

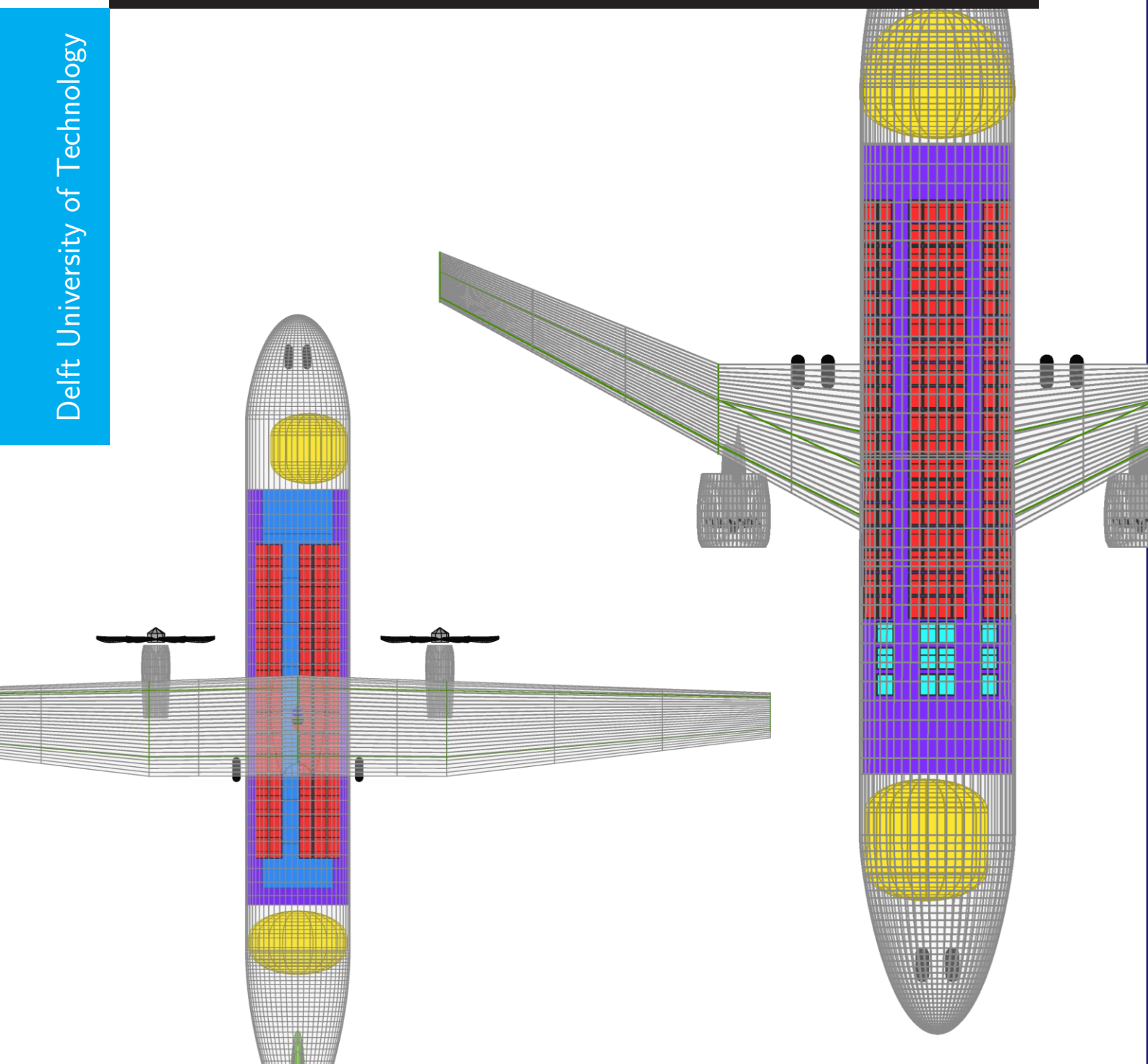
Fuel Tank Integration for Hydrogen Airliners

Giuseppe Onorato

Supervisors: Dr.ir. M. F. M. Hoogreef

August 16, 2021

Delft University of Technology



Fuel Tank Integration for Hydrogen Airlines

by

Giuseppe Onorato

**Supervisors: Dr.ir. M. F. M. Hoogreef
August 16, 2021**

to obtain the degree of Master of Science
at the Delft University of Technology,
to be defended publicly on August 24, 2021 at 10:00 AM.

Student number:	4547098
Project duration:	November 9, 2020 – August 24, 2021
Thesis committee:	Dr.ir. M. F. M. Hoogreef, TU Delft, supervisor
	Ir. P.-J. Proesmans, TU Delft
	D.Ir. G. la Rocca, TU Delft
	Dr. F. Yin, TU Delft

An electronic version of this thesis is available at <http://repository.tudelft.nl/>.

PREFACE

This report presents the work accomplished during the nine-month-long master's thesis project that I performed at the Delft University of Technology, Faculty of Aerospace Engineering, Department of Flight Performance and Propulsion, from November 9th 2020 to August 24th 2021.

Special thanks go to Dr.ir. M. F. M. Hoogreef, who gave me the opportunity to perform research in the ever-fascinating field of hydrogen aircraft, and to Ir. P.-J. Proesmans, who provided valuable feedback along the process. Gratitude goes also to Dr. A. Gangoli Rao, Dr.ir. R. Vos and Dr. F. Oliviero, for their feedback on our one-time meetings. Fundamental to the quality of this thesis was the support from my brother L. Onorato, which was sitting next to me for almost the entirety of the past year. Credits go also to M. Vasiliadis, who gifted me with the viewpoint of an experienced pilot. I am grateful to my parents for the emotional and financial support, that they unconditionally gave me for the last 25 years. Appreciation goes to D. Jawoszek, who endured me working during the weekends.

*Giuseppe Onorato
Delft, August 2021*

SUMMARY

Zero-carbon-dioxide-emitting hydrogen-powered aircraft have, in recent decades, come back on the stage as promising protagonists in the fight against global warming. Nevertheless, most recent studies agree that hydrogen aircraft would underperform their kerosene counterparts in terms of operative empty mass and specific energy consumption. The main cause for the drop in performance lays in the fuel storage, as not only the liquid hydrogen has to be kept in cryogenic conditions and pressurised, but for the same energy content, it has four times the volume of kerosene. The inevitable consequences are an increase in fuselage size, which adds mass and drag to the aircraft, and the addition of a heavy fuel storage and distribution system. On the other side, hydrogen has 2.8 times higher specific energy, and the consequent reduction in fuel mass could balance the previously mentioned drawbacks. Literature on the topic shows that the optimal fuel storage solution depends on the aircraft mission, but most studies disagree on what solutions are optimal for each aircraft range category.

The objective of this research was to identify and compare possible solutions to the integration of the hydrogen fuel containment system on short, medium and long-range airliners. The capabilities of an automated synthesis program for CS-25 aircraft have been expanded with validated structural and thermodynamic physics-based tank design models, to allow for the design and analysis of liquid hydrogen aircraft.

Studies were performed on several design options. The effect of using an integral tank structure was found to be negligible for short-range aircraft, but increasingly more beneficial for medium and long-range aircraft. The effect of increasing the fuselage diameter was found to be favourable, especially when seats abreast could be added without the addition of one aisle. The effect of using a combination of an aft and a forward tank was found to be detrimental in terms of operational empty mass, beneficial in terms of specific energy consumption and negligible in terms of maximum take-off mass. The use of spherical tanks was found to be slightly beneficial, but only when compared to a non-spherical tank version using the same tank layout, non-integral tank structure, and same cabin layout. The study on the venting pressure revealed that with increasing aircraft size the optimal venting pressure in terms of main aircraft performance decreases whereas the sensitivity to those same parameters to the choice of venting pressure increases. The use of direct gas venting as a means to contain the pressure rise did not appear to provide significant performance improvements.

The optimal designs, in terms of operational empty mass, maximum take-off mass and specific energy consumption, feature increased fuselage diameters, the use of the aft & forward tank layout, non-spherical tanks and no direct venting. The short-range aircraft uses non-integral tanks and high venting pressure, while the medium and the long-range aircraft benefit from an integral tank structure and a lower venting pressure. Nevertheless, the sensitivity to these design choices is not significant, meaning that with a different set of assumptions and/or requirements different design choices may become optimal.

The overall best performing LH2 aircraft for the short, medium and long-range categories were found to have respectively 8%, 24% and 22% higher operative empty mass, -2%, 1% and -5% higher maximum take-off mass and 5%, 13% and 5% higher specific energy consumption than their kerosene versions.

CONTENTS

Preface	i
Summary	ii
List of Figures	v
List of Tables	viii
Nomenclature	x
1 Introduction	1
1.1 Hydrogen fuel to reduce aviation emissions	1
1.2 Focus of this research	2
1.3 Structure of report	3
2 Literature Review	4
2.1 Fuel tank layout philosophies for tube-and-wing aircraft	4
2.1.1 Aft tanks	4
2.1.2 Combination of forward and aft tanks	12
2.1.3 Wing tanks	19
2.1.4 Overhead tanks	20
2.1.5 Podded tanks	23
2.2 Tank conceptual design	24
2.2.1 Studies contexts and tank requirements	24
2.2.2 Tank shape and integration	24
2.2.3 Tank materials	27
2.2.4 Heat transfer and pressure fluctuations inside tank	29
2.2.5 Tank mechanical design	31
2.2.6 Tank gravimetric index	32
2.3 Excursus on relevant hydrogen aspects	33
2.3.1 Hydrogen availability	33
2.3.2 Hydrogen-combustion emissions	34
2.3.3 Hydrogen safety	36
3 Methodology	37
3.1 Selected aircraft design tool: the Initiator	37
3.2 Adaptation of the aircraft design tool	38
3.2.1 Fuselage adaptation to tank integration	38
3.2.2 Tank sizing	40
3.2.3 Fuel system sizing	55
3.2.4 Propulsion system and wing	57
3.3 Validation of the tool	58

4 Own studies	59
4.1 Baseline aircraft	59
4.2 Tank structure: integral vs. non-integral	61
4.3 Fuselage diameter: regular vs. increased	64
4.4 Tank layout: aft vs. aft & fwd.	68
4.5 Tank shape: spherical vs. non-spherical	74
4.6 Venting pressure: low vs. high.	78
4.7 Pressure control options: gas venting vs. no gas venting	80
4.8 Optimal designs & comparison to baselines	85
4.8.1 Short-range	85
4.8.2 Medium-range	95
4.8.3 Long-range	105
4.9 Sensitivity analysis	115
4.9.1 Insulator performance: effective conductivity	115
4.9.2 Structural performance: allowable tensile stress	117
4.9.3 Range requirement	119
5 Own results compared with literature	121
5.1 Aircraft level performances	121
5.2 Tank level performance	122
6 Conclusions	124
Bibliography	126
A Example of XML input file for LH2 aircraft	130

LIST OF FIGURES

1.1	Aviation CO ₂ emissions forecast. Despite the efficiency improvement, CO ₂ emissions are rising. Source: adapted from [1].	1
1.2	Airbus ZEROe concept aircraft. Source: adapted from [2].	2
2.1	Tupolev Tu-155. Source: [3].	4
2.2	Tupolev Tu-154. Source: [4].	5
2.3	Small regional aircraft with aft tank. Source: adapted from [5].	6
2.4	Short-range aircraft powered by hybrid H ₂ propulsion. Source: adapted from [6].	7
2.5	Three-side view of the baseline concept. Dimensions in <i>m</i> . Source: [7].	9
2.6	Payload-range diagram for the Reference (A320neo), the Baseline 4 (Baseline) and the three LH ₂ concepts. Source: [7].	10
2.7	Geometry of rear integrated tank concept with the outer shape a) and the visualization of the two tanks b). Source: [7].	11
2.8	Visualization of major effects at the block-energy compared with the Baseline. Source: [7].	12
2.9	General arrangement of LH ₂ passenger aircraft. Source: [8].	13
2.10	Size comparison between H ₂ and Jet A passenger aircraft. Source: [8].	14
2.11	Long-range aircraft and catwalk located in its forward tank. Source: adapted from [5].	16
2.12	Illustration of the Hyliner (2.0) aircraft, which features a combination of forward and aft tank. Source: [9].	17
2.13	Medium-range aircraft powered by H ₂ turbines. Source: adapted from [6].	18
2.14	Long-range aircraft powered by H ₂ turbines. Source: adapted from [6].	19
2.15	High-altitude, subsonic reconnaissance airplane. Tanks are in the fuselage, in the wings and in the podded drop tanks. Source: adapted from [10].	20
2.16	Modified A380 for short-range operation. Source: [5].	20
2.17	Medium-range aircraft with part of the LH ₂ stored in overhead tanks. Source: [5].	21
2.18	Liquid Hydrogen Commercial Transport, LH ₂ -400. Source: [11].	22
2.19	Geometry of top integrated tank concept with the outer shape a) and the visualization of the two tanks b). Source: [7].	23
2.20	Geometry of podded tank concept. Source: [7].	24
2.21	Approximate size and location of LH ₂ tank, Study 1 . Source: adapted from [12].	25
2.22	The different tank arrangements for the regional airliner, Study 2 . Source: [13].	26
2.23	Tank arrangement for the long-range transport aircraft, Study 2 . Source: [13].	26
2.24	Changes in cabin layout, Study 3 . Source: [14].	27
2.25	Fuel tanks structural arrangement. Forward tank on the left, aft tank on the right, Study 3 . Source: [14].	27
2.26	Adopted tank structure for both insulation options, Study 2 . Source: [13].	28
2.27	The energy derivative in function of pressure and density for para-hydrogen. Source: [15].	30
2.28	Cost overview of three hydrogen supply pathways. Source: adapted from [6].	34
2.29	Temperature Characteristics of a Combustor. Source: [16].	35
2.30	Aviation radiative forcing components. a) Aviation as a percentage of total global radiative forcing due to human activities in the year 2011. b) Forcing components within the aviation fraction. c) Breakdown of AIC radiative forcing into contrail cirrus and persistent contrails. Source: adapted from [17].	36

3.1	N ² chart of the Initiator. In red, and underlined, the addition of the Author for the design of LH2 aircraft. First loop in orange, second loop in blue, third loop in green.	38
3.2	Fuselage sections and location of LH2 tanks. Fuel tanks in yellow.	39
3.3	Tank cross section example.	41
3.4	Illustration of tank structure options. Source: [18].	42
3.5	Flow chart of tank sizing process for non-spherical tanks.	43
3.6	Flow chart of tank sizing process for spherical tanks.	44
3.7	Tank attachments to the fuselage structure. Source: [18].	45
3.8	Design stress vs. fatigue quality index. Source: [18].	46
3.9	Installation arrangement and design details of integral tank. Source: [18].	48
3.10	Dependence of energy derivative on density and tank pressure for hydrogen. Source: [19] . .	49
3.11	Tank pressure profile for one of the designed aircraft. Flight phases: Rgate (disconnect from boil-off recovery adapter), Rto (start of take-off), Rcl (start of climb), Rd (start of descent), Raltcl (start of alternative climb), Raltcr (start of alternative cruise), Raltd (start of alternative descent), Ralthold (start of hold), Raltd2, start of second alternative descent), Rl (start of landing), Rgate2 (arrival to gate, until reconnection to boil-off recovery adapter).	51
3.12	Energy derivative profile for one of the designed aircraft. Flight phases: see Figure 3.11. . . .	52
3.13	Fuel mass profile for one of the designed aircraft. Flight phases: see Figure 3.11.	52
3.14	Tank pressure profile for one of the designed aircraft for a mission shorter than the one for which the tank was designed. Flight phases: see Figure 3.11.	53
3.15	Tank pressure profile for one of the designed aircraft, venting fuel during the last 5 mission phases. Flight phases: see Figure 3.11.	53
3.16	Thermal conductivity vs. temperature for foams, rigidised silica, and microsphere insulation. Source: [18].	54
3.17	Engine fuel delivery system. Source: [18].	56
3.18	Schematic of fuel system. Source: [18].	56
3.19	Block diagram of fuel delivery system. Source: [18].	57
4.1	Top views of baseline aircraft. Fuel tanks in yellow.	60
4.2	Example of non-integral (a) and integral (b) tank. Fuel tanks in yellow.	61
4.3	Example of LH2 aircraft with fuselage diameter of kerosene baseline (a) vs. LH2 aircraft with increased fuselage diameter (b). Fuel tanks in yellow.	65
4.4	Example of loading diagram for LH2 aircraft with aft tank layout (a) and LH2 aircraft with aft & fwd tank layout (b).	69
4.5	Example of X-plot diagram for LH2 aircraft with aft tank layout (a) and LH2 aircraft with aft & fwd tank layout (b).	70
4.6	Example of LH2 aircraft with aft tank layout (a) vs. LH2 aircraft with aft & fwd tank layout (b). Fuel tanks in yellow.	71
4.7	Example of LH2 aircraft with spherical tank shape (a) vs. LH2 aircraft with non-spherical tank shape (b). Fuel tanks in yellow.	75
4.8	Effect of venting pressure at tank and aircraft level. Tank structure: non-integral. Tank shape: non-spherical. Tank layout: aft. Seats abreast: 2-3 (ATR72), 2-3-2 (A320), 3-4-3 (A330).	79
4.9	Pressure profiles of short-range LH2 aircraft not using direct gas venting (a) and LH2 aircraft using direct gas venting (b).	82
4.10	Pressure profiles of medium-range LH2 aircraft not using direct gas venting (a) and LH2 aircraft using direct gas venting (b).	83
4.11	Pressure profiles of long-range LH2 aircraft not using direct gas venting (a) and LH2 aircraft using direct gas venting (b).	84
4.12	Side views of short-range baseline aircraft (a) and short-range optimal LH2 aircraft (b). Fuel tanks in yellow.	87

4.13 Top views of short-range baseline aircraft (a) and short-range optimal LH2 aircraft (b). Fuel tanks in yellow.	88
4.14 Design point of short-range baseline aircraft (a) and short-range optimal LH2 aircraft (b). . .	89
4.15 Loading diagram of short-range baseline aircraft (a) and short-range optimal LH2 aircraft (b). . .	90
4.16 Loading diagram of short-range baseline aircraft (a) and short-range optimal LH2 aircraft (b). . .	91
4.17 <i>MTOM</i> mass breakdown of short-range baseline aircraft (a) and short-range optimal LH2 aircraft (b).	92
4.18 <i>OEM</i> mass breakdown of short-range baseline aircraft (a) and short-range optimal LH2 aircraft (b).	93
4.19 Systems mass breakdown of short-range baseline aircraft (a) and short-range optimal LH2 aircraft (b).	94
4.20 Side views of medium-range baseline aircraft (a) and medium-range optimal LH2 aircraft (b). Fuel tanks in yellow.	97
4.21 Top views of medium-range baseline aircraft (a) and medium-range optimal LH2 aircraft (b).	98
4.22 Design point of medium-range baseline aircraft (a) and medium-range optimal LH2 aircraft (b). The airport classification for the LH2 version was increased from FAA-III to FAA-IV for convergence reasons.	99
4.23 Loading diagram of medium-range baseline aircraft (a) and medium-range optimal LH2 aircraft (b).	100
4.24 Loading diagram of medium-range baseline aircraft (a) and medium-range optimal LH2 aircraft (b).	101
4.25 <i>MTOM</i> mass breakdown of medium-range baseline aircraft (a) and medium-range optimal LH2 aircraft (b).	102
4.26 <i>OEM</i> mass breakdown of medium-range baseline aircraft (a) and medium-range optimal LH2 aircraft (b).	103
4.27 Systems mass breakdown of medium-range baseline aircraft (a) and medium-range optimal LH2 aircraft (b).	104
4.28 Side views of long-range baseline aircraft (a) and long-range optimal LH2 aircraft (b). Fuel tanks in yellow.	107
4.29 Top views of long-range baseline aircraft (a) and long-range optimal LH2 aircraft (b). Fuel tanks in yellow.	108
4.30 Design point of long-range baseline aircraft (a) and long-range optimal LH2 aircraft (b).	109
4.31 Loading diagram of long-range baseline aircraft (a) and long-range optimal LH2 aircraft (b).	110
4.32 Loading diagram of long-range baseline aircraft (a) and long-range optimal LH2 aircraft (b).	111
4.33 <i>MTOM</i> mass breakdown of long-range baseline aircraft (a) and long-range optimal LH2 aircraft (b).	112
4.34 <i>OEM</i> mass breakdown of long-range baseline aircraft (a) and long-range optimal LH2 aircraft (b).	113
4.35 Systems mass breakdown of long-range baseline aircraft (a) and long-range optimal LH2 aircraft (b).	114
4.36 Sensitivity to insulator effective thermal conductivity. The optimal configurations are used for the medium and long-range. A sub-optimal configuration is used for the short-range.	116
4.37 Sensitivity to allowable tensile stress. The optimal configurations are used for the medium and long-range. A sub-optimal configuration is used for the short-range.	118
4.38 Sensitivity to range requirement. The optimal configurations are used for the medium and long-range. A sub-optimal configuration is used for the short-range	120

LIST OF TABLES

2.1 Tupolev Tu-154B [20] vs. Tupolev Tu-155 [21].	6
2.2 Top level aircraft requirements. Source: [7].	8
2.3 General characteristics and performances of the Reference, the Baseline, the Rear tanks, the Top tanks and the Podded tanks aircraft concepts. Source: [7].	8
2.4 Comparison between LH2 and Jet A passenger aircraft (400 passengers, 5500 nmi, $M = 0.85$). Source: [8].	15
2.5 Key specifications of the Hyliner (2.0) aircraft compared to the kerosene-powered reference aircraft R2040+. Source: [9].	17
2.6 Properties of Jet A-1 fuel (kerosene-based) [22] and hydrogen [23].	25
2.7 Results from Study 1 [12].	32
2.8 Results from Study 2 [13].	33
2.9 Results from Study 3 [14].	33
4.1 Aircraft main mission requirements and configuration/performance parameters for the investigated aircraft.	59
4.2 Performance comparison between short-range aircraft using integral tanks and aircraft using non-integral tanks.	62
4.3 Performance comparison between medium-range aircraft using integral tanks and aircraft using non-integral tanks.	63
4.4 Performance comparison between long-range aircraft using integral tanks and aircraft using non-integral tanks.	64
4.5 Performance comparison between short-range aircraft with same fuselage diameters of kerosene baseline and aircraft with larger fuselage diameters.	66
4.6 Performance comparison between medium-range aircraft with same fuselage diameters of kerosene baseline and aircraft with larger fuselage diameters.	67
4.7 Performance comparison between long-range aircraft with same fuselage diameters of kerosene baseline and aircraft with larger fuselage diameters.	68
4.8 Performance comparison between short-range aircraft featuring an aft tank layout and an aft & fwd tank layout.	72
4.9 Performance comparison between medium-range aircraft featuring an aft tank layout and an aft & fwd tank layout.	73
4.10 Performance comparison between long-range aircraft featuring an aft tank layout and an aft & fwd tank layout.	74
4.11 Performance comparison between short-range aircraft featuring a spherical and a non-spherical tank shape.	76
4.12 Performance comparison between medium-range aircraft featuring a spherical and a non-spherical tank shape.	77
4.13 Performance comparison between long-range aircraft featuring a spherical and a non-spherical tank shape.	78
4.14 Performance comparison between short-range aircraft using no direct gas venting and using direct gas venting.	80
4.15 Performance comparison between medium-range aircraft using no direct gas venting and using direct gas venting.	81

4.16 Performance comparison between long-range aircraft using no direct gas venting and using direct gas venting.	81
4.17 Performance comparison between the optimal LH2 short-range aircraft and its kerosene counterpart.	86
4.18 Performance comparison between the optimal LH2 medium-range aircraft and its kerosene counterpart.	96
4.19 Performance comparison between the optimal LH2 long-range aircraft and its kerosene counterpart.	106
5.1 Comparison table for aircraft level performance of short-range aircraft designed in this research and regional aircraft from the Cryoplane project [5]. Performance values relative to the kerosene baselines of the respective studies.	121
5.2 Comparison table for aircraft level performance of medium-range aircraft designed in this research and medium-range aircraft from Silberhorn et al. [7]. Performance values relative to the kerosene baselines of the respective studies.	122
5.3 Comparison table for aircraft level performance of long-range aircraft designed in this research and long-range aircraft from McKinsey & Company [6] and the Cryoplane project [5]. Performance values relative to the kerosene baselines of the respective studies.	122
5.4 Comparison table for tank level performance of short-range aircraft designed in this research and short-range aircraft from Verstraete et al. [13].	122
5.5 Comparison table for tank level performance of medium-range aircraft designed in this research and medium-range aircraft from Silberhorn et al. [7].	123
5.6 Comparison table for tank level performance of long-range aircraft designed in this research and long-range aircraft from Verstraete et al. [13].	123

NOMENCLATURE

Abbreviations

AIC	Aircraft-induced clouds
ATAG	Air Transport Action Group
EC	Economy Class
fwd	forward
GH2	Gaseous hydrogen
ICAO	International Civil Aviation Organization
IWTI	Inner wetted thermal insulation
LH2	Liquid hydrogen
MLI	Multi-layer insulation
NACA	National Advisory Committee for Aeronautics

Molecular formulas

CO ₂	Carbon dioxide
H ₂ O	Dihydrogen monoxide
H ₂	Dihydrogen
O ₂	Dioxygen
NO _x	Nitrogen oxides

Symbols

A	outer tank surface	[m ²]
b	Wingspan	[m]
b_f	maximum width of the fuselage	[m]
b_s	structural Wingspan $b / \cos(\Lambda_{0.5})$	[m]
$BSFC$	brake-specific fuel consumption	[g/(kWh)]
$C_{D_{0,fus}}$	fuselage parasite drag coefficient	[-]
$C_{D_{0,ht}}$	horizontal tail parasite drag coefficient	[-]
C_{D_0}	aircraft parasite drag coefficient	[-]
$\left(\frac{dP}{dt}\right)$	pressure change rate	[Pa/s]

e_w	safety factor, Joint efficiency in ASME Code	[-]
g	gravitational acceleration	[m/s^2]
h_f	maximum height of the fuselage	[m]
h_{lg}	latent heat of vaporization	[J/kg]
K	coefficient for the linear acceleration	[-]
k_{fs}	fuel system fraction	[-]
k_{ins}	effective thermal conductivity of the insulation material	[$W/(mK)$]
k_{wf}	constant of proportionality equal to 0.23	[-]
L	characteristic length in the direction of the acceleration	[m]
L/D	lift-over-drag ratio	[-]
$L/D_{mid-cruise}$	lift-over-drag ratio in mid-cruise	[-]
l_t	wing root quarter-chord to horizontal tail distance	[m]
l_{fus}	fuselage length	[m]
l_{tank}	external length of tank	[m]
LHV	Lower heating value	[J/kg]
\dot{m}_{out}	mass flow rate leaving the tank	[kg/s]
FM	fuel mass	[kg]
M	Mach number	[-]
m_{crit}	critical aircraft mass for wing mass sizing	[kg]
$m_{fuelSys}$	fuel system mass (excluding LH2 tank)	[kg]
m_{fus}	fuselage structure mass	[kg]
m_g	mass flow rate of the gaseous phase	[kg/s]
m_{ht}	horizontal tail mass	[kg]
m_l	mass flow rate of the liquid phase	[kg/s]
m_{tank}	fuel tank mass	[kg]
m_w	wing mass	[kg]
MAC	mean aerodynamic chord	[m]
MLM	Maximum landing mass	[kg]
$MTOM$	Maximum take-off mass	[kg]
$MTOW$	Maximum take-off weight	[N]

$MZFM$	Maximum zero-fuel mass	[kg]
PLM	payload mass	[kg]
N_e	number of engines	[-]
N_{ft}	number of fuel tanks	[-]
n_{ult}	ultimate load factor	[-]
OEM	Operational empty mass	[kg]
OEW	Operational empty weight	[N]
P	tank pressure	[Pa]
p	tank pressure	[Pa]
P_{amb}	external tank pressure	[Pa]
P_{min}	minimum pressure	[Pa]
P_{vent}	venting pressure	[Pa]
\dot{Q}	tank heating rate	[W]
Q_w	tank heating rate	[W]
r_{fus}	fuselage radius	[m]
r_{shell}	tank structural shell radius	[m]
r_{tank}	tank outer radius	[m]
S	wing surface area	[m ²]
S/V	tank surface-to-volume ratio	[1/m]
S_G	entire outer surface of the fuselage	[m ²]
S_h	horizontal tail surface area	[m ²]
SEC	specific energy consumption	[J/pax/m]
t	time	[s]
T/W	thrust-to-weight ratio	[-]
T_{amb}	external tank temperature	[K]
T_{fuel}	fuel temperature	[K]
t_{ins}	insulation layer thickness	[m]
t_r	taper ratio	[-]
t_{shell}	structural shell thickness	[m]
$TSFC$	thrust-specific fuel consumption	[kg/(Ns)]

u	specific internal energy of tank fluid	$[J/kg]$
V	tank fluid (liquid and vapour) volume	$[m^3]$
V_D	dive speed	$[m/s]$
V_{ft}	fuel volume in liters	$[liter]$
W/P	weight-to-power ratio	$[N/W]$
W/S	wing loading	$[N/m^2]$
W_f	Fuel weight	$[N]$
W_t	Tank weight	$[N]$
W_{mix}	rate of work done on the fluid	$[W]$
x	Fuel quality	$[-]$
$\Delta P_{hydrost}$	hydrostatic pressure increment from aircraft accelerations	$[Pa]$
$\Delta x_{c.g.}$	center of gravity range normalised with MAC	$[-]$
η_{grav}	tank gravimetric index (m_{tank}/FM)	$[-]$
ϕ	energy derivative of hydrogen	$[Pa \cdot m^3/J]$
ρ_{al}	density of 2019-T851 aluminium alloy	$[kg/m^3]$
ρ_g	density of the gaseous phase	$[kg/m^3]$
ρ_{ins}	density of polyurethane foam	$[kg/m^3]$
ρ_l	density of the liquid phase	$[kg/m^3]$
ρ_{mean}	fuel mean density	$[kg/m^3]$
σ	allowable tensile stress of the structural shell material	$[Pa]$

INTRODUCTION

The introduction to this report begins with an overview of the reasons that made hydrogen aircraft concepts worthy of investigation. It continues by specifying the focus of this literature study and ends with the outline of the report structure.

1.1. HYDROGEN FUEL TO REDUCE AVIATION EMISSIONS

In line with the 2015 Paris Agreement, the Air Transport Action Group (ATAG) has set the goal of reducing, by 2050, the aviation's net CO₂ emissions to 50% of their 2005 levels [1, 6]. In the last 30 years, a combination of technology developments in aircraft engines and airframe, in the way these aircraft are operated, in the infrastructure environment and in the utilisation of assets has brought a 54% decrease in fuel consumption per passenger per *km* [1]. Nevertheless, in the same time span, demand for air travel has more than tripled [24] and is forecast to increase from 3% to 4% per year until 2050 [1, 6, 25]. The consequence of this growth is that even if efficiency improvements would accelerate from 1.5% to 2% per year, as targeted by the ICAO (International Civil Aviation Organization), by 2050 CO₂ emissions from aviation instead of halving will almost double (see Figure 1.1). Therefore, to respect the Paris Agreement and to meet the ATAG target, further and more decisive decarbonisation measures will be required.

The COVID-19 crisis is having a disruptive impact on aviation, equivalent to the 9/11, the SARS, the global financial crisis and the Eyjafjallajökull eruption airspace closure events taken together [1]. The final impact this crisis will have is not yet quantifiable but, due to its unprecedented size, its implication will be surely felt for many years [1]. In any event, history has shown that air transport and the desire to travel eventually returns [1], so the environmental problem and the consequent need for a radical change will persist.

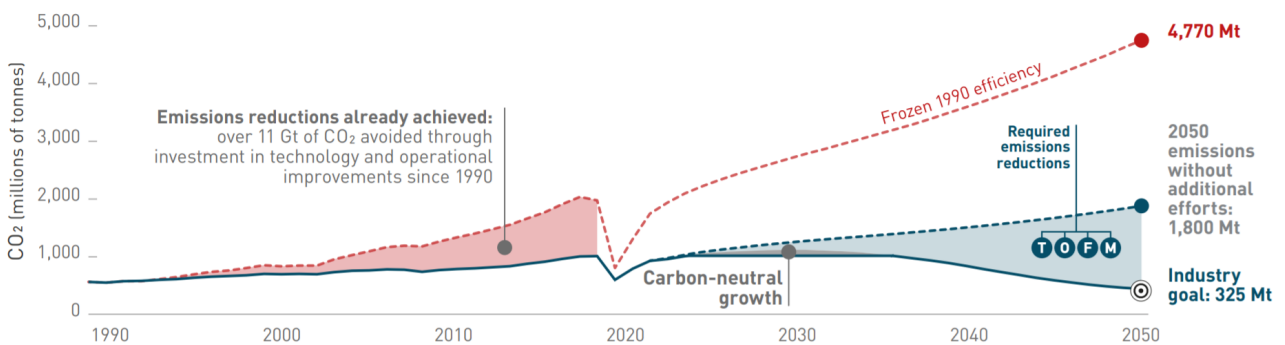


Figure 1.1: Aviation CO₂ emissions forecast. Despite the efficiency improvement, CO₂ emissions are rising. Source: adapted from [1].

Research in the possibility of using hydrogen as an alternative aviation fuel to kerosene dates back to several decades. Hans von Ohain (hydrogen-powered turbojet engine HeS 1, in 1937 [26]), NACA (Lewis Flight Propulsion laboratory on hydrogen potential, in 1955 [27, 28]), the US Air Force (B-57 on hydrogen fuel, in 1957 [29]), Lockheed (Lockheed CL-400 Suntan, in the 1950s [30]), the Soviet Union (Tupolev Tu 155 Laboratory aircraft, in 1988 [31]), and Europe (several projects in the 1990s [32]) have since long recognised the attractive combustion characteristics and high specific energy of hydrogen. Yet, these two hydrogen

qualities alone have, evidently, not been enough to outweigh clear disadvantages, such as its low energy density and its difficult handling, so hydrogen planes never went past the experimental phase. In the last decades, however, hydrogen was recognised to have another fundamental advantage to kerosene: a zero (direct) CO₂ emission energy production, either through combustion or via a fuel cell. This feature places it among the most promising solution to sustainable air travel and indeed, in the last two decades, several government-backed studies were conducted to investigate both hydrogen-combustion-powered [5] and fuel-cell-powered [33] aircraft.

Most recently, in September 2020, Airbus revealed its plan to develop three new aircraft concepts that will combine these two hydrogen-based technologies, by using direct combustion of hydrogen through a modified gas turbine which also features an embedded electric motor (powered by fuel cells). These aircraft, whose configurations and main characteristics are displayed in Figure 1.2, should enter the short-range and the medium-range market segments in 2035. Airbus's solution to the tank integration problem for the turboprop and turboprop concepts, consists in embedding the tank in the fuselages, by lengthening and increasing the diameter of the lasts [2].



Figure 1.2: Airbus ZEROe concept aircraft. Source: adapted from [2].

1.2. FOCUS OF THIS RESEARCH

Despite the tank integration solution envisioned by Airbus (aft tank) appears to be straightforward, the introduction of a large in-flight centre of gravity variation, especially for long-range missions, causes most studies to disagree on its optimality or even feasibility for other than short-range airliners. The Cryoplane Project [5] relegated its adoption to small regional aircraft, and only with the use of artificial stability. The Clean Sky 2 study [6] set the size limit for the aft tank layout to the short-range aircraft category (165 passengers, 2000 km range). Verstraete et al. [13] investigated this tank option for a regional airliner and excluded it from the design of a long-range aircraft. The Tupolev Tu-155, designed to replace the medium-range Tu-154, could carry in its aft tank enough hydrogen to fly only a short-range type mission (1700 km with 90 passengers). The single study in which the aft tank configuration used on a medium-range aircraft appears to be, if not optimal, at least feasible, is the recent study conducted by Silberhorn et al. [7], which concluded that for a 165 passengers and 5741 km mission, a hydrogen version of the aircraft (with 2045 entry-into-service) would have a 3.5% lower maximum take-off mass, 11% higher operational empty mass and a 7% higher specific energy consumption than its kerosene counterpart. The reasons for the lack of

consistency among the conclusions of these studies are multiple: the technological levels considered represented different periods, the design assumptions led to different sizing processes, and the design and analysis tools used were of different levels of fidelity.

The objective of this research is to identify and compare possible solutions to the integration of the hydrogen fuel system on short, medium and long-range airliners, by establishing a design and analysis framework capable of consistently considering the effects that different combinations of tank layout, tank structure and shape generate at aircraft level.

The maximum take-off mass (*MTOM*), the operational empty mass (*OEM*) and the specific energy consumption per passenger per *km* (*SEC*) are the three performance parameters used in literature to assess the technical feasibility of replacing a kerosene-fuelled aircraft with a hydrogen-fuelled one and will be considered the main aircraft performance parameters when assessing the aircraft relative performances in this research. The *MTOM* and the *OEM* are relevant as they are directly used to size the engines, the wing (or the high lift devices) and the landing gear, and because they are a good measure of aircraft cost. The *SEC* directly impacts the operating costs and the aircraft emissions. Naturally, through the snowball effect, these three parameters influence each other, however, it is not uncommon to find studies where a hydrogen aircraft has a lower *MTOM* but higher *OEM* and *SEC* than its kerosene counterpart¹.

1.3. STRUCTURE OF REPORT

This report observes the following structure. Chapter 2 is the literature study, where the main LH2 tank layout philosophies, namely aft tanks, a combination of forward and aft tanks, wing tanks, overhead tanks and podded tanks are introduced. This chapter also discusses some tank structural and thermal design options and sizing procedures, using contextualised examples to provide gravimetric index (η_{grav}) estimates. It then finally reviews briefly the hydrogen availability, emissions and safety aspects. Chapter 3 describes the functioning and the capabilities of the aircraft design tool adopted for this research. It then presents how it was adapted to work with LH2 aircraft and lastly shows its validation. Chapter 4 Presents the studies that have been made, using the modified tool, to investigate the impact of the tank design choices on three aircraft representing the short, medium and long-range categories. Chapter 5 compares the results of this research with the ones found in literature, both in terms of aircraft level performance and in tank level performance. Finally, in Chapter 6, the conclusion of this research and key recommendation for future work are outlined.

¹When using the word counterpart, it is meant that the aircraft is designed for the same mission (same payload / number of passengers and same range).

LITERATURE REVIEW

This chapter starts by investigating the technical feasibility of integrating, at an acceptable price in terms of *MTOM*, *OEM* and *SEC* penalties, the fuel storage system in LH2 airliners (section 2.1). It then proceeds to discuss some tank structural and thermal design options and sizing procedures, using contextualised examples to provide η_{grav} estimates (section 2.2). Lastly, to complement the researcher's knowledge on the topic, a brief literature review on other relevant hydrogen aspects, such as hydrogen availability, emission and safety, has been conducted and the key findings are presented (section 2.3).

2.1. FUEL TANK LAYOUT PHILOSOPHIES FOR TUBE-AND-WING AIRCRAFT

This section discusses the main tank layout philosophies which have been adopted through the years for the design of LH2 short, medium, and long-range tube-and-wing transport aircraft. Five subsections will present respectively aft tanks, a combination of forward and aft tanks, wing tanks, overhead tanks and podded tanks.

2.1.1. AFT TANKS

The simplest way to integrate a hydrogen fuel system into a tube-and-wing commercial aircraft is by placing a single large tank at the back of the fuselage. The small tank surface-to-volume ratio (S/V) minimises η_{grav} and the fuselage presents none to small differences with respect to a kerosene powered aircraft. The main disadvantage is the unavoidable centre of gravity (*c.g*) variation between the full and the empty-tank condition.

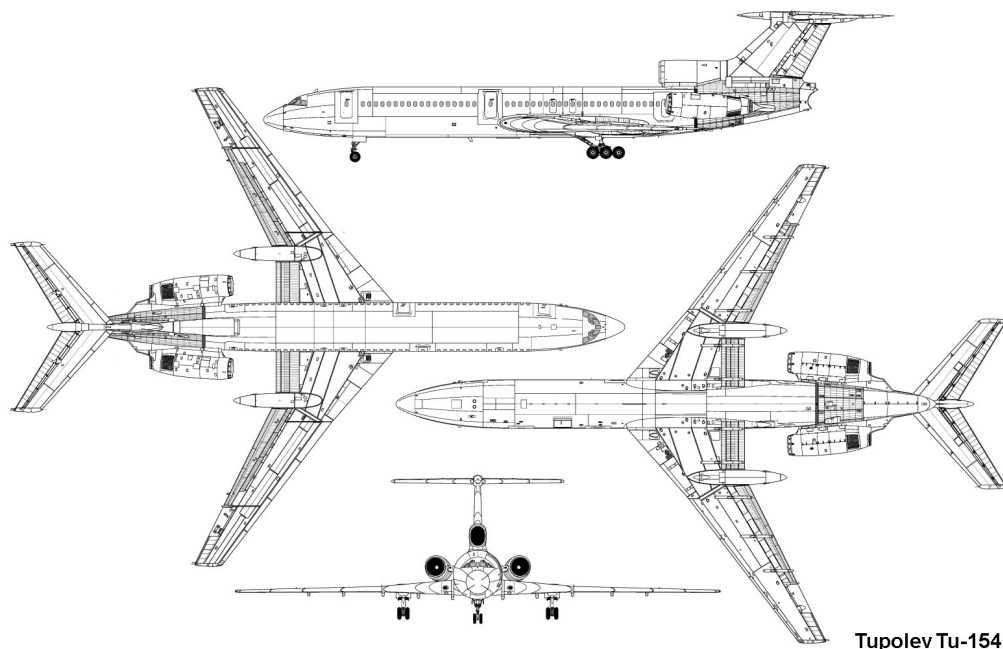
An example of hydrogen-powered aircraft in the short/medium-range category, featuring a single hydrogen aft tank, is the Tupolev Tu-155 (see Figure 2.1).



Figure 2.1: Tupolev Tu-155. Source: [3].

As a consequence of the energy crisis of the 1970's, the USSR Academy of Sciences, in collaboration with experts and scientists from different institutions, launched a program for the introduction of hydrogen as a fuel source for several sectors of the economy. In the aviation sector, a flying laboratory that would use LH₂ fuel was built. This aircraft, designed based on the commercial model Tu-154B, was called Tu-155 and flew first in April 1988 [21, 34]. Only one of the three aircraft engines was powered by hydrogen (the experimental NK-88 engine), with the remaining two working on kerosene. The cryogenic fuel was placed in a 17.5 m³ fuel tank, located in the tail section of the passenger cabin [34]. Knowing the tank volume and the LH₂ density (see Table 2.6), and assuming the entire volume being filled with LH₂, the hydrogen mass can be computed to be around 1242 kg. This hydrogen mass would allow 2 hrs of cruise at 850 km/h, starting with a MTOM of 98000 kg [21]. The tail section of the passenger cabin was kept at a lower pressure than the passenger cabin, to prevent hydrogen from reaching the crew area in the event of a leak. A pneumatically rather than electrically powered fuel pump was used to avoid the hazard of sparks. An air-to-hydrogen heat exchanger was used to boil the liquid hydrogen before combustion. The combustion chamber, the fuel injection nozzles, and the engine controls were the only modified engine components [18]. Table 2.1 compares the Tu-154B and the Tu-155 characteristics. It can be seen that, rather than introducing a fuselage extension to fit the LH₂ tank, the passenger cabin was shortened. This solution appears to have nullified the impact of the hydrogen integration to the aircraft design: the OEM and the MTOM, the range, the payload (mass) capability, the airframe geometry, the thrust and cruise speed (and thus the drag) did not vary significantly. Another aspect of the Tu-155 design, which surprisingly appears to not have been significantly impacted, is the longitudinal stability and controllability. In fact, by confronting Figure 2.1 with Figure 2.2 neither the wing nor the horizontal tail positions and sizes appear to have been modified. Nevertheless, it is possible that the aircraft longitudinal stability and controllability did change, but the engineers, rather than modifying the Tu-154 airframe, accepted the stability penalty and a shrunk flight envelope.

What did change, however, is the passenger cabin (or cargo) volume, which in turn increased the SEC.



Tupolev Tu-154

Figure 2.2: Tupolev Tu-154. Source: [4].

Table 2.1: Tupolev Tu-154B [20] vs. Tupolev Tu-155 [21].

Property	Tu-154B	Tu-155
Maiden flight year	1968	1988
Length (<i>m</i>)	47.9	47.9
Wingspan (<i>m</i>)	37.55	37.55
Height (<i>m</i>)	11.4	11.4
Wing Area (<i>m</i> ²)	201.45	202.00
OEM (<i>kg</i>)	50700	52000
MTOM (<i>kg</i>)	98000	98000
Range (<i>km</i>)	2780	2800
Cruise speed (<i>km/h</i>)	850	850
Engine	NK-8-2, 3 x 23150 lb	2 NK-8-2 + 1 NK-88, 3 x 23150 lb

An exploratory study on this tank layout was also conducted by Airbus amid the 1999 Cryoplane project [5]. Despite recognising that having a single tank behind the aft pressure bulkhead is the simplest solution, Airbus underlined that from a *c.g* shift perspective this layout can only work when the fuel mass fraction ($m_{fuel}/MTOM$) is small (regional aircraft segment). Moreover, to reduce the *c.g* variation, the aircraft concept was designed with a larger fuselage diameter (see Figure 2.3). The study found that this measure was still insufficient to contain the *c.g* travel and this resulted in the necessity to combine a fly-by-wire (artificial stability) and a large horizontal tail, detrimental for the *SEC* [5].

Compared to kerosene fuelled aircraft of the same category, this LH2 concept aircraft was estimated to have 0.3% higher *MTOM*, 16.5% higher *OEM* and 14% higher *SEC* [5].

**Figure 2.3:** Small regional aircraft with aft tank¹. Source: adapted from [5].

Another example of short/medium-range hydrogen aircraft with aft tank layout is provided by Clean Sky 2 in its 2020 report Hydrogen-Powered Aviation [6]. Unlike the Tupolev Tu-155 and the rest of the aircraft presented in this chapter, this concept uses hybrid propulsion: it uses a fuel-cell-powered electric motor to drive the fan shaft during cruise and it activates the hydrogen-combustion-powered turbine when major thrust is required at take-off and climb. The main aircraft characteristics and performances are presented in Figure 2.4. Worth noting is that the *SEC* (in that study referred to as "energy demand") of this aircraft

¹In reality, two tanks were used for regulatory reasons.

is lower than its kerosene counterpart. Note that this aircraft was designed to be hydrogen-powered and to contain a large tank and indeed, unlike the Tu-155, the fuselage was extended by approximately five meters to integrate the two² LH₂ tanks behind the passenger cabin [6].

Nevertheless, this study acknowledged that some design issues still needed to be addressed. First, a system for safe and reliable LH₂ distribution from the back to the fuselage to the two wing-mounted engines still needed to be devised. Second, the fuel cell system's power rating of more than 10 megawatts requires a considerable apparatus of heat exchangers. Third, the use of a parallel hybrid system makes the development and certification of the propulsion system complex [6].

Exhibit 8

Short-range aircraft powered by hybrid H₂ propulsion

Revolutionary aircraft

Design mission: 165 PAX, 2,000 km range, cruise speed Mach 0.72

- 2 LH₂ tanks behind PAX cabin -added weight: 4 tons
- Fuel cell system (11 MW) powering electric motors
- Electric motor driving main turbine fan shaft during cruise, while H₂ turbine is turned off



1. Major assumptions: 35% gravimetric index of LH₂ tank, 91% useable LH₂ fuel, FCS mass 2 kW/kg (incl. cooling) and 60% peak efficiency (LHV), e-motors and PMAD with 97% efficiency, battery with 0.6 kWh/kg, H₂-turbine with 45% cruise efficiency
2. Cost per available seat kilometer
3. Maximum take off weight



Figure 2.4: Short-range aircraft powered by hybrid H₂ propulsion³. Source: adapted from [6].

The last example comes from an interesting study that analysed different hydrogen tanks layouts for a medium-range aircraft with potential entry-into-service in 2045 [7].

To create a baseline aircraft for performance comparison, firstly an A230neo reference aircraft with current A320neo technology was selected (see Table 2.2). Secondly, technology factors were applied on fuselage structural mass (0.85), wing structural mass (0.8-0.85), furnishing (0.9) and engine performance (0.85), considering the 2045 entry-into-service year. In the third and last step to obtain the baseline aircraft, the configuration was modified to best exploit the consequences of these technological improvements (see Figure 2.5).

²See footnote 1.

³The gravimetric index in [6] is defined as the mass of the LH₂ fuel mass in relation to the full mass of the LH₂ tank filled with maximum LH₂ fuel.

Table 2.2: Top level aircraft requirements. Source: [7].

Parameter	Value
Design range (<i>km</i>)	5741
M_{cruise}	0.78
Take-off field length (SL ISA+15K) (<i>m</i>)	2200
Landing field length (SL ISA+0K) (<i>m</i>)	1850
ICAO Aerodrome Reference Code	Code C
Maximum payload (<i>kg</i>)	20000
Design payload (<i>kg</i>)	17000
Design cargo mass (<i>kg</i>)	2150
Maximum cargo mass (<i>kg</i>)	5150
Alternate distance (<i>nm</i>)	370
Loiter time (<i>min</i>)	30
Contingency (%)	3
Number of passengers (design, 2 class)	165
Mass per passenger (design) (<i>kg</i>)	90
Approach speed (with <i>MLM</i>) (<i>kt</i> , CAS)	131.5
Wing span limit (<i>m</i>)	36

Table 2.3: General characteristics and performances of the Reference, the Baseline, the Rear tanks, the Top tanks and the Podded tanks aircraft concepts. Source: [7].

Parameter	Reference	Baseline	Rear	Top	Podded
<i>MTOM</i> (<i>kg</i>)	79016	70276	67819	66045	64584
<i>OEM</i> (<i>kg</i>)	44294	39838	44334	42605	41084
<i>MZFM</i> (<i>kg</i>)	64294	59838	64334	62605	61084
<i>MLM</i> (<i>kg</i>)	67400	62040	65069	63331	61823
Design block-energy (<i>GJ</i>)	657.9	498.2	533.0	530.3	535.6
Thrust-to-weight ratio	0.311	0.288	0.300	0.310	0.319
Wing loading (<i>kg/m</i> ²)	635.2	674.2	620.4	620.7	621.8
Aspect ratio	10.3	12.4	11.9	12.2	12.5
Wing span (<i>m</i>)	36	36	36	36	36
Insulation thickness (<i>cm</i>)	-	-	7	10	9
Fuel system mass (excl. tank) (<i>kg</i>)	-	-	781	627	630
Fuel tank (<i>kg</i>)	-	-	1651	2429	2190
Rel. trip boil-off (%)	-	-	1.9	2.5	2.0

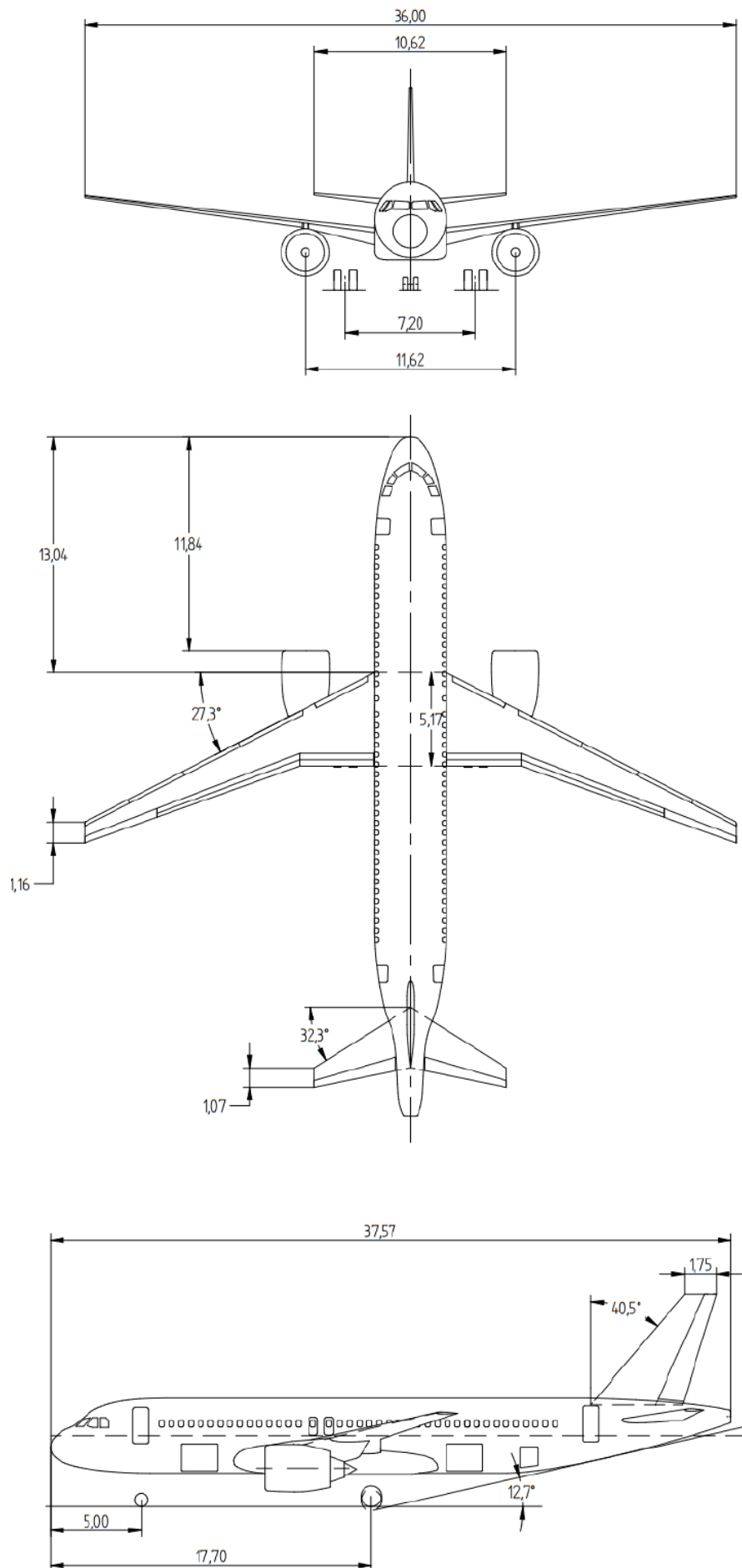


Figure 2.5: Three-side view of the baseline concept. Dimensions in *m*. Source: [7].

A first downselection excluded the investigations of:

- tanks inside the wing, due to the lack of available volume,
- tanks below the cabin inside the cargo compartment and below and beside the fuselage, mainly due to safety reasons
- tank between cockpit and cabin, due to the negative structural mass effect connected to the creation of a catwalk

The concepts for which the investigations were pursued are:

- non-integral⁴ tank behind the cabin (see Figure 2.7)
- non-integral tanks above the fuselage (see Figure 2.19)
- integral tanks in pods installed below the wing (see Figure 2.20)

Important to notice is that instead of designing the hydrogen aircraft for the design mission used for performance comparison (Kerosene Design Point in Figure 2.6), the hydrogen aircraft were designed to somewhat cover the market of the baseline aircraft. This resulted in the hydrogen concepts not being optimised, but rather over-designed for the design mission used for the performance comparison, which is the design mission of the baseline aircraft (see Figure 2.6). Note also that the engine thrust-to-weight ratio and the cruise altitude of the hydrogen concept were not kept the same as the baseline ones, but optimised.

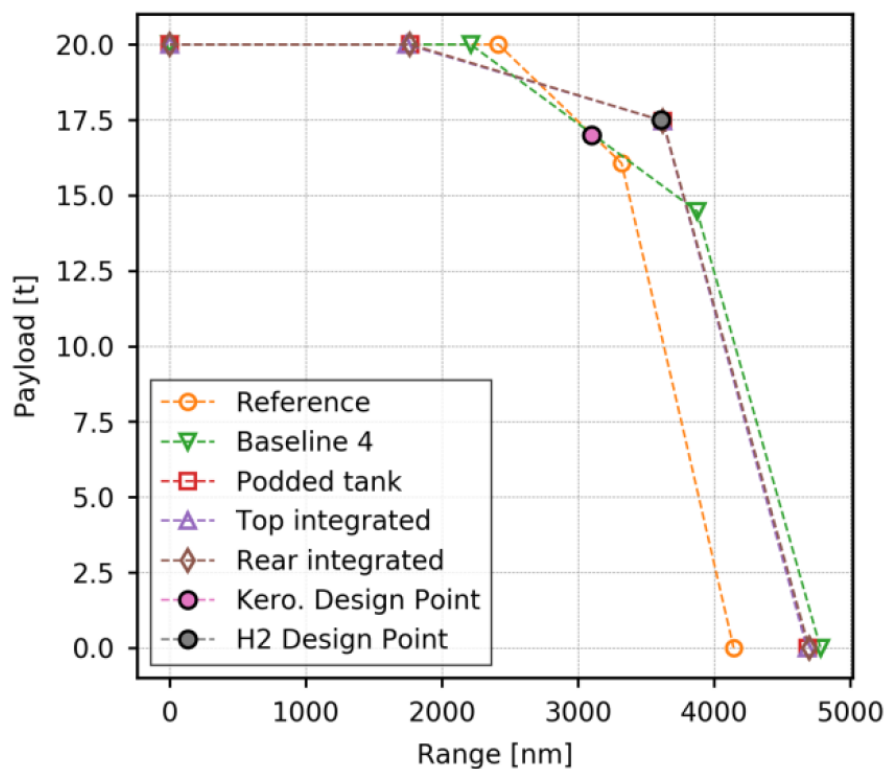


Figure 2.6: Payload-range diagram for the Reference (A320neo), the Baseline 4 (Baseline) and the three LH2 concepts. Source: [7].

The main differences between the rear integrated tank concept (see Figure 2.7) and the baseline (see Figure 2.5) are the decreased L/D (-5%) and increased fuselage mass (+28%) due to the increased fuselage

⁴This piece of information is not found in the paper, but was obtained, upon request, from one of the author of the study and is not explicitly mentioned in [7].

length (now 45.7 m). Note that the nose and main landing gear mass grow, as a consequence of the increased gear height necessary to maintain ground clearance. Together with the fuel containment and additional system mass, these factors led to an 11% higher *OEM*. Further information is given in Table 2.3 and Figure 2.8. Worth noting is that despite the in-flight centre of gravity shift due to the tank position was taken into account⁵, the horizontal tail did not significantly increase in size.

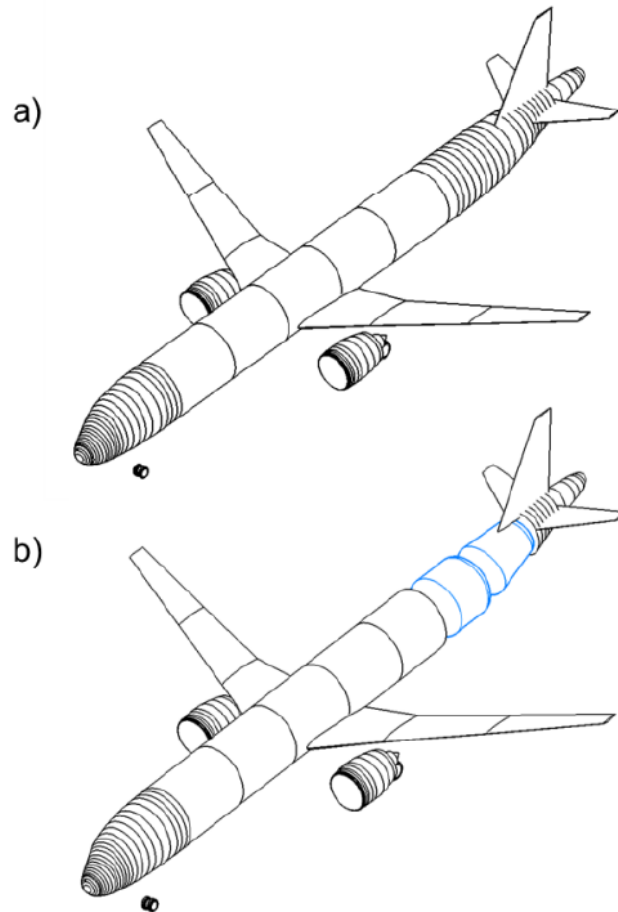


Figure 2.7: Geometry of rear integrated tank concept with the outer shape a) and the visualization of the two tanks b). Source: [7].

⁵See footnote 4

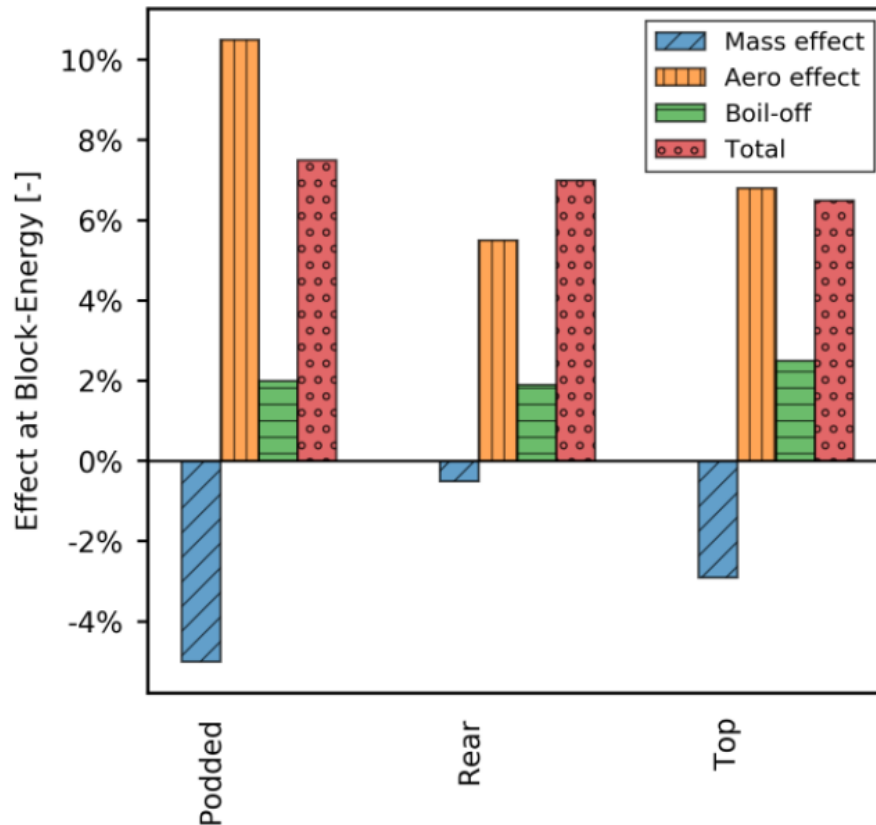


Figure 2.8: Visualization of major effects at the block-energy⁶ compared with the Baseline. Source: [7].

2.1.2. COMBINATION OF FORWARD AND AFT TANKS

In subsection 2.1.1 it was shown how the use of a single aft tank was considered to be the simplest option to integrate a hydrogen fuel system into a tube-and-wing commercial aircraft. In subsection 2.1.1 it was also stressed that the main disadvantage of this configuration is the unavoidable $c.g$ variation between the full and the empty tank condition. This section presents a tank layout configuration that eliminates this problem, at the price of a higher η_{grav} and a slightly longer fuselage (or, equivalently, shorter passenger cabin). As the $c.g$ variation problem increases with increasing $m_{fuel}/MTOM$, the aircraft designed with this tank layout are prevalently of the long-range category.

An example of a hydrogen-powered aircraft concept featuring a combination of forward and aft tanks was studied by G. D. Brewer at Lockheed in 1976 (see Figure 2.9) [8].

⁶Block-energy is the total energy required for the flight and is the sum of the Taxi energy, the Trip energy, the Contingency energy, the Alternate energy, the Final Reserve energy, the Additional energy and any Extra energy carried.

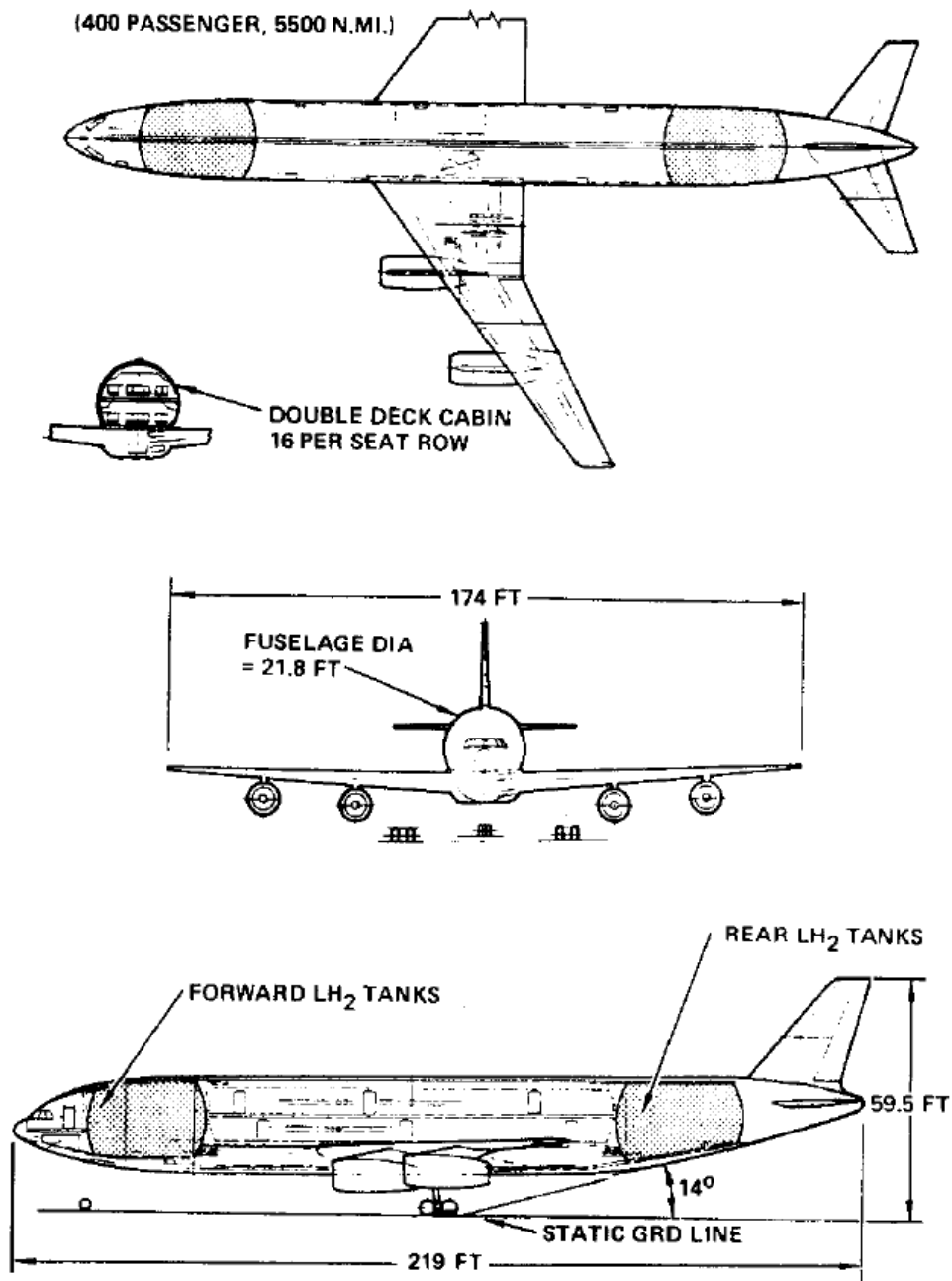


Figure 2.9: General arrangement of LH₂ passenger aircraft. Source: [8].

As in the USSR (see subsection 2.1.1), the 70's energy crisis raised the demand for an alternative fuel to replace petroleum-based kerosene in the USA too. The hydrogen potential in meeting economics, safety, performance and environmental requirements meant that studies were performed to investigate the feasibility, practicability and potential advantages of using LH₂ as fuel in commercial transport aircraft [8]. Brewer designed a kerosene (Jet A in Figure 2.10 and Table 2.4) and an LH₂ aircraft for an identical mission and he then compared performance parameters like masses, dimensions and efficiencies to find that the last aircraft outmatched the first on all three aspects (see Figure 2.10 and Table 2.4).

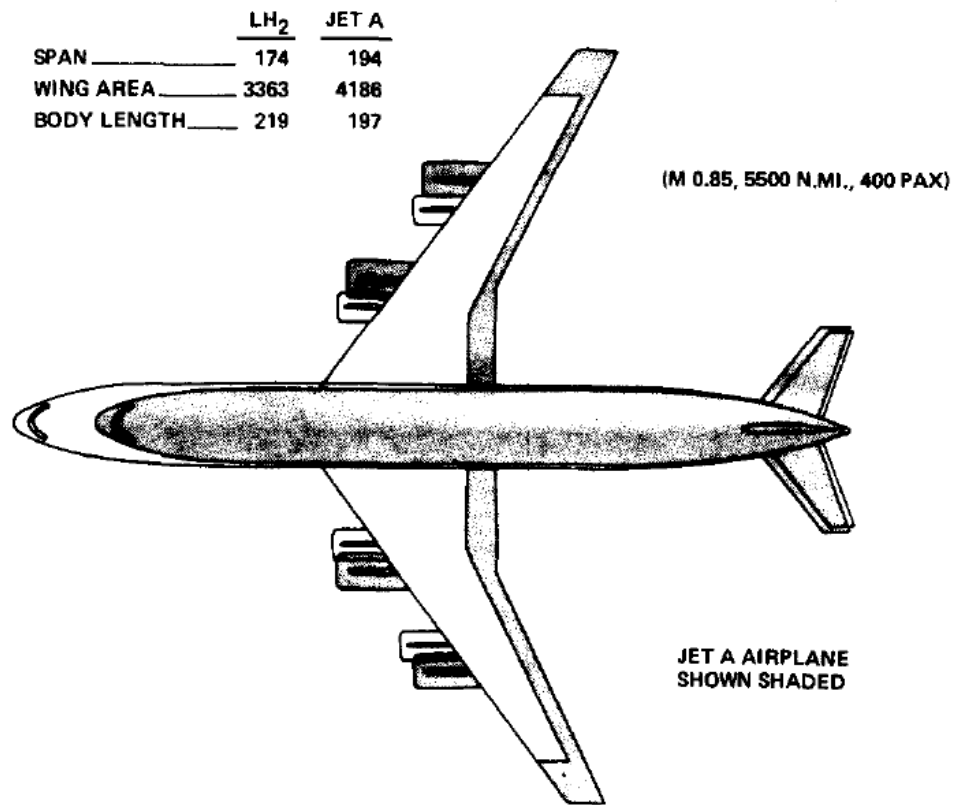


Figure 2.10: Size comparison between H₂ and Jet A passenger aircraft. Source: [8].

Table 2.4: Comparison between LH2 and Jet A passenger aircraft (400 passengers, 5500 nmi, $M = 0.85$).
Source: [8].

		LH ₂	JET A	FACTOR (JET A/LH ₂)
GROSS WEIGHT	LB	391,700	523,200	1.34
OPERATING EMPTY WEIGHT	LB	242,100	244,400	1.01
BLOCK FUEL WEIGHT	LB	52,900	165,500	3.13
THRUST PER ENGINE	LB	28,700	32,700	1.14
SPAN	FT	174	194.1	1.12
HEIGHT	FT	59.5	60.2	1.01
FUSELAGE LENGTH	FT	219	197	0.90
WING AREA	FT ²	3363	4186	1.24
L/D (CRUISE)		16.1	17.9	1.11
SFC (CRUISE)	$\frac{\text{LB}}{\text{HR}} / \text{LB}$	0.199	0.581	2.92
FAR T.O. DISTANCE	FT	6240	7990	1.28
FAR LANDING DISTANCE	FT	5810	5210	0.90
AIRCRAFT PRICE	$\$10^6$	26.9	26.5	0.99
ENERGY UTILIZATION	BTU/SEAT N.MI.	1239	1384	1.12

During the 1999 Cryoplane project conducted by Airbus and already mentioned in subsection 2.1.1 [5], a feasibility study was conducted on this tank layout option too.

Airbus reasoned that for long-range aircraft the fuselage diameter is large enough to allow for a lateral catwalk between the cockpit and the passenger cabin (see Figure 2.11). It added, however, that if the cockpit-passenger cabin interconnection could be eliminated, this layout would be feasible for aircraft with narrower fuselage too. Compared to kerosene fuelled aircraft of the same category, this LH2 concept aircraft was estimated to have 14.8% lower *MTOM*, 25.2% higher *OEM* and 9% higher *SEC* [5]. It must be mentioned that Airbus stated in the same report that neither the structural aspects of the front tank as part of the pressure vessel nor the cockpit-cabin interconnection had been examined.

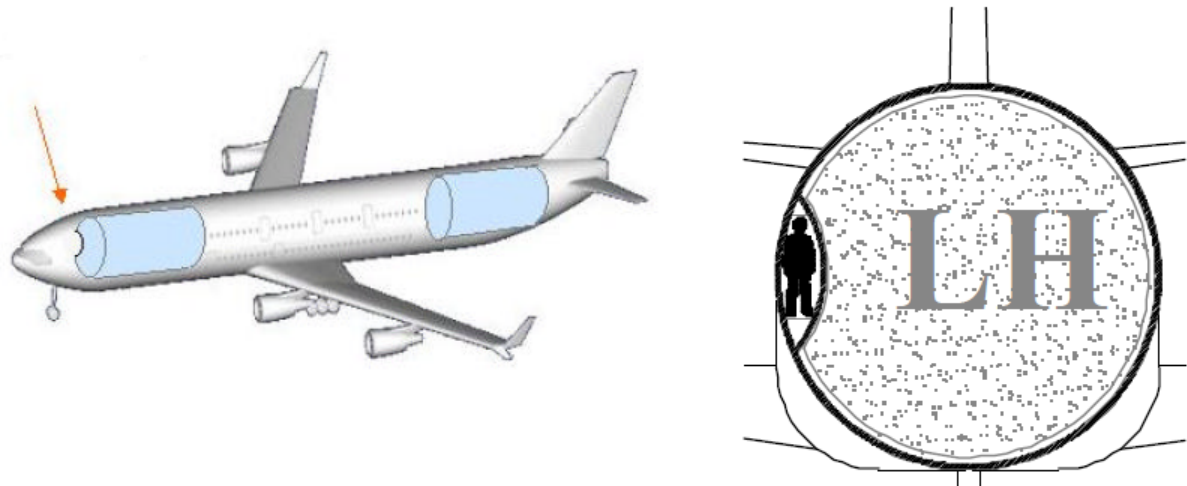


Figure 2.11: Long-range aircraft and catwalk located in its forward tank. Source: adapted from [5].

A recent study, performed by Troeltsch et al. [9], presented the conceptual design of a long-range LH2 aircraft (Hyliner (2.0), see Figure 2.12) derived from a conventional kerosene airliner with technology level representative of a 2040 entry-into-service. The tank layouts analysed in this study were: a combination of forward and aft tanks, a single overhead tank, and various combinations of forward, aft and overhead tanks. The combination of forward and aft tanks was found to be the most efficient, with the overhead tank leading to a 13% higher fuel consumption and the combinations of forward, aft and overhead tank leading to at least 15% higher fuel consumption. Compared to kerosene fuelled aircraft of the same category, the Hyliner (2.0) concept aircraft was estimated to have 26% lower *MTOM*, 7% higher *OEM* and 9% higher *SEC* [9]. Further information is given in Table 2.5.

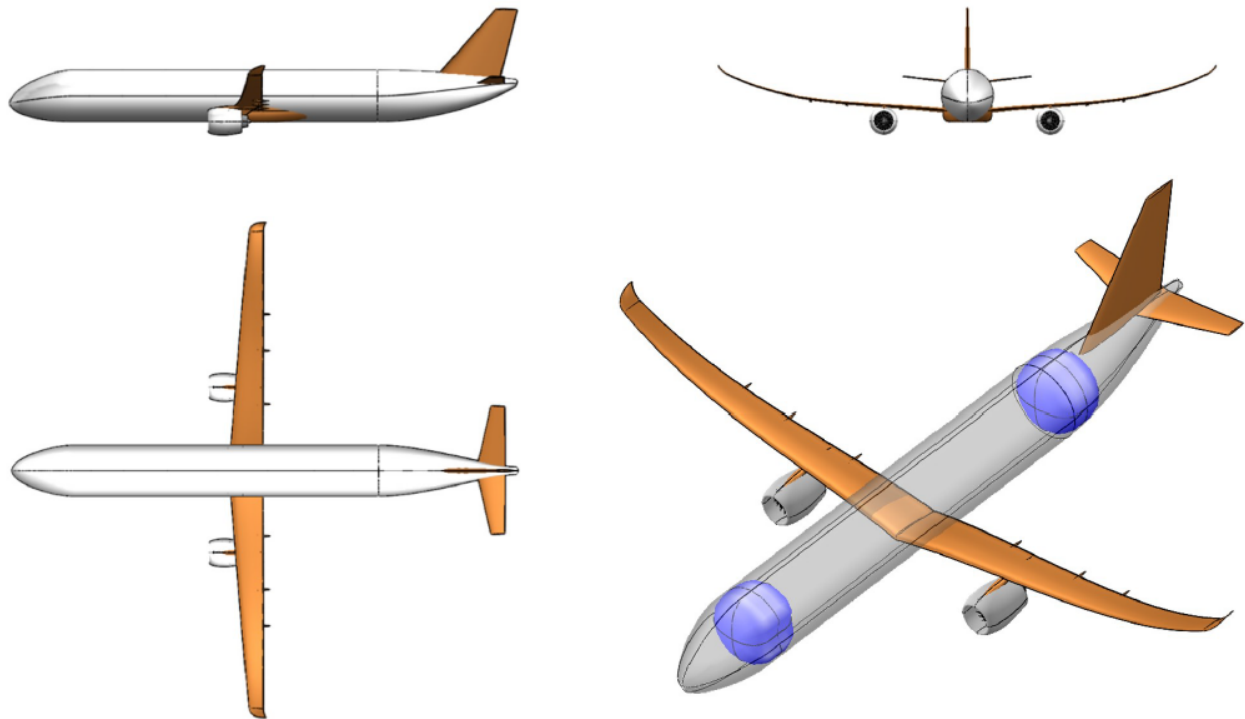


Figure 2.12: Illustration of the Hyliner (2.0) aircraft, which features a combination of forward and aft tank. Source: [9].

Table 2.5: Key specifications of the Hyliner (2.0) aircraft compared to the kerosene-powered reference aircraft R2040+. Source: [9].

Parameter	R2040+	Hyliner (2.0)
<i>MTOM</i> (kg)	264000	196000
<i>OEM</i> (kg)	138000	128000
Payload mass (kg)	46000	46000
Design range (km)	11852	11852
Wing loading (kg/m^2)	713	588
Aspect ratio	12	19.5
Wing span (m)	67	81
M_{cruise}	0.82	0.7
Fuel mass (kg)	72500	18600
Fuel tank volume (m^3)	128	371

Two final examples of hydrogen-powered aircraft featuring a combination of forward and aft tanks are given in the Clean Sky 2 report [6].

Note that the availability of two aircraft of different categories designed within the same study, not only provides absolute performance data on those aircraft but also offers information on the impact on performance from scaling-up in terms of passenger number and range. The medium-range and the long-range aircraft main characteristics and performances are presented respectively in Figure 2.13 and Figure 2.14. The medium-range aircraft required a 10 m longer fuselage compared to a kerosene aircraft, to accommodate the two LH2 tanks, while the fuselage extension of the long-range one was given to be 30% of the

original length. The report states for both the aircraft that a system to safely and reliably distribute the LH2 from the aft and the forward tank to the two wing-mounted engines had still to be developed.

Exhibit 9

Medium-range aircraft powered by H₂ turbines

Evolutionary aircraft

Design mission: 250 PAX, 7,000 km range, cruise speed Mach 0.82

- 2 LH₂ tanks in front and back of PAX cabin - added weight: 29 tons
- H₂ turbines generating propulsion power



1. Major assumptions: 37% gravimetric index of LH₂ tank, 92% useable LH₂ fuel, 47% H₂ turbine cruise efficiency, 80% fan efficiency
2. Cost per available seat kilometer
3. Maximum take off weight

Figure 2.13: Medium-range aircraft powered by H₂ turbines⁷. Source: adapted from [6].

⁷See footnote 3.

Exhibit 10

Long-range aircraft powered by H₂ turbines

Evolutionary aircraft

Design mission: 325 PAX, 10,000 km range, cruise speed Mach 0.85

- 2 LH₂ tanks in front and back of PAX cabin - added weight: 52 tons
- H₂ turbines generating propulsion power



1. Major assumptions: 38% gravimetric index of LH₂ tank, 92% useable LH₂ fuel, 50% H₂ turbine cruise efficiency, 80% fan efficiency
2. Cost per available seat kilometer
3. Maximum take off weight



Figure 2.14: Long-range aircraft powered by H₂ turbines⁸. Source: adapted from [6].

2.1.1.3. WING TANKS

Integrating tanks in the wing structure has one fundamental problem: it results in tanks with high S/V and consequent high η_{grav} . Moreover, given the 4 times lower energy density compared to kerosene and the fact that kerosene aircraft already use most of the available wing volume, it would be difficult to store sufficient LH₂ in the wing only.

An example of wing integrated tank can be found in the report by Silverstein and Hall [10] (A more recent overview of this report can be found in [35]). Silverstein and Hall analyzed the use of liquid hydrogen for a subsonic reconnaissance airplane. This aircraft had a $MTOM$ of 40000 kg and carried hydrogen tanks in the wing, in the fuselage, and optional drop tanks for additional range. It operated at 24 km of altitude and could make observations 13500 km from its base. It was powered by advanced turbojet engines weighing about half of those in use in 1955.

Silverstein and Hall concluded that "within the state of the art and the progress anticipated, aircraft designed for liquid-hydrogen fuel may perform several important missions that comparable aircraft using hydrocarbon (JP-4) fuel cannot accomplish." but also that "substantial applied research and development effort will be required in many technical fields to achieve the goal outlined." [10].

A key assumption used by Silverstein was the feasibility of lightweight and insulated fuel tanks, suitable for liquid hydrogen. Reynolds continued his investigation and concluded that it was feasible to design a tank with η_{grav} lower than 0.15. The boil-off rate was estimated to be less than 30% of the hydrogen consumption during cruise [36].

⁸See footnote 3.

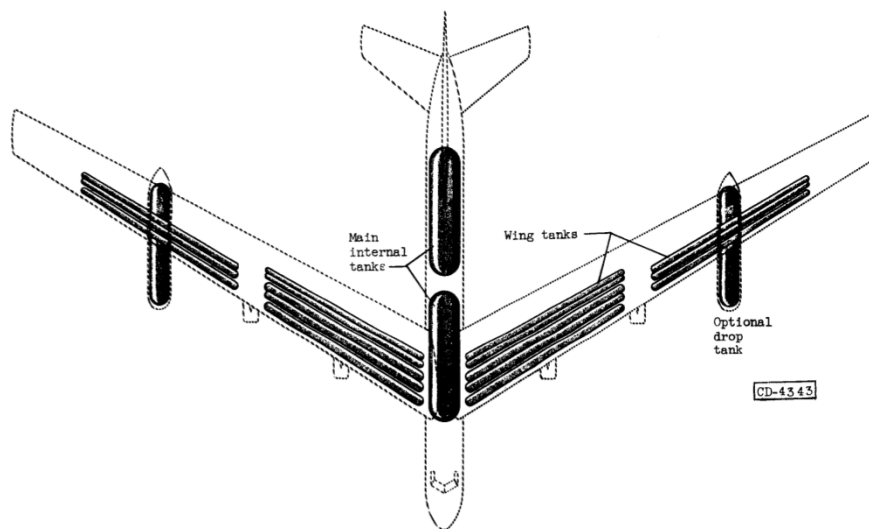


Figure 2.15: High-altitude, subsonic reconnaissance airplane. Tanks are in the fuselage, in the wings and in the podded drop tanks. Source: adapted from [10].

In the Cryoplane Project [5], Airbus assumed that a “validator” aircraft was necessary for a smooth transition to LH2. This validator would have tested the practicality of the concept and of its components and would have provided valuable operational experience. The last step of the validator strategy consisted of modifying an A380 for short-range missions. In this case, the relatively low amount of LH2 needed could have been stored in the voluminous inner wing portion with relatively low η_{grav} tanks (see Figure 2.16).

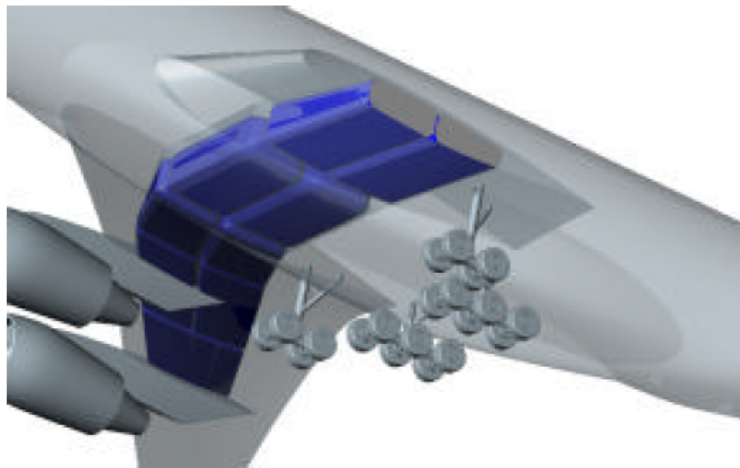


Figure 2.16: Modified A380 for short-range operation. Source: [5].

2.1.4. OVERHEAD TANKS

The tank layout philosophy consisting of positioning the tank on top of the fuselage has two main advantages: it keeps the aircraft length constant (unaltered airport handling) and prevents large variation of $c.g.$ between the full-tank and the empty-tank conditions. The main drawback of this layout is the considerable mass and drag penalty resulting from the increased fuselage cross-section, which usually also needs to deviate from the efficient circular shape.

In the Cryoplane Project (mentioned in subsection 2.1.1) [5] Airbus chose a combination of aft tank and overhead tank for the medium-range aircraft concept (see Figure 2.17). The analysis of this concept indicated a 2.7% lower *MTOM*, a 25.1% higher *OEM* and 10% higher *SEC* compared to kerosene fuelled aircraft of the same category.

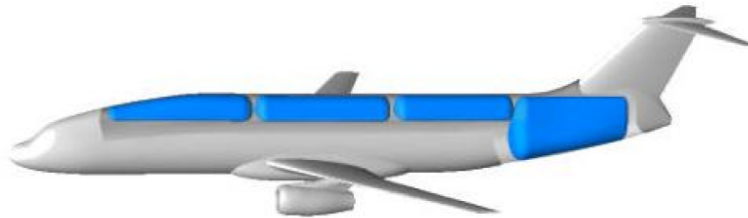


Figure 2.17: Medium-range aircraft with part of the LH2 stored in overhead tanks. Source: [5].

Another example of this tank configuration is given in the work of Maniaci [11]. He predicted the performance of an LH2 commercial transport concept, called LH2-400, compared to an energy equivalent Boeing 747-400. A detailed, componentwise drag buildup of each of the two aircraft was performed and applied to a mission analysis program. The drag buildup data was used to compare the performance at the beginning of cruise and at the end of cruise. A full mission analysis was then performed to compare the fuel burned by each aircraft. The wing loading and thrust loading of the LH2 aircraft were sized using the same take-off, climbing, and landing conditions of the Boeing 747-400 (baseline aircraft): the wing loading stayed constant while the maximum thrust required decreased due to the lower *MTOM*. The fuel tanks were initially sized with the energy requirements of the baseline aircraft and later via mission equivalence. The computed performance of the LH2 aircraft was better at the beginning of the cruise and worse toward the end of the cruise. While the total energy used for the design mission was found to be comparable, the LH2 aircraft resulted to be more sensitive to off-design missions. The author underlined that the LH2 aircraft performance could be significantly improved by lowering the cruise Mach number, as the enlarged fuselage cross-section reduced the drag divergence Mach number of the LH2 aircraft [11].

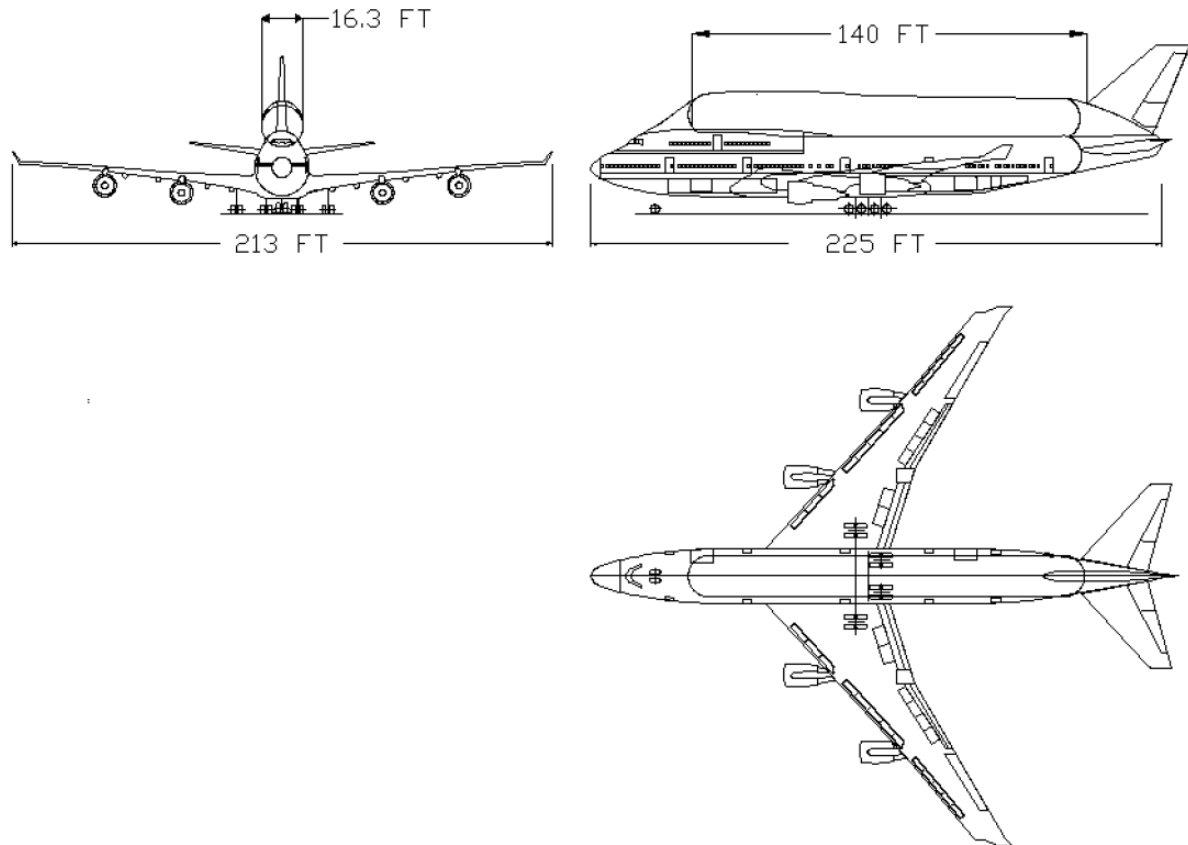


Figure 2.18: Liquid Hydrogen Commercial Transport, LH2-400. Source: [11].

One last example of overhead tank configuration is given in the same study discussed in subsection 2.1.1 (see Table 2.2 for top level aircraft requirements) [7].

This concept is the most efficient among the other two LH2 concepts analysed in the study, but it is still 6.5% less efficient than the baseline kerosene concept [7]. Further information is given in Table 2.3 and Figure 2.8.

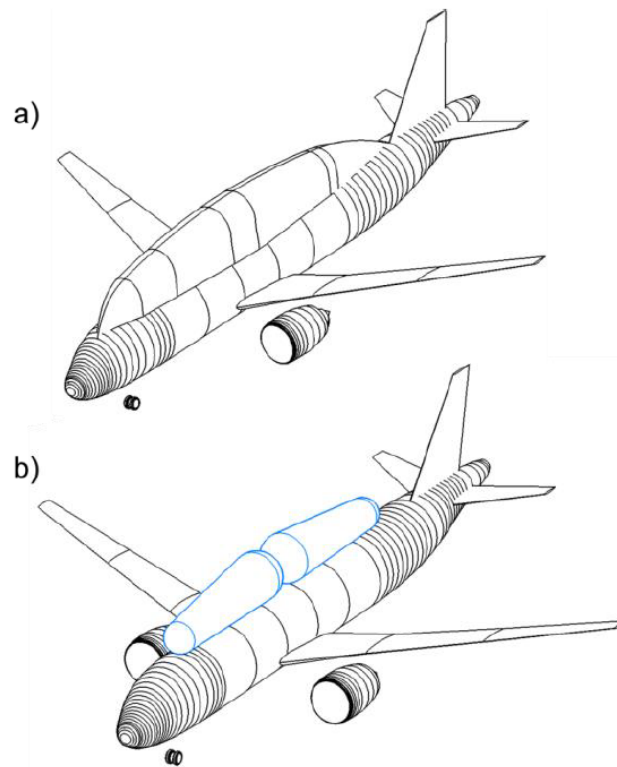


Figure 2.19: Geometry of top integrated tank concept with the outer shape a) and the visualization of the two tanks b). Source: [7].

2.1.5. PODDED TANKS

Podded tanks attached under the wing have a clear disadvantage in terms of drag penalty because of their large frontal area (e.g. see Figure 2.8) and can come with ground clearance issues. However, they present also some advantages. They can be placed close to the aircraft *c.g.* (small *c.g.* variation) and close to the engines (short fuel lines). They provide bending relief and can improve the wing aeroelastic characteristics. They offer easy accessibility for maintenance and they are placed far from the passenger cabin (improved safety). They can be swapped for larger ones when a longer range is needed and vice-versa.

One example of podded tanks configuration is given in the same study [7] discussed in subsection 2.1.1 and subsection 2.1.4 [7]. This concept is 7.5% less efficient than the baseline kerosene concept. Further information is given in Table 2.3 and Figure 2.8.

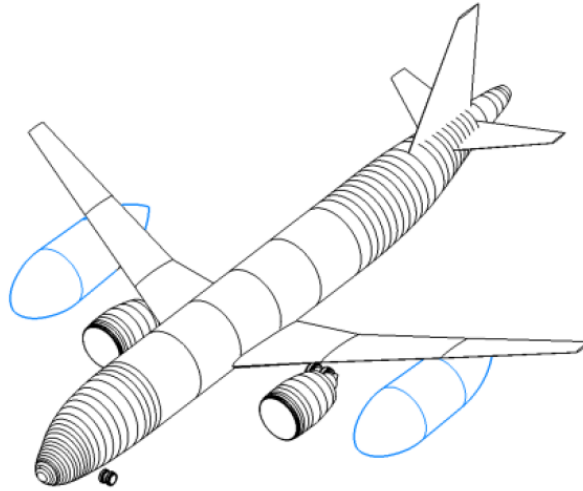


Figure 2.20: Geometry of podded tank concept. Source: [7].

One other minor example is given in the high-altitude reconnaissance aircraft described in subsection 2.1.3 [10], in which part of the fuel is stored in detachable podded tanks under the wings.

2.2. TANK CONCEPTUAL DESIGN

This section reviews the conceptual design methodology for aircraft LH2 tanks. Three studies are selected for review and comparison. The chapter starts by presenting the contexts of these studies, along with the tank requirements. It proceeds with the tank's shape and integration and with the tanks materials choices. The critical aspects of the heat transfer and the pressure fluctuations inside the tanks follow. Finally, η_{grav} , which is the tank main characteristic and the final result of the design, is reported for the three studies.

2.2.1. STUDIES CONTEXTS AND TANK REQUIREMENTS

Because the design choices and the final tank characteristics are dependent on the contexts of the studies and on the design requirements, this section gives an overview of the lasts.

The three studies reviewed in this chapter will be addressed to as **Study 1**, **Study 2** and **Study 3**.

In **Study 1**, an Airbus A320neo is reconfigured with an auxiliary power and propulsion unit (APPU) which can utilise hydrogen to generate a fraction of the aircraft thrust. Therefore, a small tank is designed to contain 400 kg of LH2, for 52.8 hrs without venting [12];

In **Study 2**, a tank design method is applied both to a typical regional airliner and to a long-range transport aircraft. The regional airliner, with a 32 passengers capacity, is designed for a 2100 km range, 9144 m cruise altitude and 0.65 cruise Mach number. The tanks are designed to store the 1150 kg of LH2 which are expected to be required to perform this mission. The long-range transport, with 400 passengers in a single deck layout or 550 passengers in a double-deck arrangement, is designed for 13890 km range. The tanks are designed to store the 40000 kg and 60000 kg respectively. [13];

In **Study 3**, the conversion to LH2 of a conventional medium-range civil transport is used as a realistic scenario to size LH2 tanks. The LH2 converted aircraft, with a 197 passengers capacity, is designed for a 9000 km range. The tanks are designed to store the 17700 kg of LH2 which are expected to be required to perform this mission [14];

2.2.2. TANK SHAPE AND INTEGRATION

Due to the very low energy density of LH2 (see Table 2.6), its cryogenic nature, its storage condition as a saturated liquid and the necessity to prevent it from entering contact with oxygen (O₂), the fuel tanks are unavoidably large and heavy. The feasibility of an LH2 aircraft relies on a successful tank integration,

which adds minimum drag and mass.

Table 2.6: Properties of Jet A-1 fuel (kerosene-based) [22] and hydrogen [23].

Property	Jet A-1	Hydrogen
Boiling point ($^{\circ}C$)	176	-252.7
Melting point ($^{\circ}C$)	-47	-259.2
Density at boiling point (kg/m^3)	804	71
Lower heating value (MJ/Kg) adiabatic	43.15	119.97
Energy density (GJ/m^3) adiabatic	34.7	8.52

One factor which influences the tank mass and the aircraft drag is the tank S/V . Minimising this ratio would minimise both the tank material (minimum tank shell volume) and the amount of heat entering the tank (thus limiting LH2 boil-off). To minimise the S/V , the tank needs to have a quasi-spherical shape and needs to be large. Such a low S/V tank can only be placed aft and/or forward of the passenger cabin. This limits the ability to use less design-disruptive volumes, such as the interior of the wing, the cargo bay or the top of the passenger cabin.

Another factor that influences the tank mass is the choice between integral and non-integral tanks. Non-integral tanks are mounted inside the fuselage and supported by it, so they have to bear only the loads connected to the fuel containment. They are simpler to manufacture and can be essentially placed anywhere on the aircraft. Integral tanks are part of the airframe structure so, on top of the load connected to the fuel containment, they have to carry the fuselage axial, bending and shear loads. They allow better utilization of the available volume inside the fuselage, which leads to a smaller fuselage, and so to lower mass and drag. Additionally, they provide better accessibility for inspection and repairs [18].

In **Study 1**, a single non-integral tank is placed in the aft cargo hold (see Figure 2.21). Its small size and elongated shape lead to a large S/V [12].

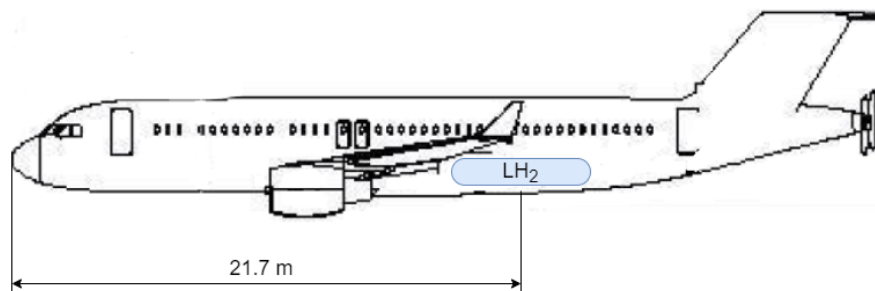


Figure 2.21: Approximate size and location of LH2 tank, **Study 1**. Source: adapted from [12].

In **Study 2**, for the regional airliner, 3 integral tanks layouts are investigated (see Figure 2.22):

- a single large quasi-spherical tank, placed aft of the passenger cabin leads to the lowest S/V .
- a combination of medium-size quasi-spherical tanks, placed both aft and forward of the cabin (without catwalk), lead to low/medium S/V ;
- Several small elongated tanks, placed on top of the cabin, plus one large quasi-spherical tank in the fuselage tail cone lead to a medium/high S/V ;

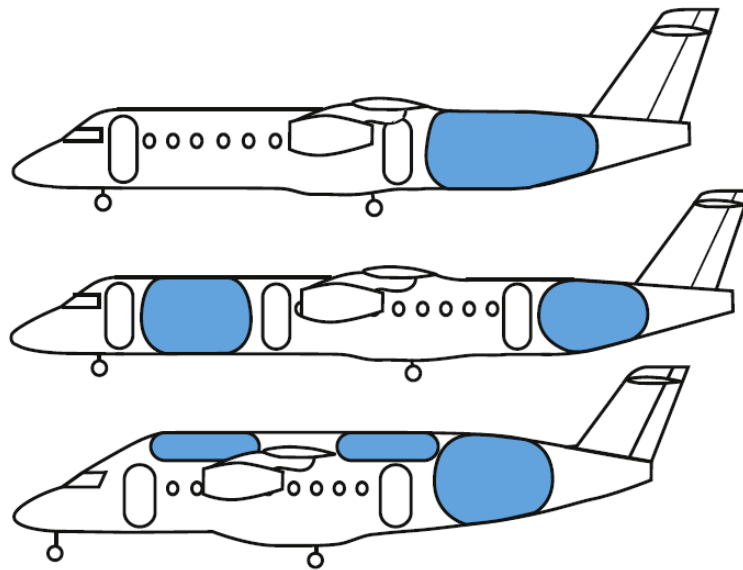


Figure 2.22: The different tank arrangements for the regional airliner, **Study 2**. Source: [13].

For the long-range transport aircraft, the fuel is stored in two integral large quasi-spherical tanks, placed both aft and forward of the cabin (without catwalk), with consequent low S/V . (see Figure 2.23) [13].

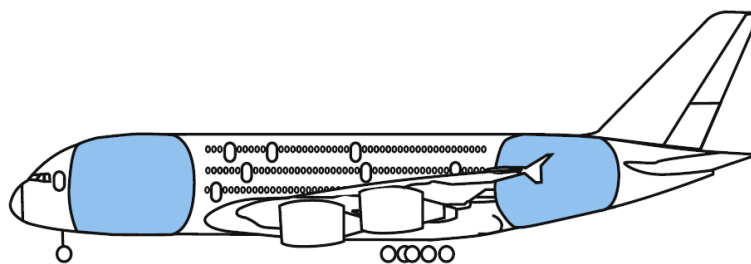


Figure 2.23: Tank arrangement for the long-range transport aircraft, **Study 2**. Source: [13].

In **Study 3**, two integral large quasi-spherical tanks, placed in the aft and forward section of passenger cabin lead to low a S/V (see Figure 2.24 and Figure 2.25). The integration of the LH2 tanks was performed such that changes in the airframe, aerodynamic shape and mass distribution were minimal. This arrangement was deemed to be the most efficient in terms of space utilisation, $c.g$ relocation and structural stiffness [18]. The airframe was redesigned following EASA CS-25 airworthiness regulations [37] and ANSI/AIAA S-080 standards for pressurized structures [14, 38].

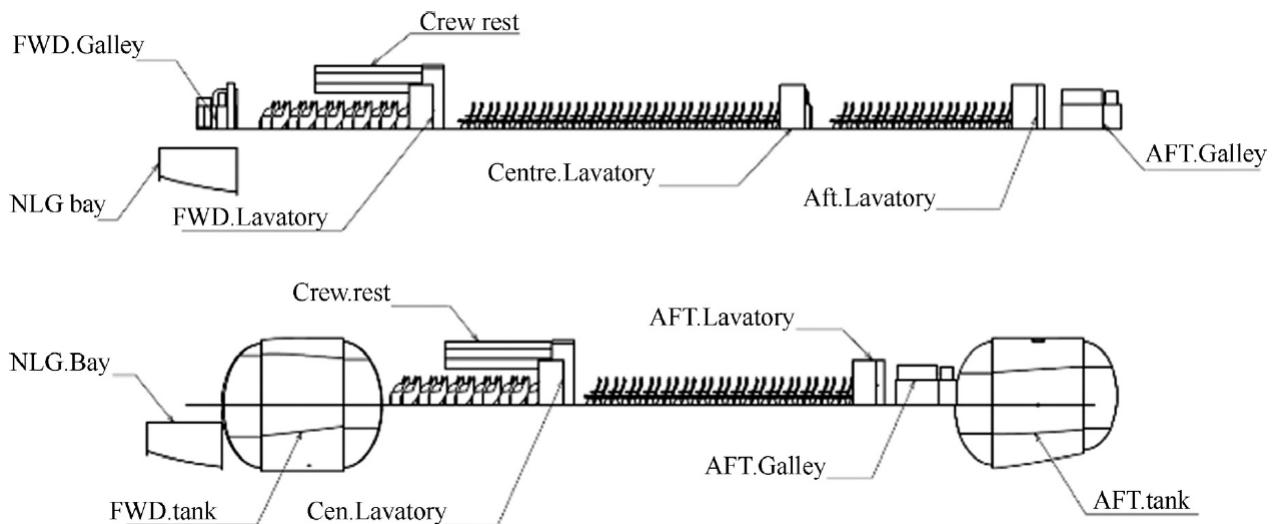


Figure 2.24: Changes in cabin layout, **Study 3**. Source: [14].

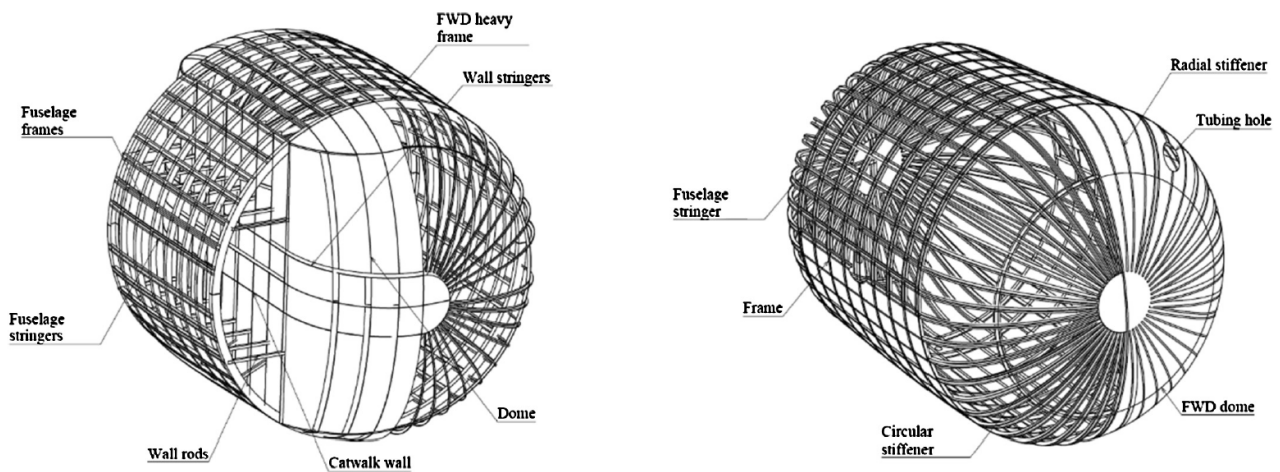


Figure 2.25: Fuel tanks structural arrangement. Forward tank on the left, aft tank on the right, **Study 3**. Source: [14].

2.2.3. TANK MATERIALS

The LH2 tanks have to be pressurised, both to maintain the hydrogen on the saturated liquid line and to prevent the oxygen from entering in contact with the hydrogen. The LH2 tanks have to be also insulated to limit the boil-off rate and thus minimise the pressure increase and/or the venting of the gaseous hydrogen (GH₂).

In subsection 2.2.2 it was mentioned that the feasibility of an LH₂ aircraft relies on a successful tank integration, which adds minimum drag and mass to the aircraft. The material choices for the tank walls and insulation have a direct impact on the tank and fuel mass and must therefore be chosen carefully.

TANK STRUCTURE MATERIALS

The ideal materials to be used for the tank walls need to possess high strength, high fracture toughness, high stiffness, low density and low permeation to H₂ [39]. The conventional material choices are the aluminium alloys [18, 40–42], but composites are also considered because of their low density and high strength. Indeed, the use of composite could achieve a 30% mass reduction and 25% cost savings if com-

pared to current metallic tanks [43] and H_2 permeability is no longer believed to form a technical barrier to the development of an unlined composite tank [44]. Nevertheless, research into composite cryogenic tanks has been done mostly for space launchers applications, where durability and safety is not as essential.

In **Study 1**, Al2219 is chosen for the inner tank wall, and a carbon-epoxy laminate, with twice the amount of fibres in tangential than in longitudinal direction, is chosen for the outer wall. The inner tank wall copes with the cyclic loading due to pressure and temperature, while the outer tank wall keeps the layers intact, protecting them from external loads [12].

In **Study 2**, two different tank structures are designed (see Figure 2.26) to integrate two different types of insulation materials (see Figure 2.2.3 for the insulation materials). Both tank structures use an aluminium alloy with ultimate stress of 234 MPa and limit stress of 172 MPa for the inner tank wall and a composite fairing for the outer tank wall, which serves as aircraft skin too. The structure using foam as insulator adopts a layer of purged open cell foam on top of the insulation layer, to accommodate dimensional changes and support the composite fairing. A vapour barrier is also added around the insulation layer and the open cell foam layer. The structure using multi-layer insulation (MLI) as the primary insulator adopts an aluminium honeycomb with two aluminium face sheets in place of the open-cell foam so that the vacuum required by the MLI can be maintained. A vapor barrier is added around an inner closed-cell foam insulation layer [13].

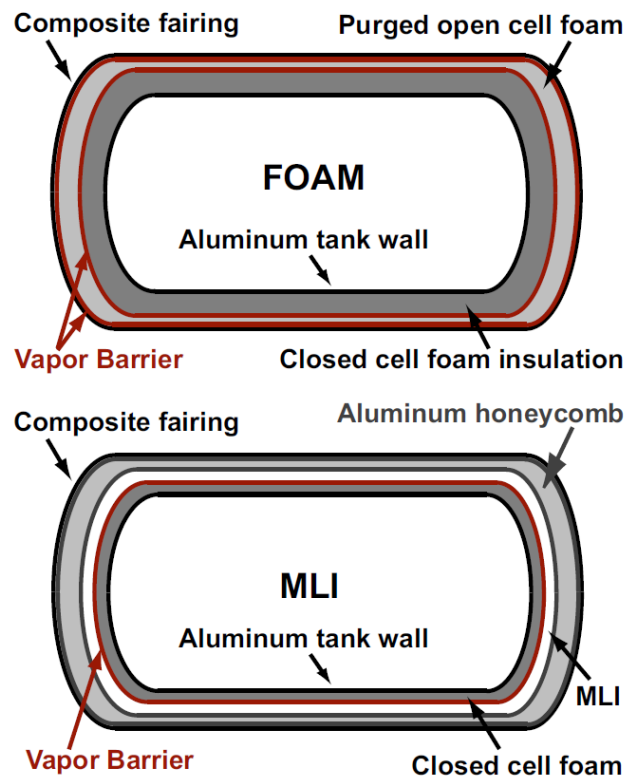


Figure 2.26: Adopted tank structure for both insulation options, **Study 2**. Source: [13].

In **Study 3**, Aluminum 2219-T87 is used for the tank skin, while the stronger Aluminum 7075-T6 is used in the structural members such as stingers and frames. Aluminum 7075-T6 is also employed in the walls of the catwalk to sustain the higher hoop stresses in this region. Ti-6Al-4V alloy is used for the stiffeners, the vertical frames and the diagonal rods located in the catwalk, which are subjected to very high hoop stresses [14].

TANK INSULATION MATERIALS

The ideal insulation materials for aeronautical applications possess low thermal conductivity, low thermal diffusivity and low mass density [39]. These characteristics are possessed by aerogels, MLI and polymer foams [39, 40]. It must be mentioned, however, that the mass fraction of the insulation layer to the empty LH2 tank mass is usually minimal [12] and, for a given allowed boil-off rate, the insulation layer thickness is the parameter that mostly affects the final drag and mass penalty from the LH2 tank.

Aerogels are gels comprised of a microporous solid in which the dispersed phase is a gas [45]. They have the lowest thermal conductivity, but they are fragile and brittle due to their high porosity [39, 40].

MLI consist of a number of alternating layers of low conductivity spacers and low emissivity foils. The heat transfer by gas conduction is minimised by operating at vacuum levels below 13 *mPa* [39]. The spacers are usually made of polyester, glass fibre paper or silk and the radiation shields are made of aluminized or goldized Mylar [46, 47]. MLI performances are exceptionally good, but they rely on the low vacuum levels and this poses a safety risk in case the vacuum is lost.

Flexible polymer foams have very low density and, being thermoformable, are easy to apply to complex shapes. Their downside is the higher thermal conductivity compared to aerogels and MLI. Rigid polymer foams have good resistance to thermal cycling and, to some degree, are thermoformable.

In **Study 1**, the insulation consists of a 15.5 *mm* thick MLI system surrounded by two 5 *mm* layers of Aero-gel (see subsection 2.2.4 for sizing procedure).

In **Study 2**, three insulation systems are considered. One uses Rohacell closed-cell polymethacrylimide (rigid) foam, one polyurethane (rigid) foam and one DAM/Tissuglass MLI [13]. The first two systems and the third system use respectively the first and the second tank structures described in subsection 2.2.3. Note that a small inner layer of closed-cell foam insulation is added to the MLI system to prevent air liquefaction upon vacuum failure [13].

In **Study 3**, the insulation system consist of a 15 *mm* thick (see subsection 2.2.4 for sizing procedure) inner wetted thermal insulation (IWTI), an insulation foam based on polyurethane with metallic liners developed for cryogenic LH2 conditions [14].

2.2.4. HEAT TRANSFER AND PRESSURE FLUCTUATIONS INSIDE TANK

The design of an LH2 aircraft tank requires a trade-off between thermal and mechanical requirements. The hydrogen boil-off due to heat entering the tank together with its consumption in the engines causes continuous pressure variations inside the tank. For an inelastic tank, when the first law of thermodynamics and conservation of mass are applied to a control volume that contains a liquid-vapour mixture and under the assumption of a homogeneous state for the mixture, the pressure fluctuation is expressed by Equation 2.1 [19, 48].

$$\frac{dp}{dt} = \frac{\phi}{V} \left[\dot{Q} - \dot{m}_{out} \cdot h_{lg} \cdot \left(x + \frac{\rho_g}{\rho_l - \rho_g} \right) \right], \quad (2.1)$$

where V is the tank volume, x is the quality of the fuel leaving the tank through the fuel lines ($x = 0$ for a saturated liquid and $x = 1$ for a saturated vapor⁹), \dot{Q} is the heat flow rate through the tank, \dot{m}_{out} is the mass flow leaving the tank, h_{lg} is the heat of vaporization at the tank pressure, ρ_g and ρ_l are the density of respectively the gas and the liquid phases and ϕ is the energy derivative, expressed by Equation 2.2.

$$\phi = \rho \left(\frac{\partial u}{\partial p} \right)_\rho \quad (2.2)$$

The energy derivative in function of pressure and density is given in Figure 2.27 for para-hydrogen. The difference with normal hydrogen is less than 1% [13].

⁹ **Study 1**, **Study 2** and **Study 3** fuel lines all remove the hydrogen from the tank in the liquid state, so in Equation 2.1 $x = 0$.

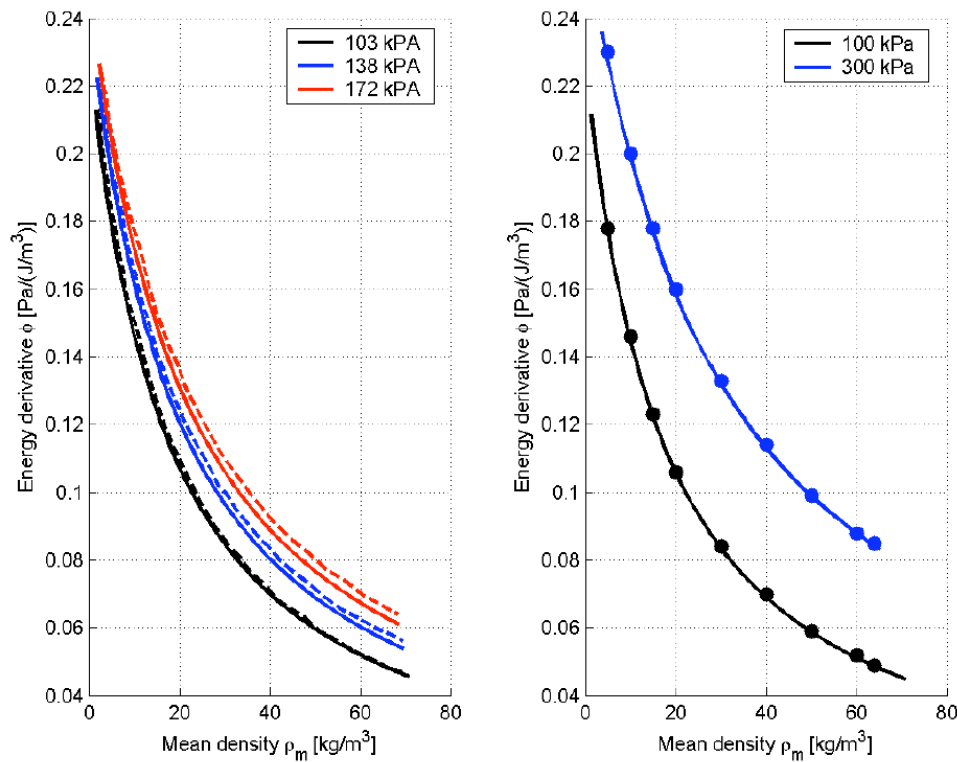


Figure 2.27: The energy derivative in function of pressure and density for para-hydrogen. Source: [15].

Potentially, there are three ways to address this internal pressure fluctuation:

- The tank could be kept at constant gauge pressure. This option would make the tank walls lighter and would effectively remove the need for quasi-spherical shapes, but when climbing the pressure would drop, the boiling point would decrease and the boil-off rate would be higher. Moreover, when descending, the pressure would increase and oxygen-rich air could enter the tank, creating an explosive mixture.
- The tank could be kept at constant absolute pressure. By choosing a pressure just above the atmospheric pressure at sea level, the tank structure would be light and the oxygen would be prevented from entering. The downside is that the hydrogen would be constantly required to either be vented or heated.
- The tank pressure could be allowed to fluctuate during flight between a minimum (fill in) and a maximum (venting) pressure (P_{vent}). This results in a heavier tank, but can drastically reduce, if not eliminate, the need for hydrogen venting.

Study 1, Study 2 and **Study 3** all allow the tank pressure to fluctuate (3rd option).

In **Study 1**, the fill in pressure is 172 kPa and P_{vent} is 300 kPa [12].

In **Study 2**, the fill in pressure is 120 kPa. A range of P_{vent} between 150 kPa and 300 kPa is analysed. [13].

In **Study 3**, the fill-in pressure is not stated and P_{vent} is set to 172 kPa. The pressure increments due to hydrogen boil-off during the flight are computed to be 20.3 kPa for the forward tank and 18.4 kPa for the aft tank. Moreover, pressure increments due to aircraft accelerations were estimated to reach a maximum of 44 kPa for the forward tank and 43 kPa for the aft tank [14].

Once the maximum and minimum pressures are defined, Equation 2.1 can be used to compute the maximum allowed heat flow rate \dot{Q} , and, with it, the insulation layers can be sized.

To compute the heat flow through the tank in relation to the insulation systems, **Study 1, Study 2** and **Study 3** all use a one-dimensional heat transfer approach.

In **Study 1**, the heat transfer is obtained by modelling the transfer through conduction and by applying a 10% increase to somewhat account for heat transfer through radiation (convective heat transfer is neglected). Moreover, the end caps are assumed to be spherical and the thermal resistance of the structural element is neglected. The insulation is designed such that no hydrogen venting is required for 52.8 *hrs*, at an ambient temperature of 45 ° and with $\dot{m}_{out} = 0$ [12].

In **Study 2**, the electrical resistance analogy with three resistances in series is used. This method is described in [15, 49]. For the first resistance, representing the heat transfer from the ambient to the fuselage, a correlation for forced convection over a flat plate is adopted and an equivalent convective heat transfer coefficient is used to account for the radiative heat transfer. The second resistance, representing the heat transfer through the tank walls (both structure and insulation layers) is modelled as pure conduction. The third resistance, representing the heat transfer from the tank walls to the hydrogen is modelled for both the liquid and the gaseous phases. For the liquid phase convection, a correlation is used to determine the Nusselt number and an equivalent convective heat transfer coefficient is used to account for the radiative heat transfer. For the gaseous phase convection, the Nusselt number is set to 17 and the radiative transfer is considered negligible. Lastly, a 30% margin is added to the heat flux obtained from the total thermal resistance to account for the additional heat that will flow into the tank through the support, the connections, and the piping. The insulation is designed such that no hydrogen venting is required during the mission [13].

In **Study 3**, a thermal resistance model similar to the one used in **Study 3** is used. The paper does however not mention how the heat transfer between the tank walls and the hydrogen is computed. It is not clear if any venting is allowed but, if there is, it must correspond to a fraction of the 5.2% allowance on the tank volume. It is not stated what value is used for \dot{m}_{out} [14].

2.2.5. TANK MECHANICAL DESIGN

Besides the load resulting from the varying internal pressure, the tank must be designed to sustain inertial load (accelerations) and, in case of integral tanks, external loads (fuselage bending etc.). A tank structure capable of sustaining the most critical combinations of these loads can then be sized using an analytical method, an empirical method, a computational method or a combination of them.

In **Study 1**, the tank is non-integral and the external loads due to accelerations of the fuel tank are carried by a support structure. This support structure translates to the tank the external loads via normal and shear stress over large contact areas. This structure, which is not part of the airframe, attaches to the airframe in six points. It must be noted that this support structure does not appear to have been sized and accounted for in the mass budget of the tank. The pressure loads, which are the ones that drive the design of the tank walls, are addressed analytically and verified with CATIA. For the inner tank wall, designed to sustain the cyclic pressure loads, a minimum required (and producible) thickness of 3 *mm* is found. For the outer wall, which besides having a fairing function bears a pressure difference of 130 *kPa* a thickness of 2 *mm* is used [12].

In **Study 2**, the tank is integral, so it is designed to resist not only the loads due to the internal tank pressure but also the one connected to the aircraft accelerations, fuel sloshing and fuselage bending. This study does not execute an independent assessment of these loads and their effect on the tank, but performs a simple pressure vessel calculation and correlates the tank wall mass to the available data from studies with similar tank operating conditions, obtained with finite element analyses [18].

In **Study 3**, the tanks are integral. They use the semi-monocoque fuselage structure for the sides and semi-elliptical domes as end caps. Both tank structures are stiffened with stringers and frames (see Figure 2.25). Located on one side of the forward tank, a vertical wall provides a boundary between the pressurized area and the catwalk. The catwalk wall is stiffened with vertical frames and longitudinal stringers. Moreover, horizontal rods are used to transfer pressure loads from the catwalk wall into the fuselage airframe. The

critical loading cases were estimated following the CS-25 airworthiness regulations and using the most critical forward and aft *c.g.*. For the forward tank, skin thicknesses of 2 mm, 2.5 mm and 5.5 mm are used respectively for the barrel section, the domes and the catwalk. For the aft tank, a skin thickness of 2 mm is used for both the barrel section and the domes.

2.2.6. TANK GRAVIMETRIC INDEX

This section presents the final results from the three studies in terms of the tank masses and η_{grav} . When the information was present in the studies, the mass components of the tank are also mentioned. Also mentioned is P_{vent} , when it is not constant across the tank types.

In **Study 1** the tank mass is 288 kg: 67 kg for the composite outer wall, 30 kg for the insulation layers and 186 kg for the aluminum alloy inner wall. Given that the tank contains 400 kg of fuel, the η_{grav} of this tank is **0.72** [12]. The results are summarised in Table 2.7.

Table 2.7: Results from **Study 1** [12].

Property	Value
Inner wall mass (kg)	186
Outer wall mass (kg)	67
Insulation layers mass (kg)	30
Tank mass (kg)	288
Fuel mass (kg)	400
η_{grav}	0.72

In **Study 2**, for the single aft tank configuration of the regional airliner, the tank η_{grav} are **0.41**, **0.46** and **0.48** for the polyurethane, Rohacell and MLI tanks respectively. These values are obtained by choosing P_{vent} of about 160 kPa, 170 kPa and 150 kPa respectively, which were found to yield the lowest η_{grav} . For the configuration with two equal sized tanks (somewhat addressing the second and third tank configurations in Figure 2.22) only the polyurethane tank was analysed. The η_{grav} of the combined two tanks are **0.52**, **0.53**, **0.62** and **0.87** for tank diameters of 3 m, 2.5 m, 2 m and 1.5 m respectively. These values are obtained by choosing P_{vent} of about 170 kPa, 185 kPa, 215 kPa and 300 kPa respectively, which were found to yield the lowest η_{grav} . For the long-range transport aircraft, instead of calculating the tank mass for the declared aircraft configuration, the tank mass was computed for individual tanks containing 15000 kg, 20000 kg, 25000 kg, 30000 kg and 35000 kg of fuel and having a fixed diameter. The tank η_{grav} associated with these fuel masses is **0.31**, **0.30**, **0.28**, **0.28** and **0.27** respectively. These values are obtained by choosing a P_{vent} of about 185 kPa, which was found to yield the lowest η_{grav} for the design where no additional heating system to heat the hydrogen at the end of the cruise is required [13]. The results are summarised in Table 2.8.

Table 2.8: Results from **Study 2** [13].

Tank Type	m_{fuel} (kg)	m_{tank} (kg)	η_{grav}	P_{vent} (kPa)
Reg. airl., single tank, polyurethane	1150	473	0.41	160
Reg. airl., single tank, Roachell	1150	526	0.46	170
Reg. airl., single tank, MLI	1150	555	0.48	150
Reg. airl., double tank, polyur., 3m diam.	1150	600	0.52	170
Reg. airl., double tank, polyur., 2.5m diam.	1150	512	0.53	185
Reg. airl., double tank, polyur., 2m diam.	1150	708	0.62	215
Reg. airl., double tank, polyur., 1.5m diam.	1150	1000	0.97	300
Long-range airliner	15000	4667	0.31	185
Long-range airliner	20000	6018	0.30	185
Long-range airliner	25000	7083	0.28	185
Long-range airliner	30000	8491	0.28	185
Long-range airliner	35000	9612	0.27	185

In **Study 3** the tank masses are 3144 kg for the forward tank and 1847 kg for the aft tank. Given that the forward and aft tank contain each 50% of the 17700 kg of fuel, their η_{grav} are **0.36** and **0.21** respectively [14]. The results are summarised in Table 2.9.

Table 2.9: Results from **Study 3** [14].

Tank Type	m_{fuel} (kg)	m_{tank} (kg)	η_{grav}
Forward tank	8850	3144	0.36
Aft tank	8850	1847	0.21

It is worth noting how both the size and the shape of the tank lead to significant differences in the η_{grav} (see Table 2.8). This is something to be aware of when selecting the tank layout.

It is also important to critically observe the large differences in η_{grav} obtained between **Study 2** and **Study 3**: the aft tank in **Study 3** has indeed a 50% lower η_{grav} than the smallest tank designed by **Study 2** for the long-range airliner, despite the last having a similar shape and almost double the size.

2.3. EXCURSUS ON RELEVANT HYDROGEN ASPECTS

This section briefly addresses the aspects of hydrogen availability, emission and safety, which, despite not being the focus of this literature study, are considered relevant to complement the researcher's knowledge on the topic.

2.3.1. HYDROGEN AVAILABILITY

The transition to LH2 will have considerable implications for the fuel supply chain, the airport infrastructure, the operations and the entire air travel system [6]. The analysis of these implications is complex and has been already performed in detail [6]. The single parameter that best captures the effects of these implications is the cost of the hydrogen to the airlines. The estimates from [6], reported in Figure 2.28, show that by 2040 the cost of hydrogen energy will be comparable to the kerosene one, as the LHV of hydrogen is 2.8 times the one of kerosene. Figure 2.28 also presents the availability of multiple feasible pathways to hydrogen production and distribution.

Cost overview of three hydrogen supply pathways

USD per kg of H₂ in 2040

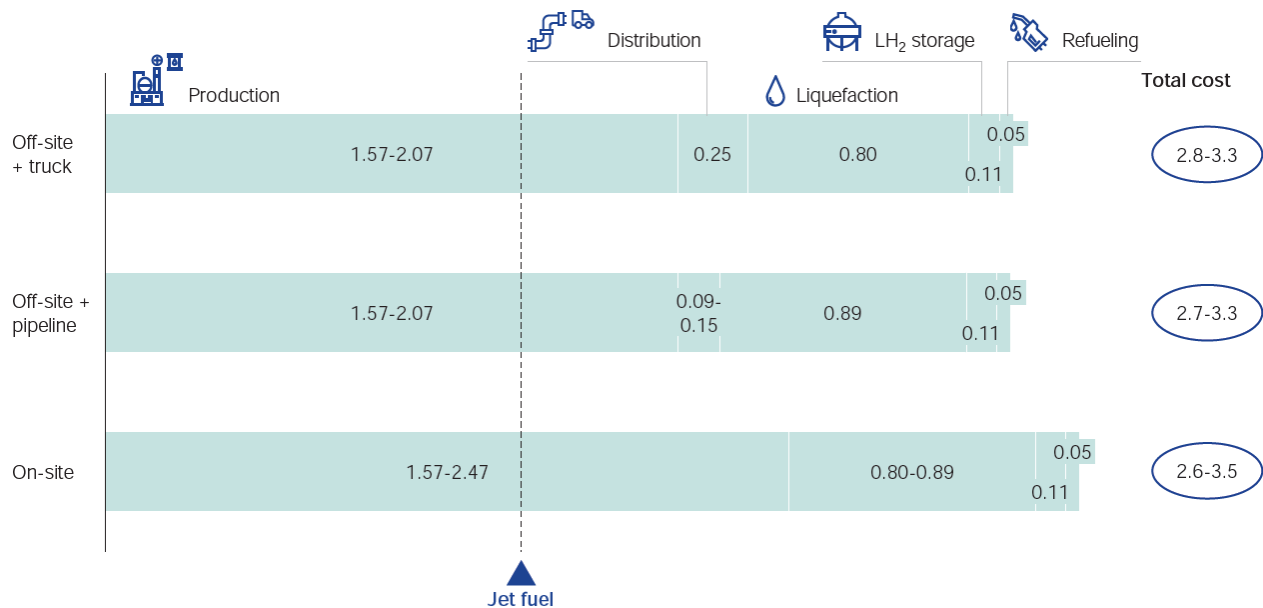


Figure 2.28: Cost overview of three hydrogen supply pathways. Source: adapted from [6].

2.3.2. HYDROGEN-COMBUSTION EMISSIONS

One fundamental aspect to remember when considering the introduction of hydrogen-combustion-powered aircraft is that the emission problem does not end with the elimination of the direct CO₂ emission. This section analyses the effect of the hydrogen-combustion NO_x emission, the increased water vapour emission and the emission-related effects (contrails and cirrus).

NO_x are gases that influence the atmospheric methane and ozone concentrations and are created through chemical reactions at high temperatures during combustion. A trade-off exists, therefore, between the engine thermodynamic efficiency, which benefits from high combustion temperatures, and NO_x production. Both kerosene and H₂ turbine aircraft rely on combustion processes and consequently emit NO_x. Nevertheless, hydrogen's wider flammability limits offer the possibility for leaner combustion, which results in lower flame temperatures (see Figure 2.29) [16]. Moreover, hydrogen's higher burning velocities and diffusivity result in higher reaction rates and in faster mixing, which translates into lower residence time. The combination of lower flame temperature and lower residence time allows to reduce the NO_x emissions by 50-80% compared to the kerosene counterpart [6].

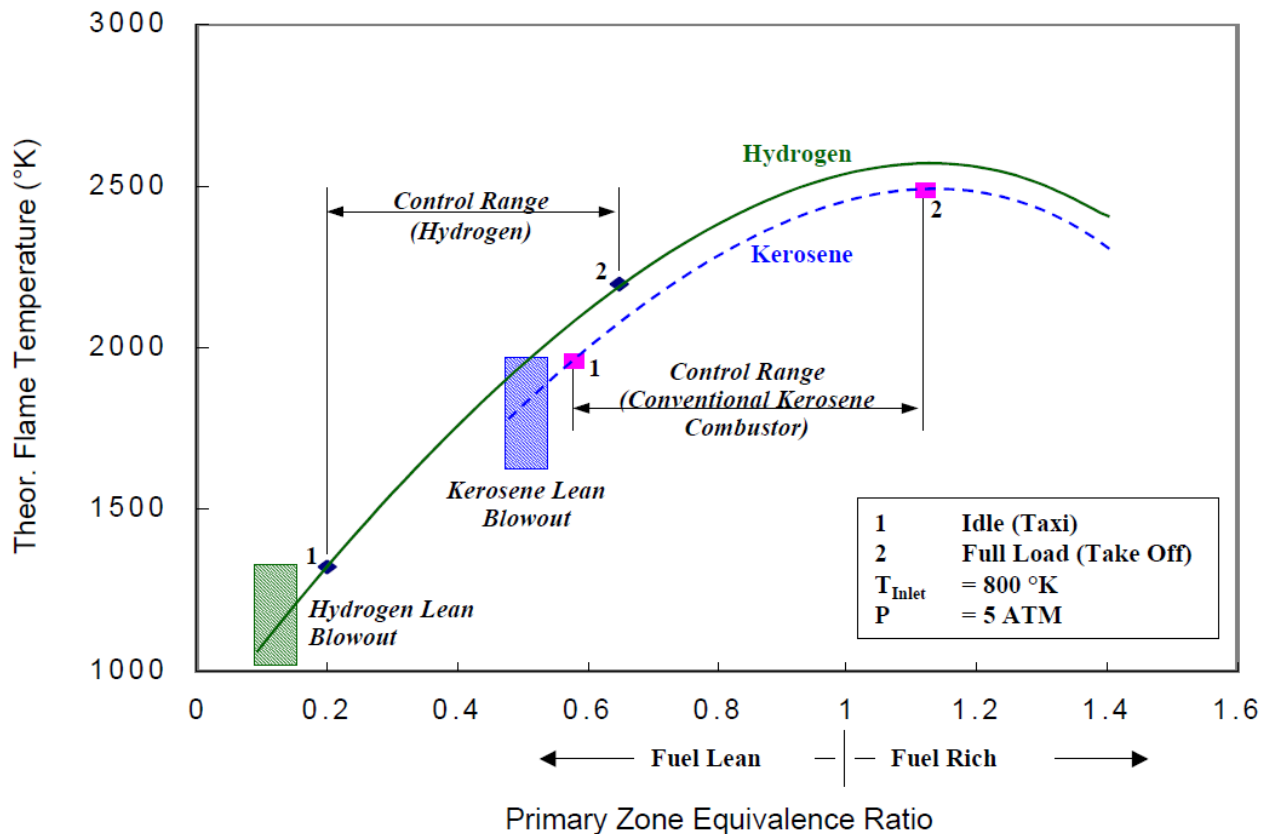


Figure 2.29: Temperature Characteristics of a Combustor. Source: [16].

Water vapour (H_2O) is, by mass and volume, the most abundant greenhouse gas in the atmosphere. When emitted in the stratosphere, H_2O has a relatively long residence time, which almost doubles for each km increase in altitude and translates into a high radiating forcing signal. A considerable amount of subsonic aircraft emissions occurs in the stratosphere. In northern/middle latitudes this fraction can be as large as 80% during winter, while comparatively small during summer, reflecting the variation of the tropopause height. In low latitudes, where the tropopause is high, aircraft flight entirely in the troposphere [50]. For the same energy content, H_2 turbines (and fuel cells), emit 2.55 times more water vapour compared to kerosene combustion, hence it is important to devise a flight strategy that minimises its radiative forcing. The annual, global-mean radiative forcing of 2012-level aviation H_2O emissions has been found to be 0.9 mW/m^2 . By comparison, the best estimate for the radiative forcing of aviation CO_2 emissions is 28 mW/m^2 [51]. The real contribution of H_2O to global warming is, in fact, indirect (contrails and cirrus).

Aircraft-induced clouds (AIC) is a term introduced in [17] to indicate persistent contrails and contrail cirrus. Contrails (condensation trails) are ice clouds generated by jet aircraft cruising in the upper troposphere (8–13 km altitude), where ice-supersaturated atmospheric conditions are present. What makes AIC different from natural cirrus is the aircraft-related formation stage, where turbine engine emissions, modified in the aircraft wake, result in a larger number of smaller ice crystals [52–54] and, consequently, lead to different evolution pathways and radiative effects. AIC are highly transparent to the incoming shortwave radiation from the Sun, reflecting only 23% back into space. They also redirect back to Earth 33% of the emitted outgoing longwave radiation. This results in a net imbalance of 10% during the day, and 33% at night [55]. Contrary to what was until recently thought, AIC represents 55% of the aviation's contribution to global warming, whereas CO_2 constitutes only 39% [17, 55].

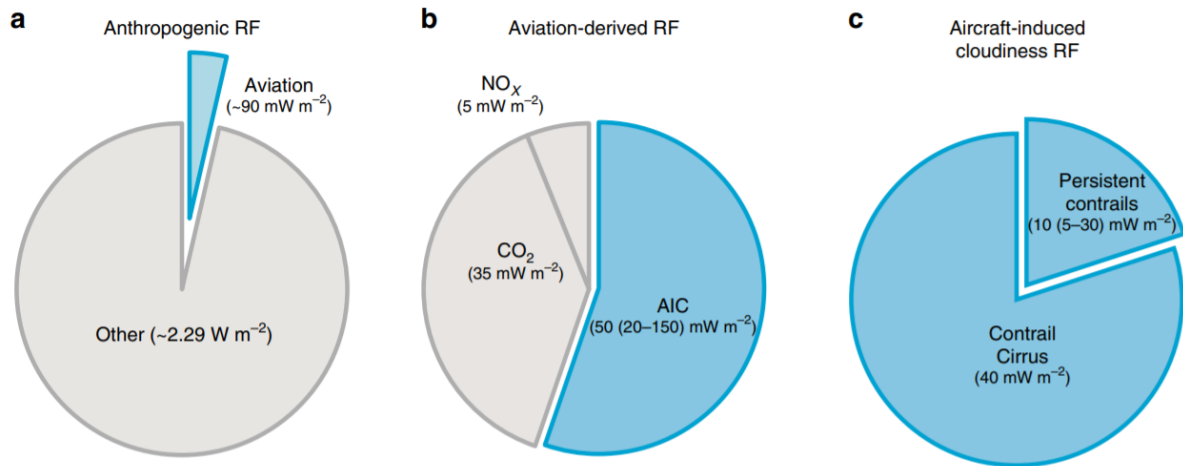


Figure 2.30: Aviation radiative forcing components. **a)** Aviation as a percentage of total global radiative forcing due to human activities in the year 2011. **b)** Forcing components within the aviation fraction. **c)** Breakdown of AIC radiative forcing into contrail cirrus and persistent contrails. Source: adapted from [17].

Despite H_2 turbines emit more water vapour, they emit fewer aerosol particles compared to the kerosene ones. Because of this, cryoplane contrails are characterised by fewer, larger ice crystals, which lower the optical depth of the contrails, rendering a larger portion of them practically invisible [56]. Overall, a contrails-related climate impact reduction between 16% and 29% in terms of radiative forcing can be achieved, according to the 2015-2050 transition scenarios from Ponater et al. [57].

2.3.3. HYDROGEN SAFETY

Investigations on the safety concerns regarding the handling and air transport of LH2 found that the hydrogen aircraft are not more dangerous than the kerosene ones, and even safer in some aspects [58, 59]. The potential hazards connected to the use of LH2 as aircraft fuel were also analysed and described by Sefain [60], who concluded that as hydrogen can cause an accident only if released and ignited, the effort should be especially placed in preventing uncontrolled hydrogen release and in removing potential sources of ignition.

METHODOLOGY

In this research, an existing aircraft conceptual design tool has been modified to make it capable of working with liquid hydrogen aircraft. This chapter first briefly describes the chosen tool functioning and capabilities, then presents how it was adapted to work with LH2 aircraft and lastly shows its validation.

3.1. SELECTED AIRCRAFT DESIGN TOOL: THE INITIATOR

The analysis tool that has been modified and employed for this research is the Initiator. The Initiator is an Automated Synthesis Program for CS-25 Aircraft that is under continuous development at the Flight Performance and Propulsion section of the Delft University of Technology Aerospace Engineering Faculty. Since its creation in 2012 by Elmendorp et al. [61] the Initiator has been continuously improved and expanded. Well-grounded works, such as "Conceptual Design and Evaluation of Blended-Wing Body Aircraft" by M. Brown and Vos [62] and "Conceptual Assessment of Hybrid Electric Aircraft with Distributed Propulsion and Boosted Turbofans" by Hoogreef et al. [63] testify to the high level of flexibility and reliability of the Initiator. The tool consists of a series of disciplinary analysis and sizing modules combined in a framework. These modules are continuously updated and improved to enhance the reliability of the results and the flexibility in the design. The modules are divided into three categories based on their functions:

- The sizing modules start from a set of top-level requirements and perform a preliminary sizing of the aircraft. They provide an initial estimation of the aircraft geometry, weights, propulsion and performance. Examples of these modules are the "Class1WeightEstimation", the "WingThrustLoading" and the "GeometryEstimation" modules.
- The Analysis modules analyse the aircraft generated by the sizing modules. Examples of these modules are the "Class2WeightEstimation", the "PerformanceEstimation", the "CleanCLmax", the "EngineModel", the "FuselageWeightEstimation" and the "MissionAnalysis" modules.
- The design modules add to or change the aircraft design. Examples of these modules are the "CabinDesign", the "ControlAllocation", the "PositionLandingGear" and the "StabilizingSurfaceSizing" modules.

The Initiator process follows three main, partially nested, convergence loops (see Figure 3.1):

- In the first convergence loop reference aircraft data and the fuel-fraction method are combined to provide a Class 1 estimate of the maximum take-off mass (MTOM). Subsequently, from the combination of a user-specified set of top-level aircraft requirements (TLARs) and performance requirements deriving from regulations (FAR/CS 25), the required thrust (or power in case of propeller aircraft) and wing size are computed. In the next step, the geometry of the aircraft is generated, using empirical sizing rules and user-specified input on the aircraft configuration. Based on this geometry, the aircraft systems masses and the aerodynamic properties are estimated (Class 2). The engine is also sized, and the newly obtained specific fuel consumption, together with the system masses and the aircraft aerodynamic properties are fed back to the start of the loop until their differences with the previous iteration values fall below a certain threshold.
- In the second loop, a more accurate mission analysis module, which is sensitive to changes in the centre of gravity and uses the trimmed drag polar replaces the fuel-fraction method. Moreover, the off-design engine performances are used to account for the effect that speed and altitude have on specific fuel consumption. In this loop, the horizontal tail is no longer sized according to empirical

tail volume coefficients, but using an X-plot method that uses requirements on stability and control. This more refined analysis impacts the fuel weight estimation and consequently the result of the Class 2 weight estimations.

- The final loop comprises the entire second loop but replaces the empirical wing mass estimation with a more refined EMWET (Elham Modified Weight Estimation Technique) [64] or FEM sizing. This analysis depends on the output of the aerodynamic analysis and on an estimate of the masses distribution. The convergence of this third loop completes the design process.

Class 1 Weight Estimation	<i>MTOM</i>	<i>MTOM</i>	<i>MTOM, FF</i>					
	Wing Thrust Loading	<i>W/S, T/W</i>			<i>T/W</i>			
		Geometry Modules	Geometry	Geometry			Wing Geometry	Fuselage Geometry
<i>OEM</i>			Class 2 Weight Estimation	<i>MTOM, FM, OEM</i>	<i>MTOM</i>	Range		
<i>L/D, C_{Dmin}, C_{Lmin}</i>	Polar	Polar		Aerodynamic Modules		Polar	Loading	Loading
<i>SFC</i>					Engine Model	<i>SFC</i>		
	<i>MTOM</i>	<u>Tank Dimensions</u>	<i>MTOM, FF</i> <u>Tank Mass</u>			Mission Analysis		
			Wing Mass				Class 2.5 Wing Weight Estimation	
			Fuselage Mass					Class 2.5 Fuselage Weight Estimation

Figure 3.1: N² chart of the Initiator. In red, and underlined, the addition of the Author for the design of LH2 aircraft. First loop in orange, second loop in blue, third loop in green.

The choice of using the Initiator lays in the accessibility to the software, in the confidence in its adequacy to provide reliable relative performance data, and in the ease with which modification can be implemented.

3.2. ADAPTATION OF THE AIRCRAFT DESIGN TOOL

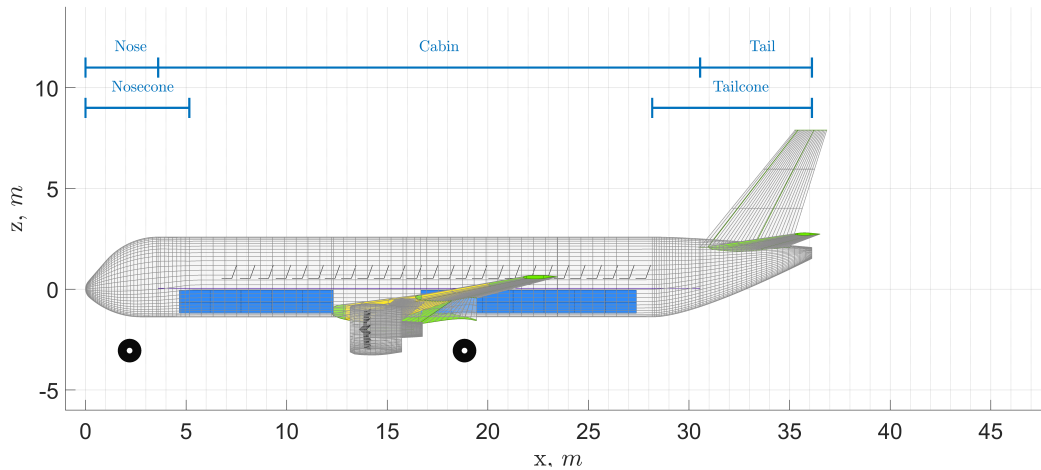
This section presents the modifications of the Initiator modules which are affected by the change in fuel type.

3.2.1. FUSELAGE ADAPTATION TO TANK INTEGRATION

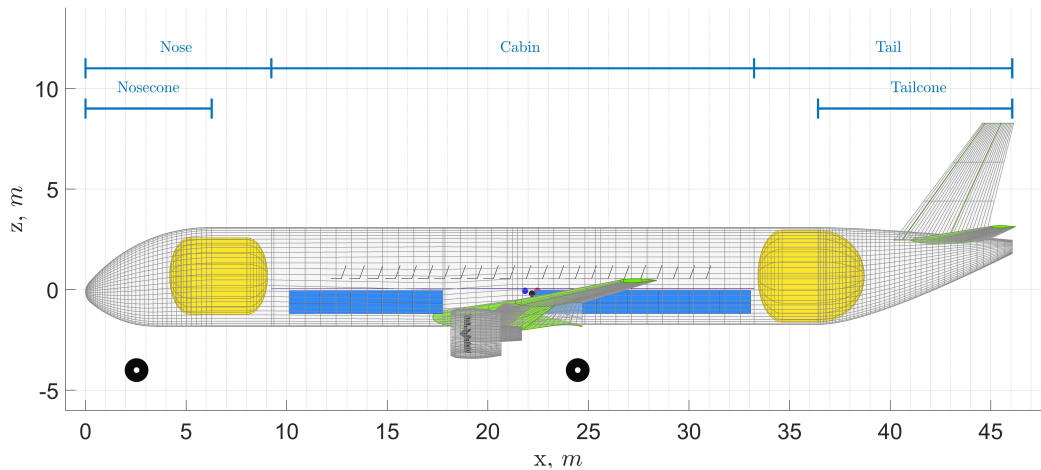
In this research, two fuselage tank layout options have been analysed. The first option consists in placing a single, large-diameter tank aft of the passenger cabin. The second option consists in using a combination of two smaller tanks: a large-diameter one placed aft of the passenger cabin and carrying most of the fuel, and a small-diameter one placed forward of the passenger cabin, which carries enough fuel to retain the small c.g. range typical of kerosene aircraft and which preserves the cabin-cockpit connection, being it laterally shifted to the fuselage centerline to create a 70 cm wide corridor.

The fuselage is modelled in the Initiator using three section compartments, namely the cabin, the nose and the tail. The nose and the tail, whose length is made proportional to the maximum fuselage radius in the kerosene aircraft, are extended in the LH2 version, to accommodate the fuel tanks. Instead, the nosecone and tailcone length, due to their aerodynamic-driven design, remain functions of the maximum fuselage radius (see Figure 3.2). The fuselage is sized with an inside-out approach. First, to be determined

are outer dimensions of the cabin section (which are circular), using the number of passengers, seating configuration, classes distribution and an airframe thickness allowance. Then the nose and tail sections lengths are computed, using the maximum cabin section radius and the tank dimensions (estimates for the first iteration). For the nose section, l_{tank} , plus an allowance, is directly added to the length proportional to the maximum cabin section radius, so that the same cockpit length available to the kerosene aircraft is maintained. The length of the tail section is, instead, the maximum between two options: l_{tank} , plus an allowance, plus the length proportional to the maximum cabin section radius, and l_{tank} , plus an allowance, minus the tank aft cap length plus the tailcone length (see Figure 3.2). This way, the tank fit is ensured and at least the same tail length available to the kerosene aircraft for the allocation of the Auxiliary Power Unit and the empennage structure is maintained.



(a) Kerosene aircraft.



(b) LH2 aircraft.

Figure 3.2: Fuselage sections and location of LH2 tanks. Fuel tanks in yellow.

The fuselage structure mass is currently¹ obtained for both the kerosene and the LH2 aircraft versions using a Class 2 estimation from Torenbeek (Equation 3.1 here, Equation 8-16 in Torenbeek [65]).

¹For this research, the Class 2.5 wing mass estimation is not used.

$$m_{fus} = k_{wf} \cdot \sqrt{V_D \cdot \frac{l_t}{b_f + h_f}} \cdot S_G^{1.2} \quad (3.1)$$

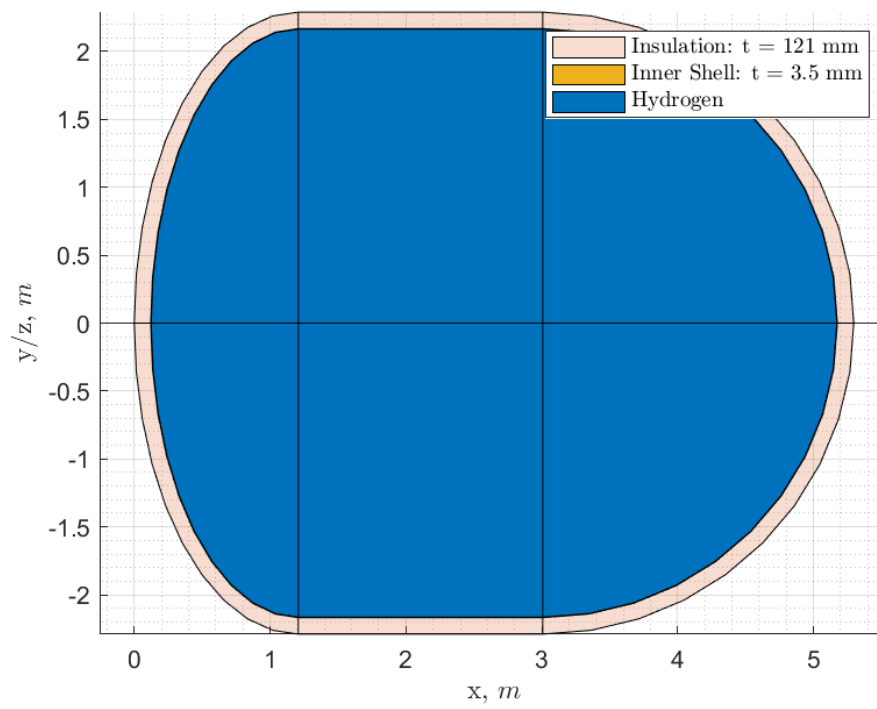
According to Equation 3.1, the fuselage structure mass (m_{fus}) is equal to a constant of proportionality equal to 0.23 (k_{wf}), multiplied by the square root of the dive speed (V_D) times the ratio between the wing root quarter-chord to horizontal tail distance (l_t) and the sum of the maximum width of the fuselage (b_f) and the maximum height of the fuselage (h_f), multiplied by the entire outer surface of the fuselage (S_G) to the power of 1.2. To m_{fus} , a further 8% is added for pressurised cabins, 4% for fuselage-mounted engines, 7% if the main landing gear is fuselage mounted and 10% for freighter aircraft.

3.2.2. TANK SIZING

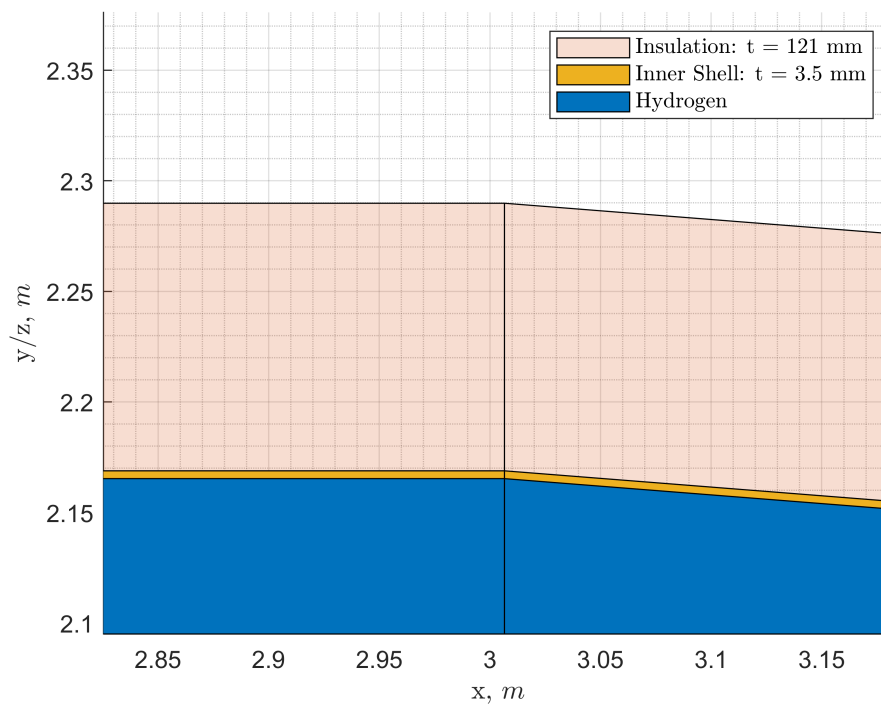
The main addition to the Initiator is the LH2 tank sizing module. This module is run at the end of each mission analysis iteration, with the last providing the total required fuel mass, the fuel consumption profile and the aircraft altitude in every segment of the extended mission (design mission plus diversion). The output of the module is the tank mass, including the tank support system, and the tank geometry.

OPTIONS

The tank is modelled as an inner structural shell externally covered by a uniform layer of insulating material (see Figure 3.3). Concerning the tank structure, the options to choose between integral and non-integral tank is available (see Figure 3.4). For the non-integral tank, the option to choose between a spherical or non-spherical (cylindrical section closed by end caps) tank is also present. Concerning the tank layout, the option to choose between a single aft tank and a combination of forward and aft tanks is available. In the latter case, the forward tank is always non-integral.

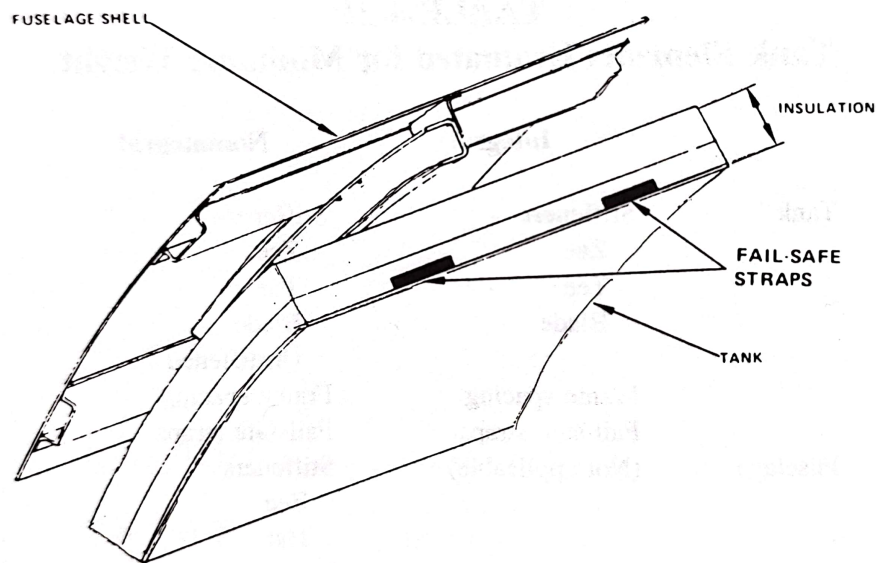


(a) Side/top view.

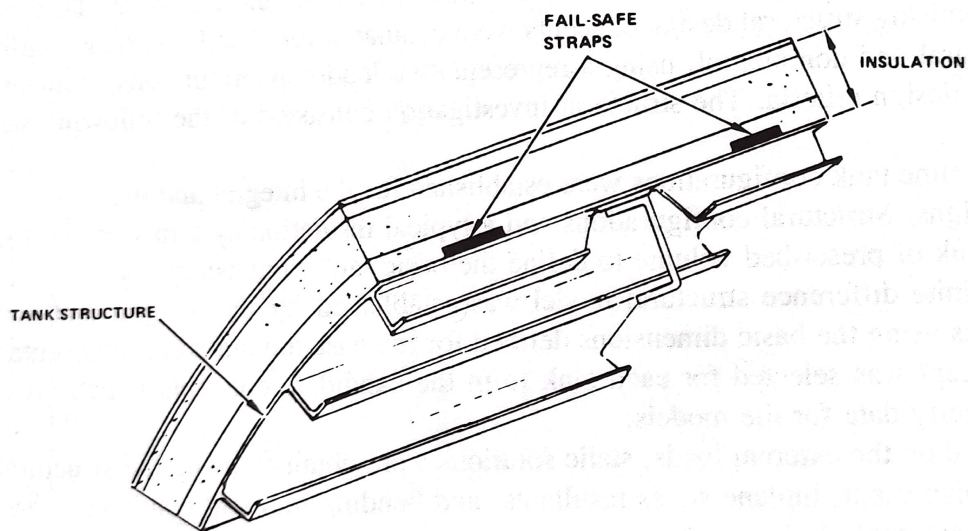


(b) Detail of inner shell and insulation.

Figure 3.3: Tank cross section example.



(a) Non-integral tank.



(b) Integral tank.

Figure 3.4: Illustration of tank structure options. Source: [18].

The tank module combines a structural and a thermodynamic model in an iterative process to determine the tank mass and dimensions. The process for the non-spherical tank is illustrated in Figure 3.5. For the spherical tank, the outer loop seen in Figure 3.5 disappears, the tank diameter becomes an output of the tank sizing module and, when this exceeds the internal fuselage diameter, the last is increased by modifying the cabin seating configuration at the next cabin design iteration (see Figure 3.6).

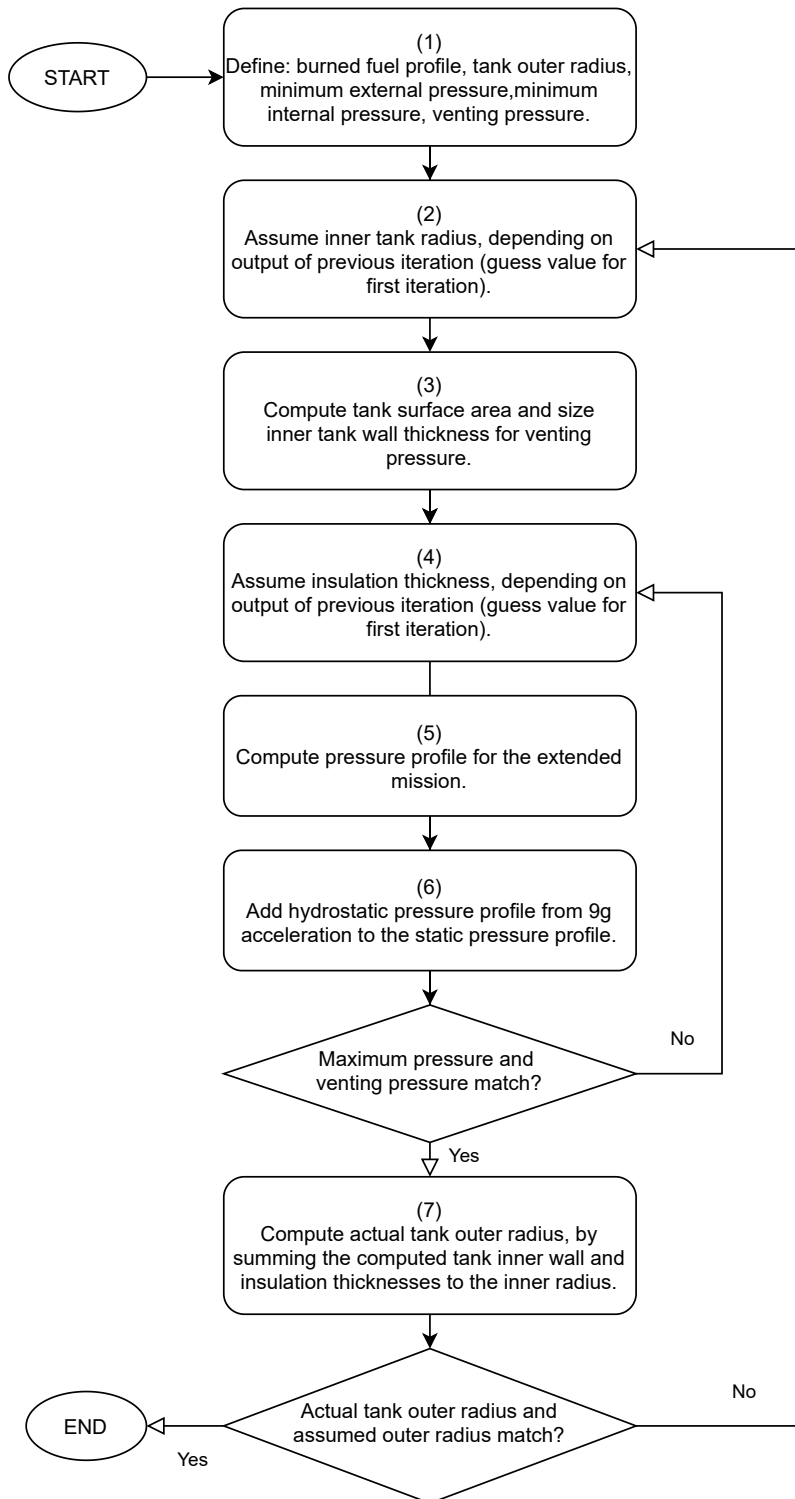


Figure 3.5: Flow chart of tank sizing process for non-spherical tanks.

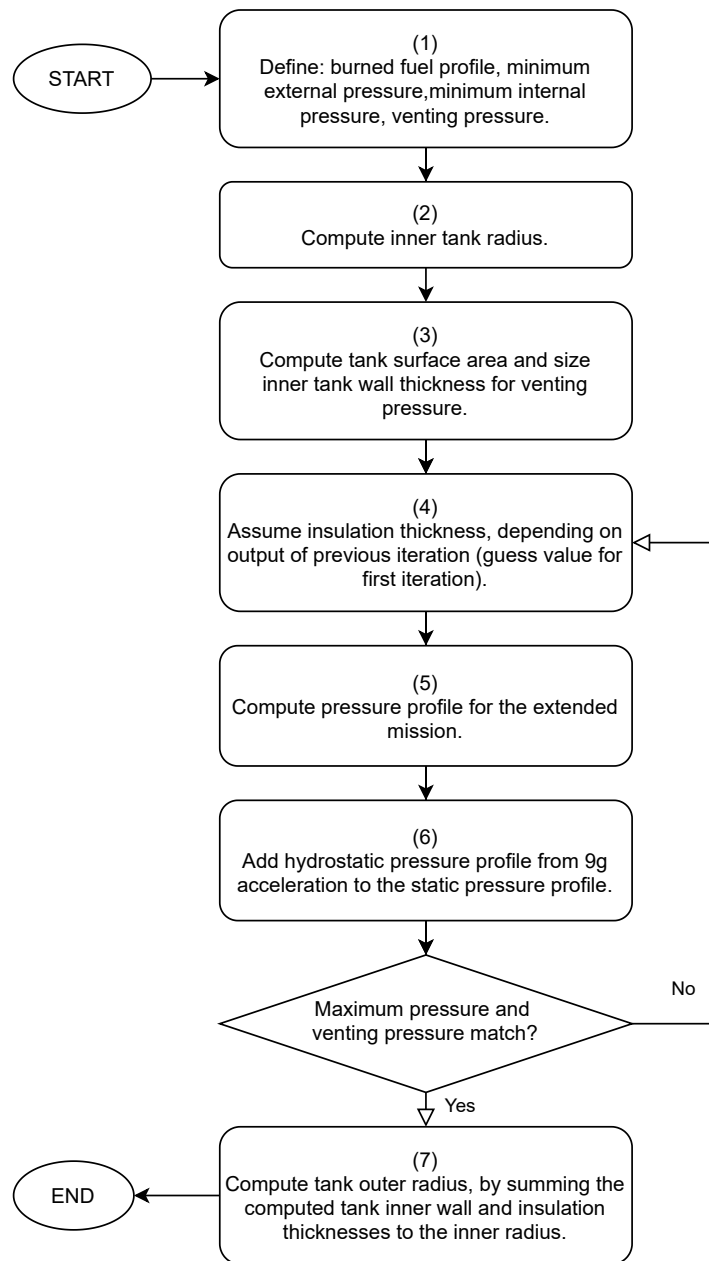
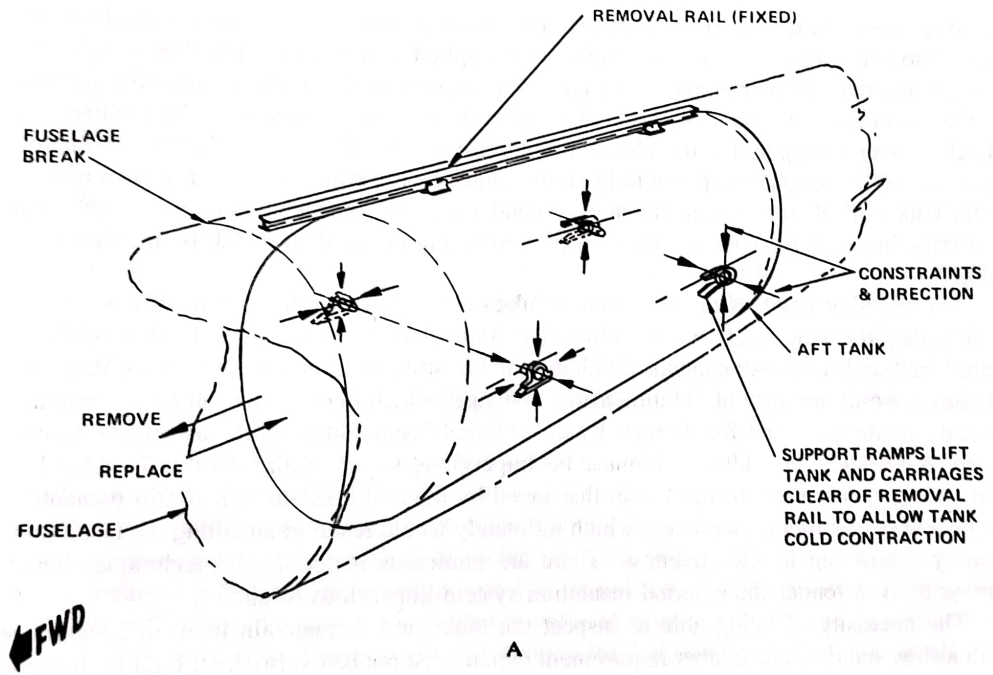
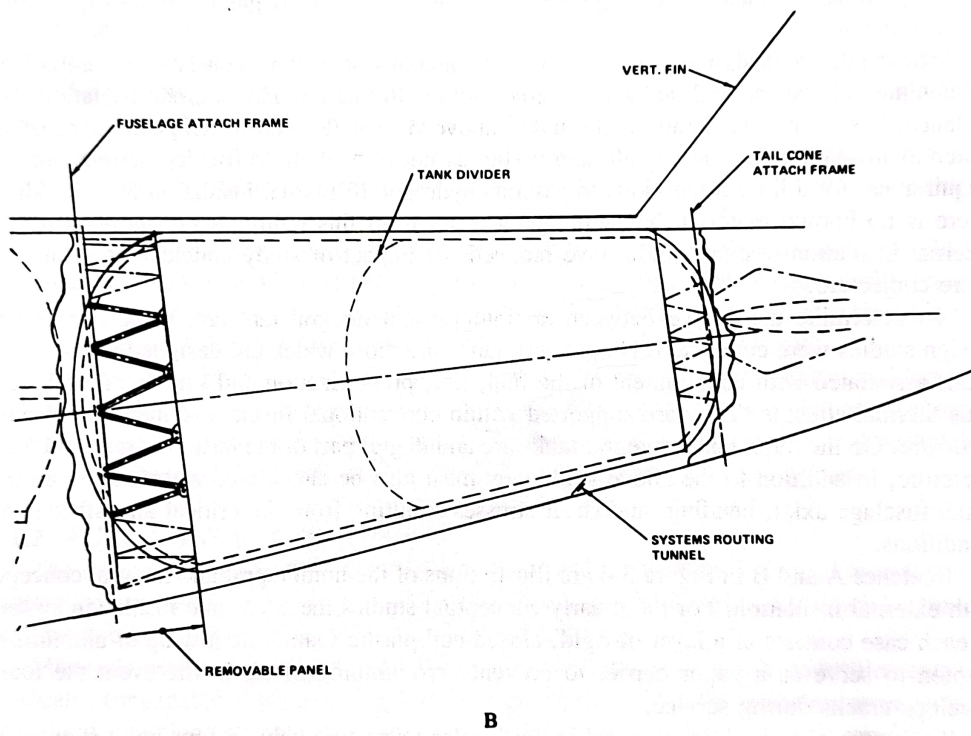


Figure 3.6: Flow chart of tank sizing process for spherical tanks.



(a) Non-integral tank.



(b) Integral tank.

Figure 3.7: Tank attachments to the fuselage structure. Source: [18].

STRUCTURE

In case a non-integral tank option is selected, a four-point tank support system connects the tank to the fuselage (see Figure 3.4a). This mounting solution, presented in Brewer's book Hydrogen Aircraft Technology [18], allows for thermal contraction and expansion and prevents the fuselage deflections from affecting the tank. Also for the non-integral tank option, the outer tank radius is set equal to 93.4% of the external fuselage radius (less in the case of a forward tank) to provide space for the fuselage structure and system routing. This value represents the cabin radius to the outer fuselage radius of the A320-200. In case the integral tank option is selected, a stiffened tank structure replaces the fuselage section at the tank location. Truss structures connect the tank to the fuselage section forward and aft of it. A protective fairing is placed on top of the insulation and equipment and system routing tunnels are added on top of it (see Figure 3.4a). With the integral tank option, the outer tank radius is set equal to the fuselage external radius. For both tank options the structural shell, which resists the pressure load only, is sized using Equation 3.2 (Barlow's formula).

$$t_{shell} = \frac{(P_{vent} - P_{amb}) \cdot r_{shell}}{\sigma \cdot e_w} \quad (3.2)$$

According to Equation 3.2 the structural shell thickness (t_{shell}) is equal to the difference between the venting pressure (P_{vent}) and the external tank pressure (P_{amb}), multiplied by the the tank structural shell radius (r_{shell}), divided by the allowable stress (σ) and a safety factor (e_w) equal to 0.8. For the non-integral tank, P_{amb} is set equal to the cabin pressure at minimum cabin altitude (2400 m), whereas for the integral tank it is set equal to the atmospheric pressure at the maximum flight altitude encountered in the flight profile. A value of 172 MPa is used for σ , as this represents the allowable stress for 2019-T851 aluminium alloy ($\rho_{al} = 2840 \text{ kg/m}^3$) at -252° , for 40000 cycles and with a fatigue quality index of 5 (see Figure 3.8)[18] (this value was also used by Verstraete et al. [13]).

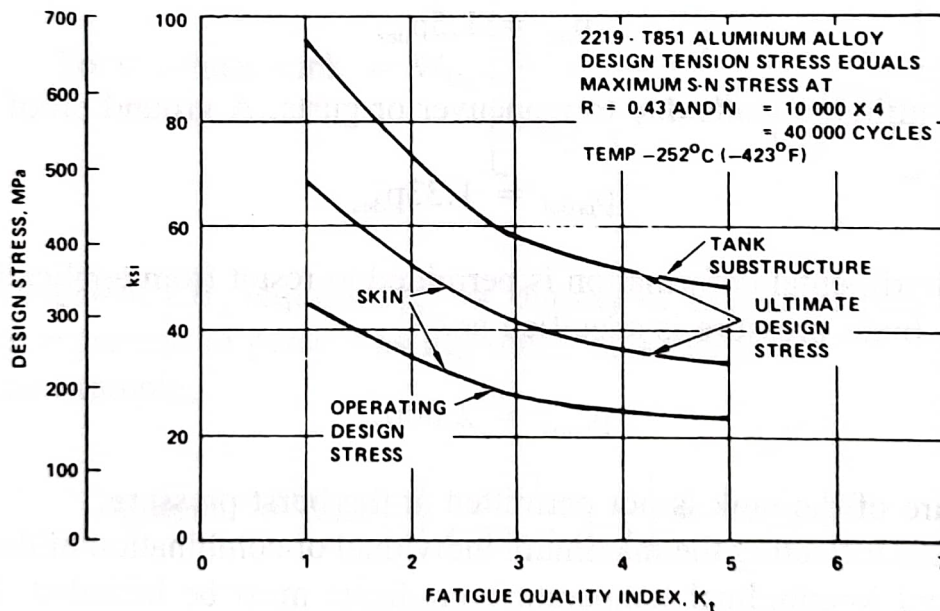


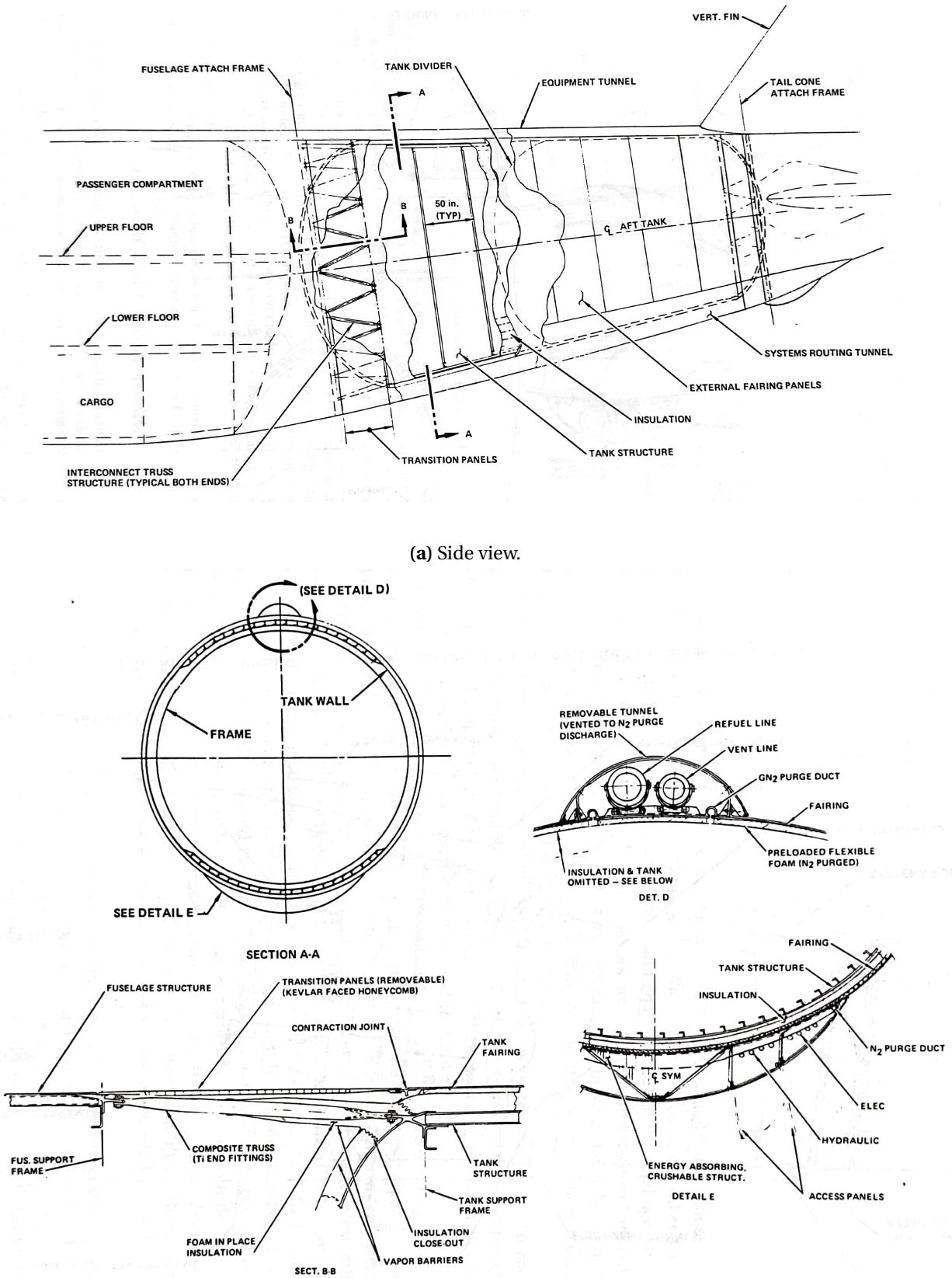
Figure 3.8: Design stress vs. fatigue quality index. Source: [18].

For the non-spherical tank, the thickness obtained for the cylindrical section is also applied to the ellipsoidal end caps, which in most cases have a 2:1 major to minor axis ratio².

²For the aft cap of the aft tank of the turbofan aircraft, a 1:1 ratio is used to use the tailcone space not belonging to the tail section.

For the non-integral tank option, the mass of the tank support system is set equal to 1.8% of the tank mass (including fuel), being this the fraction found by Brewer [18] for this type of support system for its case study aircraft and assuming that the tank support system mass is linearly proportional to the mass it supports. The tank fuselage section is sized as if the section belonged to the passenger cabin because the two sections have similar volume densities. For the integral tank option, the masses of the shell stiffening elements, the truss structures, the outer protective fairing and the equipment and system routing tunnels are assumed to be equal to the mass of the fuselage section that the integral tank replaces (see Figure 3.9). This means that the tank structure itself is sized as if it was non-integral, but using a larger radius and not adding the mass of the tank support system.

Despite the approach used for the integral tank is conservative, as it does not consider the tank inner shell contribution to the bending and shear loads, it was still preferred to a detailed structural analysis because it decouples the tank sizing from the fuselage sizing and this suits well the Initiator. Lastly, independently from the shape or structural choices but depending on the number of engines and tank layout, a tank divider is present to comply with the FAA requirement of having each engine supplied by a different tank during take-off. The mass of this tank divider is set equal to the mass of the forward cap, as the two would have a similar structure.



(b) Cross section.

Figure 3.9: Installation arrangement and design details of integral tank. Source: [18].

THERMODYNAMICS

The hydrogen boil-off due to heat entering the tank together with its consumption in the engines causes continuous pressure variations inside the tank. Lin et al. [19] investigated methods of pressure control for LH₂ tanks using a homogeneous thermodynamic model, with liquid and vapour phases at a uniform temperature equal to the saturation temperature of the cryogenic fluid at the total tank pressure. Among their proposed pressure control systems, the one including fluid mixing and direct venting was selected. The pressure fluctuation for this system is expressed by Equation 3.3.

$$\frac{dP}{dt} = \frac{\phi}{V} \cdot \left[Q_w + W_{mix} - m_g \cdot h_{lg} \cdot \left(1 + \frac{\rho_g}{\rho_l - \rho_g} \right) - m_l \cdot h_{lg} \cdot \left(\frac{\rho_g}{\rho_l - \rho_g} \right) \right], \quad (3.3)$$

where the energy derivative (ϕ) is expressed by Equation 3.4.

$$\phi = \left(\rho_{mean} \cdot \left(\frac{\partial u}{\partial P} \right)_{\rho_{mean}} \right)^{-1} \quad (3.4)$$

According to Equation 3.3, the pressure change rate $\left(\frac{dP}{dt} \right)$ is equal to the ratio between the energy derivative of hydrogen (ϕ) and the tank fluid volume (V), multiplied by the summation of four terms. The first term is the tank heating rate (Q_w), and the way it is obtained is explained later in this section. The second term is the rate of work done on the fluid (W_{mix}). The fluid mixing is used to destroy the fluid temperature stratification and to induce condensation at the liquid-vapour interface, resulting in a reduction of the tank pressure. The mixer power required to circulate the tank fluid adds to the system a certain amount of energy which eventually becomes heat and increases the net fuel energy [19]. The third term is the venting of the gaseous phase, equal to the mass flow rate of the gaseous phase (m_g), times the latent heat of vaporization (h_{lg}), times 1 plus the ratio between the density of the gaseous phase (ρ_g) and the difference between the density of the liquid phase (ρ_l) and the density of the gaseous phase. The fourth term is the venting of the liquid phase, equal to the mass flow rate of the liquid phase (m_l), times the latent heat of vaporization, times the ratio between the density of the gaseous phase and the difference between the density of the liquid phase and the density of the gaseous phase. According to Equation 3.4, the energy derivative is equal to the reciprocal of the product between the fuel mean density (ρ_{mean}) and the partial derivative of the specific internal energy (u) to the tank pressure. The values for ϕ are obtained here by interpolation and extrapolation from Figure 3.10 rather than by applying the formula.

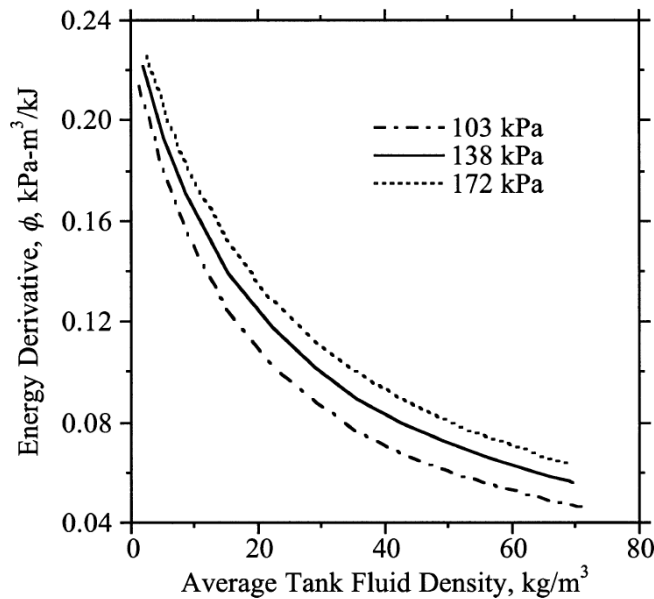


Figure 3.10: Dependence of energy derivative on density and tank pressure for hydrogen. Source: [19]

For this research, the venting of fluid and gas has been separated into two components to highlight that they represent different functions. The venting of the liquid phase represents the fuel drawn by the tank to feed the engines, whereas the venting of the gaseous phase represents direct venting to the exterior of the aircraft system, with the sole purpose of lowering the tank pressure. Equation 3.3 is integrated with a time step of 10 s from the moment the aircraft is disconnected from the refuelling station and the boil-off recovery adapter to the moment the aircraft has landed and is reconnected to the boil-off recovery adapter (see Figure 3.11). The starting pressure is set equal to P_{min} and measures 125 kPa. This pressure is sufficient to prevent air from entering the tank, with some safety margin [18]. Figure 3.12 and Figure 3.13 show respectively the energy derivative profile and fuel mass profile belonging to the pressure profile in Figure 3.11. As indicated by Brewer [18], through the boil-off recovery adapter, the aircraft operator can return gaseous boil-off to ground facilities for reliquefaction, during refuelling or prolonged periods at the gate with full tanks.

The mission for which the tank is being sized is the harmonic (plus diversion), but logically this also becomes the maximum fuel mission. When the tank designed for this mission is used for a shorter mission, the values for ρ_{mean} are lower, and as a consequence, the value for ϕ are higher. Despite this increases the pressurisation rate, the shorter mission time for which Equation 3.3 is integrated was found to be the dominant factor, therefore these missions are non-critical (see Figure 3.14).

In case direct gas venting is used, the most efficient moment to vent is the end of the mission, where ϕ has the largest values (see Figure 3.12), as the pressure drop due to venting is proportional to ϕ (see Equation 3.3). Moreover, it could be argued that by designing a tank that reaches venting pressure just after the regular mission time and starts venting gaseous hydrogen during the extended mission phases a lighter tank could be designed, without the drawback of a larger effective energy consumption due to vented hydrogen. This is the case because for a regular mission no venting would be required and the excess hydrogen carried for the venting, necessary in the eventuality of a mission extension, could be recovered on ground. The pressure profile for this type of mission is presented in Figure 3.15.

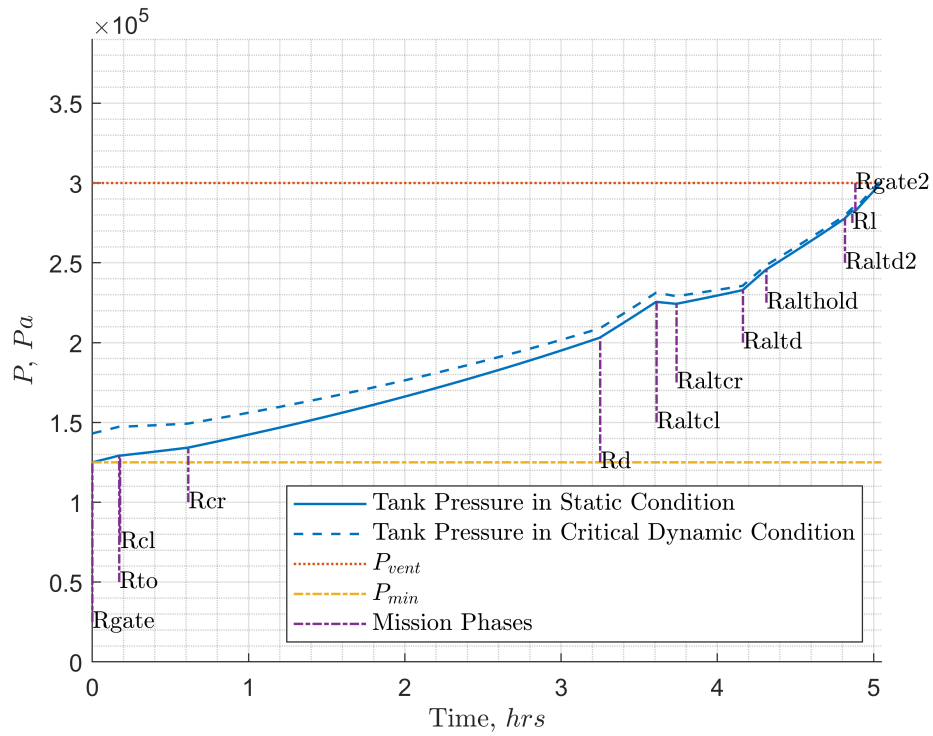


Figure 3.11: Tank pressure profile for one of the designed aircraft. Flight phases: Rgate (disconnect from boil-off recovery adapter), Rto (start of take-off), Rcl (start of climb), Rd (start of descent), Raltcl (start of alternative climb), Ralter (start of alternative cruise), Raltd (start of alternative descent), Ralthold (start of hold), Raltd2, start of second alternative descent), Rl (start of landing), Rgate2 (arrival to gate, until reconnection to boil-off recovery adapter).

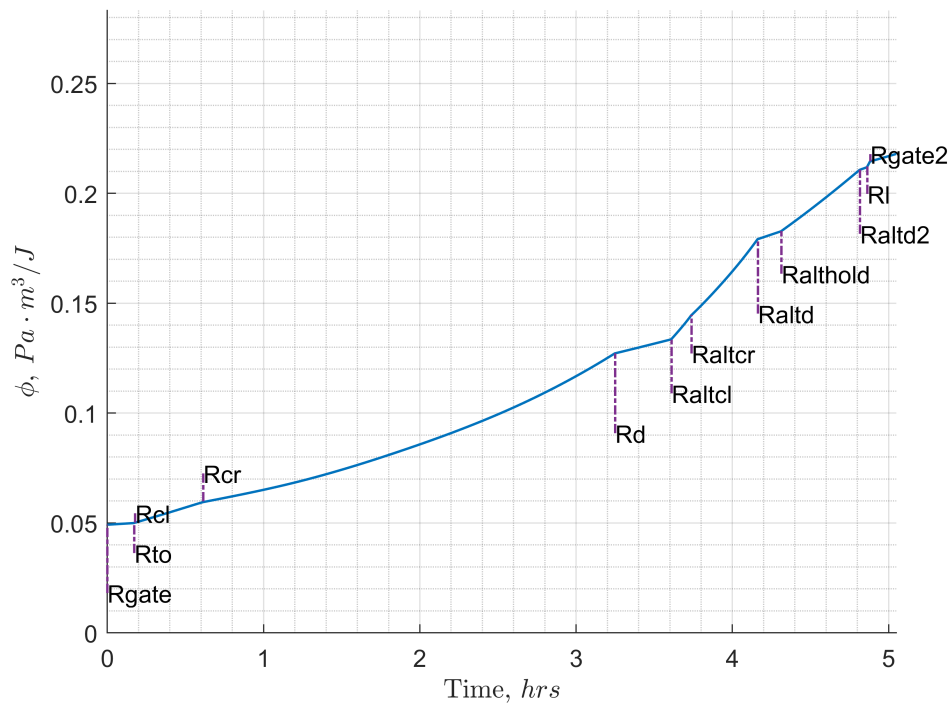


Figure 3.12: Energy derivative profile for one of the designed aircraft. Flight phases: see Figure 3.11.

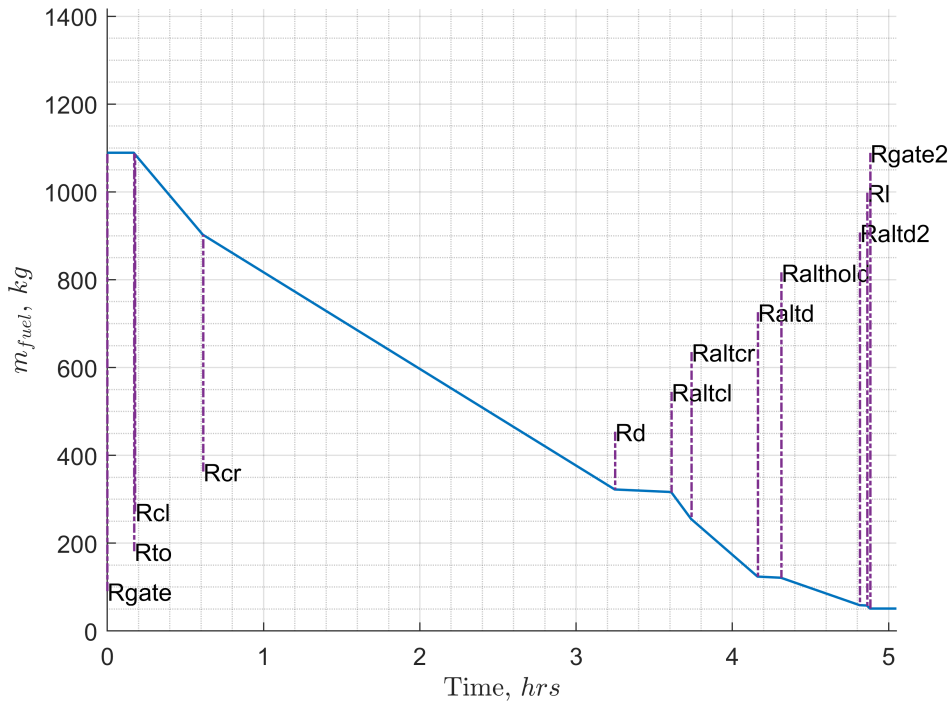


Figure 3.13: Fuel mass profile for one of the designed aircraft. Flight phases: see Figure 3.11.

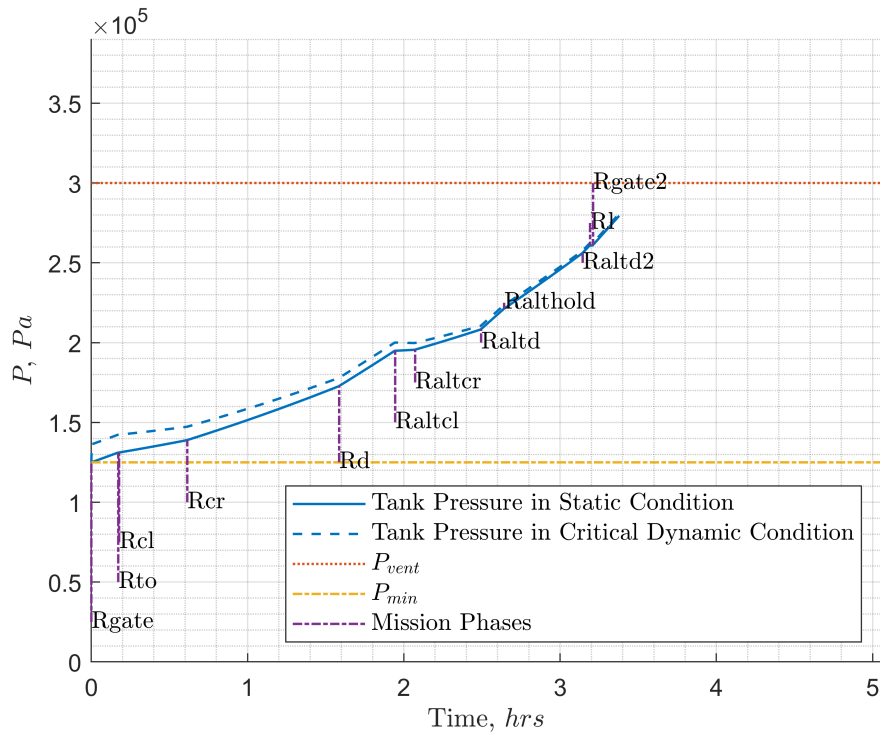


Figure 3.14: Tank pressure profile for one of the designed aircraft for a mission shorter than the one for which the tank was designed. Flight phases: see Figure 3.11.

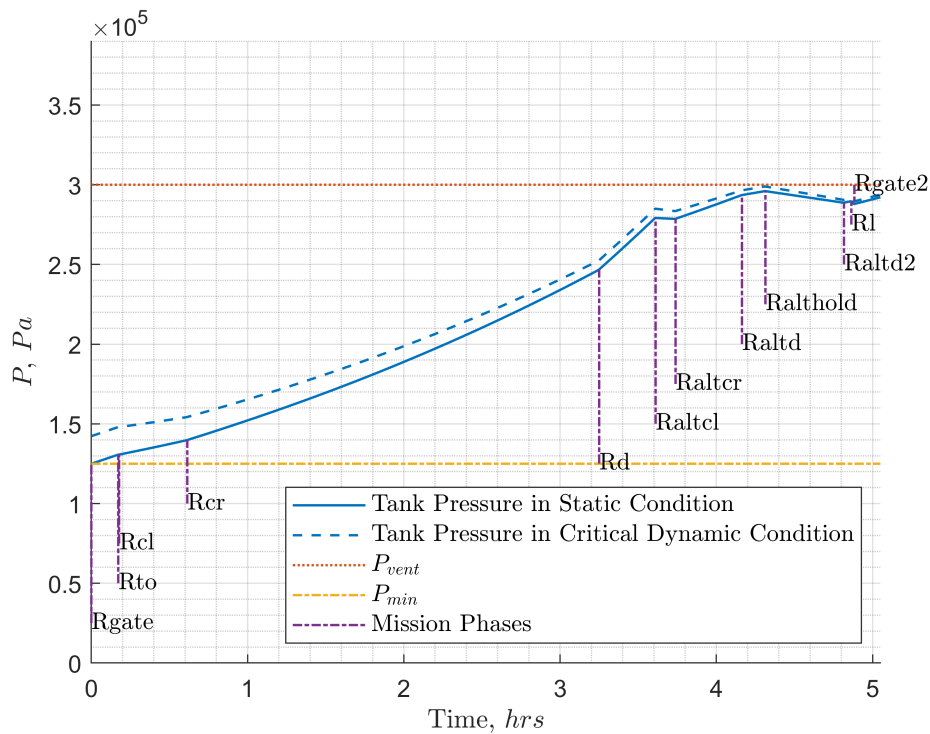


Figure 3.15: Tank pressure profile for one of the designed aircraft, venting fuel during the last 5 mission phases. Flight phases: see Figure 3.11.

The heat flow through the tank is computed by considering only conduction through a single insulation layer with uniform thermal properties. Indeed, the hydrogen itself, being kept as a homogeneous liquid-gaseous fuel mixture at the saturation temperature, does not offer any thermal resistance, and the inner tank surface can be equalled to the fuel temperature. At the same time, by disregarding the additional insulating action of the air around the tank and neglecting the radiative heat balance at the tank surface (the effective thermal resistances of these two components are difficult to estimate), the outer tank surface temperature can be equalled to the external tank temperature. To use a conservative approach, the external tank temperature was set at 320 K (47°C) throughout the whole integration period. The simple solution to the heat conduction through flat plate (Equation 3.5) is used, being t_{ins} an order of magnitude smaller than the tank radius.

$$Q_w = \frac{(T_{amb} - T_{fuel}) \cdot k_{ins} \cdot A}{t_{ins}} \quad (3.5)$$

According to Equation 3.5, the tank heating rate is equal to the difference between the external tank temperature (T_{amb}) and the fuel temperature (T_{fuel}), times the effective thermal conductivity of the insulation material (k_{ins}), times the outer tank surface (A), divided by the insulation layer thickness (t_{ins}). The value of k_{ins} at $T = (T_{amb} + T_{fuel})/2$ was selected to approximate the overall performance of the insulation layer. k_{ins} of polyurethane foam ($\rho_{ins} = 32 \text{ kg/m}^3$) at 170 K is 0.022 W/(mK) (see Figure 3.16) [18].

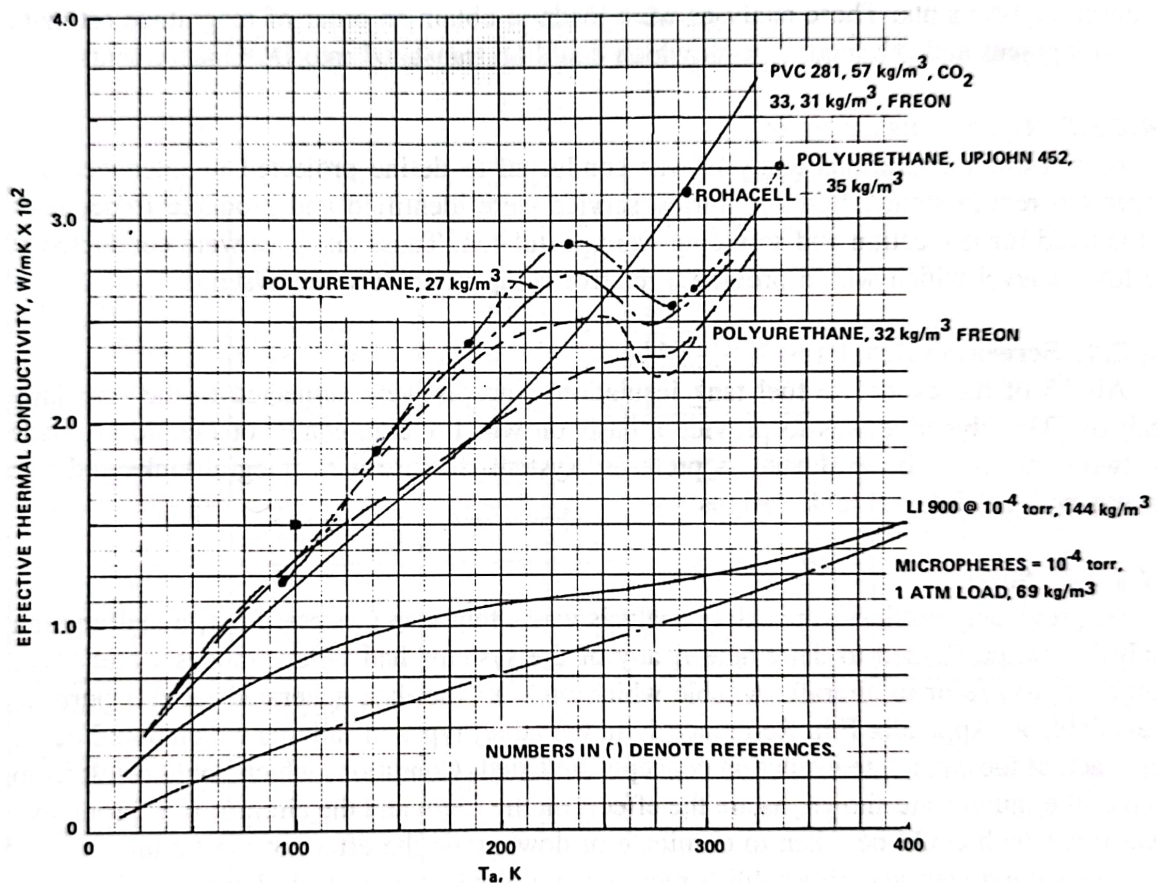


Figure 3.16: Thermal conductivity vs. temperature for foams, rigidised silica, and microsphere insulation. Source: [18].

Finally, Q_w is increased by 30% to account for the extra heat leaking through the support structure and the

pipng, as suggested by Verstraete [15].

HYDROSTATIC

Besides the increase in pressure due to hydrogen evaporation, the tank also experiences hydrostatic pressure increments from aircraft accelerations. These pressure increments depend linearly on the magnitude and direction of the aircraft accelerations and the tank dimensions. A simple model to estimate these pressure increments, taken from the CS-25 regulations and also used for LH2 aircraft by Gomez and Smith [14], is expressed by Equation 3.6.

$$\Delta P_{hydrost} = \rho_{mean} \cdot K \cdot g \cdot L \quad (3.6)$$

According to Equation 3.6, the hydrostatic pressure increment from aircraft accelerations ($\Delta P_{hydrost}$) is equal to the fuel mean density, times a coefficient for the linear acceleration (K), times the gravitational acceleration (g), times the characteristic length in the direction of the acceleration (L). Note that ρ_{mean} is computed at every integration step, the critical value of 9 for forward acceleration is used for K and l_{tank} is used for L .

ALLOWANCES

The mass of fuel required in the tank the moment the aircraft is disconnected from the refuelling station is the sum of the fuel burned during the extended mission, plus the mass of GH2 vented during flight (if any), plus a 0.3% trapped fuel allowance, plus a pressurisation fuel allowance. The pressurisation fuel allowance accounts for the mass of GH2 present in the tank at the end of the extended mission (4.3% of the burned mass at $P_{vent} = 250 \text{ kPa}$). From a mass perspective, these unusable fuel components are added to the tank mass. From an energy perspective, except for the GH2 vented during flight, these components are not accounted for because recovered on the ground. The internal volume of the tank is computed by adding to the fuel volume a 0.9% tank contraction-expansion allowance, a 2% ullage allowance and a 0.6% internal equipment allowance. The values of these allowances are retrieved from Brewer [18], except for the pressurisation fuel allowance, which is dependent on the choice of venting pressure.

3.2.3. FUEL SYSTEM SIZING

The Initiator computes the fuel system mass for the turbine kerosene aircraft using a Class 2 estimation from Torenbeek (Equation 3.7 here, Table 8.9 in Torenbeek [65]).

$$m_{fuelSys} = 36.3 \cdot (N_e + N_{ft} - 1) + 4.366 \cdot N_{ft}^{0.5} \cdot V_{ft}^{0.333} \quad (3.7)$$

According to Equation 3.7, the fuel system mass (excluding LH2 tank) ($m_{fuelSys}$) is equal to the summation of two terms. The first term is equal to 36.3 times the sum of the number of engines (N_e) and the number of fuel tanks (N_{ft}) minus 1. The second term is equal to 4.366 times the number of fuel tanks to the power of 0.5, times the fuel volume in litres (V_{ft}) to the power of 0.333.

The fuel system for a tube-and-wing turbine LH2 airliner has been meticulously designed and described by Brewer [18]. This fuel system consists of a vent system, insulated fuel supply lines to the engines, heat exchangers to transfer the engine and the airframe heat to the cryogenic fuel, fuel quantity gauging equipment, refuelling and defuelling systems, fuel jettison system, pumps, valves, seals etc. (see Figure 3.17, Figure 3.18, Figure 3.19).

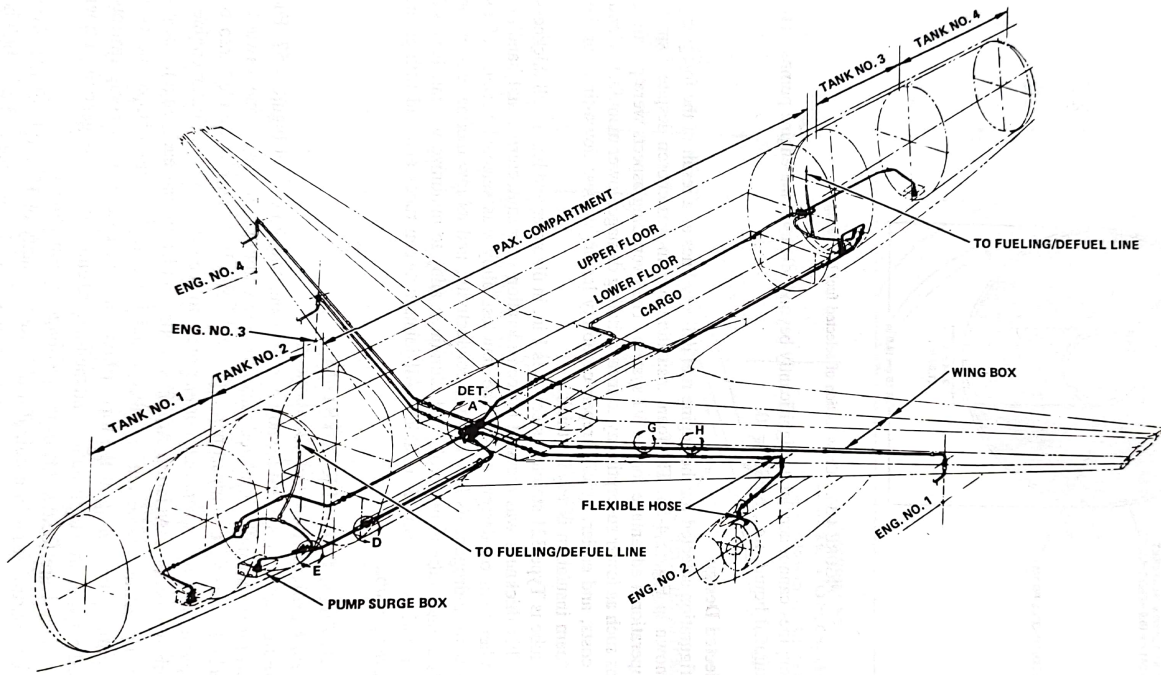


FIGURE 4-57. Diagram: engine fuel delivery system.

Figure 3.17: Engine fuel delivery system. Source: [18].

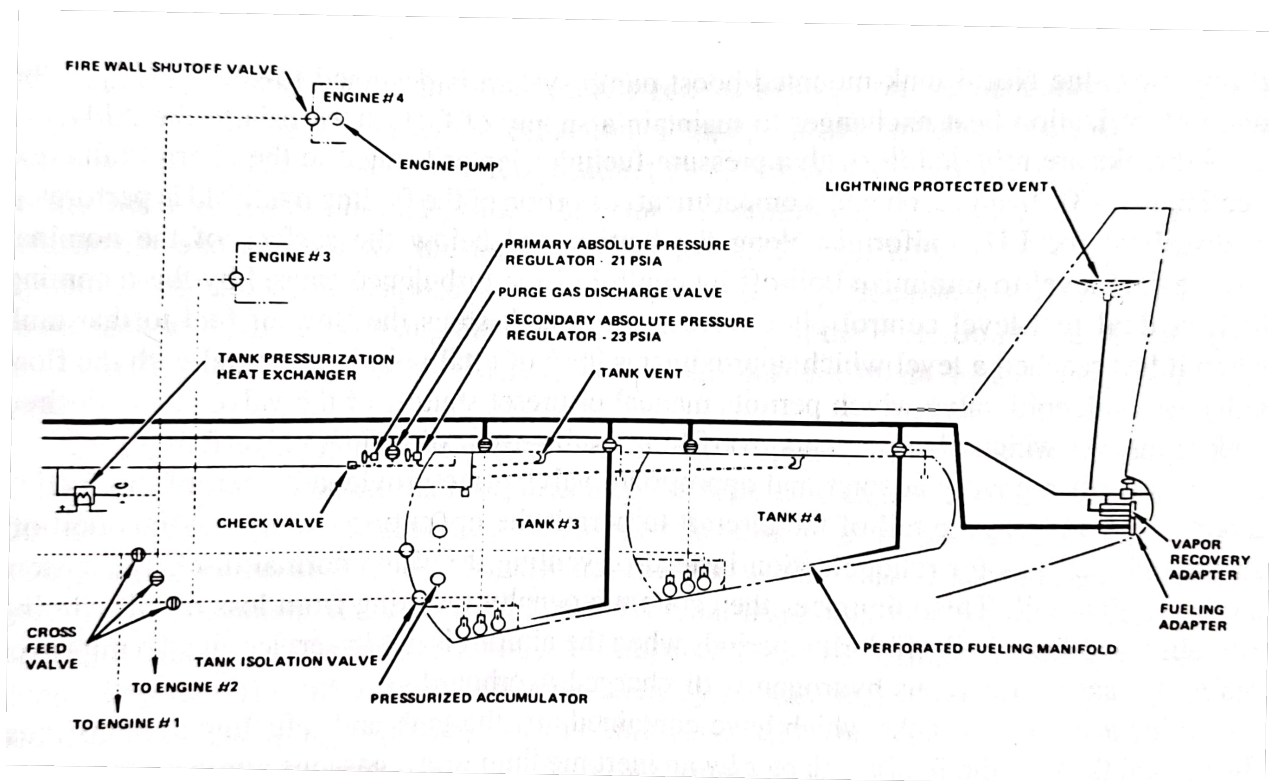


Figure 3.18: Schematic of fuel system. Source: [18].

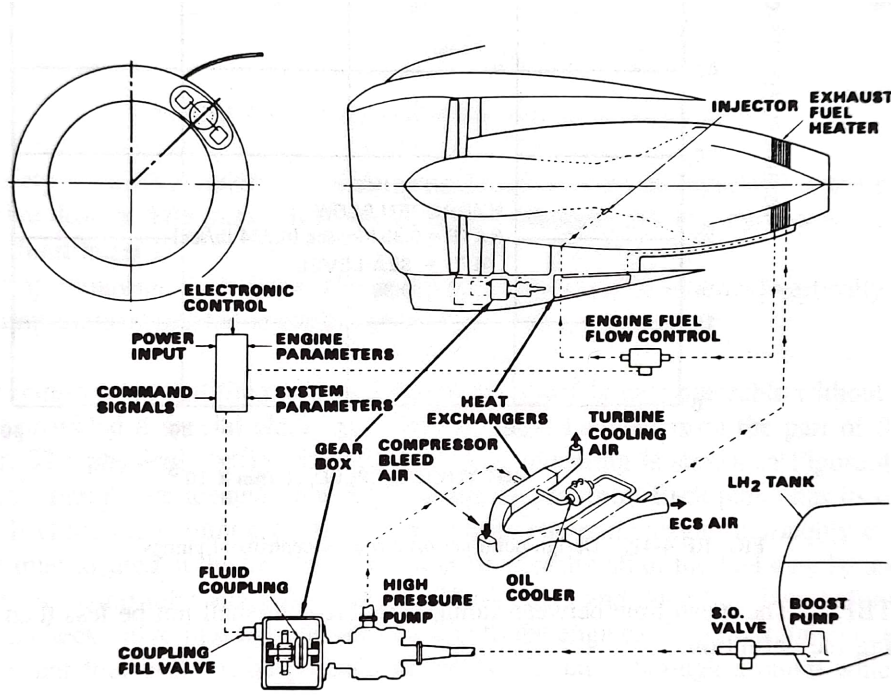


Figure 3.19: Block diagram of fuel delivery system. Source: [18].

When applying Equation 3.7 to the LH2 aircraft designed by Brewer, the value obtained for the fuel system is a fraction ($k_{fs} = 0.50$) of the one by him reported. It is believed that by using Equation 3.7 and dividing the results by k_{fs} a reasonable estimate for the LH2 fuel system can be obtained for the aircraft under investigation in this research.

3.2.4. PROPULSION SYSTEM AND WING

The propulsion system is also affected by the change in fuel type, but while the change in specific fuel consumption has been scaled with the change in fuel calorific value (x2.8), the mass estimation methods used remain the ones implemented for kerosene aircraft, since the change in mass and volume of the system is known to be negligible [18].

For this research, the final Initiator loop was removed and the wing mass remains sized using the estimation from Torenbeek (Equation 3.8 here, Equation 8.12 in Torenbeek [65]).

$$m_w = m_{crit} \cdot 6.67 \cdot 10^{-3} \cdot b_s^{0.75} \cdot \left(1 + \sqrt{\frac{1.905}{b_s}}\right) \cdot n_{ult}^{0.55} \cdot \left(\frac{b_s/t_r}{m_{crit}/S}\right)^{0.30} \quad (3.8)$$

According to Equation 3.8, the wing mass (m_w) is equal to the critical aircraft mass for wing mass sizing (m_{crit}), times $6.67 \cdot 10^{-3}$, times the structural wingspan (b_s) to the power of 0.75, times 1 plus the square root of 1.905 divided by the structural wingspan, times the ultimate load factor (n_{ult}) to the power of 0.55, times the ratio between the structural wingspan over the taper ratio (t_r) and the aircraft mass for wing mass sizing over the wing surface area, to the power of 0.3. To m_w , a further 2% is added for spoilers and speed brakes, a 5% is detracted for each couple of wing-mounted engines and a 5% is detracted if the main landing gear is not wing-mounted. A further correction is applied when composite materials are used. Nevertheless, while for the kerosene aircraft m_g is set equal to the *MZFM* (as indicated by Torenbeek for the transport category), for the LH2 aircraft the *MTOM* is used, as the absence of wing bending relief from the fuel makes the *MTOM* the critical, sizing condition.

3.3. VALIDATION OF THE TOOL

Due to the complete absence of currently operational or even experimental LH2 airliners, a validation of the complete tool using experimental data is not possible. Nevertheless, there is reason to believe in its suitability for obtaining meaningful data. The kerosene version of the tool, which serves as the backbone for the automated aircraft design, has been validated by Elmendorp et al. [61]. On the other side, the newly added LH2 tank sizing module and the modification made to the fuel system, wing, and fuselage sizing methods require some argumentation:

- Concerning the tank sizing module, the point is made that only proven structural (Barlow's equation, allowances and correlation data from Brewer [18], hydrostatic pressure increment from CS-25 regulations) and thermodynamic models (model from Lin et al. [19], heat conduction through a flat plate) have been combined, using conservative assumptions.
- Concerning the fuel system sizing method, the semi-empirical Torenbeek mass estimation [65] was multiplied with a correction factor extracted from Brewer [18]. This modified equation was applied to the case study from Silberhorn et al. (rear tank option) [7] and a mass of 766 kg was obtained, rather than the 781 kg indicated by the study.
- Concerning the wing sizing method, the Torenbeek semi-empirical equation [65] was modified for LH2 aircraft to use *MTOM* rather than *MZFM* as the critical, sizing condition. For kerosene aircraft, *MTOM* would not be the critical sizing condition because the wing-located fuel would provide bending relief. As the LH2 aircraft has the fuel located in the fuselage, it makes sense to use *MTOM* as aircraft mass for the critical sizing condition.
- Concerning the fuselage sizing, the mass estimation was kept unaltered, on the assumption that the fuselage section at the tank location did not need significant reinforcement. This assumption was formulated once noticed that the linear density of the tank section (tank mass, plus fuel system mass, plus maximum fuel mass) was comparable to the one of the cabin section (payload mass, plus furnishing mass, plus cargo containers mass). The extent to which these densities are comparable depends on the aircraft size. For the optimal short-range aircraft (see Chapter 4), the linear densities of the cabin and tank sections are respectively 862 kg/m and 481 kg/m, for the optimal medium-range they are 1135 kg/m and 1039 kg/m and for the optimal long-range aircraft they are 1677 kg/m and 1949 kg/m.
- Concerning the fuselage geometrical adaptation necessary to create the fuselage space to accommodate the tanks, validation could be done by visual inspection, as the aircraft geometry, together with the aircraft main components, could be 3D-plotted.

The Initiator, now bolstered with LH2 aircraft design capabilities (Revision 2409), was used to design LH2 aircraft versions of a short-range turboprop, a medium-range turbofan and a long-range turbofan aircraft. The aircraft are designed for their harmonic mission, but note that for the LH2 ones this corresponds to the maximum fuel mission too.

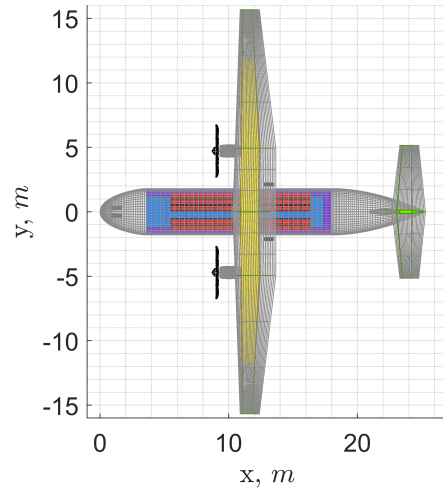
This chapter presents the results from the studies that have been made to investigate the impact of the tank design choices on the three aircraft main performance parameters.

4.1. BASELINE AIRCRAFT

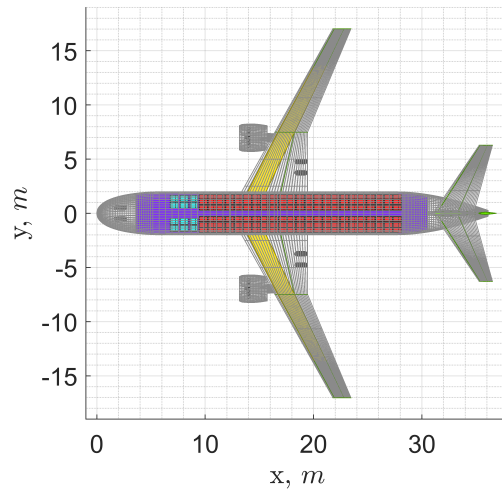
The baseline kerosene aircraft selected for these studies are initiator generated versions of the ATR72-600, the A320neo and the A330-300, representing respectively a short, a medium and a long-range aircraft, with some design modifications. The cabin layouts, or more in particular the seats abreast configurations for the economy class (EC) are chosen such that the aircraft versions with lowest *OEM*, *MTOM* and *SEC* are obtained. This modification will allow for a fair comparison with the LH2 aircraft versions. Moreover, for the ATR72-600, the aft and forward cargo bays are substituted with a single cargo bay under the cabin floor. The mission requirements and the main performance and configuration input parameters, listed in Table 4.1, are equal for both the kerosene and the LH2 version. Only the brake-specific and the thrust-specific fuel consumption differ, as explained in subsection 3.2.4.

Table 4.1: Aircraft main mission requirements and configuration/performance parameters for the investigated aircraft.

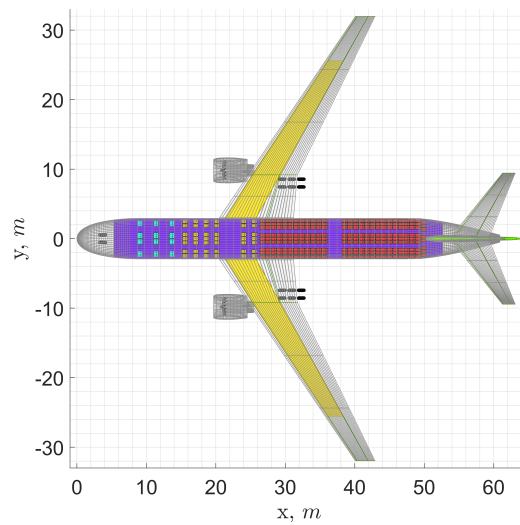
Parameters	ATR72	A320	A330
Number of passengers	72 (1 class)	150 (2 classes)	295 (3 classes)
Payload mass (<i>t</i>)	7.55	19.30	51.70
M_{cruise}	0.40	0.78	0.82
h_{cruise} (<i>m</i>)	7000	11278	11887
Range (<i>km</i>)	1530	4550	8000
Take-off distance (<i>m</i>)	1333	2180	2320
Landing Distance (<i>m</i>)	915	1440	1600
Approach speed (<i>m/s</i>)	N/A	70	70
Airworthiness Reg.	FAR-25	FAR-25	FAR-25
Loiter time (<i>min</i>)	30	30	30
Diversion range (<i>km</i>)	306	370	370
$C_{L_{max}}$ landing	2.7	2.6	2.5
$C_{L_{max}}$ take-off	2.2	2.1	2.0
Aspect ratio	12	9.5	10.0
BSFC (<i>g/(kWh)</i>)	300 (107 for LH2)	N/A	N/A
TSFC (<i>kg/(Ns)</i>)	N/A	1.501E-5 (5.36E-6 for LH2)	1.590E-5 (5.678E-6 for LH2)



(a) ATR72, tank level



(b) A320, tank level

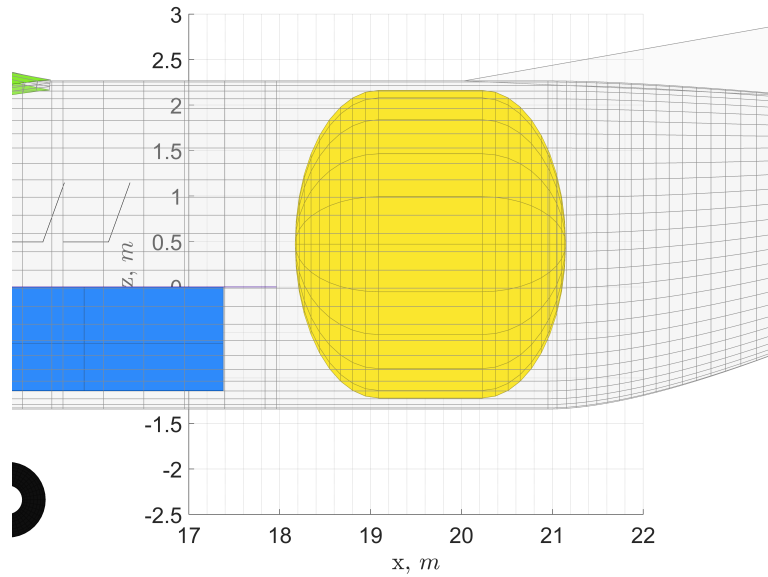


(c) A330, tank level

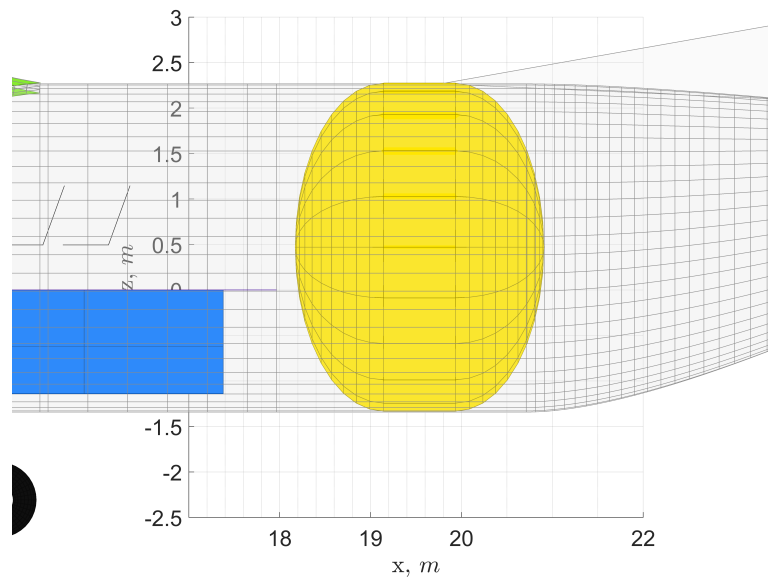
Figure 4.1: Top views of baseline aircraft. Fuel tanks in yellow.

4.2. TANK STRUCTURE: INTEGRAL VS. NON-INTEGRAL

This section investigates the extent to which using integral tanks, which are more volumetrically efficient than non-integral tanks (see Figure 4.2), increases the aircraft performances. Table 4.2, Table 4.3 and Table 4.4 presents the performance comparison for the aircraft representing the three aircraft categories respectively.



(a) ATR72LH2(aft-nonintegral-23)



(b) ATR72LH2(aft-integral-23)

Figure 4.2: Example of non-integral (a) and integral (b) tank. Fuel tanks in yellow.

The use of integral tanks appears to be increasingly beneficial with aircraft size. Note that the tank itself is heavier for the integral case, because of the lower tank external pressure and the larger tank structural shell radius. Nevertheless, the larger tank radius translates into a shorter tank length and the resulting mass and parasite drag savings from the consequently shorter fuselage more than compensate for the increase in tank mass.

Table 4.2: Performance comparison between short-range aircraft using integral tanks and aircraft using non-integral tanks¹.

Parameters	ATR72	
	non-integral	integral
Tank structure		
Seats abreast EC		2-3
Cryotank layout		aft
Cryotank shape		non-spherical
P_{vent} (kPa)		300
Direct venting		No
t_{ins} (mm)	138	140 (+1.4%)
t_{shell} (mm)	2.5	3.1 (+24%)
m_{tank} (kg)	438	469 (+7.1%)
η_{grav}	0.415	0.444 (+7%)
r_{tank} (m)	1.69	1.8 (+6.5%)
l_{tank} (m)	2.98	2.74 (-8.1%)
l_{fus} (m)	28.2	27.9 (-1.1%)
m_{fus} (t)	3.93	3.87 (-1.5%)
$C_{D_{0,fus}}$	0.00652	0.00648 (-0.6%)
OEM (t)	18.42	18.38 (-0.2%)
$MTOM$ (t)	27.03	26.99 (-0.1%)
SEC (J/pax/m)	862	862.5 (+0.1%)
Input file name	ATR72LH2 (aft-nonintegral-23)	ATR72LH2 (aft-integral-23)

¹The trailing zeroes in decimal numbers are removed.

Table 4.3: Performance comparison between medium-range aircraft using integral tanks and aircraft using non-integral tanks.

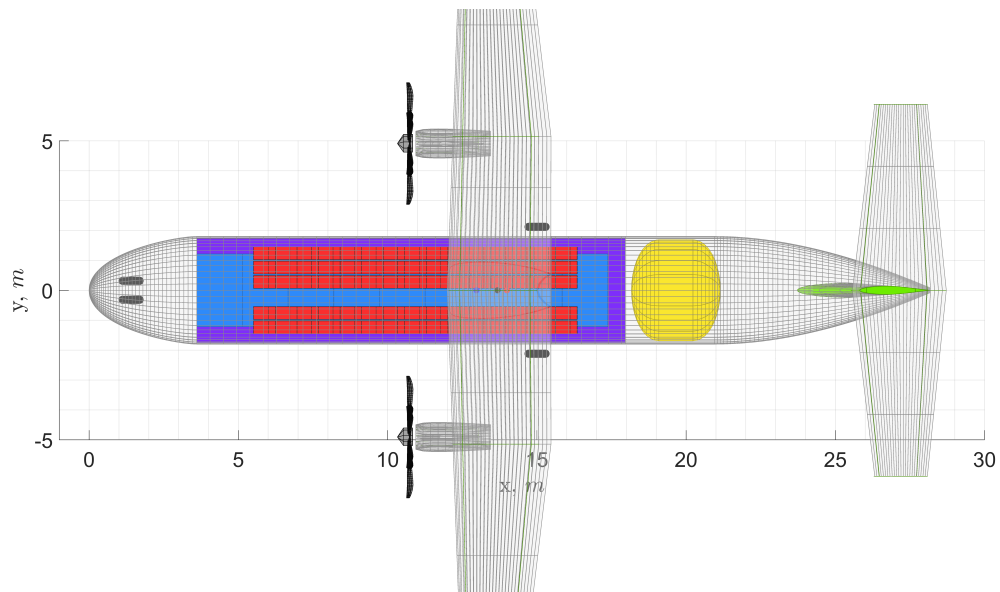
Parameters	A320	
	non-integral	integral
Tank structure		
Seats abreast EC		2-3-2
Cryotank layout		aft
Cryotank shape		non-spherical
P_{vent} (kPa)		300
Direct venting		No
t_{ins} (mm)	106	105 (-0.9%)
t_{shell} (mm)	3.6	4.7 (+30.6%)
m_{tank} (kg)	2049	2239 (+9.3%)
η_{grav}	0.322	0.354 (+9.9%)
r_{tank} (m)	2.29	2.44 (+6.6%)
l_{tank} (m)	8.05	7.24 (-10.1%)
l_{fus} (m)	44	43 (-2.3%)
m_{fus} (t)	12.2	11.63 (-4.7%)
$C_{D_{0,fus}}$	0.00776	0.00763 (-1.7%)
OEM (t)	51.65	51.36 (-0.6%)
MTOM (t)	77.31	76.98 (-0.4%)
SEC (J/pax/m)	912.3	907.1 (-0.6%)
Input file name	A320LH2 (aft-nonintegral-232)	A320LH2 (aft-integral-232)

Table 4.4: Performance comparison between long-range aircraft using integral tanks and aircraft using non-integral tanks.

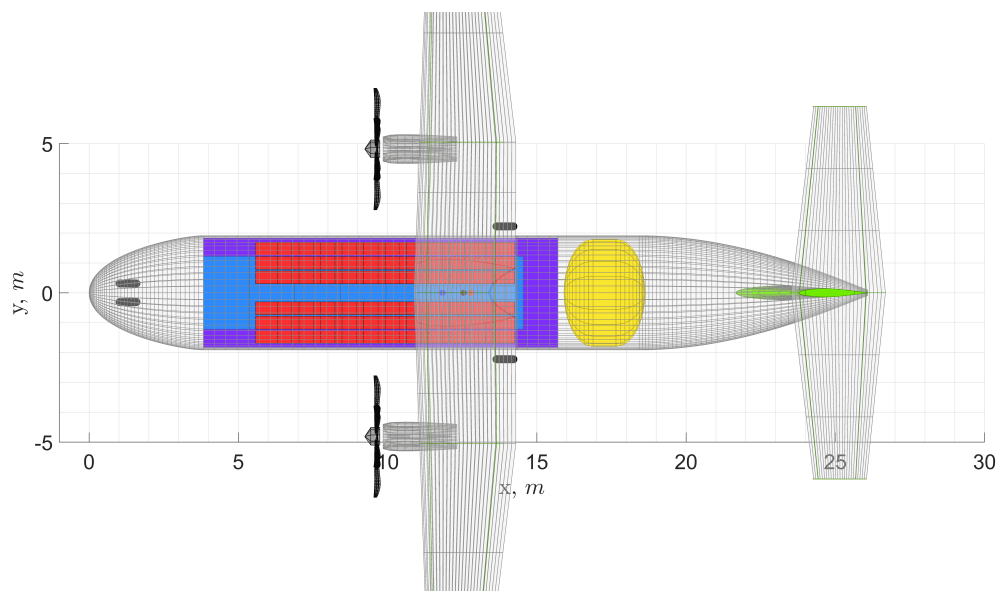
Parameters	A330	
	non-integral	integral
Tank structure		
Seats abreast EC		3-4-3
Cryotank layout		aft
Cryotank shape		non-spherical
P_{vent} (kPa)		300
Direct venting		No
t_{ins} (mm)	113	108 (-4.4%)
t_{shell} (mm)	4.7	6.3 (+34%)
m_{tank} (kg)	8054	8486 (+5.4%)
η_{grav}	0.284	0.305 (+7.4%)
r_{tank} (m)	2.99	3.19 (+6.7%)
l_{tank} (m)	19.03	16.59 (-12.8%)
l_{fus} (m)	79.7	77.1 (-3.3%)
m_{fus} (t)	43.73	40.86 (-6.6%)
$C_{D_{0,fus}}$	0.00513	0.00506 (-1.4%)
OEM (t)	176.21	172.03 (-2.4%)
MTOM (t)	256.25	251.6 (-1.8%)
SEC (J/pax/m)	1263.8	1242.9 (-1.7%)
Input file name	A330LH2 (aft-nonintegral-343)	A330LH2 (aft-integral-343)

4.3. FUSELAGE DIAMETER: REGULAR VS. INCREASED

The addition of the fuel tank behind the unmodified cabin of an existing kerosene aircraft increases the fuselage length and consequently brings the fuselage slenderness ratio beyond its optimal point. This section investigates whether an increase in fuselage diameter is beneficial for an LH2 aircraft. Because the fuselage design is inside-out, the fuselage diameter is increased by increasing the number of the seats abreast in the economy class (EC) (see Figure 4.3). Table 4.5, Table 4.6 and Table 4.7 present the performance comparison for three aircraft representing the short, medium and long-range aircraft categories respectively.



(a) ATR72LH2(aft-nonintegral-23)



(b) ATR72LH2(aft-nonintegral-33)

Figure 4.3: Example of LH2 aircraft with fuselage diameter of kerosene baseline (a) vs. LH2 aircraft with increased fuselage diameter (b). Fuel tanks in yellow.

The increase in fuselage diameter appears to be beneficial under all the main three performance parameters for both the short and the long-range aircraft. Conversely, for the medium-range aircraft, the improvements in *OEM* and *MTOM* are less pronounced, with the *SEC* being even deteriorated. The reason is that while for the short and long-range aircraft the increase in diameter would directly translate into an increase in seats abreast and thus a decrease in cabin length, for the medium-range aircraft the first increase in diameter serves to create the space for a second aisle.

Table 4.5: Performance comparison between short-range aircraft with same fuselage diameters of kerosene baseline and aircraft with larger fuselage diameters.

Parameters	ATR72	
	non-integral	non-integral
Tank structure	non-integral	non-integral
Seats abreast EC	2-3	3-3
Cryotank layout	aft	aft
Cryotank shape	non-spherical	non-spherical
P_{vent} (kPa)	300	300
Direct venting	No	No
m_{tank} (kg) (aft+fwd)	438	447 (+2.1%)
η_{grav} (aft+fwd)	0.415	0.434 (+4.6%)
l_{tank} (m) (aft + fwd)	2.98	2.71 (-9.1%)
r_{fus} (m)	1.8	1.92 (+6.7%)
l_{fus} (m)	28.2	26.1 (-7.4%)
m_{fus} (t)	3.93	3.52 (-10.4%)
$C_{D_{0,fus}}$	0.00652	0.00672 (+3.1%)
$\Delta x_{c.g.}$	0.357	0.343 (-3.9%)
S_h/S	0.348	0.364 (+4.6%)
m_{ht} (t)	0.54	0.56 (+3.7%)
$C_{D_{0,ht}}$	0.00243	0.00254 (+4.5%)
C_{D_0}	0.02063	0.02097 (+1.6%)
$L/D_{mid-cruise}$	19.9	19.6 (-1.5%)
OEM (t)	18.42	17.44 (-5.3%)
MTOM (t)	27.03	26.02 (-3.7%)
SEC (J/pax/m)	862	843.5 (-2.1%)
Input file name	ATR72LH2 (aft-nonintegral-23)	ATR72LH2 (aft-nonintegral-33)

Table 4.6: Performance comparison between medium-range aircraft with same fuselage diameters of kerosene baseline and aircraft with larger fuselage diameters.

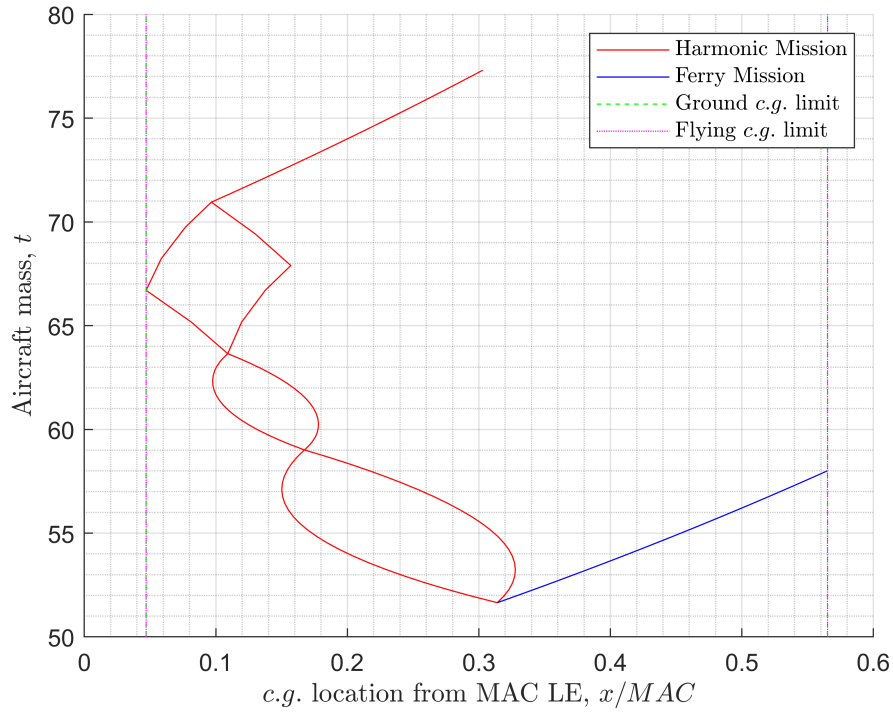
Parameters	A320		
Tank structure		non-integral	
Seats abreast EC	3-3	2-3-2	2-4-2
Cryotank layout		aft	
Cryotank shape		non-spherical	
P_{vent} (kPa)		300	
Direct venting		No	
m_{tank} (kg) (aft+fwd)	2016	2049 (+1.6%)	2125 (+5.4%)
η_{grav} (aft+fwd)	0.321	0.322 (+0.3%)	0.333 (+3.7%)
l_{tank} (m) (aft + fwd)	11.55	8.05 (-30.3%)	6.94 (-39.9%)
r_{fus} (m)	1.99	2.44 (+22.6%)	2.69 (+35.2%)
l_{fus} (m)	48.3	44 (-8.9%)	42.1 (-12.8%)
m_{fus} (t)	13.11	12.2 (-6.9%)	11.76 (-10.3%)
$C_{D_{0,fus}}$	0.007	0.0078 (11.4%)	0.0083 (+18.6%)
$\Delta x_{c.g.}$	0.607	0.518 (-14.7%)	0.475 (-21.7%)
S_h/S	0.389	0.418 (+7.5%)	0.436 (+12.1%)
m_{ht} (t)	2.17	2.32 (+6.9%)	2.45 (+12.9%)
$C_{D_{0,ht}}$	0.0029	0.0031 (+6.9%)	0.0033 (+13.8%)
C_{D_0}	0.0224	0.0233 (+4%)	0.0238 (+6.3%)
$L/D_{mid-cruise}$	16	15.7 (-1.9%)	15.4 (-3.7%)
OEM (t)	52.18	51.65 (-1%)	50.68 (-2.9%)
MTOM (t)	77.75	77.31 (-0.6%)	76.36 (-1.8%)
SEC (J/pax/m)	900.1	912.3 (+1.4%)	914.3 (+1.6%)
Input file name	A320LH2 (aft-nonintegral-33)	A320LH2 (aft-nonintegral-232)	A320LH2 (aft-nonintegral-242)

Table 4.7: Performance comparison between long-range aircraft with same fuselage diameters of kerosene baseline and aircraft with larger fuselage diameters.

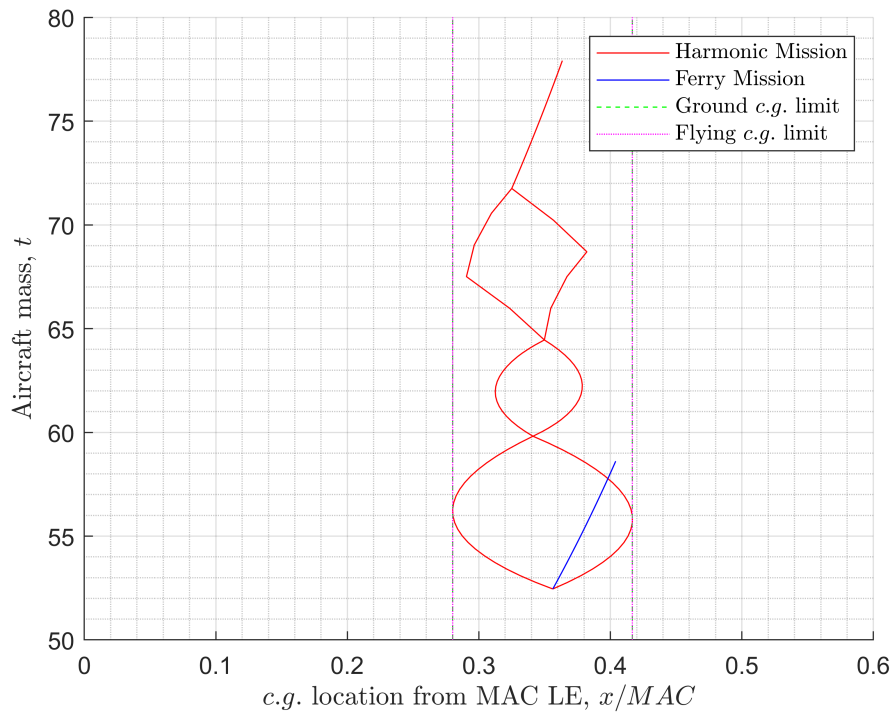
Parameters	A330		
Tank structure		non-integral	
Seats abreast EC	3-3-3	3-4-3	3-5-3
Cryotank layout		aft	
Cryotank shape		non-spherical	
P_{vent} (kPa)		300	
Direct venting		No	
m_{tank} (kg) (aft+fwd)	8161	8054 (-1.3%)	8063 (-1.2%)
η_{grav} (aft+fwd)	0.284	0.284 (0%)	0.284 (0%)
l_{tank} (m) (aft + fwd)	22.53	19.03 (-15.5%)	16.41 (-27.2%)
r_{fus} (m)	2.93	3.19 (+8.9%)	3.44 (+17.4%)
l_{fus} (m)	84.1	79.7 (-5.2%)	75.8 (-9.9%)
m_{fus} (t)	46.02	43.73 (-5%)	41.68 (-9.4%)
$C_{D_{0,fus}}$	0.0049	0.0051 (+4.1%)	0.0053 (+8.2%)
$\Delta x_{c.g.}$	0.557	0.535 (-3.9%)	0.46 (-17.4%)
S_h/S	0.254	0.266 (+4.7%)	0.258 (+1.6%)
m_{ht} (t)	4.63	4.65 (+0.4%)	4.56 (-1.5%)
$C_{D_{0,ht}}$	0.0018	0.0019 (+5.6%)	0.0018 (0%)
C_{D_0}	0.018	0.0183 (+1.7%)	0.0184 (+2.2%)
$L/D_{mid-cruise}$	18.9	18.7 (-1.1%)	18.6 (-1.6%)
OEM (t)	181.2	176.21 (-2.8%)	174.71 (-3.6%)
$MTOM$ (t)	261.6	256.25 (-2%)	254.8 (-2.6%)
SEC (J/pax/m)	1281	1263.8 (-1.3%)	1265.9 (-1.2%)
Input file name	A330LH2 (aft-nonintegral-333)	A330LH2 (aft-nonintegral-343)	A330LH2 (aft-nonintegral-353)

4.4. TANK LAYOUT: AFT VS. AFT & FWD

The use of a single fuel tank placed behind the cabin increases the $\Delta x_{c.g.}$ of the aircraft and with it the horizontal tail size. By placing a second tank in front of the cabin, a smaller $\Delta x_{c.g.}$ can be obtained, and the horizontal tail size can be reduced (see Figure 4.4 and Figure 4.5). The addition of the forward tank comes at the expense of a longer fuselage, as the forward tank has a smaller radius to allow for the corridor preserving the cabin-cockpit connection (see Figure 4.6). Because the forward tank uses the fuselage volume inefficiently, and because the centre of gravity shift from the fuel does not have to be zero to make $\Delta x_{c.g.}$ fuel independent, less than half of the fuel is placed in the forward tank (40%, for this study).

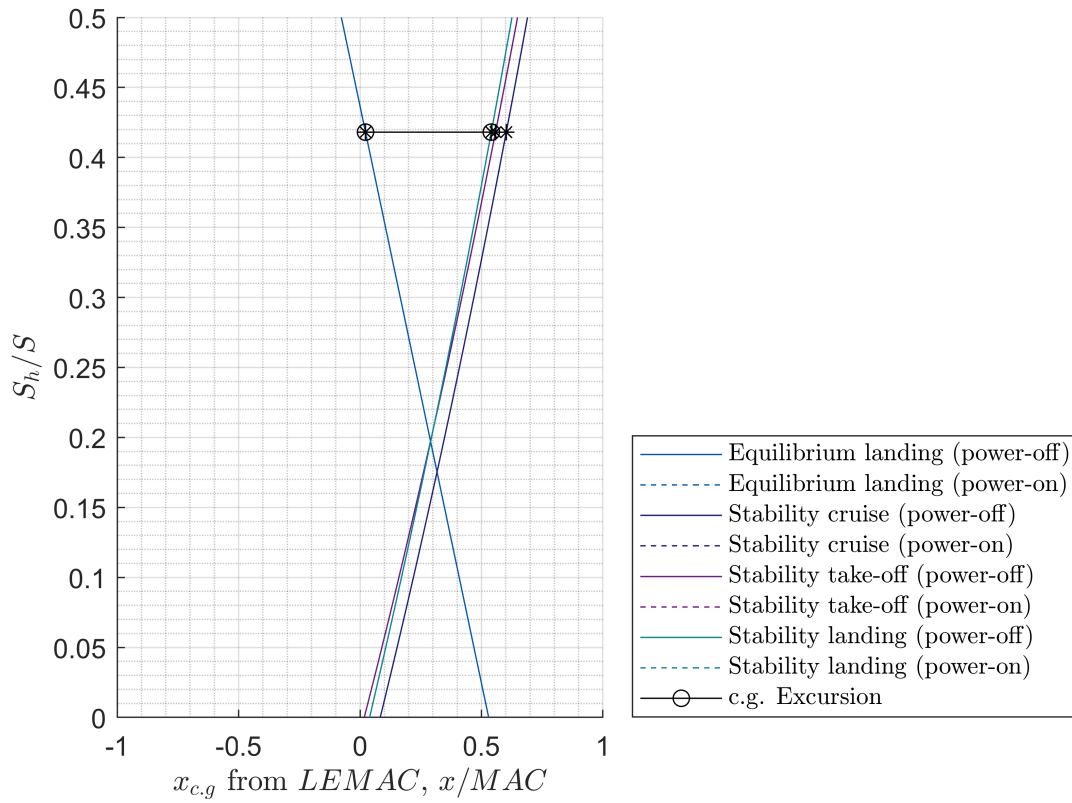


(a) A320LH2(aft-nonintegral-232)

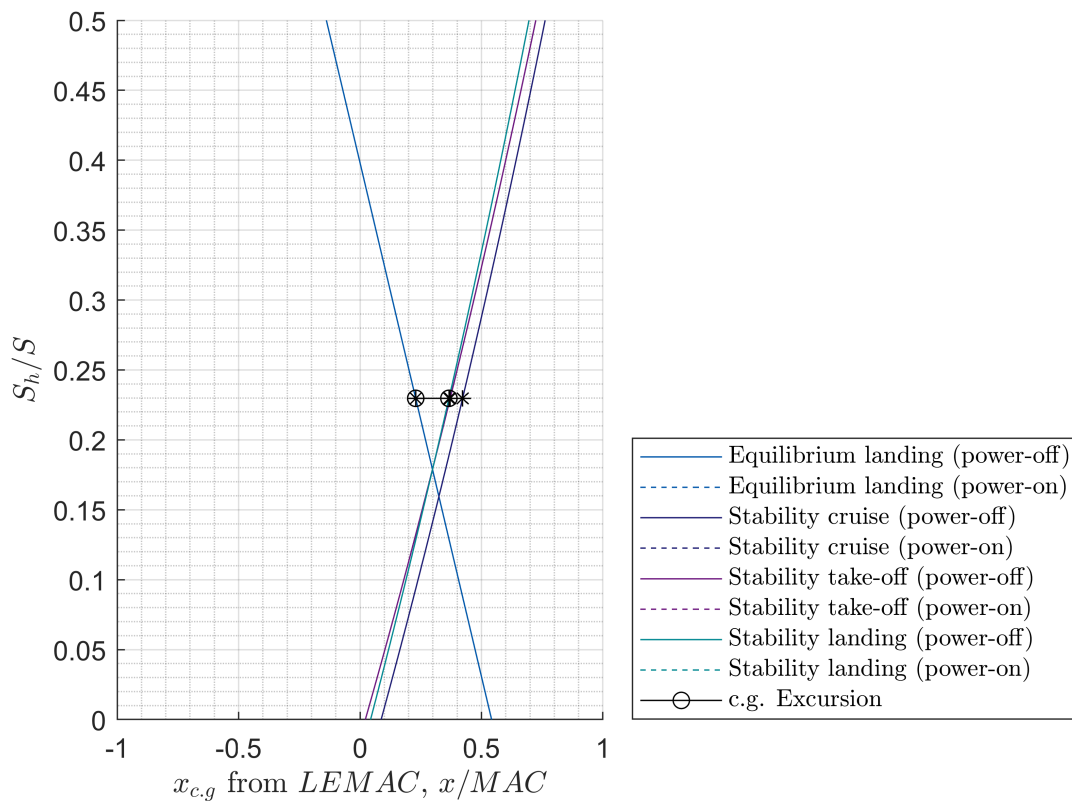


(b) A320LH2(aftFwd-nonintegral-232)

Figure 4.4: Example of loading diagram for LH2 aircraft with aft tank layout (a) and LH2 aircraft with aft & fwd tank layout (b).

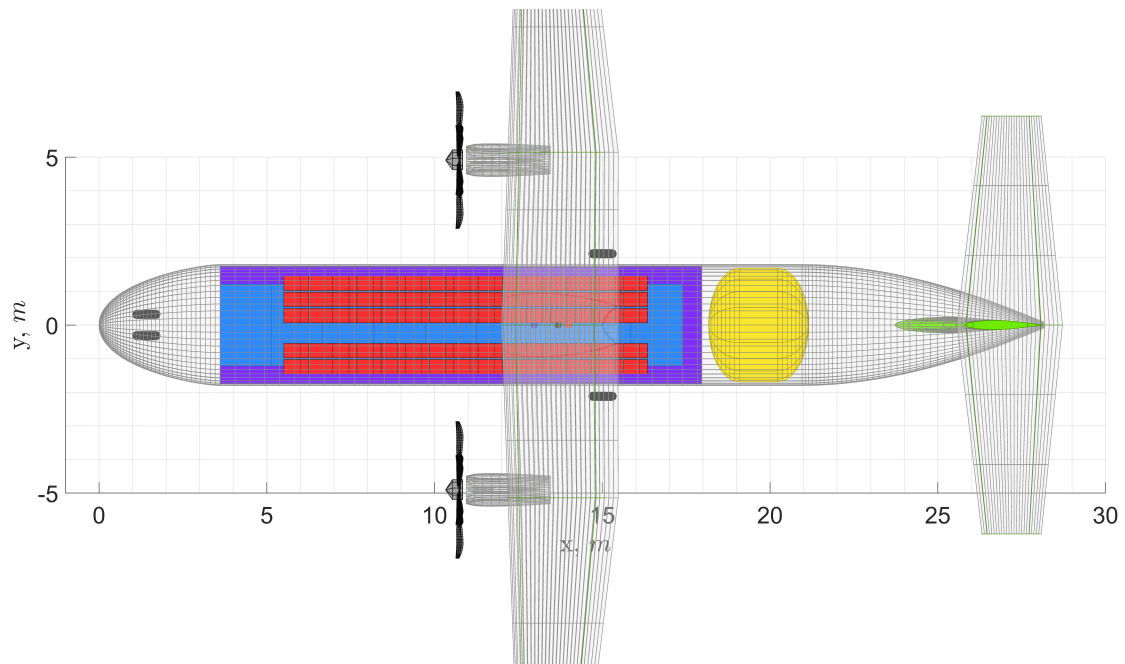


(a) A320LH2(aft-nonintegral-232)

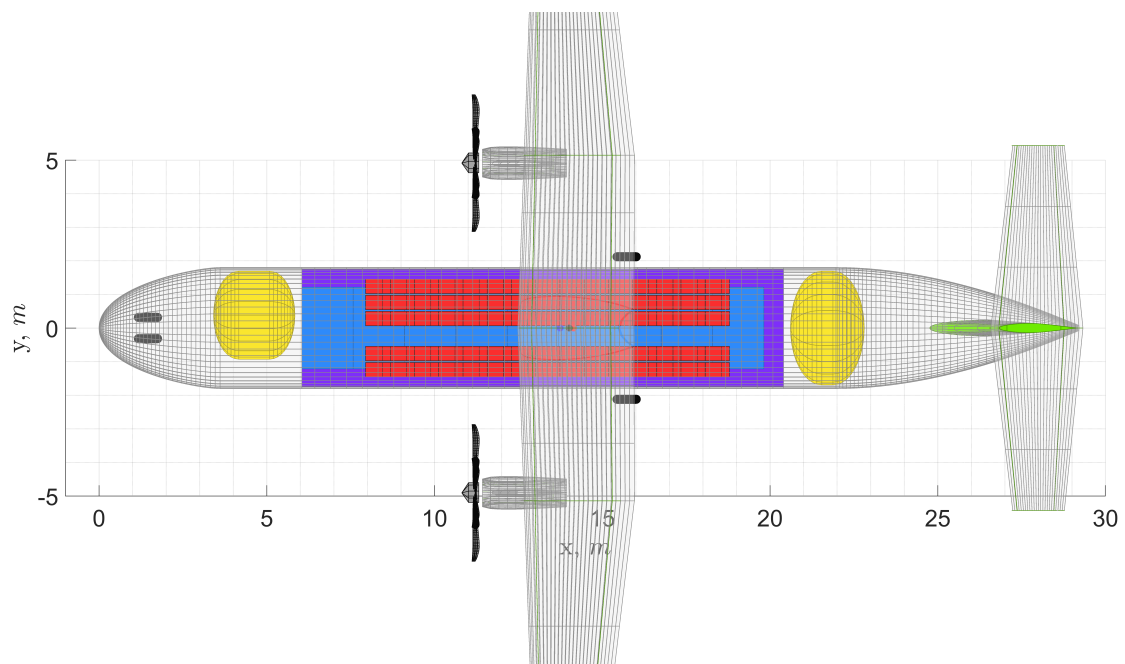


(b) A320LH2(aftFwd-nonintegral-232)

Figure 4.5: Example of X-plot diagram for LH2 aircraft with aft tank layout (a) and LH2 aircraft with aft & fwd tank layout (b).



(a) ATR72LH2(aft-nonintegral-23)



(b) ATR72LH2(aftFwd-nonintegral-23)

Figure 4.6: Example of LH2 aircraft with aft tank layout (a) vs. LH2 aircraft with aft & fwd tank layout (b). Fuel tanks in yellow.

Table 4.8, Table 4.9 and Table 4.10, present the performance comparison for three aircraft representing the short, medium and long-range aircraft categories respectively.

The addition of a forward tank appears to be detrimental in terms of *OEM*, negligible in terms of *MTOM* and beneficial in terms of *SEC* for the medium and long-range aircraft. For the short-range aircraft, *OEM* and *MTOM* remains equal, while the *SEC* improves slightly.

Table 4.8: Performance comparison between short-range aircraft featuring an aft tank layout and an aft & fwd tank layout.

Parameters	ATR72	
Tank structure	non-integral	
Seats abreast EC	2-3	
Cryotank layout	aft	aft & fwd
Cryotank shape	non-spherical	
P_{vent} (kPa)	300	
Direct venting	No	
m_{tank} (kg) (aft+fwd)	438	479 (+9.4%)
η_{grav} (aft+fwd)	0.415	0.457 (+10.1%)
l_{tank} (m) (aft + fwd)	2.98	4.62 (+55%)
l_{fus} (m)	28.2	29.2 (+3.5%)
m_{fus} (t)	3.93	4.15 (+5.6%)
$C_{D_{0,fus}}$	0.0065	0.0067 (+3.1%)
$\Delta x_{c.g.}$	0.357	0.139 (-61.1%)
S_h/S	0.348	0.266 (-23.6%)
m_{ht} (t)	0.54	0.29 (-46.3%)
$C_{D_{0,ht}}$	0.0024	0.0019 (-20.8%)
C_{D_0}	0.0206	0.0203 (-1.5%)
$L/D_{mid-cruise}$	19.9	20.1 (+1%)
<i>OEM</i> (t)	18.42	18.41 (-0.1%)
<i>MTOM</i> (t)	27.03	27.01 (-0.1%)
<i>SEC</i> (J/pax/m)	862	852.5 (-1.1%)
Input file name	ATR72LH2 (aft-nonintegral-23)	ATR72LH2 (aftFwd-nonintegral-33)

Table 4.9: Performance comparison between medium-range aircraft featuring an aft tank layout and an aft & fwd tank layout.

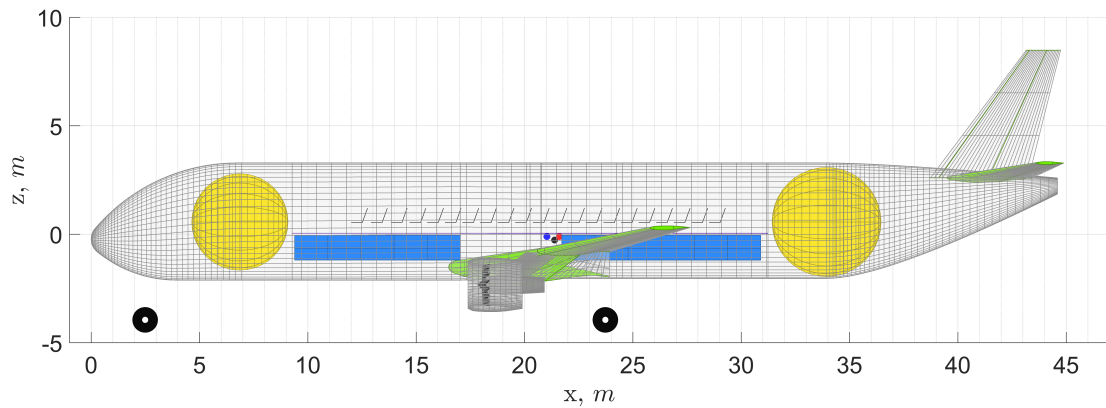
Parameters	A320	
Tank structure	non-integral	
Seats abreast EC	2-3-2	
Cryotank layout	aft	aft & fwd
Cryotank shape	non-spherical	
P_{vent} (kPa)	300	
Direct venting	No	
m_{tank} (kg) (aft+fwd)	2049	2057 (+0.4%)
η_{grav} (aft+fwd)	0.322	0.334 (+3.7%)
l_{tank} (m) (aft + fwd)	8.05	10.17 (+26.3%)
l_{fus} (m)	44	46.1 (+4.8%)
m_{fus} (t)	12.2	13.85 (+13.5%)
$C_{D_{0,fus}}$	0.0078	0.008 (+2.6%)
$\Delta x_{c.g.}$	0.518	0.137 (-73.6%)
S_h/S	0.418	0.23 (-45%)
m_{ht} (t)	2.32	1.17 (-49.6%)
$C_{D_{0,ht}}$	0.0031	0.0018 (-41.9%)
C_{D_0}	0.0233	0.0221 (-5.2%)
$L/D_{mid-cruise}$	15.7	16.4 (+4.5%)
OEM (t)	51.65	52.45 (+1.5%)
MTOM (t)	77.31	77.91 (+0.8%)
SEC (J/pax/m)	912.3	883.6 (-3.1%)
Input file name	A320LH2 (aft-nonintegral-232)	A320LH2 (aftFwd-nonintegral-332)

Table 4.10: Performance comparison between long-range aircraft featuring an aft tank layout and an aft & fwd tank layout.

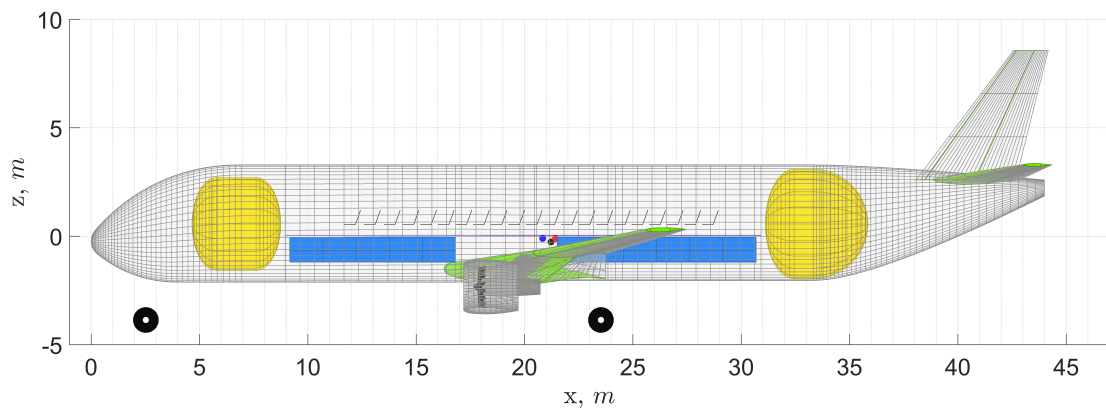
Parameters	A330	
Tank structure	non-integral	
Seats abreast EC	3-4-3	
Cryotank layout	aft	aft & fwd
Cryotank shape	non-spherical	
P_{vent} (kPa)	300	
Direct venting	No	
m_{tank} (kg) (aft+fwd)	8054	7947 (-1.3%)
η_{grav} (aft+fwd)	0.284	0.29 (+2.1%)
l_{tank} (m) (aft + fwd)	19.03	22 (+15.6%)
l_{fus} (m)	79.7	82.7 (+3.8%)
m_{fus} (t)	43.73	48.77 (+11.5%)
$C_{D_{0,fus}}$	0.0051	0.0052 (+2%)
$\Delta x_{c.g.}$	0.535	0.126 (-76.4%)
S_h/S	0.266	0.108 (-59.4%)
m_{ht} (t)	4.65	1.69 (-63.7%)
$C_{D_{0,ht}}$	0.0019	0.0008 (-57.9%)
C_{D_0}	0.0183	0.0173 (-5.5%)
$L/D_{mid-cruise}$	18.7	19.5 (+4.3%)
OEM (t)	176.21	178.76 (+1.4%)
MTOM (t)	256.25	257.87 (+0.6%)
SEC (J/pax/m)	1263.8	1221.8 (-3.3%)
Input file name	A330LH2 (aft-nonintegral-343)	A330LH2 (aftFwd-nonintegral-343)

4.5. TANK SHAPE: SPHERICAL VS. NON-SPHERICAL

The use of spherical tanks (see Figure 4.7) would halve the circumferential stresses in the tank structural shell and consequently would reduce the tank mass. On the other side, the spherical shape uses less efficiently the fuselage volume. Most importantly, fitting a single spherical tank could drive the fuselage diameter to extreme values.



(a) A320LH2(aftFwd-nonintegral-spheric)



(b) A320LH2(aftFwd-nonintegral-332)

Figure 4.7: Example of LH2 aircraft with spherical tank shape (a) vs. LH2 aircraft with non-spherical tank shape (b). Fuel tanks in yellow.

As explained in subsection 3.2.2 when using spherical tanks the fuselage diameter (and consequently the seats abreast cabin layout) is determined by the tank's size. The aircraft generated in this fashion are compared with aircraft fitted with non-spherical tanks which feature the same cabin layout. Table 4.8, Table 4.9 and Table 4.10, present the performance comparison for three aircraft representing the short, medium and long-range aircraft categories respectively.

The use of spherical tanks appears to have no effects for the short-range aircraft. The medium-range aircraft benefits from this structurally efficient tank shape, while the long-range aircraft slightly improves the *OEM* and *MTOM* and slightly worsen the *SEC*. Nevertheless, the limitation of this tank shape must be acknowledged. One of these limitations is that in case a design for an aircraft variant with a longer range is desired, a complete redesign is necessary, as the tank cannot grow in size without exceeding the fuselage diameter. Another limitation is that a tank with a spherical shape cannot be made integral.

Table 4.11: Performance comparison between short-range aircraft featuring a spherical and a non-spherical tank shape.

Parameters	ATR72	
Tank structure	non-integral	
Seats abreast EC	2-3	
Cryotank layout	aft	
Cryotank shape	spherical	non-spherical
P_{vent} (kPa)	300	
Direct venting	No	
t_{ins} (mm) (aft)	104	138 (+32.7%)
t_{shell} (mm) (aft)	1.3	2.5 (+92.3%)
m_{tank} (kg) (aft+fwd)	356	438 (+23%)
η_{grav} (aft+fwd)	0.337	0.415 (+23.1%)
r_{tank} (m) (aft)	1.68	1.69 (+0.6%)
l_{tank} (m) (aft + fwd)	3.37	2.98 (-11.6%)
l_{fus} (m)	28.6	28.2 (-1.4%)
m_{fus} (t)	4.04	3.93 (-2.7%)
$C_{D_{0,fus}}$	0.0066	0.00652 (-1.2%)
OEM (t)	18.44	18.42 (-0.1%)
$MTOM$ (t)	27.04	27.03 (-0%)
SEC (J/pax/m)	861.9	862 (0%)
Input file name	ATR72LH2	ATR72LH2
	(aft-nonintegral-spheric)	(aft-nonintegral-23)

Table 4.12: Performance comparison between medium-range aircraft featuring a spherical and a non-spherical tank shape.

Parameters	A320	
Tank structure	non-integral	
Seats abreast EC	3-3-2	
Cryotank layout	aft & fwd	
Cryotank shape	spherical	non-spherical
P_{vent} (kPa)	300	
Direct venting	No	
t_{ins} (mm) (aft)	92	119 (+29.3%)
t_{shell} (mm) (aft)	2	3.9 (+95%)
m_{tank} (kg) (aft+fwd)	1554	2123 (+36.6%)
η_{grav} (aft+fwd)	0.249	0.336 (+34.9%)
r_{tank} (m) (aft)	2.51	2.52 (+0.4%)
l_{tank} (m) (aft + fwd)	9.46	8.83 (-6.7%)
l_{fus} (m)	44.6	44 (-1.3%)
m_{fus} (t)	13.77	13.39 (-2.8%)
$C_{D_{0,fus}}$	0.00851	0.00834 (-2%)
OEM (t)	52.22	52.66 (+0.8%)
$MTOM$ (t)	77.76	78.29 (+0.7%)
SEC (J/pax/m)	895.1	909.9 (+1.7%)
Input file name	A320LH2 (aftFwd-nonintegral-spheric)	A320LH2 (aftFwd-nonintegral-332)

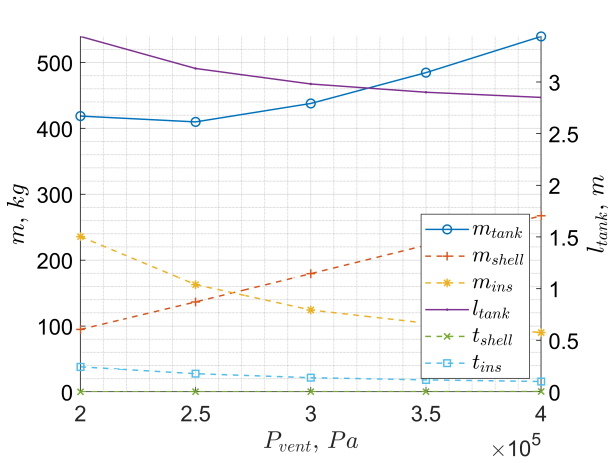
Table 4.13: Performance comparison between long-range aircraft featuring a spherical and a non-spherical tank shape.

Parameters	A330	
Tank structure	non-integral	
Seats abreast EC	2-3-5-3	
Cryotank layout	aft & fwd	
Cryotank shape	spherical	non-spherical
P_{vent} (kPa)	300	
Direct venting	No	
t_{ins} (mm) (aft)	83	109 (+31.3%)
t_{shell} (mm) (aft)	3.3	6.7 (+103%)
m_{tank} (kg) (aft+fwd)	6332	8979 (+41.8%)
η_{grav} (aft+fwd)	0.216	0.307 (+42.1%)
r_{tank} (m) (aft)	4.13	4.21 (+1.9%)
l_{tank} (m) (aft + fwd)	15.52	13.33 (-14.1%)
l_{fus} (m)	72.7	70.4 (-3.2%)
m_{fus} (t)	47.31	44.58 (-5.8%)
$C_{D_{0,fus}}$	0.00625	0.00604 (-3.4%)
OEM (t)	186.38	187.5 (+0.6%)
MTOM (t)	267.46	268.48 (+0.4%)
SEC (J/pax/m)	1311	1306.4 (-0.4%)
Input file name	A330LH2	A330LH2
	(aftFwd-nonintegral-spheric)	(aftFwd-nonintegral-2353)

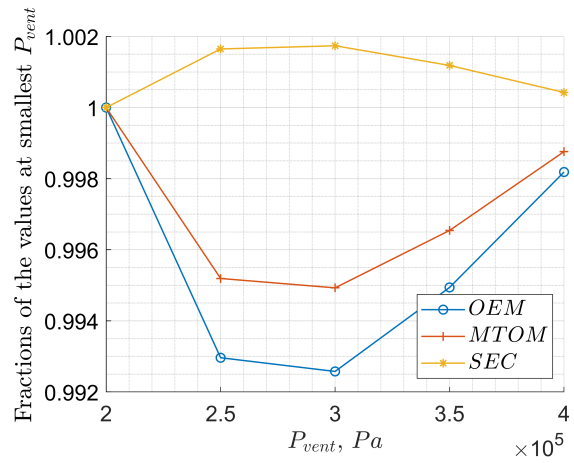
4.6. VENTING PRESSURE: LOW VS. HIGH

Another parameter of the tank design whose choice could affect the aircraft performance is the venting pressure. A lower venting pressure requires a lower structural shell thickness, but a larger insulation thickness. These thicknesses directly translate into the insulation and the structural shell masses. The insulation thickness, being at least an order of magnitude larger than the structural shell thickness, is among the two, the driver of the tank length (see Figure 3.3b). The optimal venting pressure is the one that minimises the aircraft main performance parameters and, because the minimum tank length and the minimum tank mass are not found at the same venting pressure (see Figure 4.8), an aircraft level analysis is necessary.

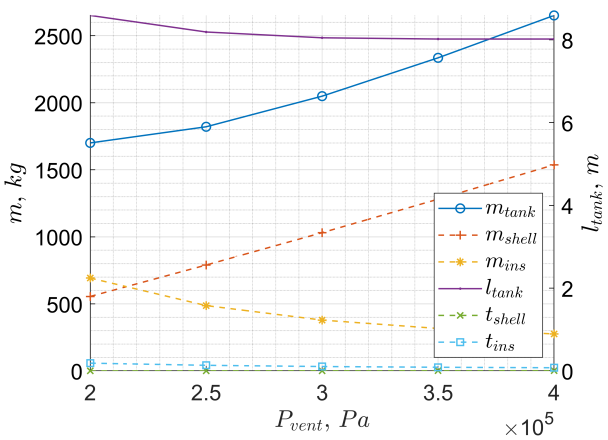
The results of this study on the optimal venting pressure are presented in Figure 4.8. It can be seen that with increasing aircraft size the optimal venting pressure decreases and the sensitivity of the main aircraft performance parameters to the choice of the venting pressure increases. For all the aircraft categories, the optimal venting pressure is higher than the venting pressure for minimum tank mass.



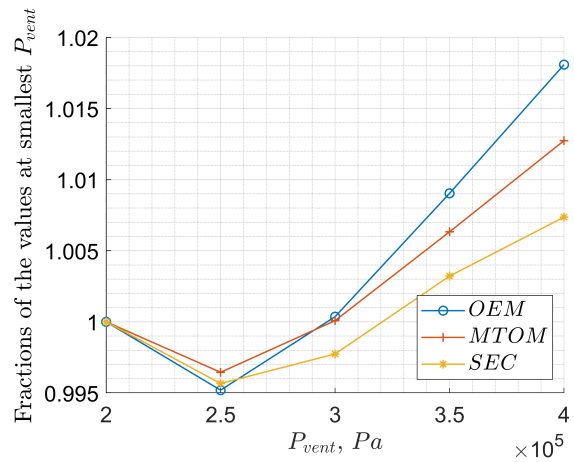
(a) ATR72, tank level



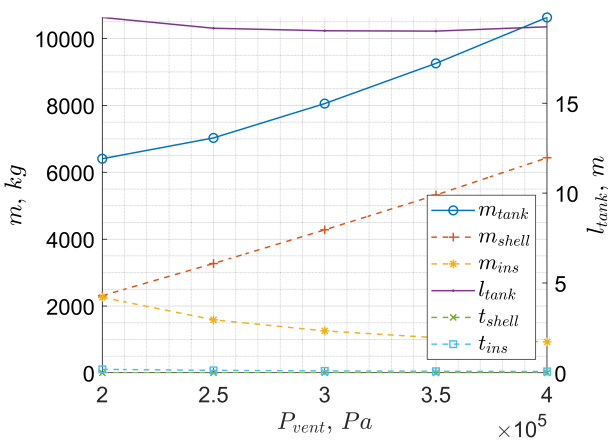
(b) ATR72, aircraft level



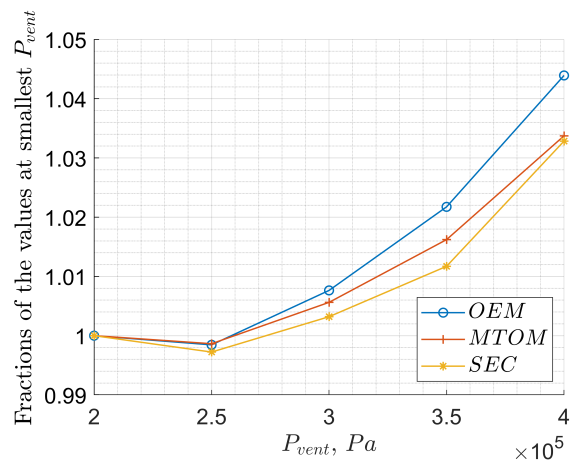
(c) A320, tank level



(d) A320, aircraft level



(e) A330, tank level



(f) A330, aircraft level

Figure 4.8: Effect of venting pressure at tank and aircraft level. Tank structure: non-integral. Tank shape: non-spherical. Tank layout: aft. Seats abreast: 2-3 (ATR72), 2-3-2 (A320), 3-4-3 (A330).

4.7. PRESSURE CONTROL OPTIONS: GAS VENTING VS. NO GAS VENTING

The insulation thickness required by the tank can be reduced by allowing part of the fuel to be vented while in the gaseous phase. This process could be particularly interesting when applied in the final phases of the extended flight mission (see subsection 3.2.2), which the tanks of the aircraft in this research are designed for.

Table 4.14, Table 4.15 and Table 4.16, present the performance comparison for three aircraft representing the short, medium and long-range aircraft categories respectively.

For all the aircraft representing the three aircraft categories, negligible benefits are observed in *OEM* and *MTOM*. The *SEC*, on the contrary, increases. Note that the *SEC* includes the energy lost in the vented fuel. The fuel actually burned ($m_{fuel_{burned}}$) is in reality minimally decreasing. Considering that the fuel venting would not be necessary during the aircraft regular missions (without alternative cruise or hold period), and that the venting system is in any case installed on the aircraft, the direct venting option could lead to minimal improvements in all three main aircraft performance parameters. Remember that once the aircraft is at the gate, after landing, the remaining fuel can be fed back to the airport facilities for reliquefaction.

Figure 4.9, Figure 4.10, Figure 4.11 show the pressure profiles for the venting case without and with venting for the aircraft representing the three aircraft categories respectively. Note that during the venting phases the pressure is not constant. This happens because the vented mass flow is set a priori, to save the computational time from an otherwise necessary iteration loop wrapping the entire tank sizing module.

Table 4.14: Performance comparison between short-range aircraft using no direct gas venting and using direct gas venting.

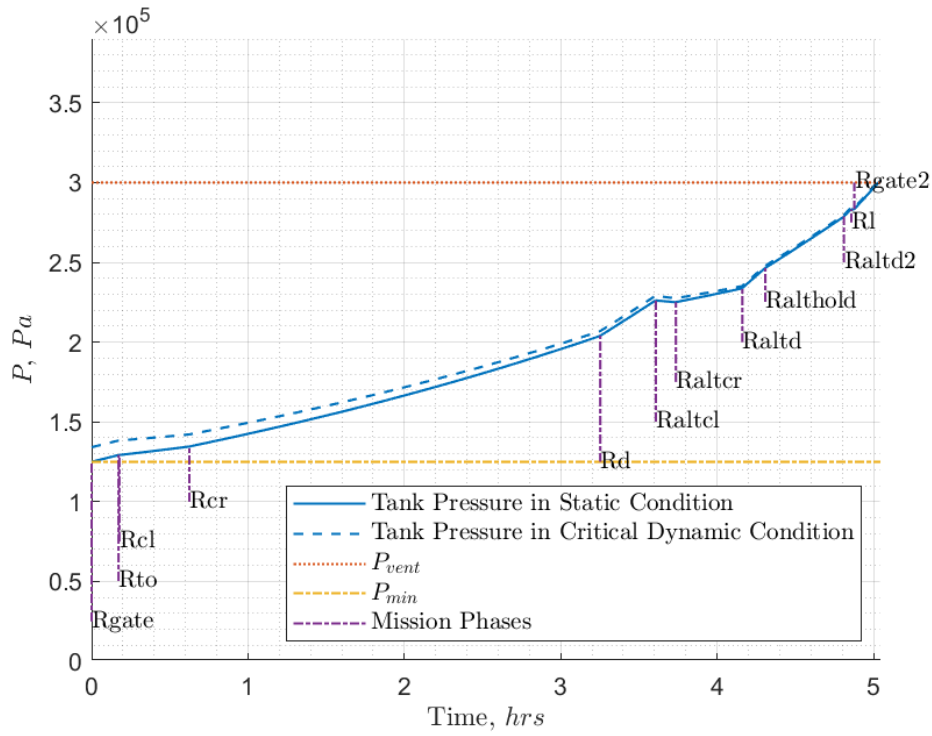
Parameters	ATR72	
Tank structure	non-integral	
Seats abreast EC	2-3	
Cryotank layout	aft	
Cryotank shape	non-spherical	
P_{vent} (kPa)	300	
Direct venting	No	Yes
t_{ins} (kg)	138	102 (-26.1%)
m_{ins} (kg)	124	91 (-26.6%)
m_{vented} (kg)	0	16
m_{tank} (kg)	438	429 (-2.1%)
l_{tank} (m)	2.98	2.84 (-4.7%)
$m_{fuelBurned}$ (kg)	1048	1046 (-0.2%)
<i>OEM</i> (t)	18.42	18.36 (-0.3%)
<i>MTOM</i> (t)	27.03	26.96 (-0.3%)
<i>SEC</i> (J/pax/m)	862	880 (2.1%)
Input file name	ATR72LH2	ATR72LH2
	(aft-nonintegral-23)	(aft-nonintegral-23-dirvent)

Table 4.15: Performance comparison between medium-range aircraft using no direct gas venting and using direct gas venting.

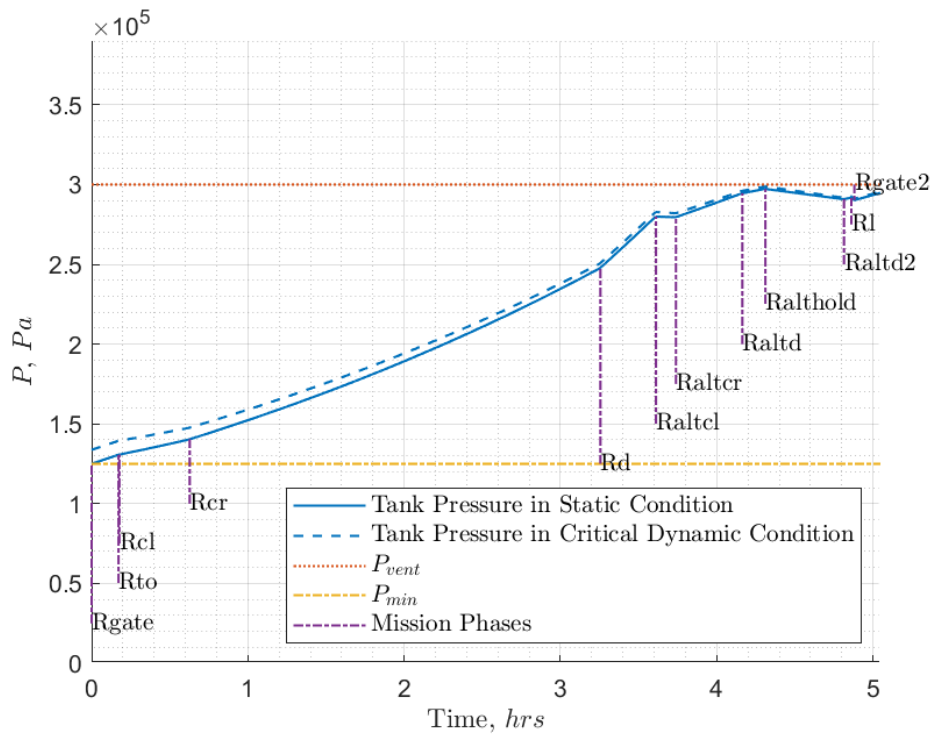
Parameters		A320
Tank structure		non-integral
Seats abreast EC		2-3-2
Cryotank layout		aft
Cryotank shape		non-spherical
P_{vent} (kPa)		300
Direct venting	No	Yes
t_{ins} (kg)	106	89 (-16%)
m_{ins} (kg)	379	316 (-16.6%)
m_{vented} (kg)	0	48
m_{tank} (kg)	2049	2050 (0%)
l_{tank} (m)	8.05	7.97 (-1%)
$m_{fuelBurned}$ (kg)	6414	6413 (-0%)
OEM (t)	51.65	51.57 (-0.2%)
MTOM (t)	77.31	77.23 (-0.1%)
SEC (J/pax/m)	912.3	920.4 (+0.9%)
Input file name	A320LH2	A320LH2
	(aft-nonintegral-232)	(aft-nonintegral-232-dirvent)

Table 4.16: Performance comparison between long-range aircraft using no direct gas venting and using direct gas venting.

Parameters		A330
Tank structure		non-integral
Seats abreast EC		3-4-3
Cryotank layout		aft
Cryotank shape		non-spherical
P_{vent} (kPa)		300
Direct venting	No	Yes
t_{ins} (kg)	113	102 (-9.7%)
m_{ins} (kg)	1257	1132 (-9.9%)
m_{vented} (kg)	0	98
m_{tank} (kg)	8054	8052 (-0%)
l_{tank} (m)	19.03	18.88 (-0.8%)
$m_{fuelBurned}$ (kg)	28560	28538 (-0.1%)
OEM (t)	176.21	175.94 (-0.2%)
MTOM (t)	256.25	255.97 (-0.1%)
SEC (J/pax/m)	1263.8	1268.7 (0.4%)
Input file name	A330LH2	A330LH2
	(aft-nonintegral-343)	(aft-nonintegral-343-dirvent)

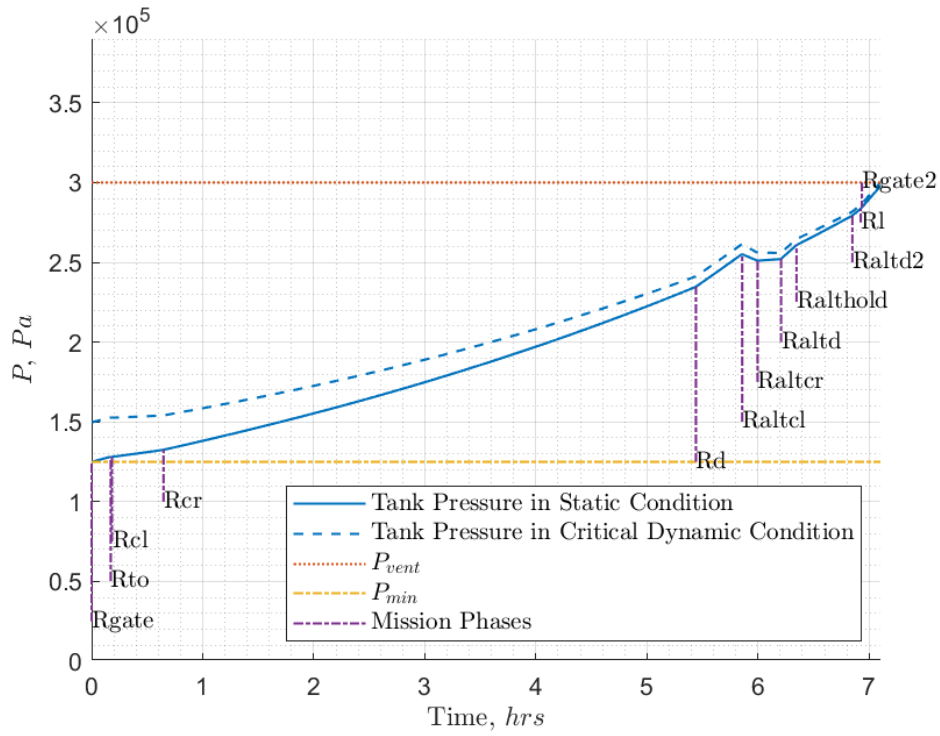


(a) ATR72LH2(aft-nonintegral-23)

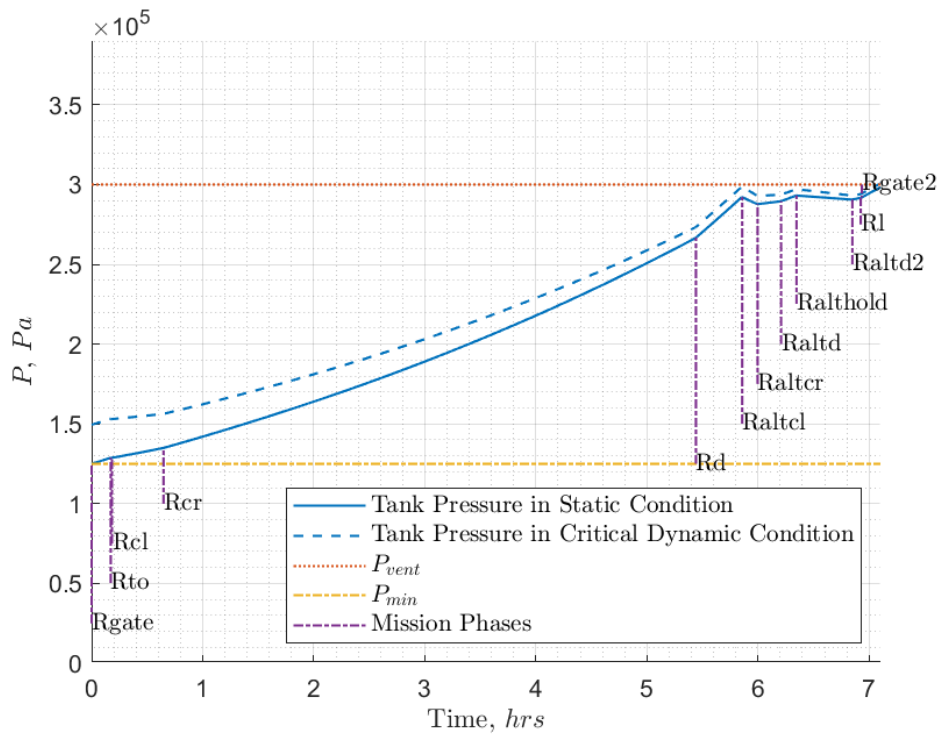


(b) ATR72LH2(aft-nonintegral-dirvent)

Figure 4.9: Pressure profiles of short-range LH2 aircraft not using direct gas venting (a) and LH2 aircraft using direct gas venting (b).

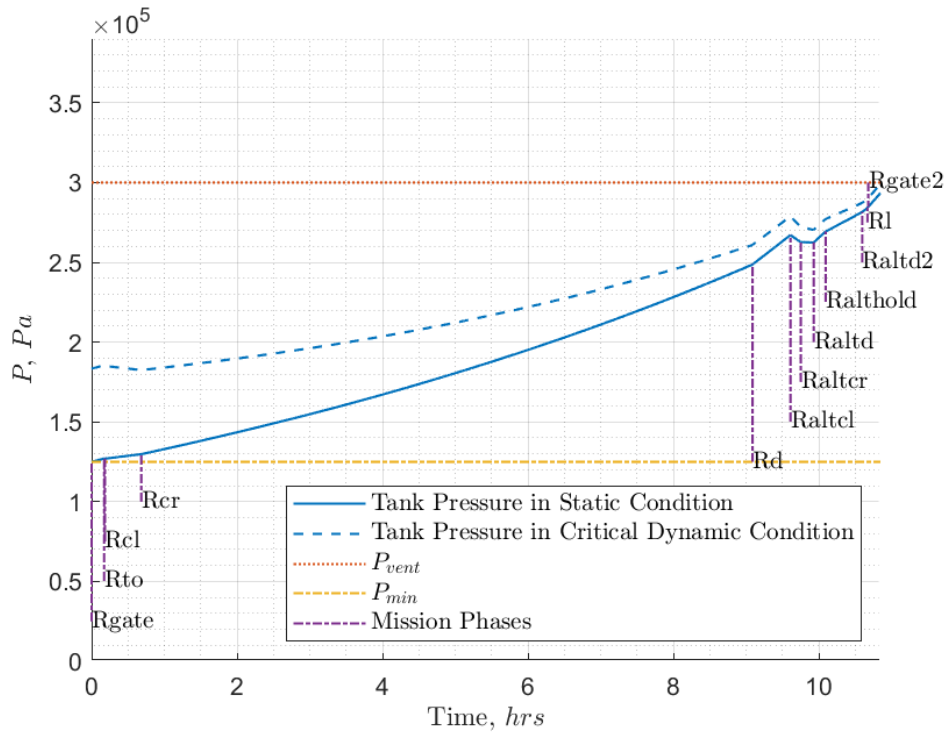


(a) A320LH2(aft-nonintegral-232)

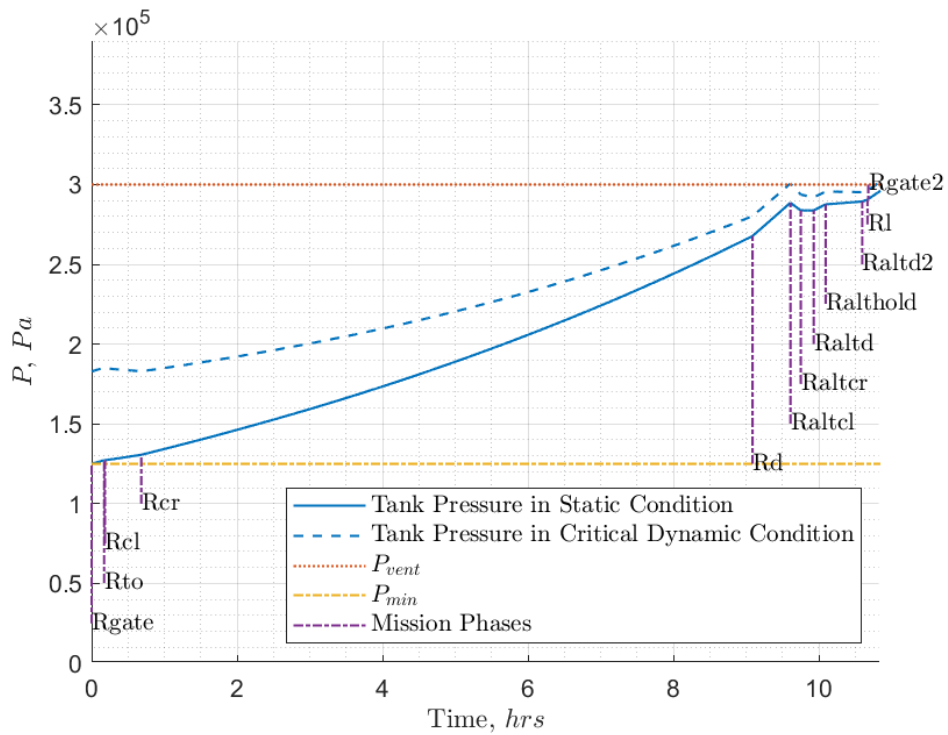


(b) A320LH2(aft-nonintegral-dirvent)

Figure 4.10: Pressure profiles of medium-range LH2 aircraft not using direct gas venting (a) and LH2 aircraft using direct gas venting (b).



(a) A330LH2(aft-nonintegral-343)



(b) A330LH2(aft-nonintegral-343-dirvent)

Figure 4.11: Pressure profiles of long-range LH2 aircraft not using direct gas venting (a) and LH2 aircraft using direct gas venting (b).

4.8. OPTIMAL DESIGNS & COMPARISON TO BASELINES

In this section, the insights gained from the previously described studies on the several design options are used to generate the optimal aircraft for the three range categories. These LH2 aircraft will then be compared to their kerosene baselines, to quantify their relative performances and identify the causes for the differences.

4.8.1. SHORT-RANGE

For the short-range aircraft, the ATR72, no significant performance differences were found when using an integral tank (see Table 4.2), hence a simpler non-integral tank is selected. A fuselage diameter capable of accommodating 6 seats abreast was found to be beneficial (see Table 4.5). The large drag reduction potential of the aft & fwd tank layout was noted in Table 4.8. The non-spherical tank shape is selected, given the results of Table 4.11. The optimal venting pressure of 300 *kPa* (see Figure 4.8a) is selected. The option to use direct gas venting is not chosen, because the performance gains on the aircraft masses were minor (see Table 4.14), and the impact on the energy used is difficult to determine. Indeed, while the burned mass itself would be slightly reduced and the non-vented gas in case of a regular mission could be reliquefied, the efficiency of the reliquefaction is, in this research not considered.

The LH2 aircraft generated combining these design options is here compared to its kerosene baseline. In terms of the aircraft main performance parameters, the LH2 version has 8% higher *OEM*, 1.5% lower *MTOM* and 5% higher *SEC*.

The higher *OEM* is a consequence of the addition of the 478 *kg* of m_{tank} , the 129% higher $m_{fuelSys}$, the 7% higher m_{ht} , the 14% higher m_{fus} , and 9% higher m_{wing} . The larger m_{fus} is caused by the 7% higher r_{fus} and 7% higher l_{fus} (see also Figure 4.12 and Figure 4.13). The larger m_{wing} is caused by the 4% larger S , in turn a consequence of the 5% lower W/S . The reduction in W/S is dictated by the landing performance (see Figure 4.14), which suffer from the higher *MLM*. The larger m_{ht} is a direct consequence of the 9% higher S_h/S and the larger S . To understand why a larger S_h/S is required despite a 25% lower $\Delta x_{c.g.}$ (see also Figure 4.15), the X-plots in Figure 4.16 come in assistance. Comparing the X-plots of the two aircraft we noticed that the "Stability" lines have similar slopes and horizontal-axis crossing points, whereas the "Equilibrium landing" lines for the LH2 version are shifted to the right. This shift to the right is the source of the increase in required S_h/S and it is caused by a larger negative value of the zero-lift pitching moment coefficient for the aircraft without tail. This larger negative value for the pitching moment is mostly due to more effective flaps (approximately 70% contribution) and to a smaller extent to the larger fuselage.

The lower *MTOM* is achieved thanks to the 62% lower *FM*. The higher *SEC* is caused by a combination of increased mid-cruise aircraft mass and 2.5% lower $L/D_{mid-cruise}$. The lower $L/D_{mid-cruise}$ is a consequence of the 3% higher C_{D_0} , mitigated by a reduction in trim drag. The first is caused by the 8% higher $C_{D_{0,ht}}$ and the 8% higher $C_{D_{0,fus}}$, which are a direct consequence of their increased geometrical sizes. The second is a consequence of the lower $\Delta x_{c.g.}$.

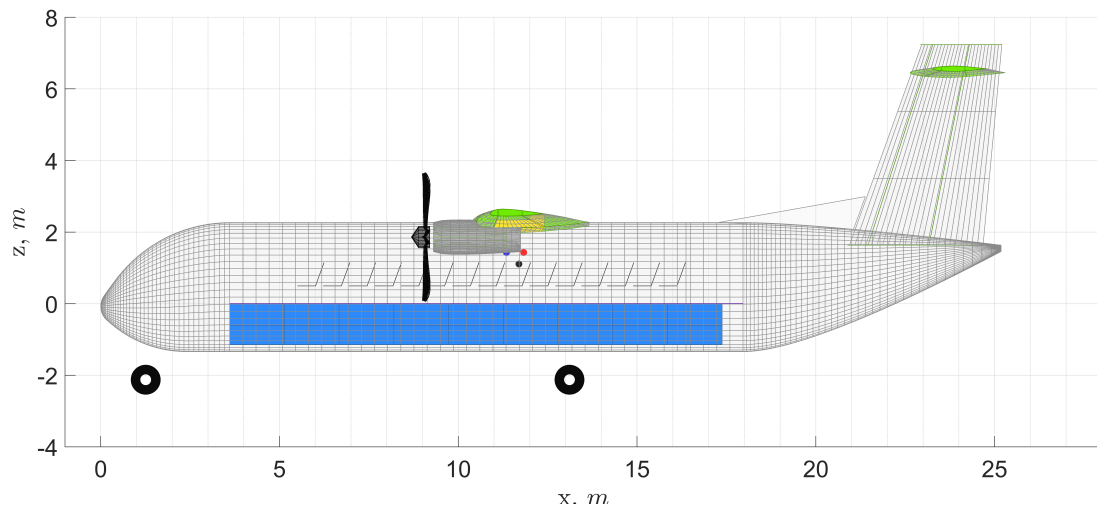
Figure 4.17 shows that for the LH2 version the *OEM* goes from representing 61% to 67% of the *MTOM*, while the *FM* goes from 10% to 4%.

Figure 4.18 shows that for the LH2 version mass of the systems goes from representing 13% to 16% of the *OEM*.

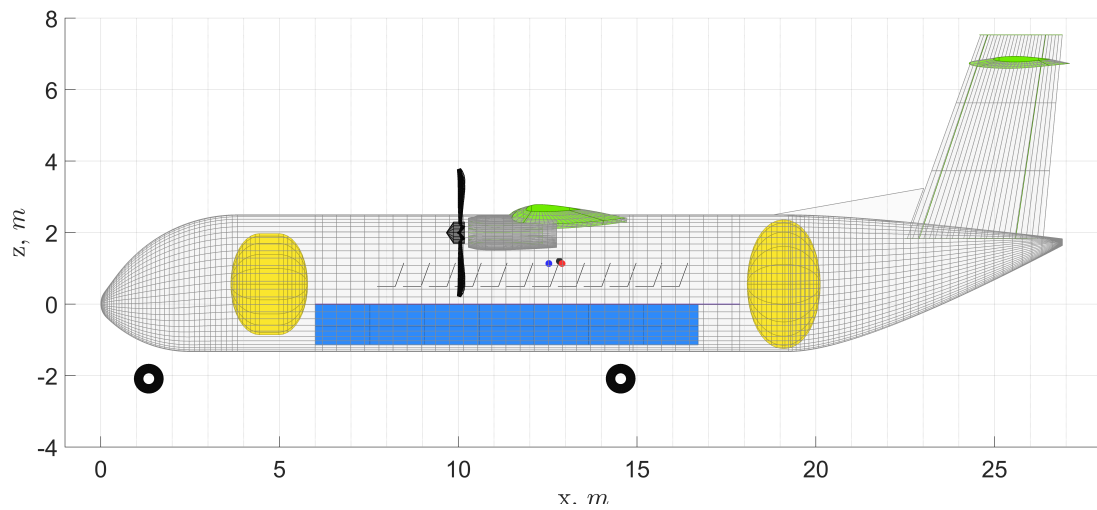
Figure 4.19 shows that for the LH2 version the fuel system mass (including the fuel tanks) goes from representing 11% to 36% of the systems' masses.

Table 4.17: Performance comparison between the optimal LH2 short-range aircraft and its kerosene counterpart.

Parameters	ATR72	
	Kerosene	LH2
Fuel type		
Tank structure	N/A	non-integral
Seats abreast EC	2-3	3-3
Cryotank layout	N/A	aft & fwd
Cryotank shape	N/A	non-spherical
P_{vent} (kPa)	N/A	300
Direct venting	N/A	No
t_{ins} (mm) (aft)	N/A	177
t_{shell} (mm) (aft)	N/A	2.6
m_{tank} (kg) (aft+fwd)	N/A	478
η_{grav} (aft+fwd)	N/A	0.47
r_{tank} (m) (aft)	N/A	1.8
l_{tank} (m) (aft+fwd)	N/A	4.19
$m_{fuelSys}$ (kg)	228	522 (+128.9%)
r_{fus} (m)	1.8	1.92 (+6.7%)
l_{fus} (m)	25.2	26.9 (+6.7%)
Wingspan (m)	31.4	32 (+1.9%)
S (m ²)	82	85 (+3.7%)
W/S (N/m ²)	3147	2982 (-5.2%)
T/W	N/A	N/A
W/P (N/W)	0.0606	0.0574 (-5.3%)
$\Delta x_{c.g.}$	0.176	0.132 (-25%)
S_h/S	0.26	0.282 (+8.5%)
m_{ht} (t)	0.28	0.3 (+7.1%)
m_{fus} (t)	3.23	3.68 (+13.9%)
m_w (t)	2.85	3.11 (+9.1%)
$C_{D_{0,ht}}$	0.0019	0.002 (+7.5%)
$C_{D_{0,fus}}$	0.0064	0.00694 (+8.3%)
C_{D_0}	0.0201	0.02064 (+2.8%)
$L/D_{mid-cruise}$	20.4	19.9 (-2.5%)
FM	2701	1019 (-62.3%)
OEM (t)	16.03	17.32 (+8%)
$MTOM$ (t)	26.28	25.89 (-1.5%)
SEC (J/pax/m)	790.9	830.2 (+5%)
Input file name	ATR72	ATR72LH2
	(23)	(aftFwd-nonintegral-33-300)

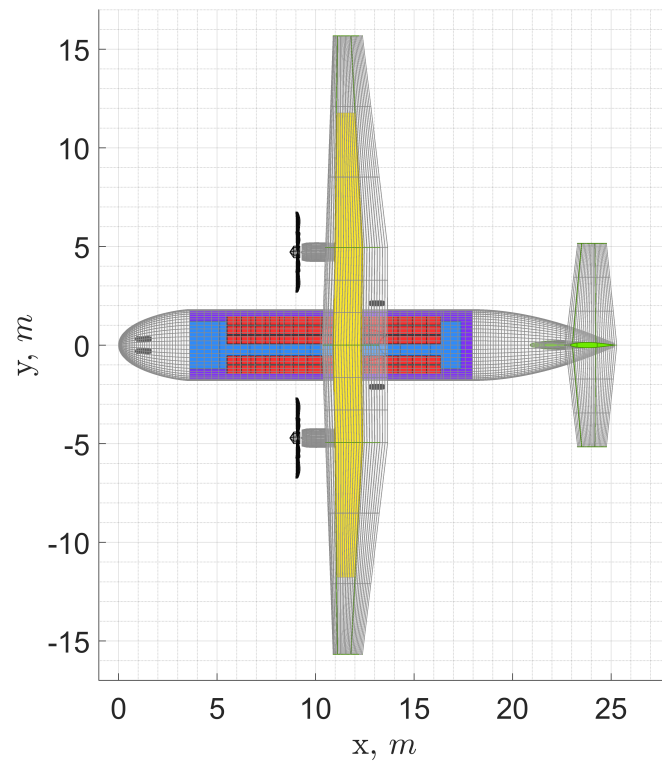


(a) ATR72(23)

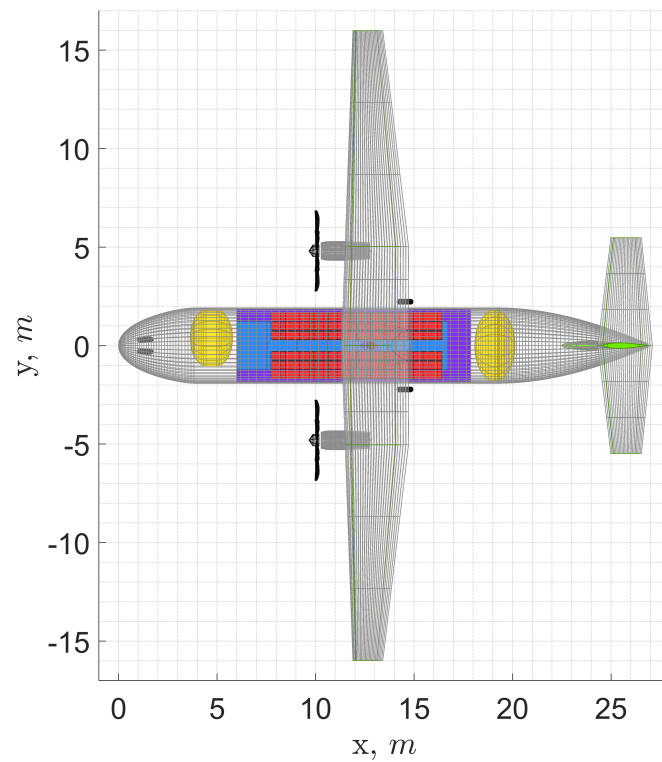


(b) ATR72LH2(aftFwd-nonintegral-33-300)

Figure 4.12: Side views of short-range baseline aircraft (a) and short-range optimal LH2 aircraft (b). Fuel tanks in yellow.

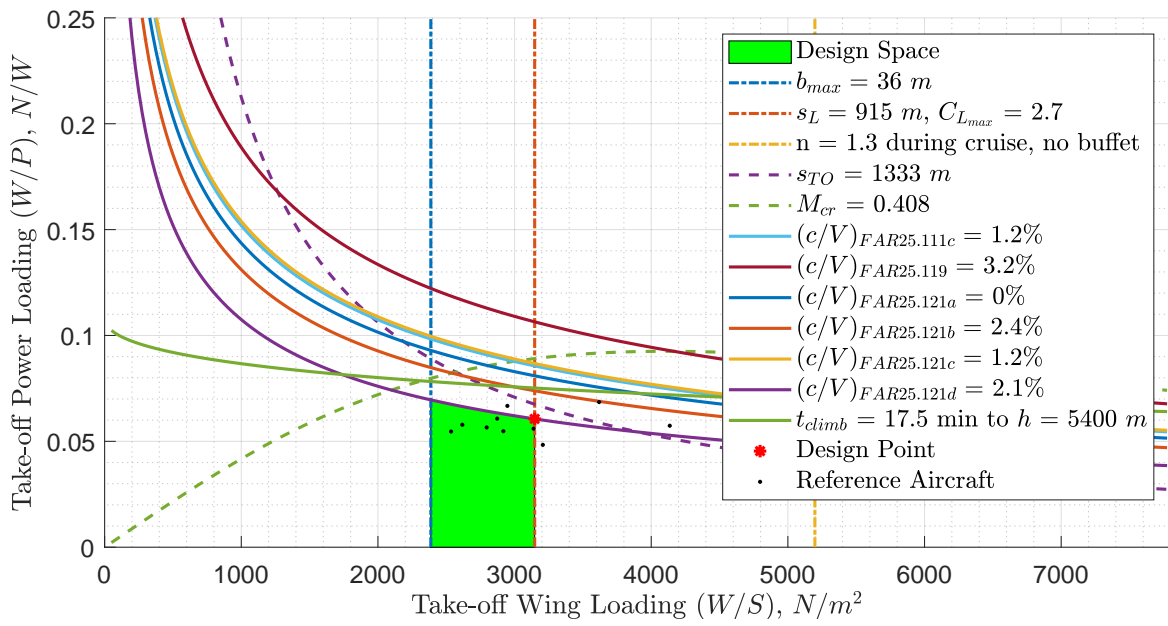


(a) ATR72(23)

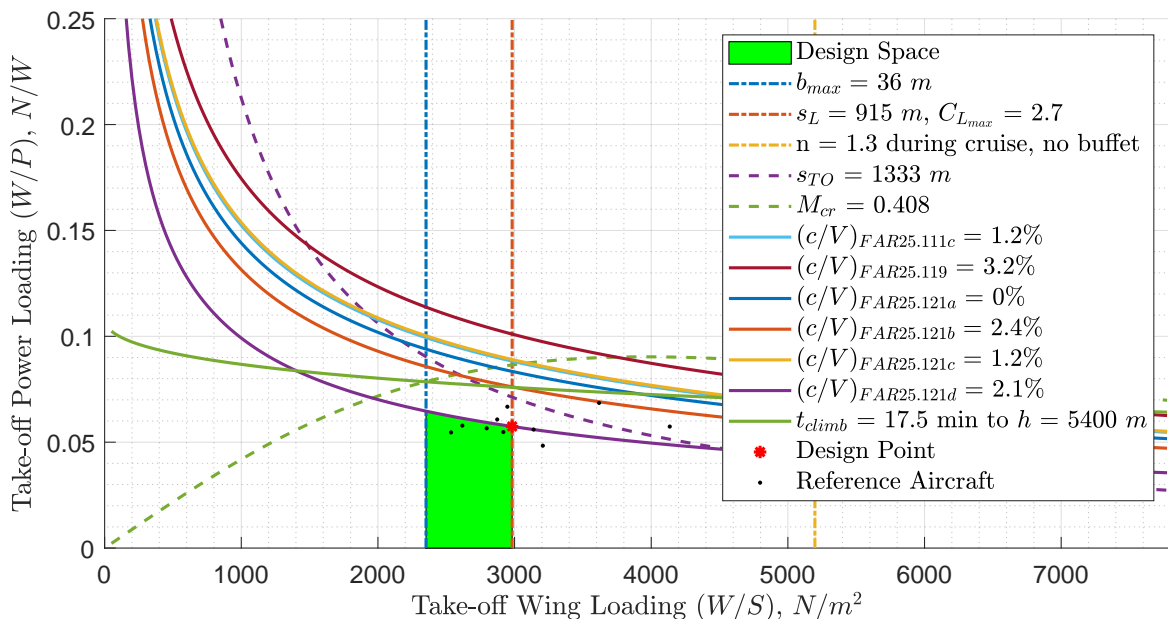


(b) ATR72LH2(aftFwd-nonintegral-33-300)

Figure 4.13: Top views of short-range baseline aircraft (a) and short-range optimal LH2 aircraft (b). Fuel tanks in yellow.

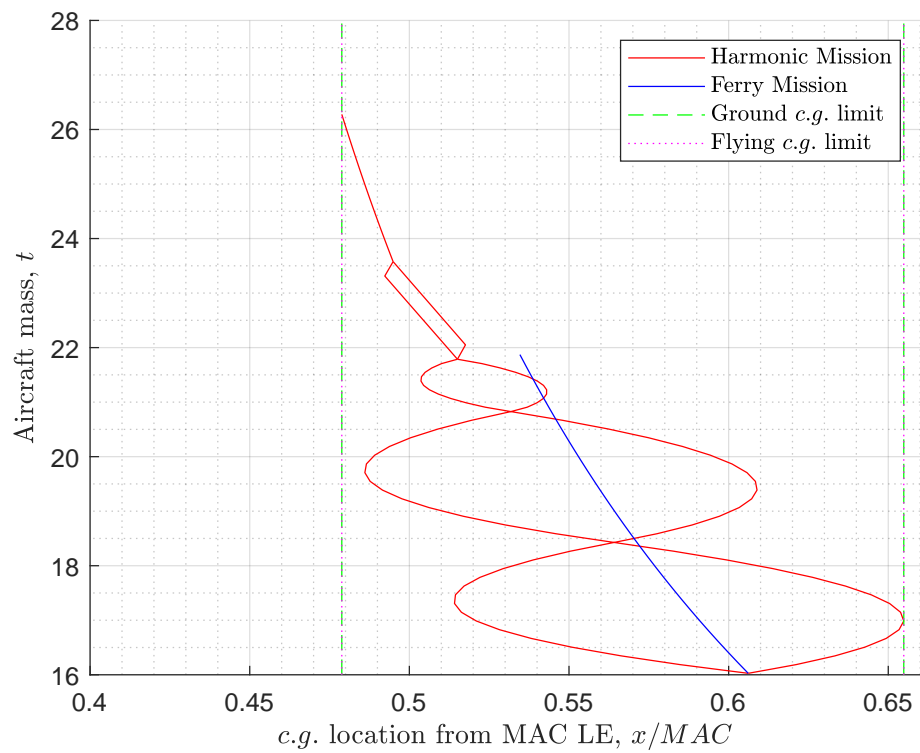


(a) ATR72(23)

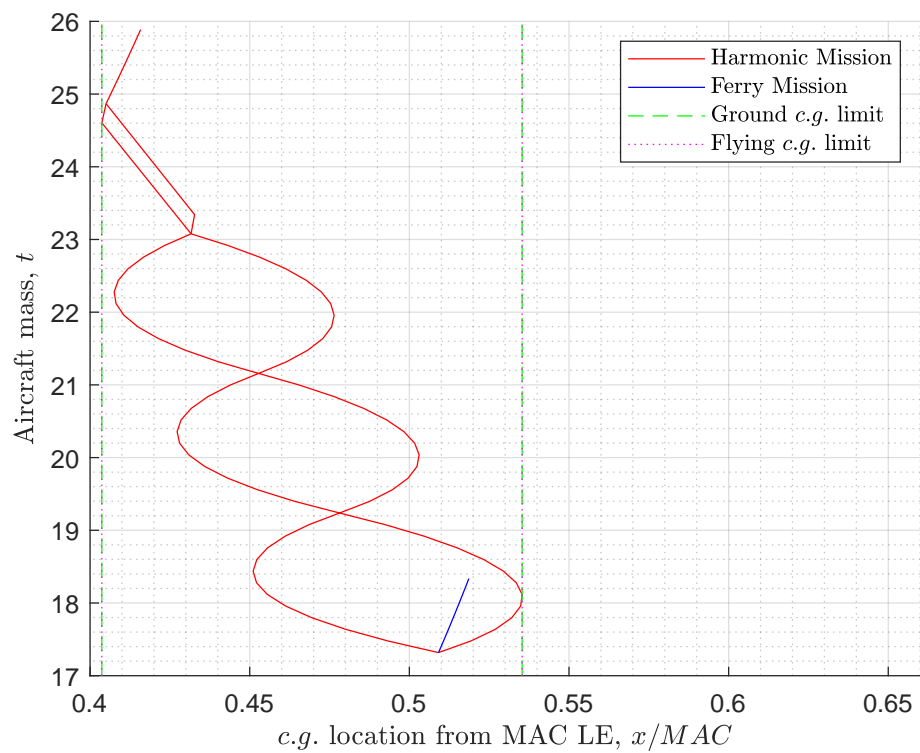


(b) ATR72LH2(aftFwd-nonintegral-33-300)

Figure 4.14: Design point of short-range baseline aircraft (a) and short-range optimal LH2 aircraft (b).

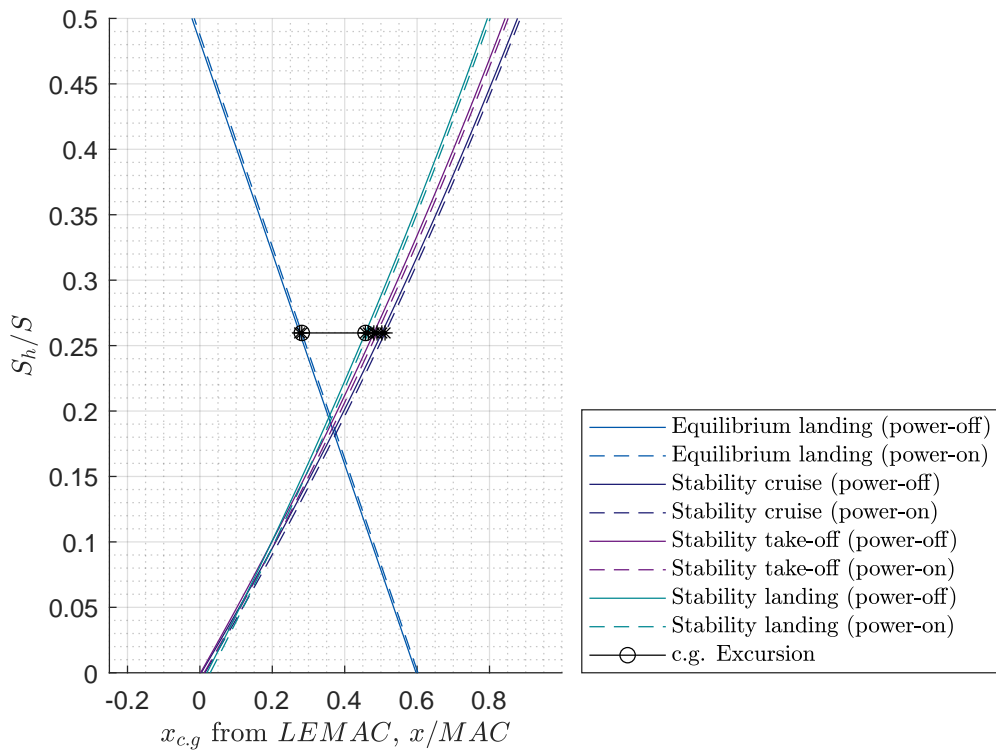


(a) ATR72(23)

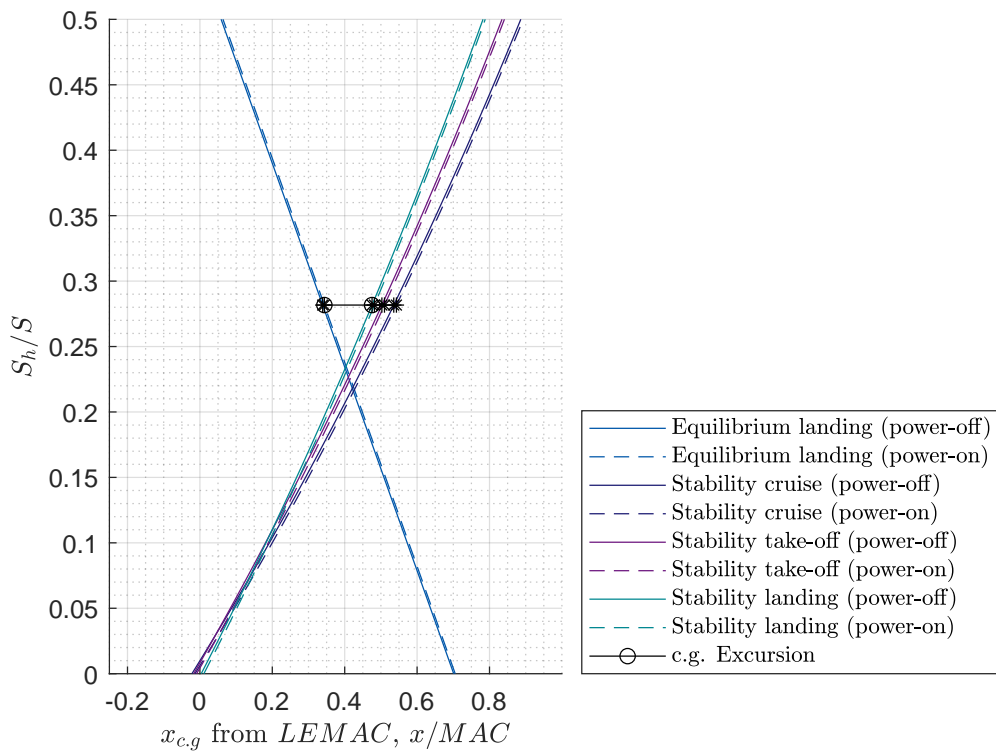


(b) ATR72LH2(aftFwd-nonintegral-33-300)

Figure 4.15: Loading diagram of short-range baseline aircraft (a) and short-range optimal LH2 aircraft (b).



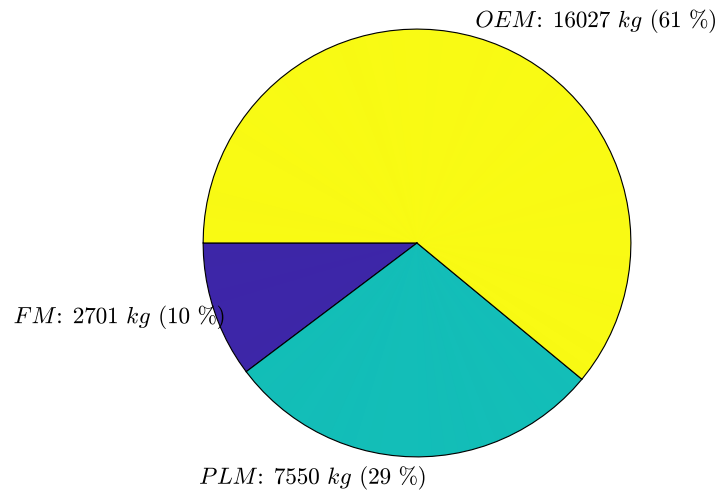
(a) ATR72(23)



(b) ATR72LH2(aftFwd-nonintegral-33-300)

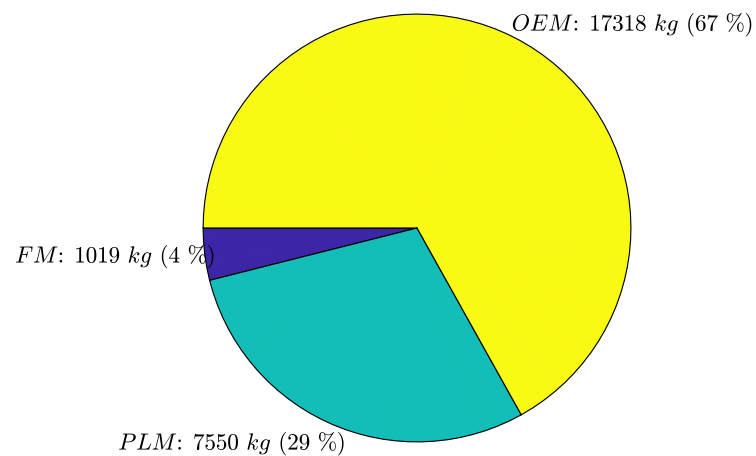
Figure 4.16: Loading diagram of short-range baseline aircraft (a) and short-range optimal LH2 aircraft (b).

$MTOM = 26277 \text{ kg}$
Block Energy (excl. reserve) = 87 GJ



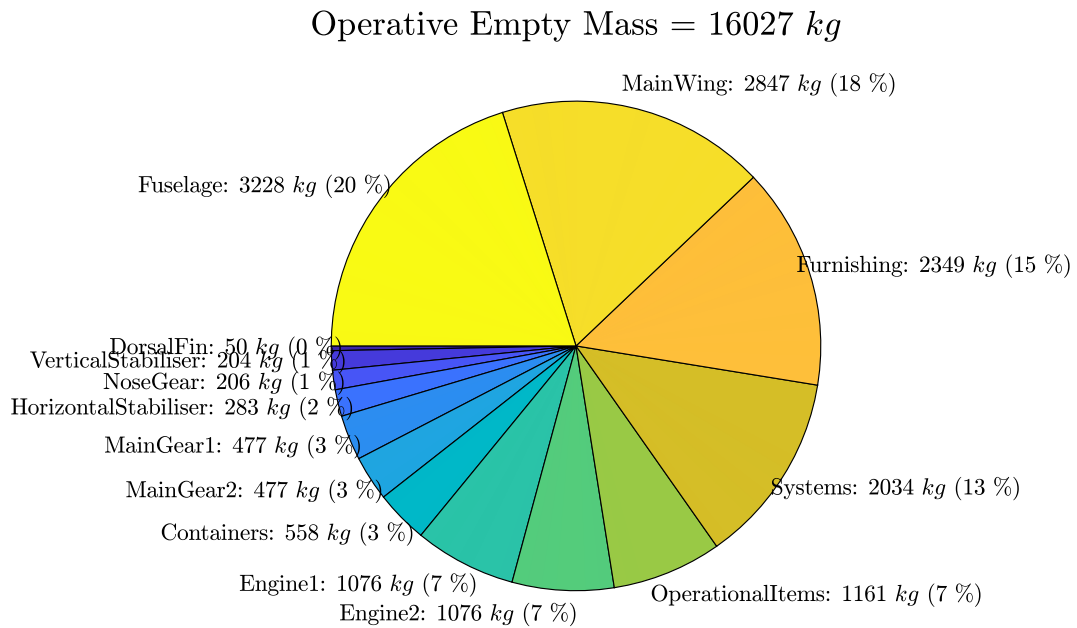
(a) ATR72(23)

$MTOM = 25887 \text{ kg}$
Block Energy (excl. reserve) = 91 GJ

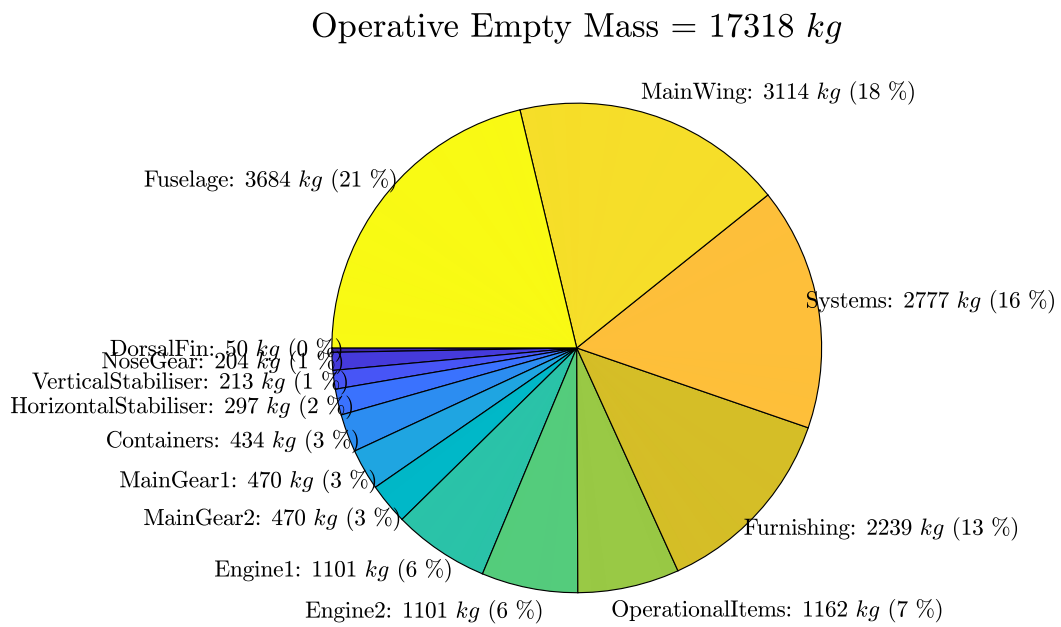


(b) ATR72LH2(aftFwd-nonintegral-33-300)

Figure 4.17: MTOM mass breakdown of short-range baseline aircraft (a) and short-range optimal LH2 aircraft (b).

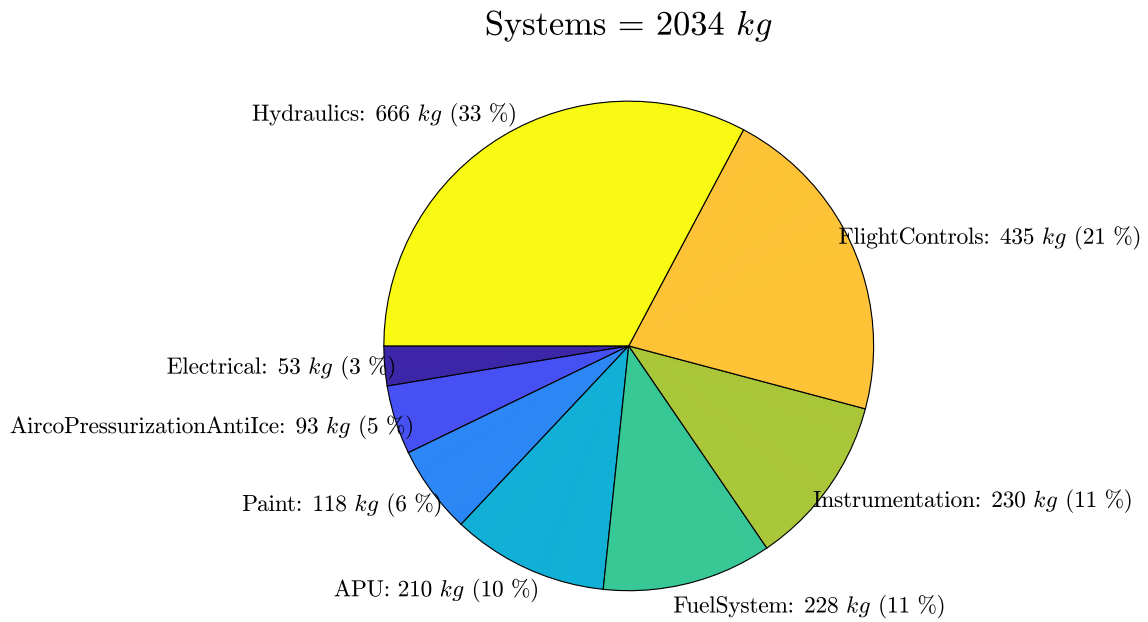


(a) ATR72(23)

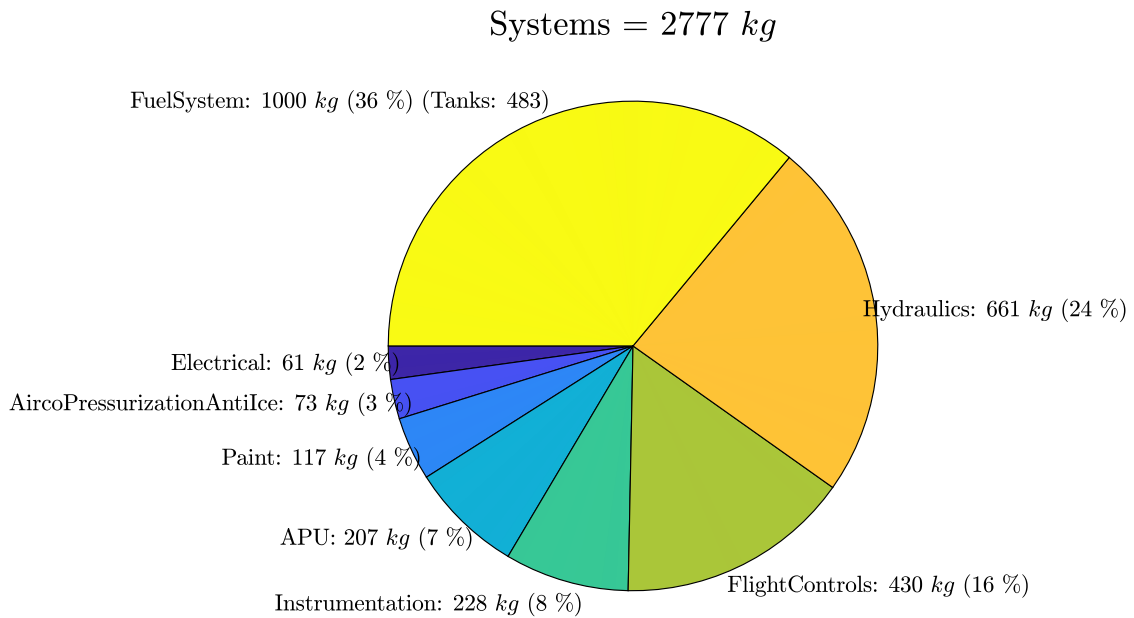


(b) ATR72LH2(aftFwd-nonintegral-33-300)

Figure 4.18: OEM mass breakdown of short-range baseline aircraft (a) and short-range optimal LH2 aircraft (b).



(a) ATR72(23)



(b) ATR72LH2(aftFwd-nonintegral-33-300)

Figure 4.19: Systems mass breakdown of short-range baseline aircraft (a) and short-range optimal LH2 aircraft (b).

4.8.2. MEDIUM-RANGE

For the medium-range aircraft, the A320, half a per cent performance improvements were found when using an integral tank (see Table 4.3), hence the integral tank option is adopted. A fuselage diameter capable of accommodating 8 seats abreast was found to be beneficial (see Table 4.6). The large drag reduction potential of the aft & fwd tank layout was noted in Table 4.9. The non-spherical tank shape is selected, despite Table 4.12 shows the advantages of the spherical tank when non-integral tanks are used, because the non-spherical tank option allows using an integral tank structure, whose benefits more than compensates for the lower performance of the non-spherical tank shape. The optimal venting pressure of 250 kPa (see Figure 4.8c) is selected. The option to use direct gas venting is not chosen, because the performance gains on the aircraft masses were minor (see Table 4.15), and the impact on the energy used is difficult to determine. Indeed, while the burned mass itself would be slightly reduced and the non-vented gas in case of a regular mission could be reliquefied, the efficiency of the reliquefaction is, in this research not considered.

The LH2 aircraft generated combining these design options is here compared to its kerosene baseline. In terms of the aircraft main performance parameters the LH2 version has 24.3% higher *OEM*, 1.3% higher *MTOM* and 13.2% higher *SEC*.

The higher *OEM* is a consequence of the added 2038 kg of m_{tank} , the 181% higher $m_{fuelSys}$, the 26% higher m_{ht} , the 64% higher m_{fus} , and 26% higher m_{wing} . The larger m_{fus} is caused by the 35% higher r_{fus} and 21% higher l_{fus} (see also Figure 4.20 and Figure 4.21). The larger m_{wing} is caused by the 12% larger S , in turn a consequence of the 10% lower W/S and higher *MTOM*. The reduction in W/S is dictated by the approach speed performance (see Figure 4.22), which suffer from the higher *MLM*. The larger m_{ht} is a direct consequence of the 10% higher S_h/S and the larger S . To understand why such a larger S_h/S is required despite a mere 1% larger $\Delta x_{c.g.}$ (see also Figure 4.23), the X-plots in Figure 4.24 come in assistance. Comparing the X-plots of the two aircraft we noticed that the source of the increase in required S_h/S for the LH2 version is the "Stability" lines shift to the left, combined with the "Equilibrium landing" lines shift to the right. The leftward shift of the x-axis crossing point of the stability lines, which corresponds to the aerodynamic centre of the aircraft without tail, is entirely caused by the large increase in fuselage size. The rightward shift of the x-axis crossing point of the controllability lines, which corresponds to the aerodynamic centre of the aircraft without tail minus the ratio between the aerodynamic moment coefficient and the lift coefficient of the aircraft without tail, is caused by a larger negative value of the zero-lift pitching moment coefficient for the aircraft without tail. This larger negative value for the pitching moment is mostly due to the larger fuselage (approximately 80% contribution) and to a smaller extent to the more effective flaps. Worth noting is that the 1% increase in $\Delta x_{c.g.}$ for the LH2 is not caused by an inefficient fuel distribution, but by a more demanding passenger boarding procedure (see Figure 4.23). Indeed, the addition of a second aisle, allows 4 rather than 2 passengers per row to board the aircraft in the first boarding phase (first "bubble" in the loading diagram).

The lower *MTOM* is achieved thanks to the 59% lower *FM*. The higher *SEC* is caused by a combination of increased mid-cruise aircraft mass and 4.7% lower $L/D_{mid-cruise}$. The lower $L/D_{mid-cruise}$ is a consequence of the 10% higher C_{D_0} . The second is caused by the 9% higher $C_{D_{0,m}}$ and the 40% higher $C_{D_{0,fus}}$, which are a direct consequence of their increased geometrical sizes. Note that the trim drag remains almost unvaried, following the negligible change in $\Delta x_{c.g.}$.

Figure 4.25 shows that for the LH2 version the *OEM* goes from representing 54% to 67% of the *MTOM*, while the *FM* goes from 20% to 8%.

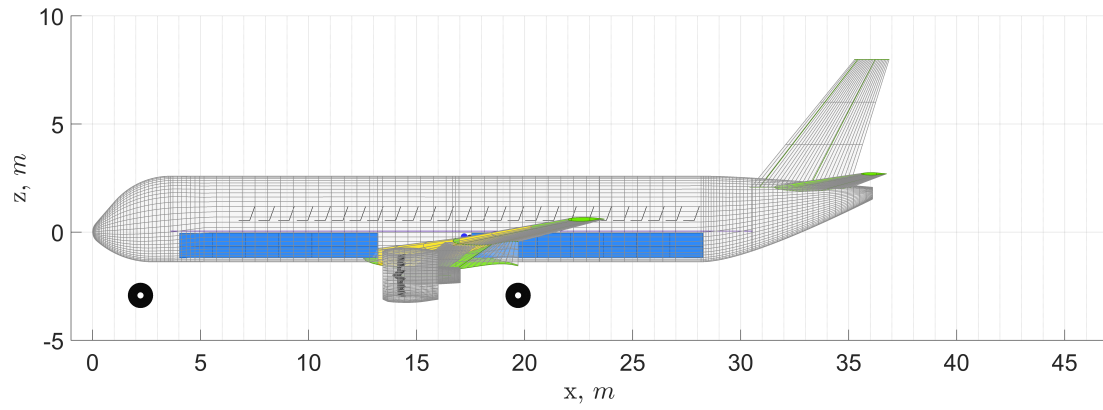
Figure 4.26 shows that for the LH2 version mass of the systems goes from representing 13% to 16% and the fuselage mass from 19% to 26% of the *OEM*.

Figure 4.27 shows that for the LH2 version the fuel system mass (including the fuel tanks) goes from representing 5% to 35% of the systems' masses.

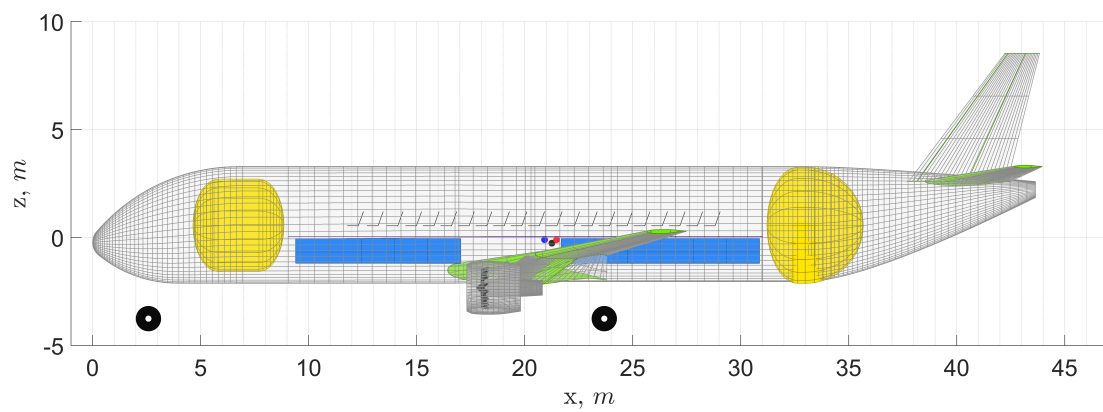
Table 4.18: Performance comparison between the optimal LH2 medium-range aircraft and its kerosene counterpart².

Parameters	A320	
	Kerosene	LH2
Fuel type		
Tank structure	N/A	integral
Seats abreast EC	3-3	2-4-2
Cryotank layout	N/A	aft & fwd
Cryotank shape	N/A	non-spherical
P_{vent} (kPa)	N/A	250
Direct venting	N/A	No
t_{ins} (mm) (aft)	N/A	154
t_{shell} (mm) (aft)	N/A	4.2
m_{tank} (kg) (aft+fwd)	N/A	2038
η_{grav} (aft+fwd)	N/A	0.328
r_{tank} (m) (aft)	N/A	2.69
l_{tank} (m) (aft+fwd)	N/A	8.67
$m_{fuelSys}$ (kg)	272	764 (+180.9%)
r_{fus} (m)	1.99	2.69 (+35.2%)
l_{fus} (m)	36.1	43.7 (+21.1%)
Wingspan (m)	33.9	36 (+6.2%)
S (m ²)	121	136 (+12.4%)
W/S (N/m ²)	6145	5515 (-10.3%)
T/W	0.3157	0.2945 (-6.7%)
W/P (N/W)	N/A	N/A
$\Delta x_{c.g.}$	0.123	0.124 (+0.8%)
S_h/S	0.23	0.253 (+10%)
m_{ht} (t)	1.01	1.27 (+25.7%)
m_{fus} (t)	7.95	13.07 (+64.4%)
m_w (t)	7.61	9.59 (+26%)
$C_{D_{0,ht}}$	0.00182	0.00198 (+8.8%)
$C_{D_{0,fus}}$	0.00605	0.00847 (+40%)
C_{D_0}	0.02069	0.02269 (+9.7%)
$L/D_{mid-cruise}$	16.9	16.1 (-4.7%)
m_{fuel}	15190	6206 (-59.1%)
OEM (t)	41.09	51.05 (+24.2%)
MTOM (t)	75.58	76.56 (+1.3%)
SEC (J/pax/m)	787.4	891.3 (+13.2%)

²For the A320(33) the DC tolerance setting was increased from 1E-3 to 1E-4.

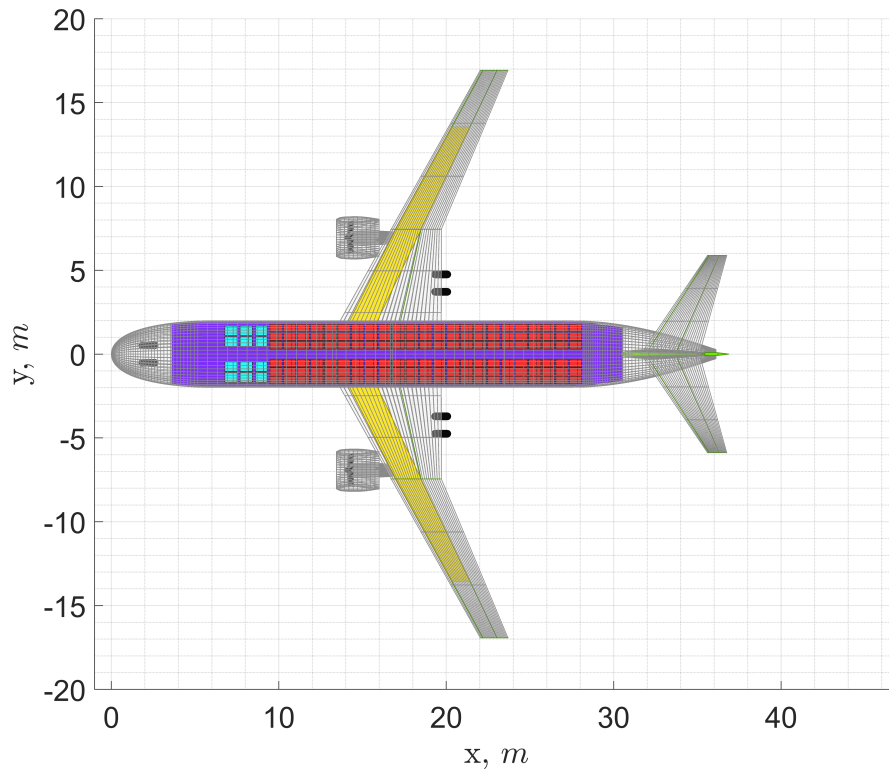


(a) A320(33)

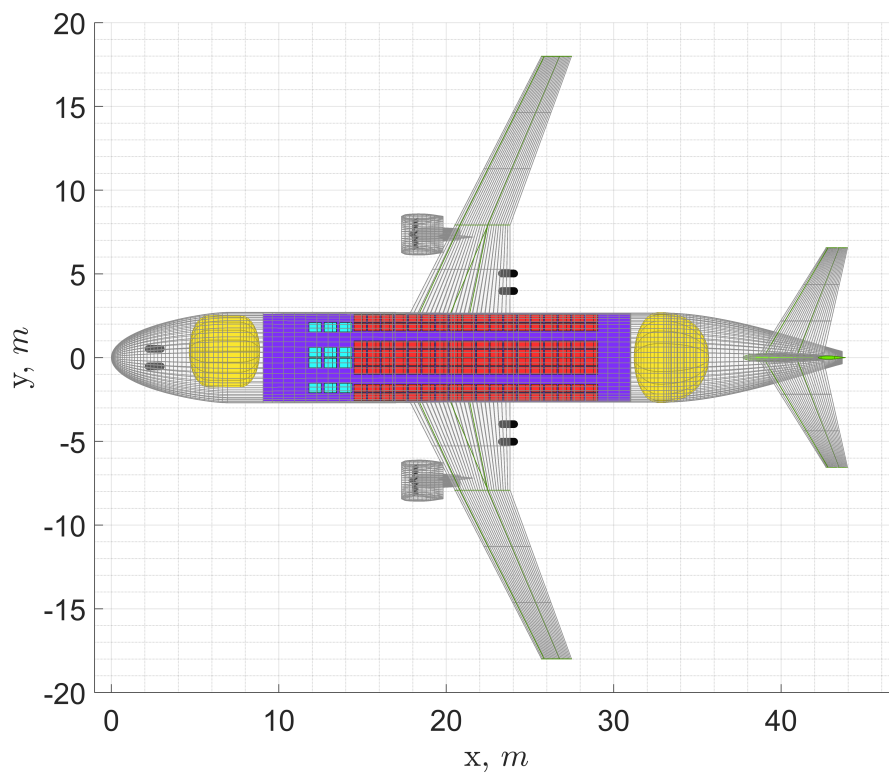


(b) A320LH2(aftFwd-nonintegral-33-300)

Figure 4.20: Side views of medium-range baseline aircraft (a) and medium-range optimal LH2 aircraft (b). Fuel tanks in yellow.

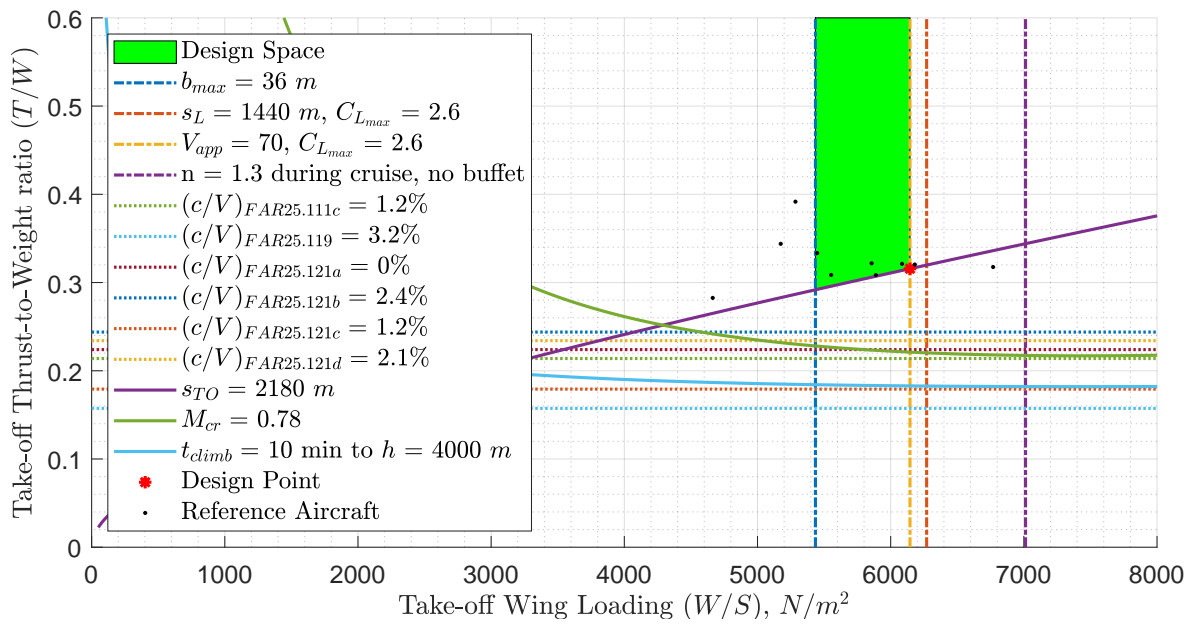


(a) A320(33)

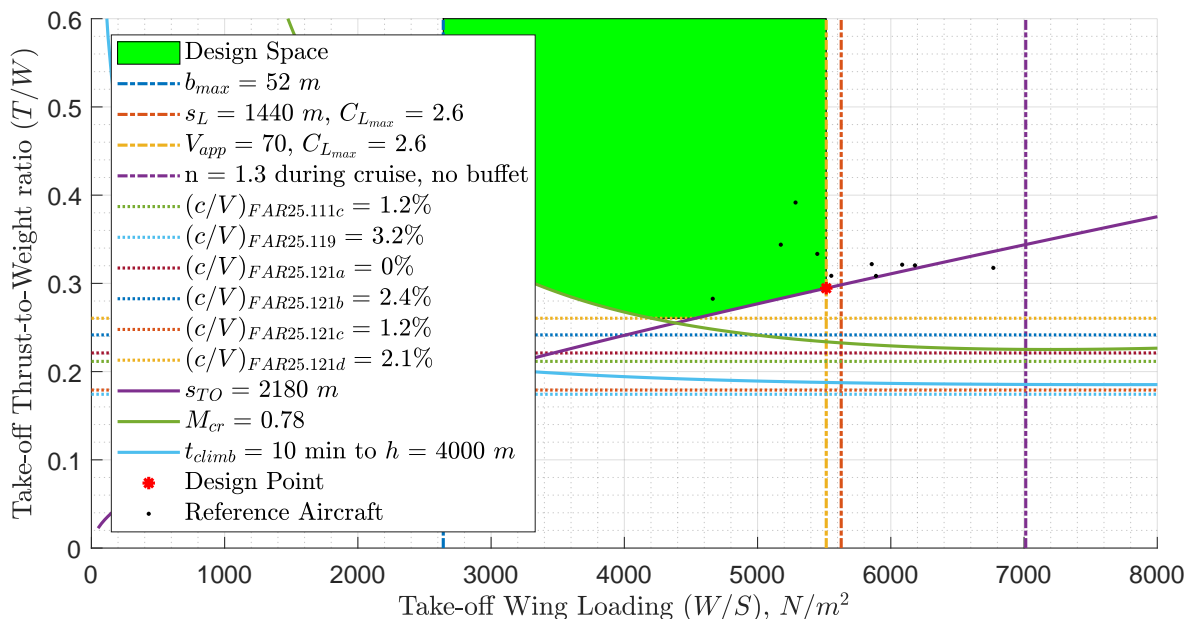


(b) A320LH2(aftFwd-integral-242-250)

Figure 4.21: Top views of medium-range baseline aircraft (a) and medium-range optimal LH2 aircraft (b).

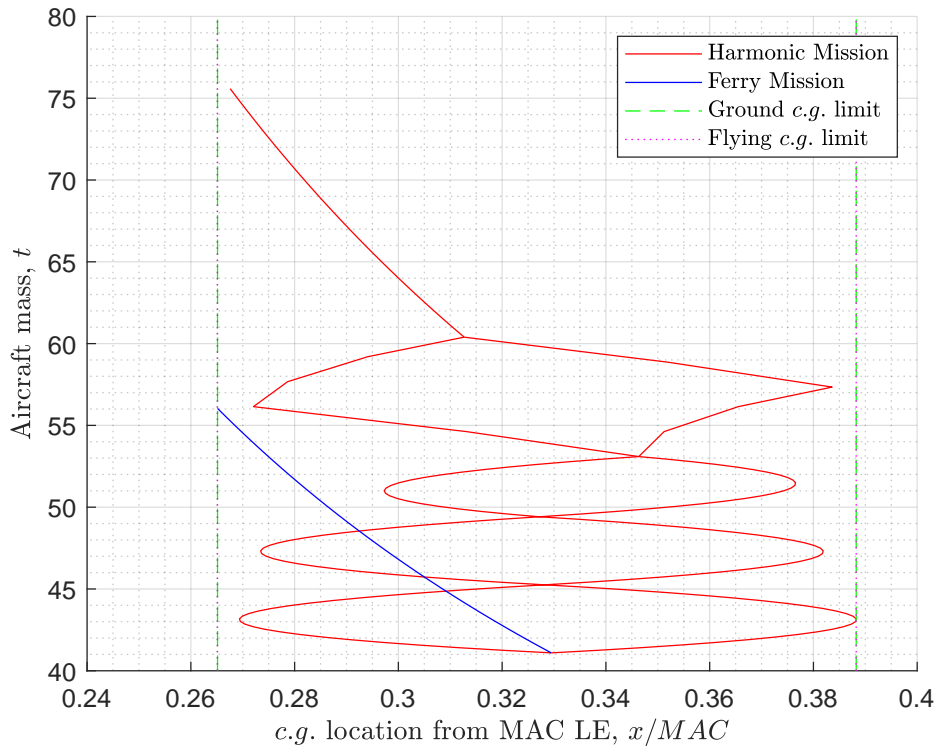


(a) A320(33)

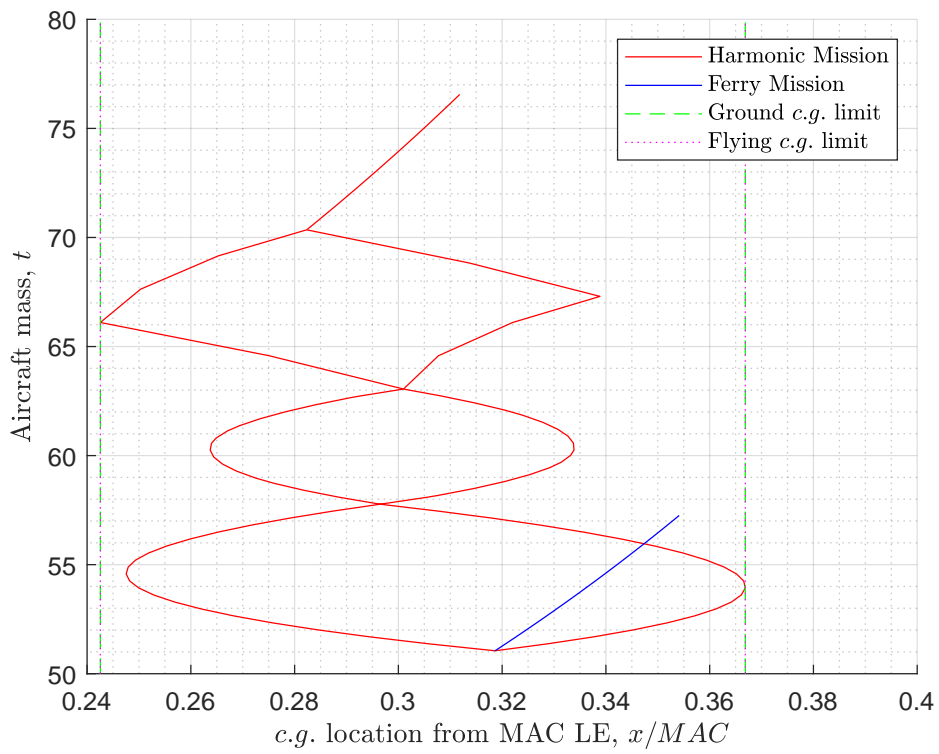


(b) A320LH2(aftFwd-integral-242-250)

Figure 4.22: Design point of medium-range baseline aircraft (a) and medium-range optimal LH2 aircraft (b). The airport classification for the LH2 version was increased from FAA-III to FAA-IV for convergence reasons.

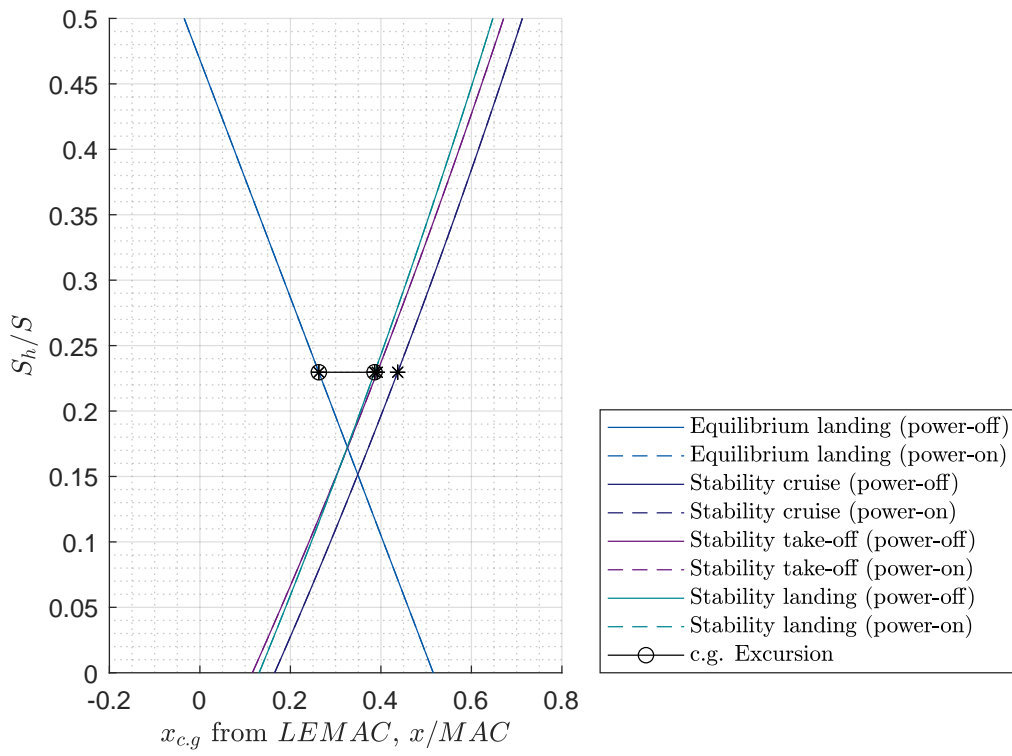


(a) A320(33)

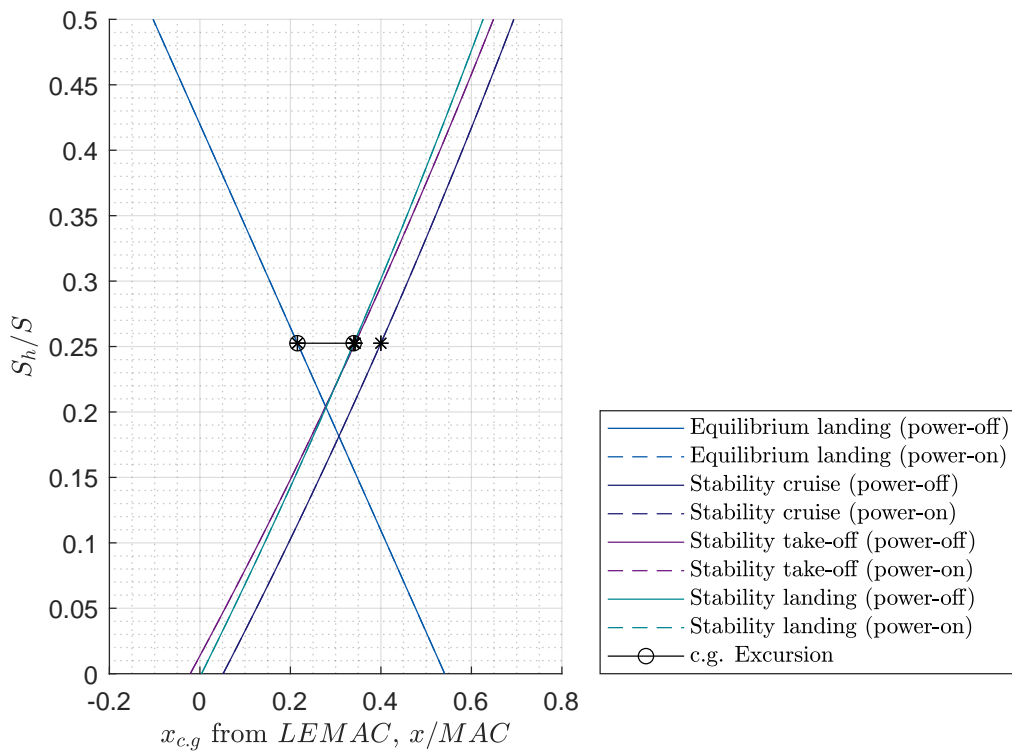


(b) A320LH2(aftFwd-integral-242-250)

Figure 4.23: Loading diagram of medium-range baseline aircraft (a) and medium-range optimal LH2 aircraft (b).



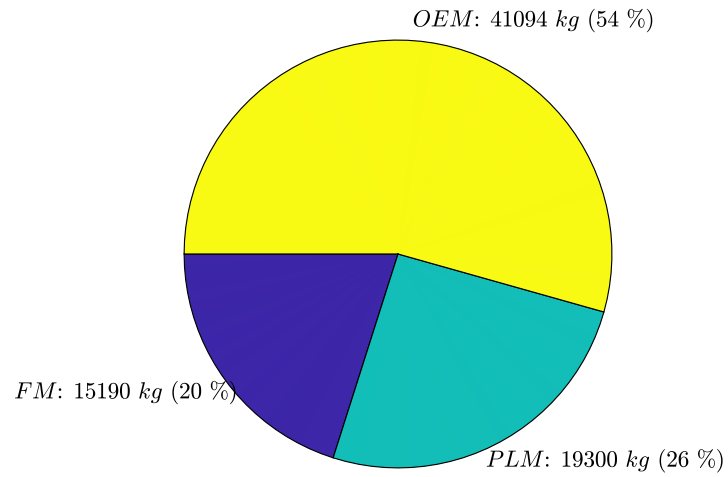
(a) A320(33)



(b) A320LH2(aftFwd-integral-242-250)

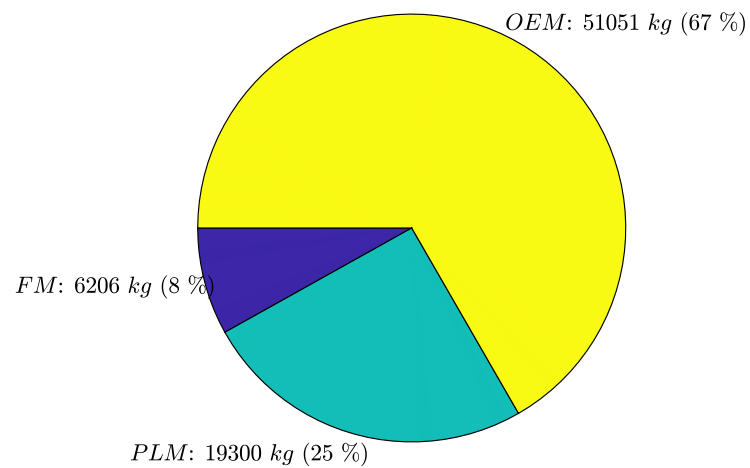
Figure 4.24: Loading diagram of medium-range baseline aircraft (a) and medium-range optimal LH2 aircraft (b).

$MTOM = 75584 \text{ kg}$
Block Energy (excl. reserve) = 537 GJ



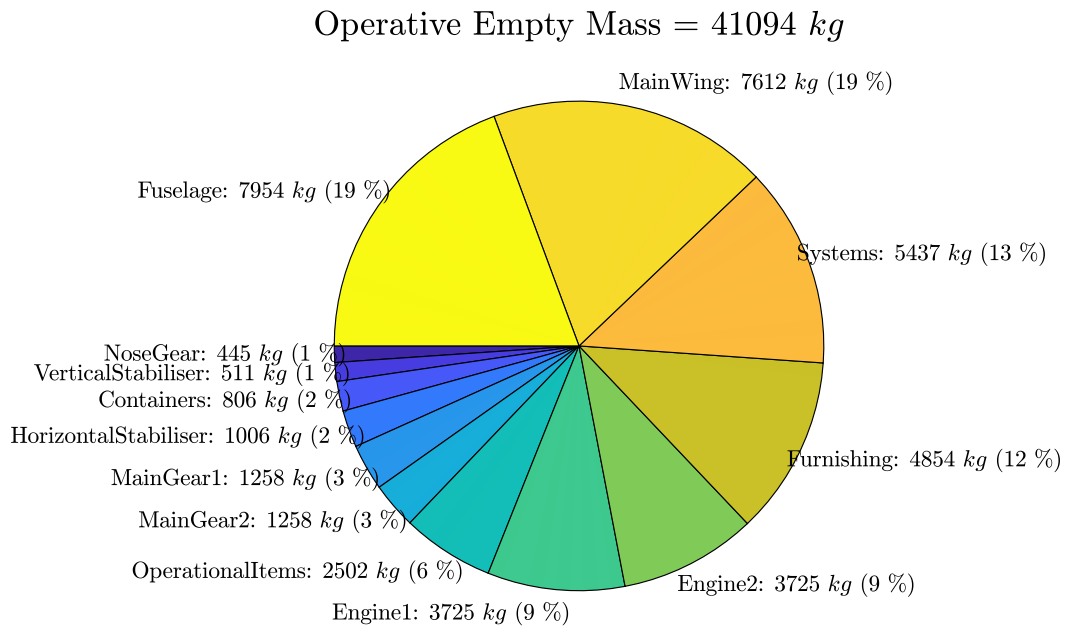
(a) A320(33)

$MTOM = 76557 \text{ kg}$
Block Energy (excl. reserve) = 608 GJ

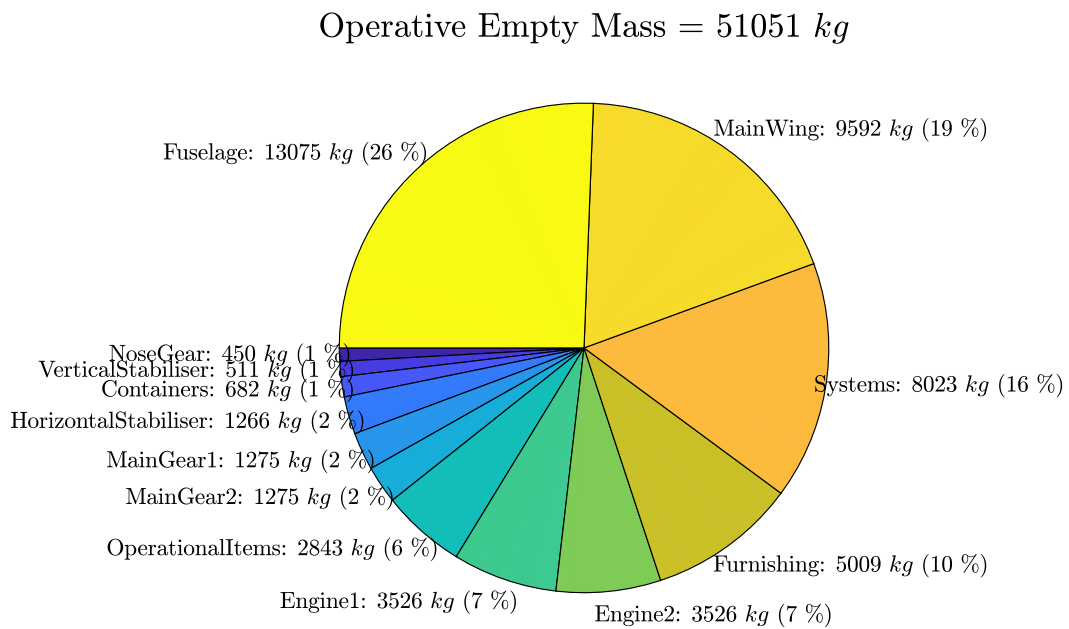


(b) A320LH2(aftFwd-integral-242-250)

Figure 4.25: *MTOM* mass breakdown of medium-range baseline aircraft (a) and medium-range optimal LH2 aircraft (b).

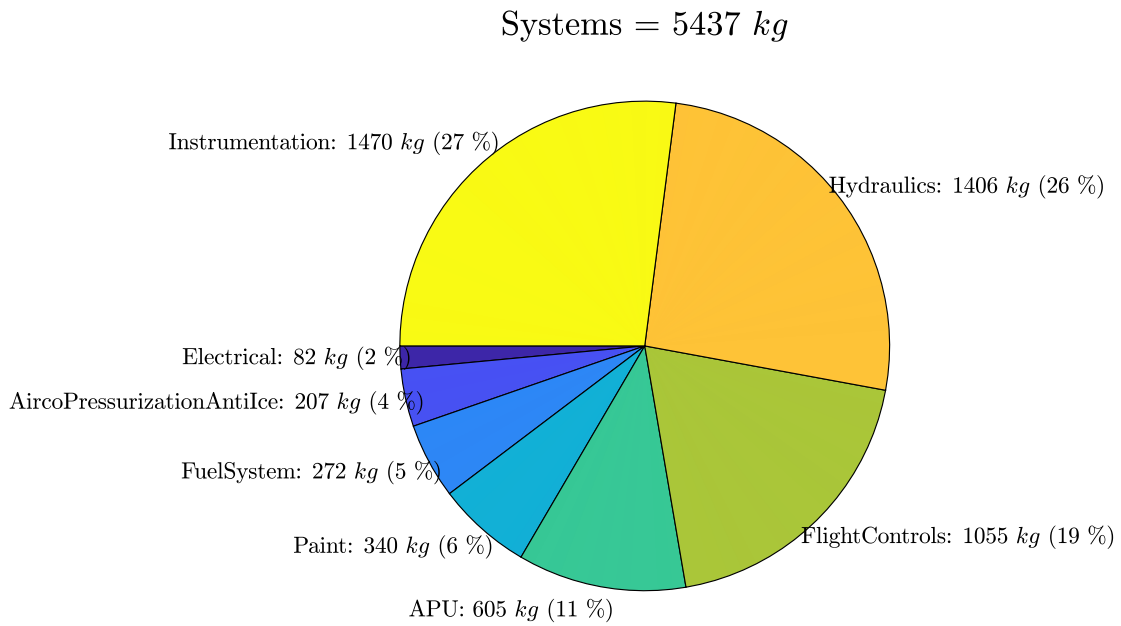


(a) A320(33)

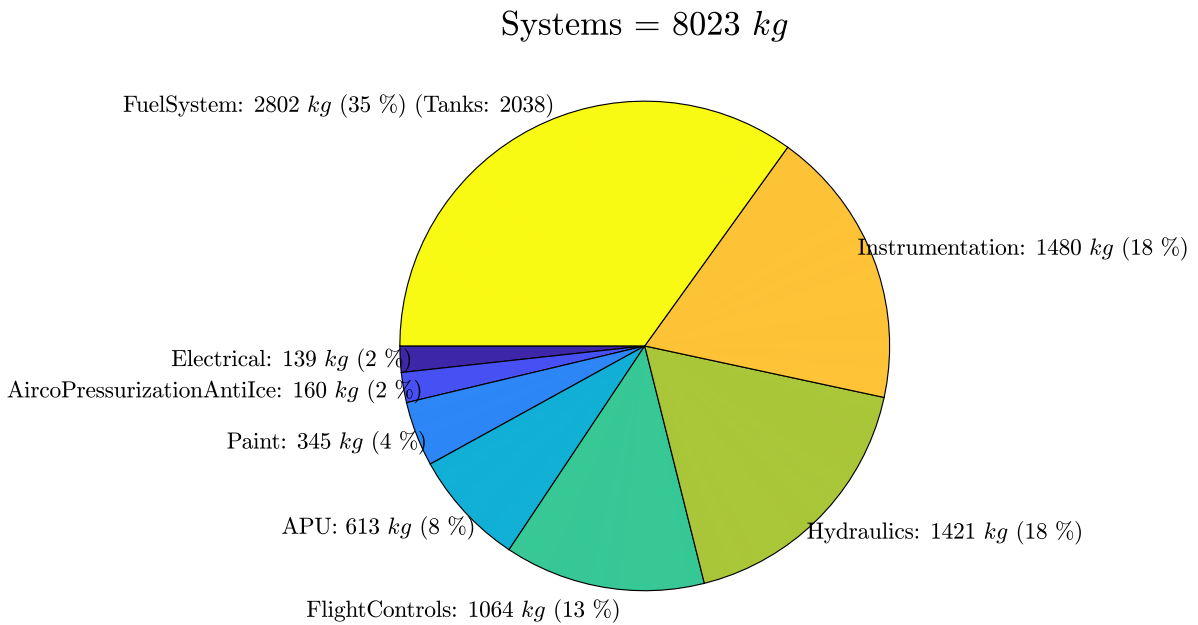


(b) A320LH2(aftFwd-integral-242-250)

Figure 4.26: OEM mass breakdown of medium-range baseline aircraft (a) and medium-range optimal LH2 aircraft (b).



(a) A320(33)



(b) A320LH2(aftFwd-integral-242-250)

Figure 4.27: Systems mass breakdown of medium-range baseline aircraft (a) and medium-range optimal LH2 aircraft (b).

4.8.3. LONG-RANGE

For the long-range aircraft, the A330, noticeable performance improvements were found when using an integral tank (see Table 4.4), hence the integral tank option is adopted. A fuselage diameter capable of accommodating 11 seats abreast was found to be beneficial (see Table 4.7). The large drag reduction potential of the aft & fwd tank layout was noted in Table 4.10. The non-spherical tank shape is selected, despite Table 4.13 shows the advantages of the spherical tank when non-integral tanks are used, because the non-spherical tank option allows using an integral tank structure, whose benefits more than compensates for the lower performance of the non-spherical tank shape. The optimal venting pressure of 250 kPa (see Figure 4.8e) is selected. The option to use direct gas venting is not chosen, because the performance gains on the aircraft masses were minor (see Table 4.16), and the impact on the energy used is difficult to determine. Indeed, while the burned mass itself would be slightly reduced and the non-vented gas in case of a regular mission could be reliquefied, the efficiency of the reliquefaction is, in this research not considered.

The LH2 aircraft generated combining these design options is here compared to its kerosene baseline. In terms of the aircraft main performance parameters the LH2 version has 22.3% higher *OEM*, 4.9% lower *MTOM* and 5% higher *SEC*.

The higher *OEM* is a consequence of the added 7268 kg of m_{tank} , the 170% higher $m_{fuelSys}$, the 66% higher m_{fus} , and 26% higher m_{wing} , mitigated by the 22% lower m_{ht} . The larger m_{fus} is caused by the 17% higher r_{fus} and 27% higher l_{fus} (see also Figure 4.28 and Figure 4.29). The larger m_{wing} is caused by the 11% larger S , in turn a consequence of the 14% lower W/S . The reduction in W/S is dictated by the approach speed performance (see Figure 4.30), which suffer from the higher *MLM*. This time a 22% smaller m_{ht} is obtained, thanks to the 26% lower S_h/S . To understand why a smaller S_h/S is required, loading diagram in Figure 4.31 and the X-plots in Figure 4.24 come in assistance. Figure 4.31.a shows how the large fuel mass fraction, typical of aircraft of this category, can become the driver for the $\Delta x_{c.g.}$ for a kerosene aircraft with fuel entirely located in the main wing. Figure 4.31.b shows instead how the use of two fuel tanks in the LH2 aircraft can bring a 47% reduction in $\Delta x_{c.g.}$. Comparing the X-plots of the two aircraft (see Figure 4.24) we can still notice a small leftward shift of the x-axis crossing point of the stability lines and a small rightward shift of the x-axis crossing point of the controllability lines, with the same sources explained for the medium-range aircraft. Nevertheless, the extreme reduction in $\Delta x_{c.g.}$ is the prevailing factor and a 26% reduction in S_h/S is still obtained.

The lower *MTOM* is achieved thanks to the 62% lower *FM*. The higher *SEC* is caused by a combination of increased mid-cruise aircraft mass and 1.5% lower $L/D_{mid-cruise}$. The lower $L/D_{mid-cruise}$ is a consequence of the 4% higher C_{D_0} , mitigated by the reduction in trim drag. The first is caused by the 31% higher $C_{D_{0,fus}}$, mitigated by the 24% lower $C_{D_{0,ht}}$, which are a direct consequence of their increased and decrease in geometrical sizes respectively. The second stems from the smaller $\Delta x_{c.g.}$.

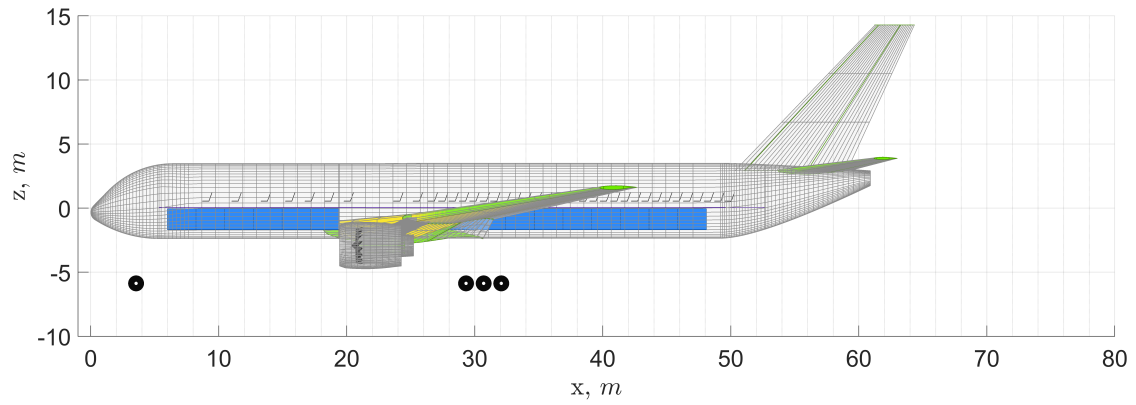
Figure 4.33 shows that for the LH2 version the *OEM* goes from representing 53% to 68% of the *MTOM*, while the *FM* goes from 27% to 11%.

Figure 4.34 shows that for the LH2 version mass of the systems goes from representing 10% to 13% and the fuselage mass from 19% to 26% of the *OEM*.

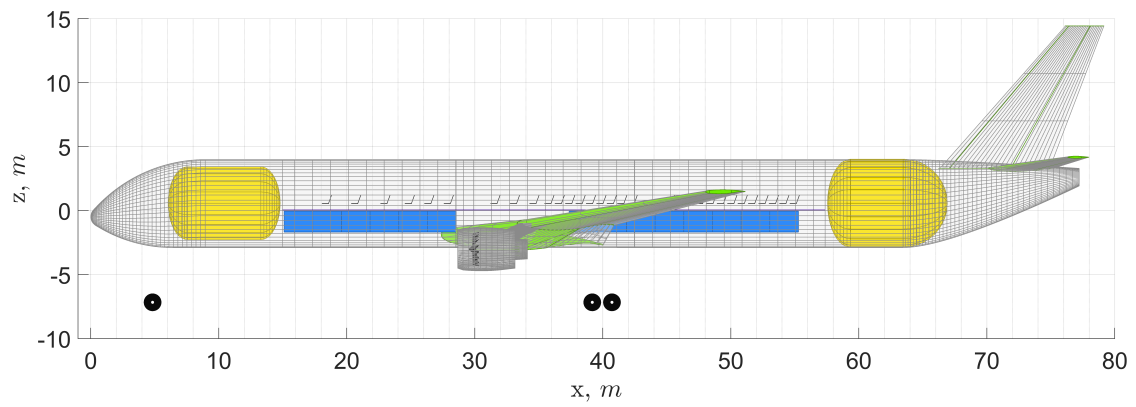
Figure 4.35 shows that for the LH2 version the fuel system mass (including the fuel tanks) goes from representing 3% to 38% of the systems' masses.

Table 4.19: Performance comparison between the optimal LH2 long-range aircraft and its kerosene counterpart.

Parameters	A330	
	Kerosene	LH2
Fuel type		
Tank structure	N/A	integral
Seats abreast EC	3-3-3	3-5-3
Cryotank layout	N/A	aft & fwd
Cryotank shape	N/A	non-spherical
P_{vent} (kPa)	N/A	250
Direct venting	N/A	No
t_{ins} (mm) (aft)	N/A	145
t_{shell} (mm) (aft)	N/A	5.5
m_{tank} (kg) (aft+fwd)	N/A	7268
η_{grav} (aft+fwd)	N/A	0.27
r_{tank} (m) (aft)	N/A	3.44
l_{tank} (m) (aft+fwd)	N/A	18.1
$m_{fuelSys}$ (kg)	403	1088 (+170%)
r_{fus} (m)	2.93	3.44 (+17.4%)
l_{fus} (m)	60.9	77.2 (+26.8%)
Wingspan (m)	63.8	67.2 (+5.3%)
S (m ²)	407	451 (+10.8%)
W/S (N/m ²)	6329	5428 (-14.2%)
T/W	0.2949	0.268 (-9.1%)
W/P (N/W)	N/A	N/A
$\Delta x_{c.g.}$	0.253	0.135 (-46.6%)
S_h/S	0.166	0.123 (-25.9%)
m_{ht} (t)	2.39	1.86 (-22.2%)
m_{fus} (t)	27.01	44.94 (+66.4%)
m_w (t)	39.34	49.38 (+25.5%)
$C_{D_{0,ht}}$	0.00124	0.00094 (-24.2%)
$C_{D_{0,fus}}$	0.00416	0.00546 (+31.3%)
C_{D_0}	0.01703	0.01766 (+3.7%)
$L/D_{mid-cruise}$	19.6	19.3 (-1.5%)
FM	70999	26918 (-62.1%)
OEM (t)	139.72	170.94 (+22.3%)
$MTOM$ (t)	262.42	249.56 (-4.9%)
SEC (J/pax/m)	1143.7	1200.9 (+5%)
Input file name	A330 (333)	A330LH2 (aftFwd-integral-(353-250))

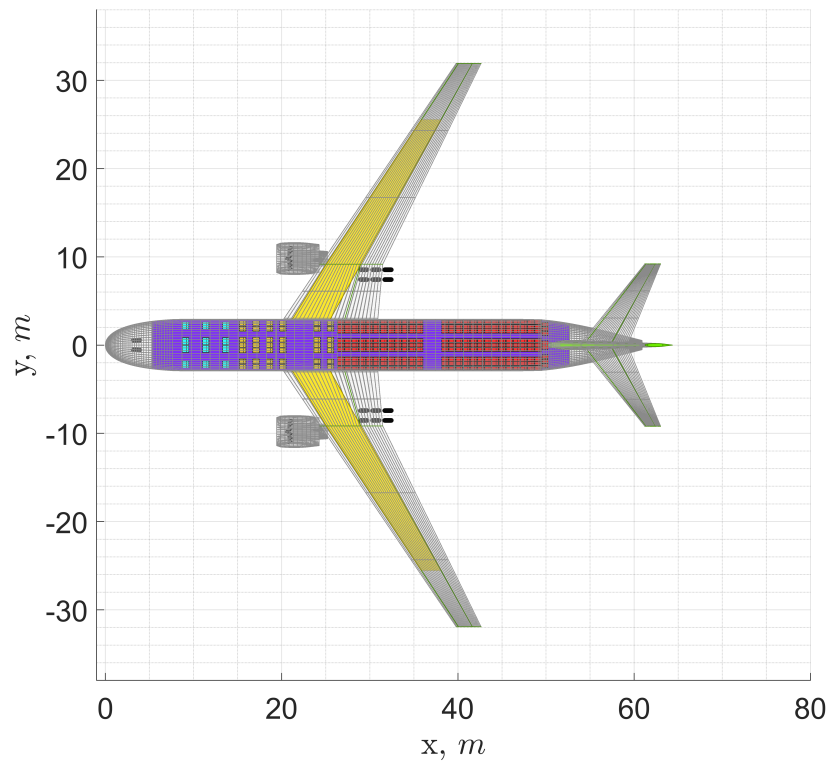


(a) A330(333)

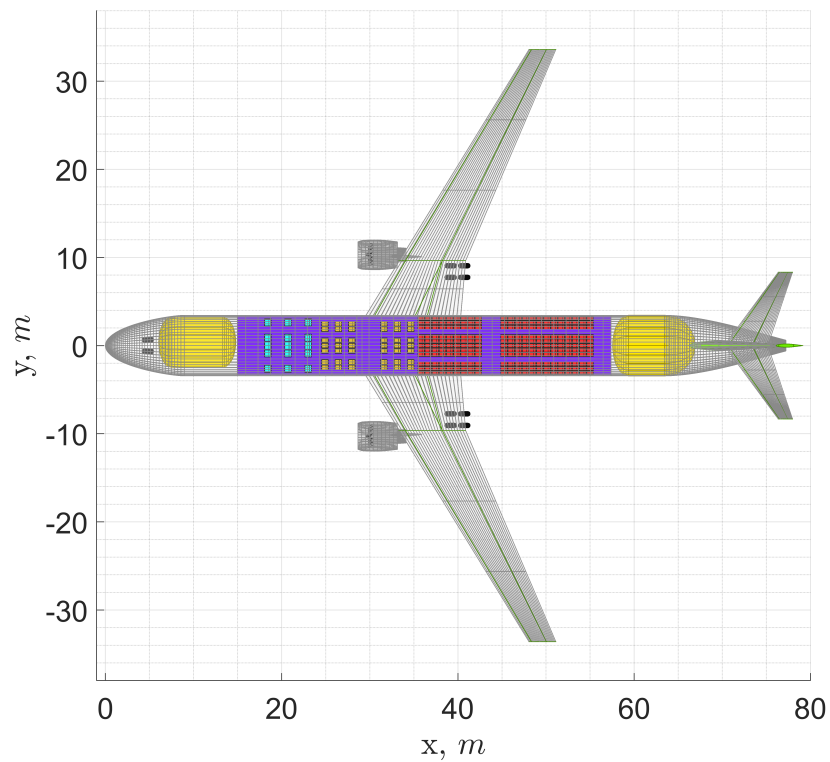


(b) A330LH2(aftFwd-nonintegral-33-300)

Figure 4.28: Side views of long-range baseline aircraft (a) and long-range optimal LH2 aircraft (b). Fuel tanks in yellow.

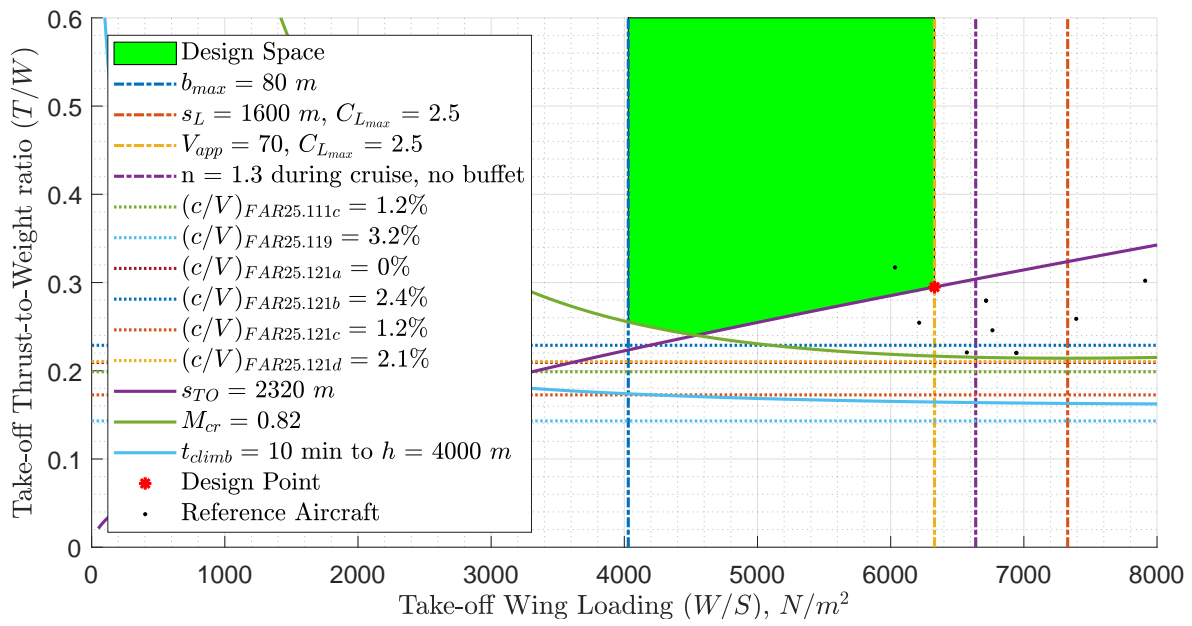


(a) A330(333)

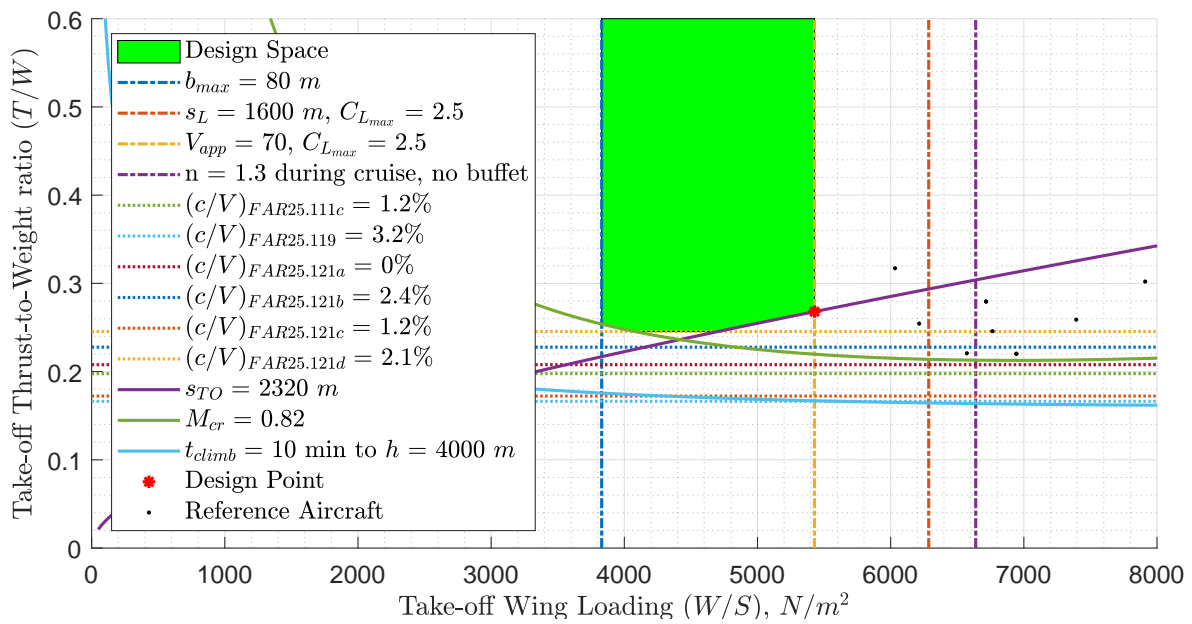


(b) A330LH2(aftFwd-integral-(353-250))

Figure 4.29: Top views of long-range baseline aircraft (a) and long-range optimal LH2 aircraft (b). Fuel tanks in yellow.

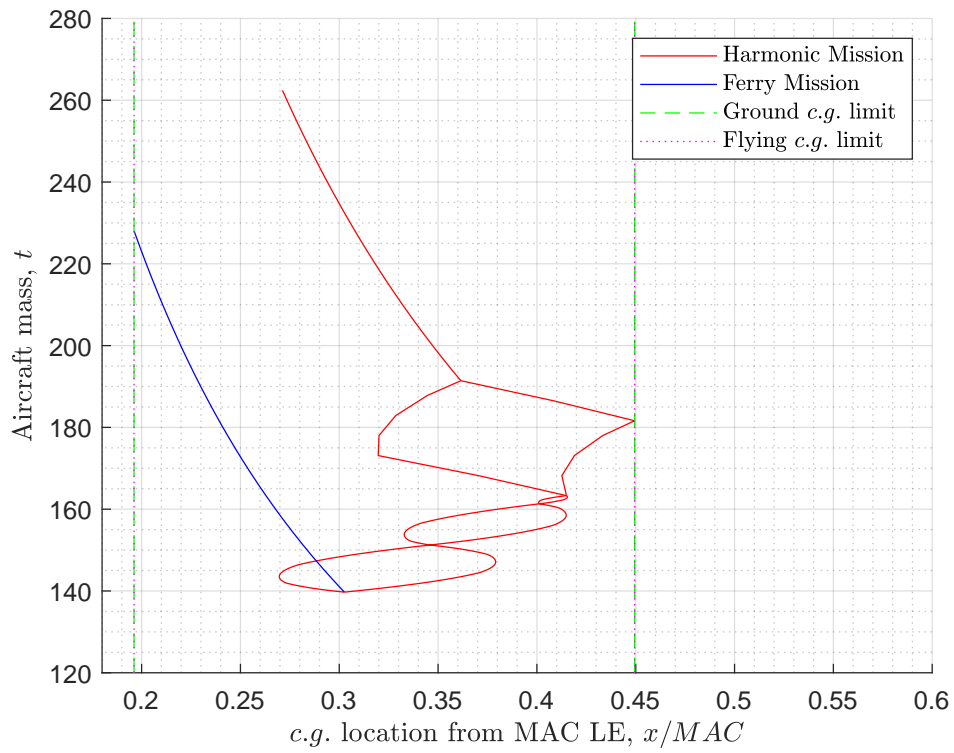


(a) A330(333)

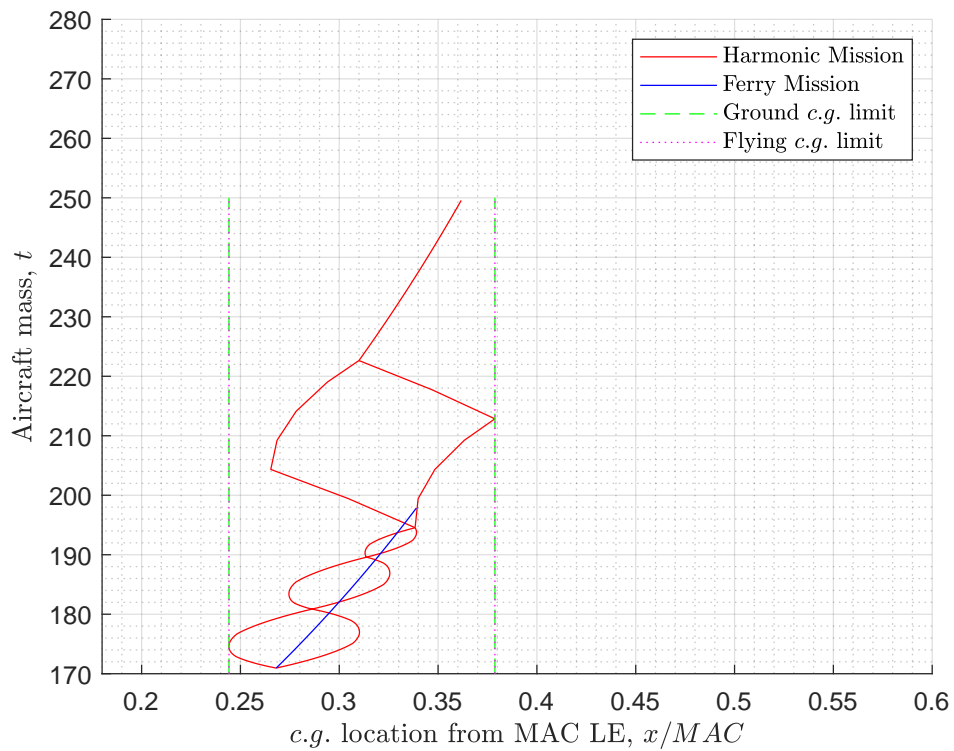


(b) A330LH2(aftFwd-integral-(353-250))

Figure 4.30: Design point of long-range baseline aircraft (a) and long-range optimal LH2 aircraft (b).

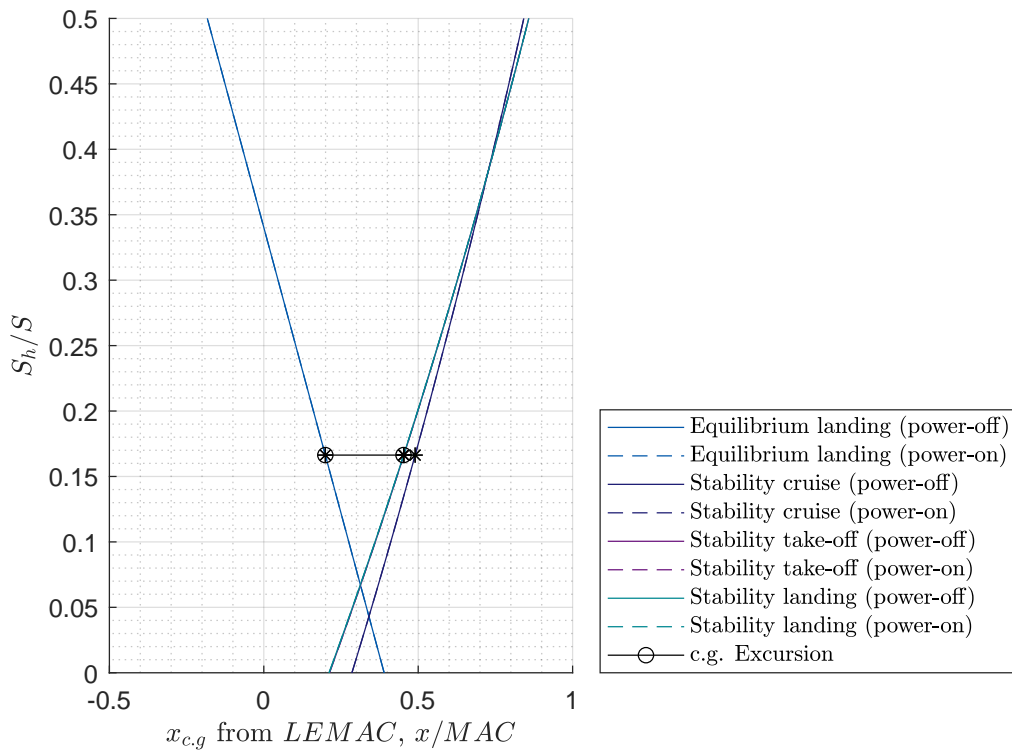


(a) A330(333)

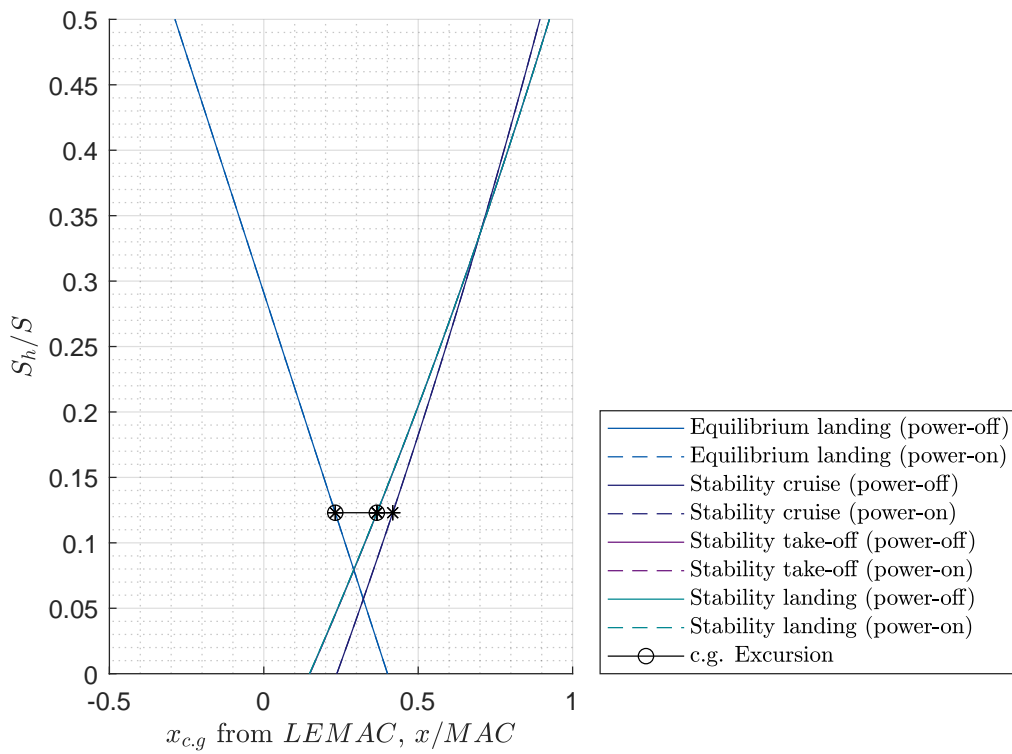


(b) A330LH2(aftFwd-integral-353-250)

Figure 4.31: Loading diagram of long-range baseline aircraft (a) and long-range optimal LH2 aircraft (b).



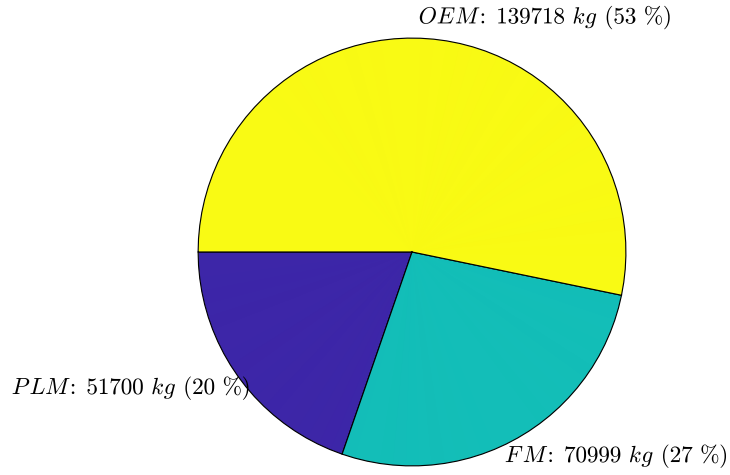
(a) A330(333)



(b) A330LH2(aftFwd-integral-353-250)

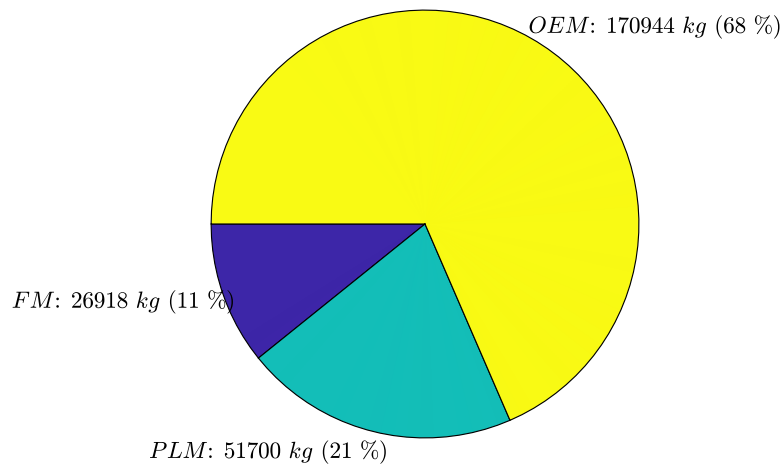
Figure 4.32: Loading diagram of long-range baseline aircraft (a) and long-range optimal LH2 aircraft (b).

$MTOM = 262417 \text{ kg}$
 Block Energy (excl. reserve) = 2699 GJ



(a) A330(333)

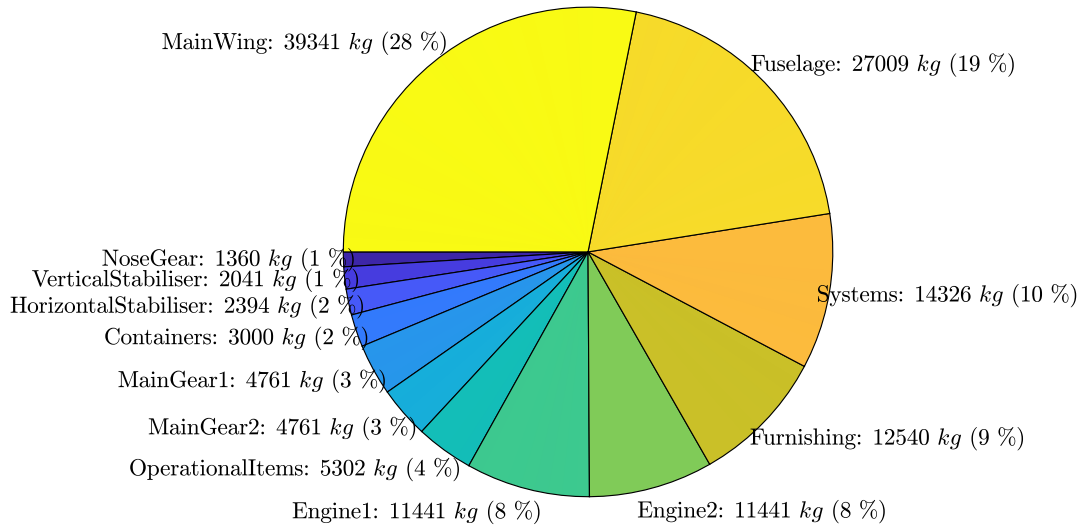
$MTOM = 249562 \text{ kg}$
 Block Energy (excl. reserve) = 2834 GJ



(b) A330LH2(aftFwd-integral-(353-250))

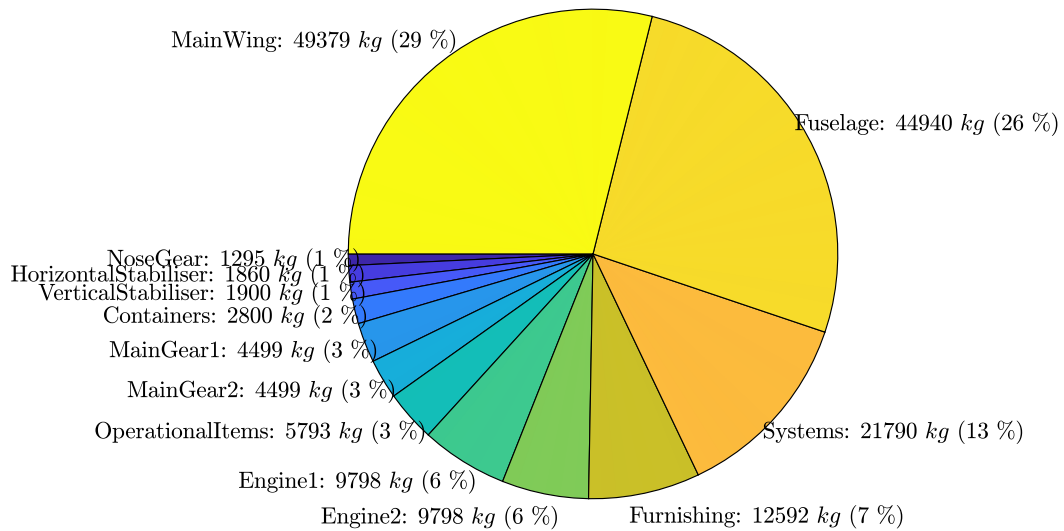
Figure 4.33: *MTOM* mass breakdown of long-range baseline aircraft (a) and long-range optimal LH2 aircraft (b).

Operative Empty Mass = 139718 kg



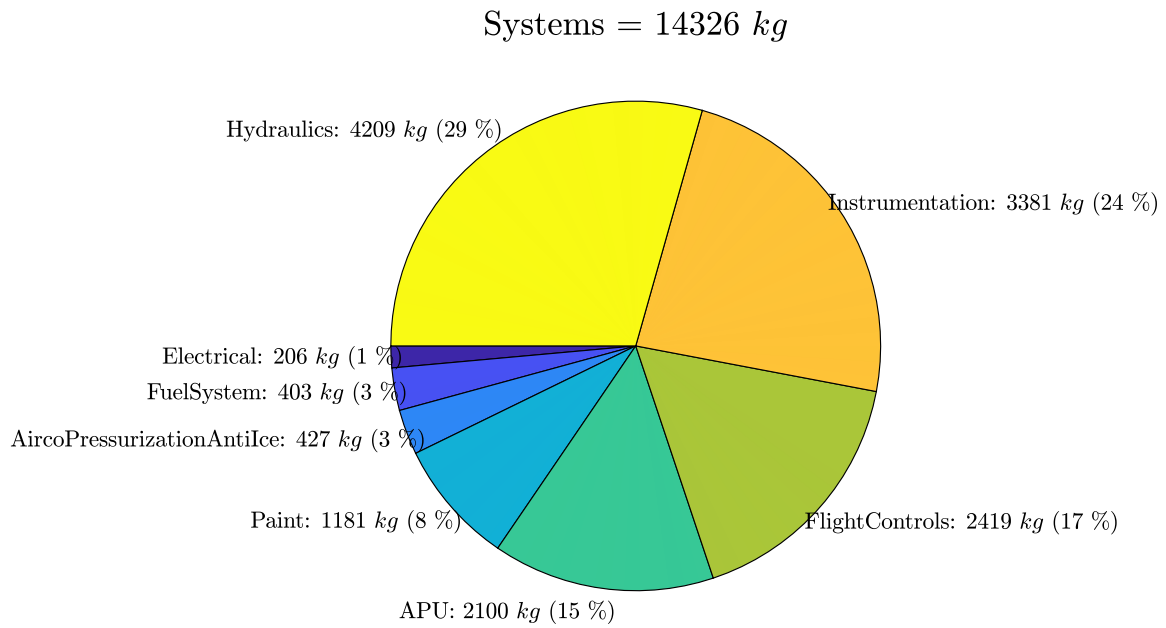
(a) A330(333)

Operative Empty Mass = 170944 kg

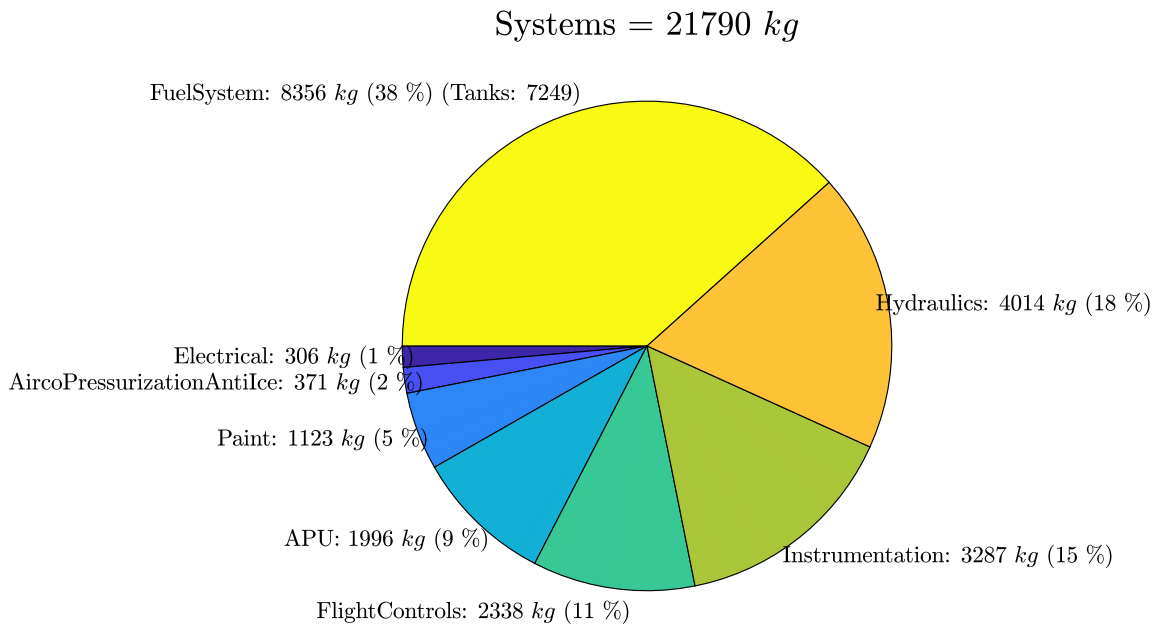


(b) A330LH2(aftFwd-integral-(353-250))

Figure 4.34: OEM mass breakdown of long-range baseline aircraft (a) and long-range optimal LH2 aircraft (b).



(a) A330(333)



(b) A330LH2(aftFwd-integral-(353-250))

Figure 4.35: Systems mass breakdown of long-range baseline aircraft (a) and long-range optimal LH2 aircraft (b).

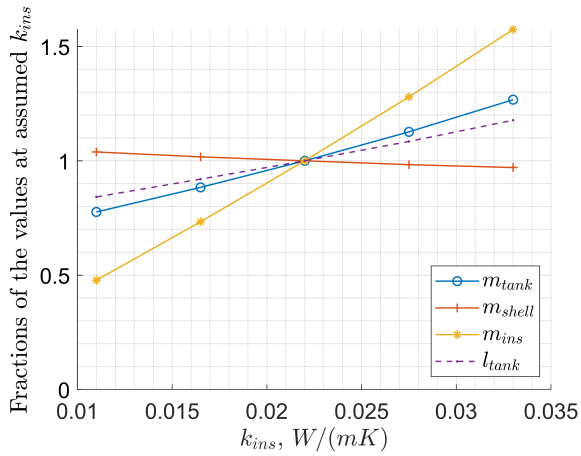
4.9. SENSITIVITY ANALYSIS

This section investigates the amount of variation experienced by the main aircraft performance parameters in response to changes in key inputs, such as the effective thermal conductivity of the insulator material, the allowable tensile stress of the structural shell material, and the required mission range. The reference aircraft for these sensitivities analysis are the optimal designs described in section 4.8, except for the short-range aircraft, which uses a 5 rather than 6 seats abreast layout³.

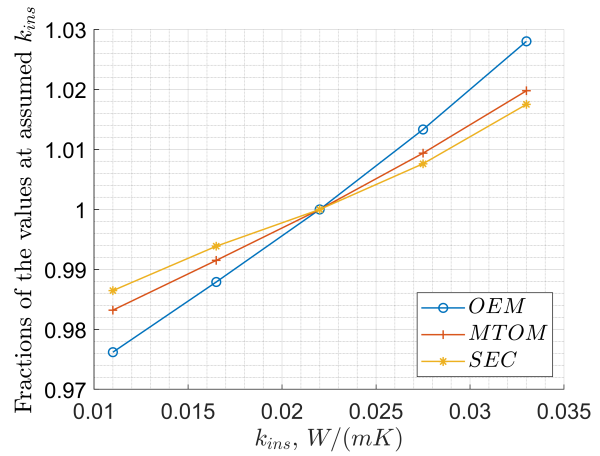
4.9.1. INSULATOR PERFORMANCE: EFFECTIVE CONDUCTIVITY

The effective thermal conductivity of the insulator material is increased and decreased by 25% and 50%. The consequences at the tank level and at the aircraft level are presented in Figure 4.36. The first noticeable effects are that all three aircraft categories respond similarly to the change in k_{ins} and their response is linear. At the tank level, a 50% increase in k_{ins} yields approximately a 55% increase in m_{ins} , a 17-27% increase in m_{tank} and a 8-18% increase in l_{fus} , with the smaller values belonging to the largest aircraft. At the aircraft level the increases due to a 50% higher k_{ins} are in the order of to 2-3% for both the *OEM* and 1-2% for the *MTOM* and the *SEC*.

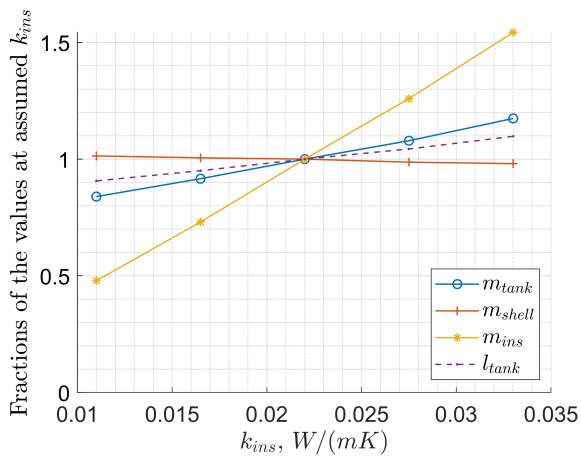
³The use of the 6 seats abreast would have created problems in the design of the aft tank as the reduction in insulation thickness and the reduction in mission range would have reduced the cylindrical section to negative values.



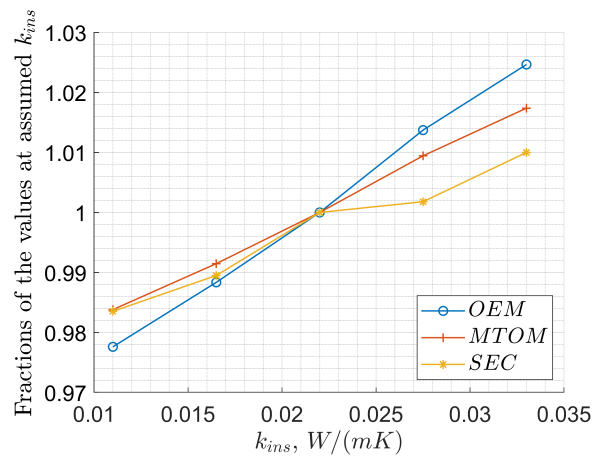
(a) ATR72, tank level.



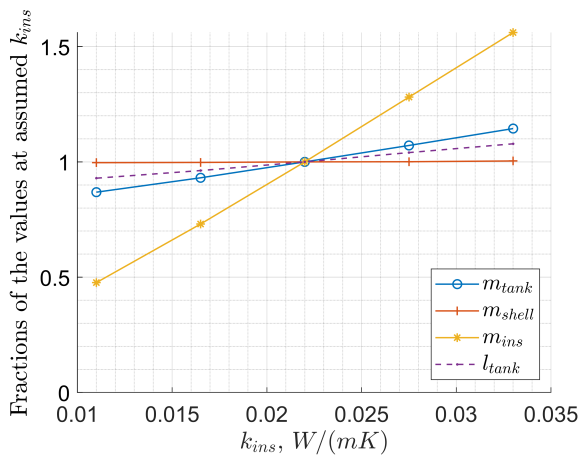
(b) ATR72, aircraft level.



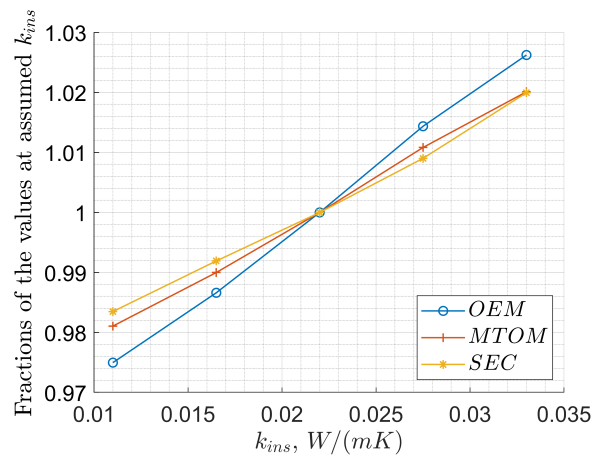
(c) A320, tank level.



(d) A320, aircraft level.



(e) A330, tank level.

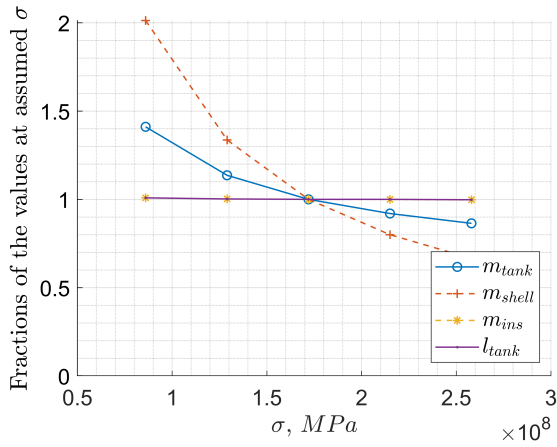


(f) A330, aircraft level..

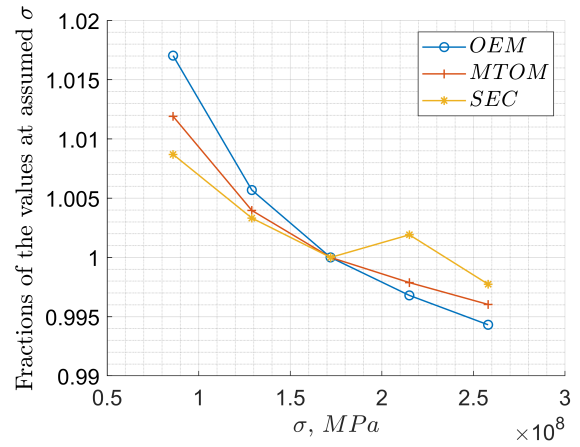
Figure 4.36: Sensitivity to insulator effective thermal conductivity. The optimal configurations are used for the medium and long-range. A sub-optimal configuration is used for the short-range.

4.9.2. STRUCTURAL PERFORMANCE: ALLOWABLE TENSILE STRESS

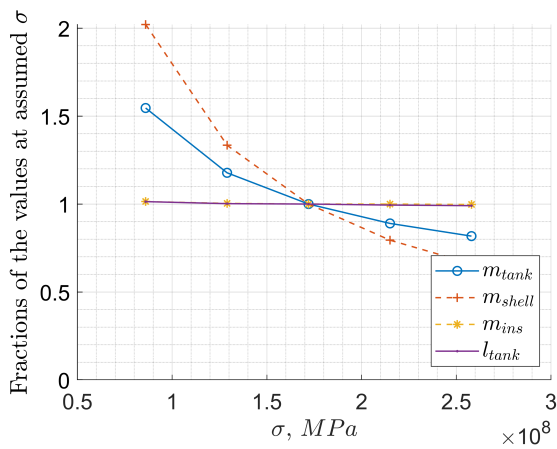
The allowable tensile stress of the structural shell material is increased and decreased by 25% and 50%. The consequences at the tank level and at the aircraft level are presented in Figure 4.37. While all three aircraft categories respond similarly to the change in σ at the tank level, at the aircraft level a response similar in shape but larger in magnitude with increased aircraft size is observed. In contrast to what was observed in the previous subsection, the response to a variation in σ appears to be not linear but quadratic. This is logical, since the structural shell mass is inversely proportional to σ , while the insulation mass is directly proportional to k_{ins} . At the tank level, the only significantly affected component is the shell, hence the tank length remains unvaried. At the aircraft level the increases due to a 50% higher σ are in the order of 1.7-5.5% for the *OEM* and 1.2-4.2% for the *MTOM* and 0.8-3% for the *SEC*, with the higher values belonging to the largest aircraft.



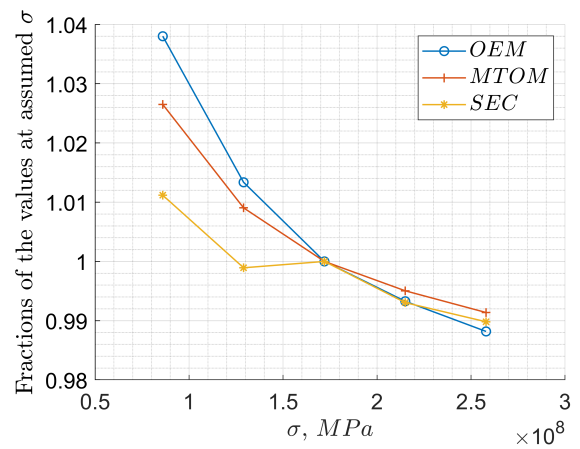
(a) ATR72, tank level.



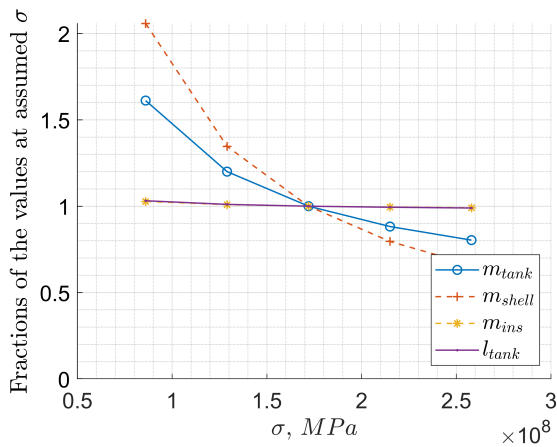
(b) ATR72, aircraft level.



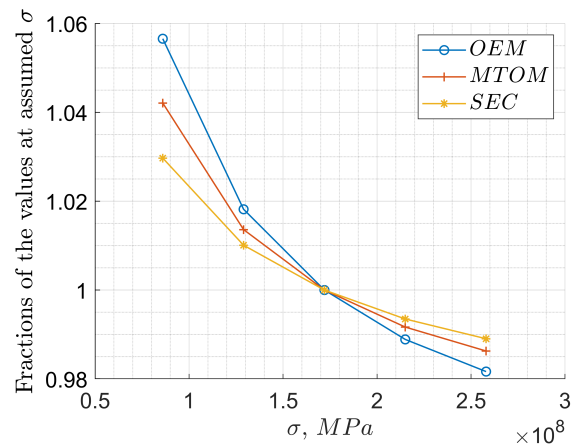
(c) A320, tank level.



(d) A320, aircraft level.



(e) A330, tank level.

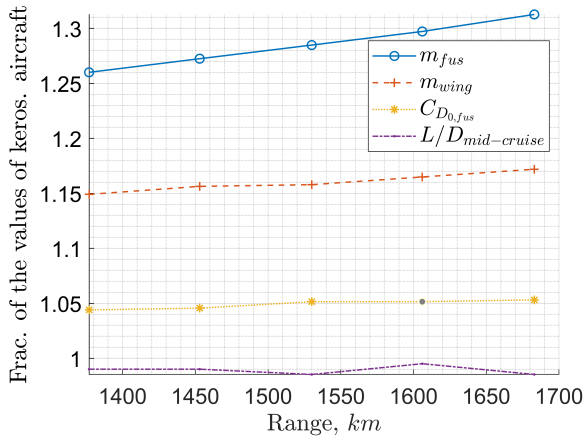


(f) A330, aircraft level.

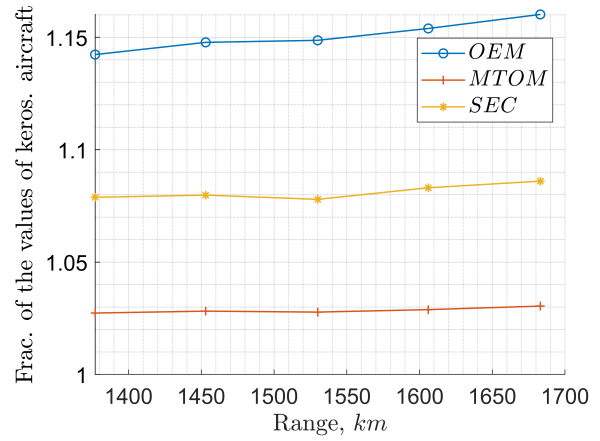
Figure 4.37: Sensitivity to allowable tensile stress. The optimal configurations are used for the medium and long-range. A sub-optimal configuration is used for the short-range.

4.9.3. RANGE REQUIREMENT

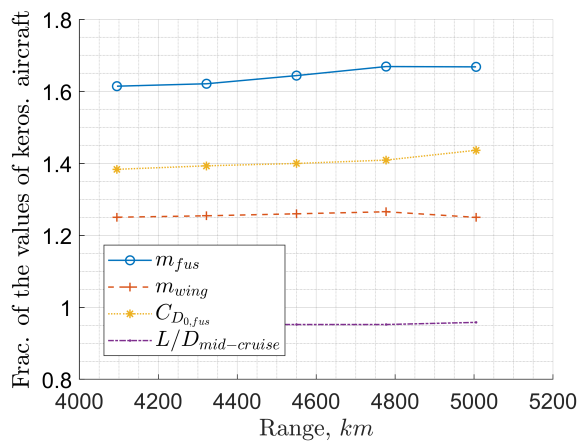
In this sensitivity analysis, the relative performance of the LH2 aircraft to the kerosene baselines is computed for mission range requirements increased and decreased by 5% and 10%. The consequences on the main performance parameters and on other key parameters are presented in Figure 4.38. For all three aircraft categories, we notice that the ratio between the fuselage mass of the LH2 aircraft and the one of the kerosene aircraft increases with increasing range. This was to be expected since the fuselage design of a kerosene aircraft is independent of the range, whereas the one of the LH2 aircraft increases in length with increasing fuel volume. m_{wing} follows the increase in OEM , $C_{D_{0,fus}}$ increases with fuselage length, while $L/D_{mid-cruise}$ remains approximately constant. In terms of the main aircraft performance parameters, a 10% increase in range translates into a 1% increase in OEM for all three aircraft categories. With respect to the $MTOM$ and the SEC , the short-range aircraft sees negligible changes, while the medium and long-range aircraft actually see improvements in the relative performances. With respect to the sharp improvement in the LH2 medium-range aircraft relative performances at 110% of the mission range, the reason was found in the loading diagram of the kerosene version. Indeed, at around 105% of the mission range, the fuel fraction starts becoming a dominant component in the determination of the $\Delta x_{c.g.}$. A situation similar to the one observed for the long-range aircraft (see Figure 4.31 Figure 4.32) is obtained, where the horizontal tail of the kerosene version increases in size, adding mass and drag to the aircraft.



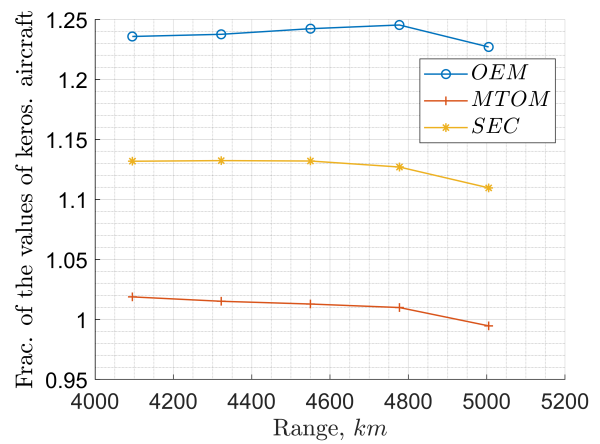
(a) ATR72, relevant parameters.



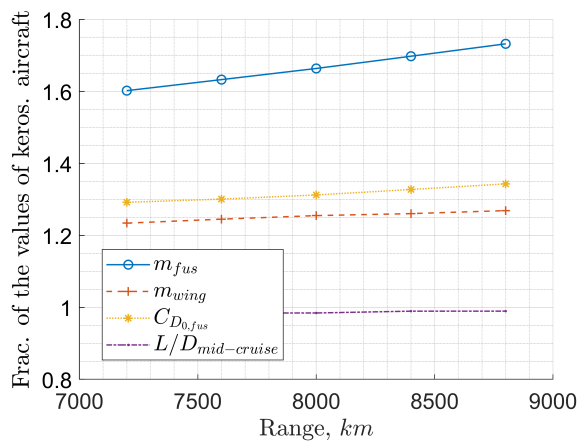
(b) ATR72, main performance parameters.



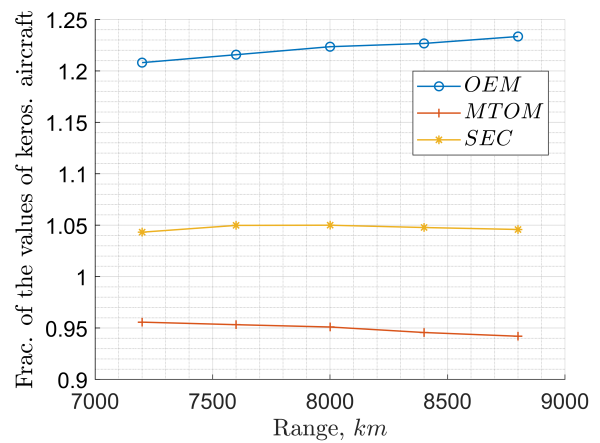
(c) A320, relevant parameters.



(d) A320, main performance parameters.



(e) A330, relevant parameters.



(f) A330, main performance parameters.

Figure 4.38: Sensitivity to range requirement. The optimal configurations are used for the medium and long-range. A sub-optimal configuration is used for the short-range

OWN RESULTS COMPARED WITH LITERATURE

This chapter compares the results of this research with the ones found in literature, both in terms of the aircraft level performances and in the tank level performances.

5.1. AIRCRAFT LEVEL PERFORMANCES

For the short-range category the ATR72 LH2 version with 5 seats abreast aft tank layout is compared to the small regional aircraft from the Cryoplane project [5] (see Figure 2.3 and section 2.1). The relative values of the main aircraft performance parameters with respect to their kerosene baselines are reported in Table 5.1. Both studies estimate a significant increase in *OEM* and *SEC* and a negligible increase in *MTOM*.

Table 5.1: Comparison table for aircraft level performance of short-range aircraft designed in this research and regional aircraft from the Cryoplane project [5]. Performance values relative to the kerosene baselines of the respective studies.

Parameters	Short range	
	ATR72LH2(aft-nonintegral-23-300)	Cryoplane project
<i>OEM</i>	+15%	+17%
<i>MTOM</i>	+3%	+0.3%
<i>SEC</i>	+9%	+14%

For the medium-range category the A320 LH2 version with 6 seats abreast and an aft tank layout is compared to the A320-like LH2 aircraft with aft tank layout designed by Silberhorn et al. [7] (see Figure 2.7 and section 2.1). The relative values of the main aircraft performance parameters with respect to their kerosene baselines are reported in Table 5.2. It appears that under all the main performance parameters the aircraft designed in this research underperforms the one from Silberhorn et al.. One contributor to this drop in performances is the larger relative increase in fuselage length, which directly affects the fuselage mass and the mid-cruise lift-over-drag ratio. The larger increase in fuselage length can be explained by the 80% larger fuel mass (see Table 5.5). Note that the Silberhorn et al. aircraft was designed for 2045 entry-into service year, so a 0.85 technology factor was applied to the engine performance, reducing the required fuel mass.

Table 5.2: Comparison table for aircraft level performance of medium-range aircraft designed in this research and medium-range aircraft from Silberhorn et al. [7]. Performance values relative to the kerosene baselines of the respective studies.

Parameters	Medium-range	
	A320LH2(aft-nonintegral-33)	Silberhorn et al.
l_{fus}	+34%	+22%
m_{fus}	+52%	+28%
$L/D_{mid-cruise}$	-18%	-5%
OEM	+27%	+11%
$MTOM$	+3%	-9%
SEC	+14%	+7%

For the long-range category the A330 LH2 version with 11 seats abreast and an aft & fwd tank layout is compared to the long-range aircraft from McKinsey & Company [6] (see Figure 2.14) and the one from the Cryoplane project [5](see Figure 2.11). The relative values of the main aircraft performance parameters with respect to their kerosene baselines are reported in Table 5.3. With respect to the McKinsey & Company study, the results from this research appear extremely optimistic. Nevertheless, the extremely high 1.63 tank gravimetric index used by McKinsey & Company, which they take as an assumption, is completely out of line with the rest of the literature, and probably the cause of the much worse performances of their aircraft. The results from this research align much better with the ones from the Cryoplane project. What is unexpected is that despite having similar OEM and higher $MTOM$, the aircraft from this research still presents a lower SEC . Unfortunately, the lack of further data on the Cryoplane project aircraft makes it impossible to understand the cause of it.

Table 5.3: Comparison table for aircraft level performance of long-range aircraft designed in this research and long-range aircraft from McKinsey & Company [6] and the Cryoplane project [5]. Performance values relative to the kerosene baselines of the respective studies.

Parameters	Long-range		
	A330LH2(aftFwd-integral-(353-250)	McKinsey & Company	Cryoplane project
OEM	+22	-	+25%
$MTOM$	-5%	+23%	-15%
SEC	+5%	+42%	+9%

5.2. TANK LEVEL PERFORMANCE

For the short-range category, the tank belonging to the ATR72 LH2 version with 5 seats abreast and an aft tank layout is compared to the polyurethane tank of the regional aircraft from Verstraete et al. [13] (see Figure 2.22). The two tanks in question, which carry a similar amount of fuel, have almost equal tank gravimetric indexes (see Table 5.4).

Table 5.4: Comparison table for tank level performance of short-range aircraft designed in this research and short-range aircraft from Verstraete et al. [13].

Parameters	Short-range	
	ATR72LH2(aft-nonintegral-23-300)	Verstraete et al.
$m_{fuel} (kg)$	1055	1150
$\eta_{grav} (J/pax/m)$	0.42	0.41

For the medium-range category, the tank belonging to the A320 version with 6 seats abreast and an aft tank layout is compared to the aft tank of the medium-range aircraft from Silberhorn et al. [7] (see Figure 2.7). The tank of the aircraft from this research has a much lower gravimetric index, despite having a fuel mass in the same order of magnitude see Table 5.5). It is not known what is the cause for this difference as some fundamental design variables, such as the allowable material tensile stress and the nature of the support structure, are not described with sufficient detail by the authors. On the other hand, the mass of the fuel system (excluding tanks) is found to be very similar (see Table 5.5).

Table 5.5: Comparison table for tank level performance of medium-range aircraft designed in this research and medium-range aircraft from Silberhorn et al. [7].

Parameters	Medium-range	
	A320LH2(aft-nonintegral-33)	Silberhorn et al.
$m_{fuelSys}$ (kg)	766	781
m_{fuel} (kg)	6280	3485
η_{grav} (J/pax/m)	0.321	0.47

For the long-range category, the tank belonging to the A330 LH2 version with 11 seats abreast and an aft & fwd tank layout is compared to the tanks of the long-range single-deck aircraft from Verstraete et al. [13] (see Figure 2.23). The two tanks in question, which carry amounts of fuel in the same order of magnitude, have similar tank gravimetric indexes (see Table 5.4).

Table 5.6: Comparison table for tank level performance of long-range aircraft designed in this research and long-range aircraft from Verstraete et al. [13].

Parameters	Long-range	
	A330LH2(aftFwd-integral-(353-250)	Verstraete et al.
m_{fuel} (kg)	26918	40000
η_{grav} (J/pax/m)	0.27	0.30

CONCLUSIONS

In this research, several solutions to the integration of the hydrogen fuel system on short, medium and long-range airliners have been investigated using a framework capable of consistently considering the effects that different combinations of tank layout, tank structure and shape generate at aircraft level.

The effect of using an integral tank structure was found to be negligible for short-range aircraft, but increasingly more beneficial for medium and long-range aircraft. Indeed, despite the mass of the integral is larger, the mass and parasite drag savings from the smaller fuselage extension that this tank requires are dominant. The effect of increasing the fuselage diameter was found to be favourable, especially when seats abreast could be added without the addition of one aisle. Indeed, a wider fuselage, with a shorter cabin and shorter tanks, allows restoring the fuselage slenderness ratio of the baseline kerosene aircraft. The effect of using a combination of an aft and a forward tank was found to be detrimental in terms of operational empty mass, beneficial in terms of specific energy consumption and negligible in terms of maximum take-off mass. The operational empty mass increases because the narrower forward tank, placed to the side of the cockpit-cabin connecting corridor, inevitably yields a longer fuselage. The specific energy consumption decreases because the smaller horizontal tail surface required to balance the aircraft increases the mid-cruise lift-to-drag ratio. The maximum take-off mass remains approximately equal because the lower fuel mass required balances the higher operational empty mass. Given that the corridor left to the side of the forward tank has a width independent of the fuselage diameter, the aircraft with wider fuselages benefit more from this tank layout option. The use of spherical tanks was found to be slightly beneficial, but only when compared to a non-spherical tank version using the same tank layout, non-integral tank structure, and same cabin layout. Indeed, the absence of the cylindrical section prevents the spherical tank from growing or shrinking in length to achieve the optimal slenderness and from being used as an integral part of the fuselage structure. The study on the venting pressure revealed that with increasing aircraft size the optimal venting pressure in terms of main aircraft performance decreases whereas the sensitivity to those same parameters to the choice of venting pressure increases. The use of direct gas venting as a means to contain the pressure rise did not appear to provide significant performance improvements. Nevertheless, if the extra hydrogen carried for venting in case of an extended mission can, when unused, be efficiently recovered on ground, some small mass and energy savings can be obtained.

The optimal designs, in terms of operational empty mass, maximum take-off mass and specific energy consumption, feature increased fuselage diameters, the use of the aft & forward tank layout, non-spherical tanks and no direct venting. The short-range aircraft uses non-integral tanks and high venting pressure, while the medium and the long-range aircraft benefit from an integral tank structure and a lower venting pressure. Nevertheless, the sensitivity to these design choices is not significant, meaning that with a different set of assumptions and/or requirements different design choices may become optimal. For the best performing short-range LH2 aircraft, an 8% increase in operative empty mass, a 1.5% reduction in maximum take-off mass and a 5% increase in specific energy consumption are expected compared to the kerosene version. For the medium-range LH2 aircraft, a 24% increase in operative empty mass, a 1% increase in maximum take-off mass and a 13 % increase in specific energy consumption, compared to the kerosene version. For the long-range aircraft, a 22% increase in operative empty mass, a 5% reduction in maximum take-off mass and a 5% increase in specific energy consumption, compared to the kerosene version. The sensitivity analysis on the tank insulation and structural material performances indicated that

no fundamental changes in the main aircraft performance parameters are to be expected. The sensitivity analysis on the mission range showed that an increase in range has the effect of accentuating the operational empty mass penalty but leaves the maximum take-off mass and the specific energy consumption relative values fairly unchanged. With respect to the relative performances found in the literature, the results of this research lay in the middle, being optimistic compared to some researches while pessimistic compared to others.

Two main recommendations for future research are given. Because the fuselage mass increase was found to be the main contributor to the drop in the aircraft performances and consequently probably the source to the largest relative estimation error, future research could be directed towards the use of more sophisticated fuselage mass estimation methods, for example, using the finite element method. Moreover, given that the fuselage of LH2 aircraft is always longer than the one of its kerosene counterpart, it would be worth implementing in the design tool a landing gear mass estimation method that considers the landing gear height.

BIBLIOGRAPHY

- [1] *Waypoint 2050. Balancing growth in connectivity with a comprehensive global air transport response to the climate emergency*, Tech. Rep. (Air Transport Action Group, 2020).
- [2] Airbus, *Introducing ZEROe*, https://www.youtube.com/watch?v=525YtyRi_Vc (2020), retrieved on 04/12/2020.
- [3] B. Corner, *The challenges of hydrogen*, <https://leehamnews.com/2020/08/28/bjorns-corner-the-challenges-of-hydrogen-part-6-tank-placement> (2020), retrieved on 17/12/2020.
- [4] *Tupolev Tu-154*, http://richard.ferriere.free.fr/3vues/tupolev_tu154_3v.jpg, retrieved on 17/12/2020.
- [5] *Liquid hydrogen fuelled aircraft – system analysis*, Tech. Rep. GRD1-1999-10014 (Airbus Deutschland GmbH, 2003).
- [6] *Hydrogen-powered aviation A fact-based study of hydrogen technology, economics, and climate impact by 2050*, Tech. Rep. (Clean Sky 2 JU and FCH 2 JU, 2020).
- [7] D. Silberhorn, G. Atanasov, J.-N. Walther, and T. Zill, *Assessment of Hydrogen Fuel Tank Integration at Aircraft Level*, in *Deutscher Luft- und Raumfahrtkongress 2019* (2019).
- [8] G. D. Brewer, *Aviation usage of liquid hydrogen fuel: prospects and problem*, *International Journal of Hydrogen Energy* (1976).
- [9] F. Troeltsch, M. Engelmann, A. Scholz, F. Peter, J. Kaiser, and M. Hornung, *Hydrogen Powered Long Haul Aircraft with Minimized Climate Impact*, in *AIAA Aviation 2020 forum* (2020).
- [10] A. Silverstein and E. W. Hall, *Liquid Hydrogen as a Jet Fuel for High-Altitude Aircraft*, Tech. Rep. (Lewis Flight Propulsion Laboratory, 1955).
- [11] D. C. Maniaci, *Relative Performance of a Liquid Hydrogen-Fueled Commercial Transport*, in *46th AIAA Aerospace Sciences Meeting and Exhibit* (Reno, Nevada, 2008).
- [12] D. C. Acevedo et al., *A320 Auxiliary Propulsion and Power Unit*, Tech. Rep. (Delft University of Technology, 2020).
- [13] D. Verstraete, P. Hendrick, P. Pilidis, and K. Ramsden, *Hydrogen fuel tanks for subsonic transport aircraft*, *International Journal of Hydrogen Energy* (2010).
- [14] A. Gomez and H. Smith, *Liquid hydrogen fuel tanks for commercial aviation: structural sizing and stress analysis*, *Aerospace Science and Technology* (2019).
- [15] D. Verstraete, *The Potential of Liquid Hydrogen for long range aircraft propulsion*, Ph.D. thesis, Cranfield University (2009).
- [16] J. Brand, S. Sampath, F. Shum, R. L. Bayt, and J. Cohen, *Potential Use of Hydrogen in Air Propulsion*, in *AIAA International Air and Space Symposium and Exposition: The Next 100 Years* (Dayton, Ohio, 2003).

- [17] B. Kärcher, *Formation and radiative forcing of contrail cirrus*, Nature Communications (2018).
- [18] G. D. Brewer, *Hydrogen Aircraft Technology* (CRC Press, Boca Raton, 1991).
- [19] C. S. Lin, N. T. V. Dresar, and M. M. Hasan, *Pressure Control Analysis of Cryogenic Storage Systems*, Journal of Propulsion and Power (2004).
- [20] *Tupolev Tu-154*, <https://www.airlines-inform.com/commercial-aircraft/tu-154.html> (2015), retrieved on 17/12/2020.
- [21] *Tupolev Tu-155*, <https://avia-pro.net/blog/tu-155> (2015), retrieved on 17/12/2020.
- [22] *Handbook of products*, https://web.archive.org/web/20110608075828/http://www.bp.com/liveassets/bp_internet/aviation/air_bp/STAGING/local_assets/downloads_pdfs/a/air_bp_products_handbook_04004_1.pdf (2011), retrieved on 07/12/2020.
- [23] A. Contreras, S. Yiğit, K. Özay, and T. N. Veziroğlu, *Hydrogen as aviation fuel: a comparison with hydrocarbon fuels*, International Journal of Hydrogen Energy (1997).
- [24] *Air transport, passengers carried*, <https://data.worldbank.org/indicator/IS.AIR.PSGR>, retrieved on 03/12/2020.
- [25] *Aircraft Technology Roadmap to 2050*, Tech. Rep. (IATA, 2018).
- [26] H. Peter, *Forever fuel: the story of hydrogen* (Westview Press, 1981).
- [27] B. Arrighi, *NACA Lewis's 1957 Transformation* (Glenn Research Center, Cleveland, Ohio, 2017).
- [28] J. R. Kinney, *The Power for Flight. NASA's Contributions to Aircraft Propulsion* (National Aeronautics and Space Administration, Washington, DC, 2017).
- [29] *Liquid hydrogen as a propulsion fuel, 1945-1959. Bee Project*, <https://history.nasa.gov/SP-4404/ch6-4.htm> (), retrieved on 03/12/2020.
- [30] *Liquid hydrogen as a propulsion fuel, 1945-1959. Suntan*, <https://www.hq.nasa.gov/office/pao/History/SP-4404/ch8-1.htm> (), retrieved on 03/12/2020.
- [31] P. Hoffmann, *Tomorrow's Energy: Hydrogen, Fuel Cells, and the Prospects for a Cleaner Planet* (The MIT Press, Cambridge, Massachusetts, 2001).
- [32] R. Faaß, *Cryoplane*, https://www.fzt.haw-hamburg.de/pers/Scholz/dglr/hh/text_2001_12_06_Cryoplane.pdf (2001), retrieved on 04/12/2020.
- [33] M. D. Guynn, J. E. Freeh, and E. D. Olson, *Evaluation of a Hydrogen Fuel Cell Powered Blended-Wing-Body Aircraft Concept for Reduced Noise and Emissions*, Tech. Rep. NASNTM-2004-2 12989 (NASA, 2004).
- [34] *Tu-155*, <https://www.globalsecurity.org/military/world/russia/tu-155.htm>, retrieved on 17/12/2020.
- [35] *Liquid hydrogen as a propulsion fuel, 1945-1959. Silverstein-Hall Report*, <https://history.nasa.gov/SP-4404/ch6-3.htm#t2> (), retrieved on 03/12/2020.
- [36] T. W. Reynolds, *Aircraft-Fuel-Tank Design for Liquid Hydrogen*, Tech. Rep. (Lewis Flight Propulsion Laboratory, 1955).

- [37] *Certification specifications and acceptable means of compliance for Large Aeroplanes CS-25*, European Aviation Safety Agency (2016).
- [38] *Standard: Space Systems - Metallic Pressure Vessels, Pressurized Structures, and Pressure Components*, American National Standards Institute (ANSI) (1998).
- [39] S. K. Mital, J. Z. Gyekenyesi, S. M. Arnold, R. M. Sullivan, J. M. Manderscheid, and P. L. Murthy, *Review of current state of the art and key design issues with potential solutions for liquid hydrogen cryogenic storage tank structures for aircraft applications*, Tech. Rep. NASA/TM—2006-214346 (NASA, 2006).
- [40] L. Allidieres and F. Janin, *Tanks (Including Insulation), Cryoplane project*, Tech. Rep. Cryoplane Task Technical Report 3.6.2 (Air Liquide, 2002).
- [41] R. Heydenreich, *Cryotanks in future vehicles*, Cryogenics (1998).
- [42] A. Zielinski, *Hydrogen-assisted degradation of some non-ferrous metals and alloys*, Journal of Materials Processing Technology (2001).
- [43] *Composite cryotank technologies & demonstration*, https://gameon.nasa.gov/gcd/wp-content/uploads/sites/58/2015/11/FS_CCTD_factsheet.pdf (2013), retrieved on 27/12/2020.
- [44] M. J. Robinson, J. D. Eichinger, and S. E. Johnson, *Hydrogen permeability requirements and testing for reusable launch vehicle tanks*, in *AIAA/ASME/ASCE/AHS/ASC Structures, Structural Dynamics, and Materials Conf.* (2012).
- [45] J. V. Alemán, A. V. Chadwick, J. He, M. Hess, K. Horie, R. G. Jones, P. Kratochvíl, I. Meisel, I. Mita, G. Moad, S. Penczek, and R. E. T. Stepto, *Pure And Applied Chemistry* (IUPAC Recommendations, 2007) page 1806.
- [46] G. J. Weisend, *Handbook of cryogenic engineering* (Taylor and Francis, Philadelphia, PA, 1998) pages 186-201.
- [47] C. W. Keller, G. R. Cunnington, and A. P. Glassford, *Thermal performance of multilayer insulations*, Tech. Rep. 19740014451 (NASA, 1974).
- [48] C. S. Lin, N. T. V. Dresar, and M. M. Hasan, *A Pressure Control Analysis of Cryogenic Storage Systems*, Tech. Rep. NASA TM-104409, AIAA-91-2405 (National Aeronautics and Space Administration, Lewis Research Center, 1991).
- [49] J. H. Lienhard IV and J. H. Lienhard V, *A heat transfer textbook* (Phlogiston Press, Cambridge, Massachusetts, 2004).
- [50] M. Gauss, I. S. A. Isaksen, S. Wong, and W.-C. Wang, *Impact of H₂O emissions from cryoplanes and kerosene aircraft on the atmosphere*, Journal of Geophysical Research (2003).
- [51] L. J. Wilcox, K. P. Shine, and B. J. Hoskins, *Radiative forcing due to aviation water vapour emissions*, Atmospheric Environment (2012).
- [52] O. Boucher et al., *Clouds and aerosols*, in *Climate Change 2013: The Physical Science Basis. Contribution of Working Group I to the Fifth Assessment Report of the Intergovernmental Panel on Climate Change* (Cambridge University Press, Cambridge, UK, 2013) pp. 571–657.
- [53] D. Duda, P. Minnis, and L. Nguyen, *Estimates of cloud radiative forcing in contrail clusters using GOES imagery*, Journal of Geophysical Research **106**, 4927 (2001).

- [54] C. Voigt et al., *ML-CIRRUS: The Airborne Experiment on Natural Cirrus and Contrail Cirrus with the High-Altitude Long-Range Research Aircraft HALO*, Bulletin of the American Meteorological Society (2017).
- [55] L. Sherry and T. Thompson, *Primer on Aircraft Induced Clouds and Their Global Warming Mitigation Options*, Transportation Research Record: Journal of the Transportation Research Board (2020).
- [56] S. Marquart, M. Ponater, L. Ström, and K. Gierens, *An upgraded estimate of the radiative forcing of cryoplane contrails*, Meteorologische Zeitschrift (2005).
- [57] M. Ponater, S. Pechtl, R. Sausen, U. Schumann, and G. Hüttig, *Potential of the cryoplane technology to reduce aircraft climate impact: A state-of-the-art assessment*, Atmospheric Environment (2006).
- [58] U. Schmidtchen, E. Behrend, H. W. Pohl, and N. Rostek, *Hydrogen Aircraft and Airport Safety*, Renewable and Sustainable Energy Review (1997).
- [59] B. Khandelwal, AdamKarakurt, P. R. Sekaran, V. Sethi, and R. Singh, *Hydrogen powered aircraft: the future of airtransport*, Progress in Aerospace Sciences (2013).
- [60] M. J. Sefain, *Hydrogen Aircraft Concepts & Ground Support*, Ph.D. thesis, Cranfield University (2000).
- [61] R. Elmendorp, R. Vos, and G. L. Rocca, *A Conceptual Design and Analysis Method for Conventional and Unconventional Airplanes*, in *29th Congress of the International Council of the Aeronautical Sciences* (St. Petersburg, Russia, 2014).
- [62] M. Brown and R. Vos, *Conceptual Design and Evaluation of Blended-Wing-Body Aircraft*, in *2018 AIAA Aerospace Sciences Meeting* (Kissimmee, Florida, 2018).
- [63] M. F. M. Hoogreef, R. Vos, R. de Vries, and L. L. M. Veldhuis, *Conceptual Assessment of Hybrid Electric Aircraft with Distributed Propulsion and Boosted Turbofans*, in *AIAA Scitech 2019 Forum* (San Diego, California, 2019).
- [64] A. Elham, G. La Rocca, and M. J. L. van Tooren, *Development and implementation of an advanced, design-sensitive method for wing weight estimation*, Aerospace Science and Technology (2013).
- [65] E. Torenbeek, *Synthesis of Subsonic Airplane Design* (Delft University Press and Martinus Nijhoff Publishers, Delft, 1982).

EXAMPLE OF XML INPUT FILE FOR LH2 AIRCRAFT

When you have the Initiator (Revision 2409 or newer), you can use an input file of the following type to generate an LH2 aircraft.

```

1 <?xml version="1.0" encoding="utf-8"?>
2 <initiator xmlns:xsi="http://www.w3.org/2001/XMLSchema-instance" xsi:
   noNamespaceSchemaLocation="initiator.xsd">
3   <aircraft>
4     <name>A320-NEO-LH2</name>
5     <description>Airbus A320-NEO</description>
6     <missions default="Harmonic">
7       <mission name="Harmonic">
8         <requirement>
9           <name>Pax</name>
10          <value>150</value>
11        </requirement>
12        <requirement>
13          <name>PayloadMass</name>
14          <value>19300</value>
15        </requirement>
16        <requirement>
17          <name>CruiseMach</name>
18          <value>0.78</value>
19        </requirement>
20        <requirement>
21          <name>Altitude</name>
22          <value>11278</value>
23        </requirement>
24        <requirement>
25          <name>Range</name>
26          <value>4550</value>
27        </requirement>
28        <requirement>
29          <name>TakeOffDistance</name>
30          <value>2180</value>
31        </requirement>
32        <requirement>
33          <name>LandingDistance</name>
34          <value>1440</value>
35        </requirement>
36        <requirement>
37          <name>ApproachSpeed</name>

```

```

38     <value>70</value>
39 </requirement>
40 <requirement>
41     <name>NumberOfFlights</name>
42     <value>100000</value>
43 </requirement>
44 <requirement>
45     <name>AirworthinessRegulations</name>
46     <value>FAR-25</value>
47 </requirement>
48 <requirement>
49     <name>TimeToClimb</name>
50     <!-- Time to climb to a specified altitude -->
51     <value mapType="vector">10;4000</value>
52     <!-- Time [minutes] ; Altitude [meter] -->
53 </requirement>
54 <requirement>
55     <name>LoiterTime</name>
56     <value>30</value>
57 </requirement>
58 <requirement>
59     <name>DivRange</name>
60     <value>370</value>
61 </requirement>
62 <requirement>
63     <name>AirportClassification</name>
64     <value>FAA-IV</value>
65 </requirement>
66 </mission>
67 </missions>
68 <performance>
69     <parameter>
70         <name>LDmax</name>
71         <value>18</value>
72     </parameter>
73     <parameter>
74         <name>SFC</name>
75         <value>0.1893</value>
76     </parameter>
77     <parameter>
78         <name>FuelType</name>
79         <value>LH2</value>
80     </parameter>
81     <parameter>
82         <name>CLmaxLanding</name>
83         <value>2.6</value>
84     </parameter>
85     <parameter>
86         <name>CLmaxTakeOff</name>

```

```

    <value>2.1</value>
88 </parameter>
    <parameter>
90     <name>CLmaxClean</name>
        <value>1.3</value>
92     </parameter>
</performance>
94 <configuration>
    <parameter>
96     <name>WingAspectRatio</name>
        <value>9.5</value>
98     </parameter>
    <parameter>
100     <name>WingLocation</name>
        <value>Low</value>
102     </parameter>
    <parameter>
104     <name>HasKink</name>
        <value>1</value>
106     </parameter>
    <parameter>
108     <name>TEinboardSweep</name>
        <value>0</value>
110     </parameter>
    <parameter>
112     <name>TailType</name>
        <value>Standard</value>
114     </parameter>
    <parameter>
116     <name>RootAirfoil</name>
        <value>SC20414</value>
118     </parameter>
    <parameter>
120     <name>KinkAirfoil</name>
        <value>SC20412</value>
122     </parameter>
    <parameter>
124     <name>KinkTwist</name>
        <!-- twist angle at kink, code will consider wing incidence--
>
126     <value>-3</value>
    </parameter>
128     <parameter>
        <name>TipAirfoil</name>
        <value>SC20410</value>
130     </parameter>
132     <parameter>
        <name>TipTwist</name>
134     <!-- twist angle at tip, code will consider wing incidence

```

```

and possible kink twist-->
  <value>-1.2</value>
136 </parameter>
  <parameter>
138   <name>SupercriticalAirfoil</name>
     <value>1.1</value>
140 </parameter>
  <parameter>
142   <name>Freight</name>
     <value>>false</value>
144 </parameter>
  <parameter>
146   <name>FuselageTank</name>
     <value>>false</value>
148 </parameter>
  <parameter>
150   <name>CompositeStructures</name>
     <!-- Fuselage,Wing,Empennage-->
152   <value mapType="vector">0;0;0</value>
</parameter>
  <parameter>
154   <name>TankLayout</name>
     <value>aftFwd</value>
156 </parameter>
  <parameter>
158   <name>SphericalTank</name>
     <value>>false</value>
160 </parameter>
  <parameter>
162   <name>IntegralTank</name>
     <value>>true</value>
164 </parameter>
</configuration>
<parts mainPart="Fuselage">
168   <fuselage name="Fuselage" type="Conventional">
     <paxDivision mapType="vector">1</paxDivision>
170     <!-- should sum to 1 -->
     <!-- Based on A320 Europe, Lufthansa (SeatGuru) -->
172     <!-- http://www.seatguru.com/airlines/Lufthansa/
Lufthansa_Airbus_A320-200_NEK.php -->
     <!-- Dimensions: Seat width, arm rest width, seat pitch,
seatbackspace, legspace (last 2 unused) -->
174     <cabins>
       <cabin name="Cabin1">
176         <class>
           <name>FC</name>
178           <seatingArr mapType="vector">1;2;1</seatingArr>
           <seatingDim mapType="vector">0.57;0.078;0.914;0.8;0.3</
seatingDim>

```

```

180         </class>
181         <class>
182             <name>EC</name>
183             <seatingArr mapType="vector">2;4;2</seatingArr>
184             <seatingDim mapType="vector">0.46;0.048;0.813;0.8;0.3</
seatingDim>
185         </class>
186         <classDistribution mapType="vector">0.08;0;0;0.92</
classDistribution>
187     </cabin>
188 </cabins>
189 </fuselage>
190 <wing name="Main Wing" type="MainWing"/>
191 <wing name="Horizontal Stabiliser" type="HorizontalTail"/>
192 <wing name="Vertical Stabiliser" type="VerticalTail"/>
193 <engine name="Engine-1" type="TurboFan" distributed="false">
194     <location>Main Wing</location>
195     <!-- engine x location, fraction of fuselage length for
fuselage mounted; spanwise fraction for wing/tail mounted,
negative for other wing; -->
196     <!-- offset from wing in x fraction of engine length; offset
in z fraction of engine diameter-->
197     <LocationFrac mapType="vector">0;0.4;-0.8;-0.6</
LocationFrac>
198     <bypassRatio>11</bypassRatio>
199     <motor name="Turbine-1" type="Turbine"/>
200     <fan name="Fan-1" type="Fan"/>
201 </engine>
202 <engine name="Engine-2" type="TurboFan" distributed="false">
203     <location>Main Wing</location>
204     <LocationFrac mapType="vector">0;-0.4;-0.8;-0.6</
LocationFrac>
205     <bypassRatio>11</bypassRatio>
206     <motor name="Turbine-2" type="Turbine"/>
207     <fan name="Fan-2" type="Fan"/>
208 </engine>
209 </parts>
210 </aircraft>
211 <runList>DesignConvergence,PlotTool</runList>
212 <settings>
213     <include source="defaultSettingsLH2.xml"/>
214     <setting>
215         <name>AftMinToMaj1</name>
216         <value>0.5</value>
217     </setting>
218     <setting>
219         <name>AftMinToMaj2</name>
220         <value>1</value>
221     </setting>

```

```
222 <setting>
    <name>FwdMinToMaj1</name>
224     <value>0.5</value>
    </setting>
226 <setting>
    <name>FwdMinToMaj2</name>
228     <value>0.5</value>
    </setting>
230 <setting>
    <name>LuggageMass</name>
232     <value>20</value>
    </setting>
234 <setting>
    <name>UseFemWingWeight</name>
236     <value>>false</value>
    </setting>
238 <setting>
    <name>SparPositions</name>
240     <value mapType="vector">0.10;0.6</value>
    </setting>
242 <setting>
    <name>UseAuxiliarySparForFuelTank</name>
244     <value>>false</value>
    </setting>
246 <setting>
    <name>TailControl</name>
248     <value>full moving</value>
    </setting>
250 <setting>
    <name>MainWingKinkLocation</name>
252     <value>0.44</value>
    </setting>
254 <setting>
    <name>UsableFuelVolume</name>
256     <!-- Fraction of fuel tank volume usable for fuel storage -->
    <value>1.0</value>
258 </setting>
    <setting>
260     <name>ventingPressure</name>
    <value>250000</value>
262 </setting>
    <setting>
264     <name>fuelFracAft</name>
    <value>0.60</value>
266 </setting>
    <setting>
268     <name>thermalCond</name>
    <value>2.2E-2</value>
270 </setting>
```

```
272     <setting>
        <name>sigmainnerwall</name>
        <value>172E6</value>
274     </setting>
</settings>
276 <moduleInputs>
    <input module="PlotTool">
278     <plotModules>Geometry,DesignConvergence</plotModules>
    </input>
280 </moduleInputs>
</initiator>
```

Listing A.1: XML input file for liquid hydrogen aircraft A320LH2(aftFwd-integral-242-250). Working on Revision 2409 of the Initiator